

**THE DEVELOPMENT OF L-PHENYLALANINE BIOSENSOR  
USING BORON-DOPED DIAMOND (BDD) ELECTRODE  
MODIFIED WITH POLYANILINE-POLYVINYL SULPHONATE  
COMPOSITE FILM**



UNIVERSITY *of the*  
WESTERN CAPE

**ZELO MANGOMBO**

**THE DEVELOPMENT OF L-PHENYLALANINE  
BIOSENSOR USING BORON-DOPED DIAMOND (BDD) ELECTRODE MODIFIED  
WITH POLYANILINE-POLYVINYL SULPHONATE COMPOSITE FILM**

**By**

**ZELO MANGOMBO**

**A thesis submitted in partial fulfillment of the requirements for the degree of Doctor  
Philosophiae in Department of Chemistry, University of the Western Cape.**



**UNIVERSITY of the  
WESTERN CAPE**

**Supervisors: Prof. Priscilla G.L. Baker**

**Prof. Emmanuel I. Iwuoha**

**Prof. David L. Key**

**May 2010**

**i**

## Keywords

Polyaniline

Polyvinyl sulphonate

Composite film polymers

Electrochemical enzyme biosensor

L-phenylalanine

L-tyrosine

Tyrosinase

Lipoprotein (human plasma)

Boron-doped diamond (BDD)

Cyclic voltammetry



## Abstract

The aim of this project was to develop a biosensor on a modified boron-doped diamond (BDD) platform in order to determine L-phenylalanine (L-Phe) levels in the aqueous media and real samples. A BDD electrode modified with polyaniline (PANI) film doped with polyvinyl sulphonate (PVS), containing in-situ deposited tyrosinase (Tyr) enzyme was studied with special emphasis on the detection of L-phenylalanine (L-Phe). The PANI-PVS film was electrochemically coated on the BDD surface by cyclic voltammetry (CV) at  $50 \text{ mV s}^{-1}$  (versus Ag/AgCl). An increase in current density with increasing number of cycles was an indication of the polymer growth. The morphologies of the composite films were characterized by scanning electron microscopy (SEM). The study has shown successfully doping of the PANI film by PVS and that the template PVS directed the electron transfer of both enzyme and BDD electrode. The modified electrode was further utilized to detect L-Phe. PANI-PVS film was found to be more suitable material for enzyme immobilization and biosensor development. L-Tyr standard solution was studied, characterized and used as a reference standard solution for L-Phe determination. The oxidation of L-Phe was also carried out as a function of pH. Voltammetric results inferred that Tyr immobilized on the PANI-PVS composite film retained its bioelectrocatalytic activity towards the oxidation of L-Phe and was not denatured during its immobilization. The PANI-PVS materials provided a suitable micro-environment for immobilization of Tyr and were thus applied as a mediator to enhance the direct electron transfer of Tyr on BDD electrode. The Tyr/PANI-PVS biosensor was finally applied for the detection of L-phenylalanine. The activity of Tyr was causing an increase current in its response to L-Phe. The limit of detection for L-Phe by the voltammetric method was  $1.0 \times 10^{-2} \mu\text{M}$  within a concentration range of 2-10  $\mu\text{M}$ . This study demonstrates that the developed biosensor is sensitive enough to detect the L-Phe in these matrices and could be a useful tool in screening of the L-Phe at low concentrations. The apparent Michaelis-Menten constant ( $K_m^{app}$ ) calculated for the Tyr/PANI-PVS biosensor in the presence of L-Phe was found to be  $1.39 \pm 0.01 \mu\text{M}$  and the sensitivity was  $7.19 \text{ Amol}^{-1} \text{ dm}^3$ . The low  $K_m^{app}$  value obtained for the Tyr/PANI-PVS biosensor indicates strong binding to Tyr by the substrate. The biosensor was also used in the real samples. L-Phe content of effervescent flu tablets determined using this biosensor was 9.10 % and 9.51 % (m/m) and that of an artificial sweetener containing L-Phe as a dipeptide before hydrolysis, was 25.66 % and 28.40 % (m/m).

The developed biosensor was employed for the determination of L-phenylalanine in lipoprotein (human plasma) and lemonade (soft drink). The biosensor has shown the linearity from 0.2 to  $20 \pm 0.1 \mu\text{M}$  for lipoprotein (human plasma) and 0.2 to  $22 \pm 0.1 \mu\text{M}$  for lemonade (soft drink), respectively. The detection limit was found to be  $1.0 \times 10^{-3} \pm 0.1 \mu\text{M}$  for both lipoprotein and lemonade. The biosensor exhibited high sensitivity for L-Phe detection, very good reproducibility and with a relative standard deviation (R.S.D) of 5 % (duplicate measurements) was obtained. The low R.S.D obtained for the biosensor demonstrates that its response was highly reproducible. Therefore, the biosensor is sufficient in providing high sensitivity for determination of L-Phe in real samples at residue levels.




## Declaration

I declare that *The development of L-Phenylalanine Biosensor Using Boron-Doped Diamond (BDD) Electrode Modified with Polyaniline-Polyvinyl Sulphonate Composite* is my own work, that it has not been submitted before for any degree or examination in any other university, and that all the sources I have used or quoted have been indicated and acknowledged as complete references.

**Zelo Mangombo**

Signature.....



**May 2010**

2010/09/23

**Supervisors: Prof. Priscilla G.L. Baker**

Signature.....



**Prof. Emmanuel Iwuoha**

Signature.....

**Prof. David L. Key**

Signature.....

## Acknowledgements

I would like to thank the Almighty GOD, Eternal Father, for His unconditional Love through JESUS CHRIST and renewed my strength day by day, which enabled me to complete this thesis.

(Hebrews 6: 10)

Special thanks go to my wife Meisie Mangombo, my family and family-in-Law for persevering for this time of my studies. Thank you very much for your love and encouragement. Thanks to Pastor Bienvenue Mukoko for his prayer and motivation.

I would like to acknowledge the University of the Western Cape, South Africa, for giving me the opportunity to pursue my Doctoral degree at this University. Special thanks to the Department of Chemistry and SensorLab, University of the Western Cape, for providing all the apparatus and instrumentation required for my research.

I would also like to acknowledge my Supervisors, Professor Priscilla G.L. Baker, Professor Emmanuel I. Iwuoha and Professor David L. Key for their excellent supervision, support and encouragement during this period.

Finally, I sincerely thank the National Research Foundation (NRF) of South Africa for funding this project.

Many thanks to all my family members and special friends for their patience, love, support and encouragement during this period of study and have been away from home. The support of all my colleagues in Sensor Lab, University of the Western Cape, is gratefully acknowledged. I also would like to extend my acknowledgement to the Physics department at University of the Western Cape for their assistance with SEM experiments. Special thanks to Mr. Adrian of physics department and Associated Professor Susan A. Bourne (UCT) for her encouragement.

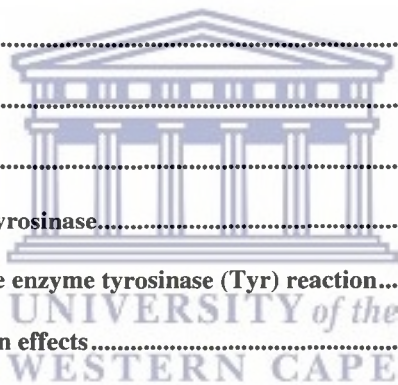
# Table of contents

<b>Title page</b> .....	<b>ii</b>
<b>Keywords</b> .....	<b>ii</b>
<b>Abstract</b> .....	<b>Error! Bookmark not defined.</b>
<b>Declaration</b> .....	<b>v</b>
<b>Acknowledgements</b> .....	<b>vii</b>
<b>Table of contents</b> .....	<b>viii</b>
<b>List of figures and tables</b> .....	<b>xv</b>
<b>List of Publications</b> .....	<b>xxi</b>
<b>Abbreviations</b> .....	<b>xxii</b>
<b>CHAPTER 1</b> .....	<b>Error! Bookmark not defined.</b>
<b>Introduction</b> .....	<b>Error! Bookmark not defined.</b>
<b>1.1 Motivation of the study</b> .....	<b>3</b>
<b>1.2 Statement of the problem</b> .....	<b>6</b>
<b>1.3 Aim and objectives</b> .....	<b>6</b>
<b>1.3.1 General objectives</b> .....	<b>6</b>
<b>1.3.2 Specific objectives</b> .....	<b>7</b>
<b>1.4 Research hypothesis</b> .....	<b>8</b>
<b>1.5 Contribution of the work described in this thesis</b> .....	<b>9</b>
<b>1.6 Research framework</b> .....	<b>10</b>
<b>1.7 Delimitations of the thesis</b> .....	<b>11</b>
<b>1.8 Proposed “KIMB*”- mechanisms</b> .....	<b>11</b>
<b>1.9 Overview of the chapters</b> .....	<b>14</b>

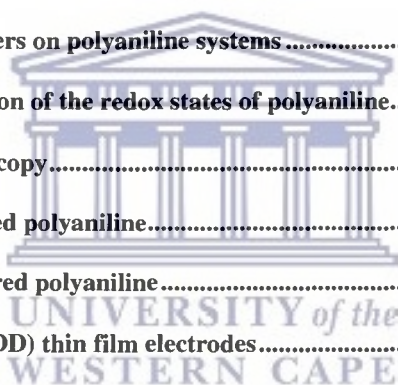




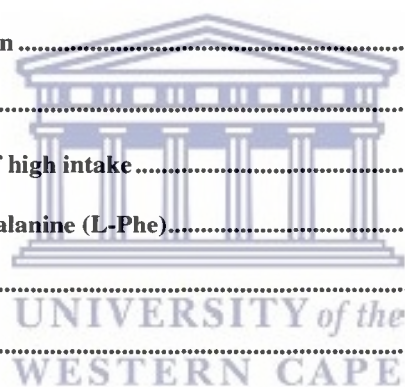
<b>CHAPTER 2 .....</b>	<b>15</b>
<b>Literature Review.....</b>	<b>15</b>
<b>2.1 Introduction .....</b>	<b>15</b>
<b>2.2 Biosensors.....</b>	<b>15</b>
<b>2.2.1 Bioreceptors/or biorecognitions .....</b>	<b>17</b>
<b>2.2.2 Transducers .....</b>	<b>19</b>
<b>2.2.3 Types of biosensors.....</b>	<b>20</b>
<b>2.3 Enzymes.....</b>	<b>23</b>
<b>2.3.1 Enzyme biosensors.....</b>	<b>25</b>
<b>2.3.1.1 Enzyme kinetics .....</b>	<b>25</b>
<b>2.3.1.2 Enzyme inhibition.....</b>	<b>27</b>
<b>2.3.1.3 Tyrosinase (Tyr) enzyme.....</b>	<b>30</b>
<b>2.3.1.3.1 Source of tyrosinase.....</b>	<b>32</b>
<b>2.3.1.3.2 Structure of tyrosinase .....</b>	<b>33</b>
<b>2.3.1.3.3 Tyrosinase functions.....</b>	<b>34</b>
<b>2.3.1.3.4 Reaction mechanisms of tyrosinase.....</b>	<b>35</b>
<b>2.3.1.3.5 Kinetics (rate) study of the enzyme tyrosinase (Tyr) reaction.....</b>	<b>39</b>
<b>2.3.1.3.6 Tyrosinase (Tyr) inhibition effects.....</b>	<b>41</b>
<b>2.4 Immobilization methods .....</b>	<b>41</b>
<b>2.4.1 Cross-linking.....</b>	<b>42</b>
<b>2.4.2 Carrier-bonding.....</b>	<b>42</b>
<b>2.4.2.1 Physical adsorption .....</b>	<b>43</b>
<b>2.4.2.2 Ionic bonding .....</b>	<b>43</b>
<b>2.4.2.3 Covalent bonding.....</b>	<b>44</b>
<b>2.4.2.4 Entrapping of enzyme .....</b>	<b>45</b>
<b>2.5 Conducting polymers (CPs).....</b>	<b>46</b>
<b>2.5.1 Historical background of electronically conducting polymers .....</b>	<b>48</b>
<b>2.5.2 Synthesis of conducting polymers .....</b>	<b>49</b>



2.5.3	Applications of conducting polymers .....	51
2.5.4	Polyaniline (PANI) as a conducting polymer .....	52
2.5.4.1	Conductivity and doping of polyaniline.....	54
2.5.4.2	The concept of sulphonated polyaniline (SPAN) .....	56
2.5.5	pH sensitivity and switching properties of polyaniline.....	57
2.5.6	Preparation of PANI composites/blends with others copolymers .....	58
2.5.7	Counter-ion induction techniques .....	59
2.5.8	Shortcomings of the solubility approach .....	59
2.5.9	Nanostructurization approaches .....	60
2.5.10	Processability .....	60
2.5.11	Electrosynthesis of polyanilines.....	63
2.5.12	Factors affecting the electrodeposition processes .....	65
2.5.13	Reported kinetic parameters on polyaniline systems .....	66
2.5.14	Spectroscopic determination of the redox states of polyaniline.....	66
2.5.15	Scanning Electron Microscopy.....	69
2.5.16	Synthesis of nanostructured polyaniline.....	69
2.5.17	Properties of nanostructured polyaniline.....	70
2.6	Boron-doped diamond (BDD) thin film electrodes.....	70
2.6.1	Introduction .....	70
2.6.2	Carrier mobility of diamond .....	72
2.6.3	Doping of diamond .....	72
2.6.4	Factors influencing the electrochemical behavior of BDD electrode .....	73
2.6.5	Boron-doped diamond (BDD) electrodes.....	74
2.6.5.1	Properties of boron-doped diamond (BDD) electrodes .....	74
2.6.5.2	Modification of BDD electrodes .....	75
2.6.6	Electrochemical techniques .....	76
2.6.7	Electrochemistry of BDD electrodes.....	78
2.6.7.1	Electrochemical studies of highly BDD in aqueous media .....	79



2.6.7.2	Electrochemical studies of highly BDD in non-aqueous media .....	79
2.6.7.3	Electrochemical studies of moderately BDD in aqueous media .....	79
2.6.7.4	Electrochemical studies of undoped diamond in aqueous media .....	80
2.6.7.5	Conducting polymer modified BDD electrodes.....	80
2.7	Application of BDD electrodes .....	83
2.7.1	Thermal applications.....	84
2.7.2	Electronic devices .....	84
2.7.3	Optical windows.....	84
2.7.4	Abrasives .....	85
2.8	L-phenylalanine (L-Phe) .....	85
2.8.1	Introduction .....	85
2.8.2	Deficiency of L-phenylalanine .....	87
2.8.3	Dosage and administration .....	87
2.8.4	Overdosage.....	88
2.8.5	Toxicity and symptoms of high intake .....	88
2.8.6	Food sources of L-phenylalanine (L-Phe).....	88
2.8.7	Actions .....	89
2.8.8	Mechanism of action.....	89
2.8.9	Indications and usage .....	89
2.8.10	Contraindications .....	90
2.8.11	Precautions.....	90
2.8.12	Adverse reactions.....	90
2.8.13	Recommendations.....	91
2.9	L-tyrosine (L-Tyr) .....	91
2.10	Phenylketonuria (PKU).....	92
2.10.1	Signs and symptoms effects .....	92
2.10.2	Nutritional therapy.....	93
2.10.3	Precautions.....	93



2.10.4	Maternal PKU effects.....	93
2.10.5	Recommendations.....	94
2.11	Conclusion and future trends .....	94
<b>CHAPTER 3 .....</b>		<b>96</b>
<b>Electrochemical techniques .....</b>		<b>96</b>
3.1	Reagents and materials .....	96
3.2	Principles of the electrochemical techniques used .....	97
3.3	Principles governing electrode processes.....	97
3.4	Electroanalytical techniques employed.....	99
3.4.1	Instrumentation .....	99
3.4.2	Cyclic voltammetry .....	103
3.4.2.1	Characteristics of reversible systems.....	106
3.4.2.2	Characteristics of quasi-reversible systems.....	107
3.4.2.3	Estimating the surface concentration of a redox couple .....	108
3.4.3	Square wave voltammetry (SWV).....	109
3.4.4	Linear sweep voltammetry (LSV).....	110
3.4.5	Electrochemical enzyme biosensors.....	112
3.4.5.1	Principles of operation .....	112
3.4.5.2	Practical aspects.....	114
3.4.5.2.1	Response time.....	114
3.4.5.2.2	Biosensor calibration.....	114
3.5	Electrochemical procedures.....	115
3.5.1	Electrochemical activation and cleaning of BDD electrodes.....	115
3.5.2	Electrochemical synthesis and characterization of polyaniline Doped with polyvinyl sulphonate (PANI-PVS) .....	116
3.5.3	Multi-scan rate studies on the electrochemical behaviour of electro- deposited PANI-PVS .....	117

3.5.3.1	Characterization of PANI-PVS in H <sub>2</sub> SO <sub>4</sub> and HCl .....	117
3.5.3.2	Characterization of the polymer composite in phosphate buffer Solution (PBS).....	117
3.5.4	Preparation and characterization of the enzyme biosensor .....	117
3.5.5	Electrochemical measurements .....	119
3.6	Graphing and data analysis .....	119
3.7	Determination of the limit of detection (LOD).....	120
 <b>CHAPTER 4 .....</b>		<b>121</b>
<b>Synthesis and characterization of Polyaniline Doped with Polyvinyl Sulphonate (PANI-PVS) .....</b>		<b>121</b>
4.1	Introduction .....	121
4.2	Electrochemical synthesis and characterization of PANI-PVS .....	122
4.3	Optimization of the stability of BDD surface electrode for Electropolymerization of PANI-PVS in 1 M HCl.....	128
4.4	Characterization of PANI-PVS films using UV-Vis spectroscopy .....	129
4.5	Characterization of PANI-PVS films using SEM .....	130
4.6	Conclusions .....	133
 <b>CHAPTER 5 .....</b>		<b>134</b>
<b>Tyr/PANI-PVS Biosensor Characterization and Optimization .....</b>		<b>134</b>
5.1	Introduction .....	134
5.2	Spectroscopic analysis of PANI-PVS and Tyr/PANI-PVS films .....	135
5.2.1	UV-Vis spectroscopy .....	135
5.2.2	Fourier transform infrared (FTIR) spectroscopy.....	137
5.3	Direct electrochemistry of Tyrosinase (Tyr) and electrochemical characterization of the Tyr/BDD biosensor.....	139

5.3.1	<b>Immobilization and characterization of Tyrosinase (Tyr) onto BDD electrode.....</b>	<b>139</b>
5.3.2	<b>Detection of L-phenylalanine (L-Phe) using Tyr/BDD biosensor.....</b>	<b>143</b>
5.4	<b>Direct electrochemistry of Tyrosinase (Tyr) and electrochemical characterization of the Tyr/PANI-PVS biosensor .....</b>	<b>145</b>
5.5	<b>Investigation of the electrocatalytic activity of the Tyr/PANI-PVS biosensor .....</b>	<b>148</b>
5.6	<b>Response time of the Tyr/PANI-PVS biosensor.....</b>	<b>152</b>
5.7	<b>Reproducibility and stability of the Tyr/PANI-PVS biosensor .....</b>	<b>152</b>
5.8	<b>Conclusions .....</b>	<b>154</b>
<b>CHAPTER 6 .....</b>		<b>155</b>
<b>Application of Tyr/PANI-PVS Biosensor for the detection of phenol compounds .....</b>		<b>155</b>
6.1	<b>Introduction .....</b>	<b>155</b>
6.2	<b>Fabrication of the Tyr/PANI-PVS biosensor .....</b>	<b>156</b>
6.3	<b>Experimental conditions .....</b>	<b>156</b>
6.4	<b>Detection of L-Tyrosine (L-Tyr) using the Tyr/PANI-PVS/BDD-biosensor.....</b>	<b>157</b>
6.5	<b>Detection of L-Phenylalanine (L-Phe) using the Tyr/PANI-PVS/BDD-biosensor.....</b>	<b>159</b>
6.6	<b>Application of Tyr/PANI-PVS biosensors .....</b>	<b>167</b>
6.6.1	<b>Electrochemical study of real samples using Tyr/PANI-PVS/BDD-biosensor.....</b>	<b>167</b>
6.6.2	<b>Determination of L-Phe in biological samples using Tyr/PANI-PVS/BDD biosensor .....</b>	<b>170</b>
6.7	<b>Discussion.....</b>	<b>175</b>

<b>CHAPTER 7 .....</b>	<b>177</b>
<b>Conclusions and Recommendations.....</b>	<b>177</b>
<b>7.1 Conclusions .....</b>	<b>177</b>
<b>7.2 Recommendations.....</b>	<b>179</b>
<b>References .....</b>	<b>180</b>



## List of Figures and Tables

### List of Figures

<b>Figure 1.1.</b> Pathways for L-phenylalanine detection using: A) phenylalanine hydroxylase (PAH) and (B) tyrosinase (Tyr), as enzymes .....	5
<b>Figure 1.2.</b> Catalytic pathways of tyrosinase for L-dopa oxidation (equation 1.1-1.4) .....	5
<b>Figure 1.3.</b> Research framework.....	10
<b>Figure 1.4a.</b> Proposed “KIMB*-1” mechanism for L-Phe detection using Tyr/PANI-PVS/BDD biosensor. “KIMB*”: Key (K), Iwuoha (I), Mangombo (M), Baker (B).....	12
<b>Figure 1.4b.</b> Proposed “KIMB*-1” mechanism for L-Phe detection using Tyr/BDD biosensor. “KIMB*”: Key (K), Iwuoha (I), Mangombo (M), Baker (B) .....	13
<b>Figure 2.1.</b> Typical diagram of a biosensor .....	17
<b>Figure 2.2.</b> Typical representation of an electrochemical enzyme biosensor .....	22
<b>Figure 2.3.</b> (a) Variation of the reaction velocity $v$ with the substrate concentration and (b) Lineweaver-Burk plots for different types of reversible enzyme inhibitors .....	26
<b>Figure 2.4.</b> Kinetic schemes for reversible enzyme inhibition .....	29
<b>Figure 2.5.</b> Tyrosinase pathway for melanin production (i-ii).....	31
<b>Figure 2.6.</b> Model structure of tyrosinase enzyme: (A) – (B) only Tyr molecule has shown, copper atoms are shown in green and in red is the molecular surface. (C) – (D) the active site for the protein sits within a pocket formed on the molecular surface of the molecule. (D) – (E) histidine amino acids are shown as a blue line representation.....	34
<b>Figure 2.7.</b> Tyrosinase pathway for providing L-dopa in the system .....	35
<b>Figure 2.8.</b> Direct oxidation by copper enzyme (two metal centers) for a two-electron oxidation .....	36
<b>Figure 2.9.</b> Catalytic cycle for the oxidation of monophenol and diphenol substrates to <i>o</i> -quinones by tyrosinase in the presence of $O_2$ .....	38



<b>Figure 2.10.</b> Mechanism of tyrosinase activity for the oxidation of monophenol and diphenol substrates to <i>o</i> -quinones in the presence of O <sub>2</sub> .....	39
<b>Figure 2.11.</b> Catalytic mechanism of tyrosinase enzyme activity for melanine production .....	40
<b>Figure 2.12.</b> Typical covalent bonds between Tyr enzyme and activated carboxylic group .....	45
<b>Figure 2.13.</b> Structures of some conducting polymers commonly used in biosensors .....	48
<b>Figure 2.14.</b> Oxidative polymerization of aniline.....	50
<b>Figure 2.15.</b> (A) The general polymeric structure of polyaniline. (B) Oxidation of aniline to polyaniline showing its redox states.....	53
<b>Figure 2.16.</b> An illustration of n and p- doping process respectively .....	55
<b>Figure 2.17.</b> An illustration of polyvinyl sulphonate (PVS) copolymer structure .....	59
<b>Figure 2.18.</b> A poly-carbonate track-etched membrane (PCM) (a) and an anodic alumina membrane (ALM) (b) showing uniformly sized nano-pores within which polymer deposition takes place .....	61
<b>Figure 2.19.</b> A schematic diagram showing the micelle-monomer orientation adopted by an anionic-surfactant in a polar solvent during template-free polymerization process .....	62
<b>Figure 2.20.</b> Typical boron-doped diamond electrode (manufactured by Windsor Scientific Limited; www.windsorscientific.co.uk) .....	75
<b>Figure 2.21.</b> Redox polymers processes in the background of p-type (semiconductor) .....	81
<b>Figure 3.1.</b> A typical electrochemical cell consisting of three electrodes: WE = working electrode, RE = reference electrode and AE = auxiliary electrode .....	101
<b>Figure 3.2.</b> A typical commonly electrodes used as working electrode: carbon, platinum, gold, graphite and diamond electrodes, respectively .....	102
<b>Figure 3.3.</b> A typical electroanalytical system used for the electrochemical measurements .....	103
<b>Figure 3.4.</b> An E-I curve (voltammogram) demonstrating the most important parameters associated with cyclic voltammetry.....	104
<b>Figure 3.5.</b> A typical cyclic voltammogram for polyaniline doped with a strong acid showing The potential regions for redox state inter-conversions.....	105
<b>Figure 3.6.</b> Potential wave form for square wave voltammetry.....	110

<b>Figure 3.7.</b> Typical linear sweep voltammogram for anodic sweep .....	<b>111</b>
<b>Figure 3.8.</b> Schematic representation of the diffusion of the substrate S and the product P in the enzymatic layer on a transducer .....	<b>113</b>
<b>Figure 3.9.</b> Calibration of an amperometric enzyme electrode for L-phenylalanine .....	<b>115</b>
<b>Figure 3.10.</b> A scheme of the steps followed during the preparation of enzyme electrodes and ultimate biosensor construction .....	<b>118</b>
<b>Figure 4.1.</b> Cyclic voltammograms for electrochemical synthesis of (PANI-PVS in 1 M H <sub>2</sub> SO <sub>4</sub> , (ii) PANI-PVS in 1 M HCl, using scan rate of 50 mV s <sup>-1</sup> .....	<b>123</b>
<b>Figure 4.2.</b> Cyclic voltammograms of PANI-PVS film electrodeposited on BDD in (iv) 1 M HCl solution at scan rates between 5 – 200 mV s <sup>-1</sup> and (v) 0.1 M PBS (pH 7.2), scan rate of 5 mV s <sup>-1</sup> .....	<b>125</b>
<b>Figure 4.3.</b> The plots obtained after the electropolymerization of PANI-PVS at BDD electrode (PANI-PVS/BDD electrode): (A) peak potentials (E <sub>p</sub> ) versus scan rate, (B) peak currents (I <sub>p</sub> ) versus scan rate and (C) peak currents (I <sub>p</sub> ) versus square root of the potential scan rate. The values of E <sub>p</sub> and I <sub>p</sub> were effectively calculated from peaks a and b' of PANI-PVS/BDD electrode at different scan rates (see Figure 4.2 (iv)), where I <sub>pa</sub> /I <sub>pc</sub> = 0.995 .....	<b>127</b>
<b>Figure 4.4.</b> CV of stability BDD/PANI-PVS in 1 M HCl with measurements performed at Different time (from 5-60 min). Only the 10 <sup>th</sup> cycle that has shown at scan rate of 50 mV s <sup>-1</sup> .....	<b>129</b>
<b>Figure 4.5.</b> UV-Vis spectra of a) PANI and b) PANI-PVS films .....	<b>130</b>
<b>Figure 4.6.</b> SEM image of a) PANI and b) PANI-PVS in 1 M HCl; (c) PANI-PVS in 1 M H <sub>2</sub> SO <sub>4</sub> and bare electrode (BDD without modification) .....	<b>132</b>
<b>Figure 5.1.</b> UV-Vis spectra for a) PANI- in DMF, b) PANI-PVS films in PBS-DMF solution, c) Tyr/PANI-PVS in PBS-DMF solution and Tyr in PBS (pH 7.2) .....	<b>137</b>
<b>Figure 5.2.</b> FTIR spectra for a) PANI- PVS film, b) Tyr/PANI-PVS film and (c) free Tyr .....	<b>139</b>
<b>Figure 5.3.</b> (a) Cyclic voltammograms of Tyr/BDD biosensor in 0.1 M PBS (pH 7.2) and (b) The plot of anodic peak current versus scan rates in 0.1 M PBS (pH 7.2) .....	<b>141</b>
<b>Figure 5.4.</b> SEM images obtained from the surfaces of a) bare electrode and (b) tyrosinase- modified BDD electrode .....	<b>142</b>
<b>Figure 5.5.</b> UV absorption for L-phenylalanine (grey), L-tyrosine (pink) and PBS only (red) .....	<b>143</b>

<b>Figure 5.6.</b> Linear sweep voltammetry of 20-160 $\mu\text{L}$ (1.32-10.66 Mm) L-phenylalanine oxidation, scan rate of 50 mV/s .....	<b>144</b>
<b>Figure 5.7.</b> UV-Vis absorption measured after oxidation of 60 $\mu\text{L}$ (red), 120 $\mu\text{L}$ (green) and 160 $\mu\text{L}$ (blue) of L-phenylalanine standard added .....	<b>144</b>
<b>Figure 5.8.</b> UV-Vis absorption of L-phenylalanine standard (in PBS) overlapped with absorption of L-dopa .....	<b>145</b>
<b>Figure 5.9.</b> (a) Cyclic voltammograms of Tyr/PANI-PVS biosensor in PBS (pH 7.2) and (b) The plot of anodic peak current versus scan rates in PBS (pH 7.2).....	<b>147</b>
<b>Figure 5.10.</b> Cyclic voltammograms of Tyr immobilized on PANI-PVS biosensor in response to Different concentrations of L-Phe (0.3, 0.5 and 0.7 $\mu\text{M}$ ) in PBS (pH 7.2), at scan rate of $\text{mV s}^{-1}$ .....	<b>149</b>
<b>Figure 5.11.</b> The proposed catalytic cycle for the Tyr/PANI-PVS biosensor in aerobic medium. PANI <sup>0/+</sup> are the PANI-PVS bound redox sites.....	<b>149</b>
<b>Figure 5.12.</b> Biosensor responses to successive addition of L-Phe in PBS at scan rate of 50 $\text{mV s}^{-1}$ .....	<b>151</b>
<b>Figure 5.13.</b> Calibration curve for the Tyr/PANI-PVS biosensor responses to different Concentration of L-Phe (2-14 $\mu\text{M}$ ).....	<b>151</b>
<b>Figure 5.14.</b> Calibration plot for the Tyr/PANI-PVS biosensor to the different concentration in the linear range between 2-10 $\mu\text{M}$ .....	<b>152</b>
<b>Figure 5.15.</b> Reproductivity and stability of the biosensor after: i) one week, ii) two weeks iii) three weeks and iv) four weeks.....	<b>154</b>
<b>Figure 6.1.</b> Cyclic voltammograms of the increasing L-tyrosine concentration (0-10 $\mu\text{M}$ ) using Tyr/PANI-PVS/BDD biosensor in 0.1 M PBS (pH 7.2), scan rate: 50 $\text{mV s}^{-1}$ , aerobic condition ....	<b>158</b>
<b>Figure 6.2.</b> Calibration plot for the Tyr/PANI-PVS biosensor to the different concentration of L-tyrosine in the linear range between 2-10 $\mu\text{M}$ .....	<b>158</b>
<b>Figure 6.3.</b> Square wave voltammetry (SWV) of the increasing L-tyrosine concentration (0-10 $\mu\text{M}$ ) using Tyr/PANI-PVS/BDD biosensor in 0.1 M PBS (pH 7.2), scan rate: 50 $\text{mV s}^{-1}$ , aerobic condition ....	<b>159</b>
<b>Figure 6.4.</b> Cyclic voltammograms of the increasing L-Phe concentration (0-10 $\mu\text{M}$ ) using Tyr/PANI-PVS/BDD biosensor in 0.1 M PBS (pH 7.2), scan rate: 50 $\text{mV s}^{-1}$ , aerobic condition.....	<b>160</b>

<b>Figure 6.5.</b> Influence of scan rates on oxidation peak current of L-Phe using TY/PANI-PVS/BDD-biosensor in 0.1 M PBS (pH 7.2). The CV has shown the increasing current with the increasing scan rate (5-50 mV s <sup>-1</sup> ) .....	161
<b>Figure 6.6.</b> The relationship between response potential and L-Phe concentration Tyr/PANI-PVS/BDD biosensor in 0.1 M PBS (pH 7.2). Linear range: 2-10 μM.....	161
<b>Figure 6.7.</b> Linear sweep voltammetry (LSV) for the conversion of L-Phe (0-10.66 mM) to the formation of L-dopa using Tyr/PANI-PVS/BDD biosensor in 0.1 M PBS (pH 7.2) .....	162
<b>Figure 6.8.</b> UV absorption for L-Phe (pink), L-Tyr (dark blue) and L-dopa (light blue) .....	163
<b>Figure 6.9.</b> UV-Vis absorption measured after oxidation of 160 μL of L-phenylalanine standard added using Tyr/PANI-PVS/BDD biosensor in 0.1 M PBS (pH 7.2).....	163
<b>Figure 6.10.</b> FTIR spectra for (i) the immobilized Tyr/PANI-PVS film with L-Phe and (ii) Tyr/PANI-PVS film in 0.1 M PBS (pH 7.2).....	164
<b>Figure 6.11.</b> Cyclic voltammograms of L-Phe (0.1 M) and mixed L-dopa with L-Phe using BDD electrode in 0.1 M HCl, scan rate: 50 mV s <sup>-1</sup> .....	166
<b>Figure 6.12.</b> Differential pulse voltammograms of L-Phe (0.1 M) using BDD electrode in 0.1 M HCl, scan rate: 50 mV s <sup>-1</sup> .....	166
<b>Figure 6.13.</b> Cyclic voltammograms of effervescent flu tablet-T1 (A) and flu tablet-T2 (B) using Tyr/PANI-PVS/BDD biosensor in 0.1 M PBS (pH 7.2), scan rate: 50 mV s <sup>-1</sup> , aerobic condition .....	169
<b>Figure 6.14.</b> Cyclic voltammograms of sugar-S1 (C) and sugar-S2 (D) using Tyr/PANI-PVS/BDD-biosensor in 0.1 M PBS (pH 7.2), scan rate: 50 mV s <sup>-1</sup> , aerobic condition .....	170
<b>Figure 6.15.</b> Cyclic voltammograms of lipoprotein (human plasma) sample using Tyr/PANI-PVS/BDD biosensor in 0.1 M PBS (pH 7.2), scan rate: 50 mV s <sup>-1</sup> , aerobic condition .....	172
<b>Figure 6.16.</b> Cyclic voltammograms of lemonade (soft drink) sample using Tyr/PANI-PVS/BDD-biosensor in 0.1 M PBS (pH 7.2), scan rate: 50 mV s <sup>-1</sup> , aerobic condition .....	172
<b>Figure 6.17.</b> Calibration plots of currents versus concentration of (A) lipoprotein (human plasma) and (B) lemonade (soft drink).....	173
<b>Figure 6.18.</b> Model structure of tyrosinase enzyme showing copper atoms (in green), the active site for the protein sits .....	174

## List of Tables

<b>Table 2.1.</b> Classification of the enzyme groups and their type of reaction catalyzed.....	<b>24</b>
<b>Table 2.2.</b> Assignments for FTIR absorption bands for polyaniline.....	<b>68</b>
<b>Table 3.1.</b> Diagnostic tests for the electrochemical reversibility of a redox couple, carried out by cyclic voltammetry .....	<b>106</b>
<b>Table 4.1.</b> Kinetic parameters of the PANI-PVS composite film in 0.1 M PBS (pH=7.2).....	<b>128</b>
<b>Table 6.1.</b> Mass % of L-phenylalanine in selected pharmaceutical preparations.....	<b>170</b>
<b>Table 6.2.</b> Response characteristics of the biosensor in the presence of lipoprotein (human plasma) and lemonade (soft drink).....	<b>173</b>



## List of Publications

**Zelo Anatole Mangombo**, David L. Key, Emmanuel I. Iwuoha, Priscilla G.L. Baker\* (2010).

Development of a tyrosinase biosensor on a novel Polyaniline-Polyvinyl Sulphonate Composite Film modified Boron-Doped Diamond (BDD) electrode. *Microchimica Acta*, Ref. Ms. No. MCA-D-10-00010, [Accepted for Publication: 15/05/2010].

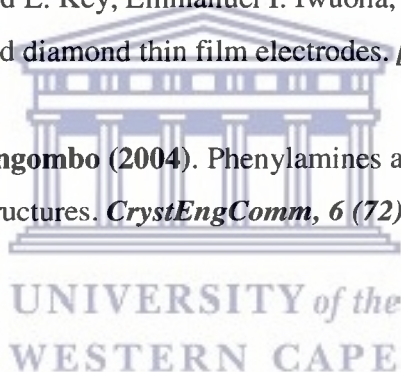
**Zelo Anatole Mangombo**, David L. Key, Emmanuel I. Iwuoha, Priscilla G.L. Baker\* (2010).

Tyrosinase modified BDD biosensor for the detection of L-Phenylalanine. [In Review].

**Zelo Anatole Mangombo**, David L. Key, Emmanuel I. Iwuoha, Priscilla G.L. Baker\* (2010).

Review: Boron doped diamond thin film electrodes. [In Review].

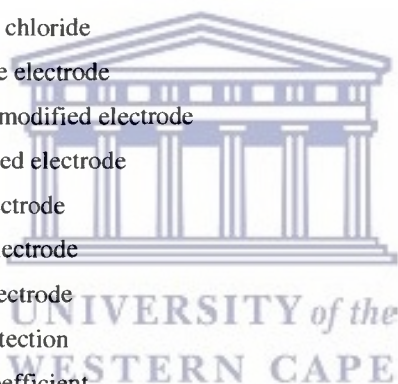
Susan A. Bourne\* and **Zelo Mangombo** (2004). Phenylamines as building blocks to layered inorganic-organic structures. *CrystEngComm*, 6 (72), 437-442.



## Abbreviations

BDD	Boron-doped diamond
L-Phe	L-phenylalanine
PANI	Polyaniline
PVS	Polyvinyl sulphonate
Tyr	Tyrosinase
CV	Cyclic voltammetry
SEM	Scanning electron microscopy
FTIR	Fourier transform infrared
UV-Vis	Ultraviolet-visible
L-Tyr	L-tyrosine
L-Dopa	L-3,4-dihydroxyphenylalanine
PKU	Phenylketonuria
CVD	Chemical vapor deposition
SAM	Self-assembled monolayer
GC	Glassy carbon
Pt	Platinum
Au	Gold
IME	Interdigitated microsensor electrode
KIMB	Key (K), Iwuoha (I), Mangombo (M), Baker (B)
ISFET	Ion-sensitive field effect transistors
SPR	Surface plasmon resonance
QCM	Quartz crystal microbalance
GOD	Glucose oxidase
PPO	Polyphenol oxidase
DA	Dopamine
CPs	Conducting polymers
VB	Valence band
CB	Conduction band
ICPs	Intrinsically conducting polymers
PPy	Polypyrrole
PTh	Polythiophene
PPV	Poly(phenylene vinylene)

SPAN	Sulphonated polyaniline
PVP	Polyvinyl pyrrolidone
PVA	Polyvinyl alcohol
PSSA	Polystyrene sulfonic acid
PAA	Polyacrylic acid
ALM	Anodic alumina membrane
AC	Alternating current
SHE	Standard hydrogen electrode
NEA	Negative electron affinity
FIA	Flow injection analysis
HPLC	High-performance liquid chromatography
SWV	Square wave voltammetry
LSV	Linear sweep voltammetry
ADC	Analog-to-digital converter
DAC	Digital-to-analog converter
SCE	Saturated calomel electrode
Ag/AgCl	Silver/silver chloride
CPE	Carbon paste electrode
CME	Chemically modified electrode
SPE	Screen-printed electrode
WE	Working electrode
RE	Reference electrode
AE	Auxiliary electrode
LOD	Limits of detection
$D_e$	Diffusion coefficient
FDA	Food and Drug Administration
UVA	Ultraviolet-A rays





# CHAPTER 1

## Introduction

In recent years, increased concerns with the electrochemical biosensors have appeared as the most frequently used technique in monitoring and diagnosis tests in various fields such as clinical, environmental and agricultural analysis [1]. Electrochemical biosensors are based on the electrochemical species consumed and or produced during a biological and chemical interaction method of a biological active substance and substrate. The key role of biosensors is to recognize substrate in solution with a specific target molecule such as antibodies, enzymes, etc. However, it is not simple to discover materials showing detection properties similar to biological receptors [2]. Biosensors, in particular, electrochemical sensors with the use of enzymes have been vigorously developed. For example, biosensors are currently available that allow patients to conveniently and highly accurately determine blood glucose level. Pei et al., have developed a simple and fast glucose biosensor based on microcantilever method. The biosensor was found to be extremely selective and particularly responsive to glucose over a wide range of concentration levels [3]. Although sensors have been developed, attempts have been recently made to determine L-phenylalanine (L-Phe). For example, there have been various methods used for L-Phe determination [4,5,6]. But there still remain a number of problems to be solved in putting the biosensor into practical use.

Nevertheless, it is desirable for patients with phenylketonuria (PKU) that L-Phe can be easily determined at home so as to monitor the blood L-Phe level and examine foods and drinks. However, it is still difficult at the present stage. PKU is a rare, inherited, metabolic disorder in the degradation of dietary phenylalanine [7]. In PKU, the liver is unable to convert L-Phe to L-tyrosine (L-Tyr). When left untreated, this result in a buildup of L-Phe in the blood, which eventually passes into the brain causing mental retardation or other neurological problems [8]. People with this disease are therefore put on a low L-Phe diet soon after being diagnosed with PKU as infants. Under these circumstances, it is an object of the present investigation to provide

L-Phe biosensor, by which L-Phe can be highly accurately, quickly and conveniently quantitated without resort to the use of many reagents.

For convenience, efficiency and lower cost, electrochemical treatment is a new alternative for this application. Several efforts to use nanostructured systems (physical and chemistry of materials), microelectronic devices (engineering and bioelectronic), or electrochemical knowledge were made for different purposes. Both conductive and semiconductive nanosized material and enzymes is probably the foremost challenging application in developing combined biochemical structures for biosensor or bioelectronic devices. This requires the correct integration between the biocatalyst and the conductive support.

Recently, the conductive diamond thin films fabricated by the use of chemical vapor deposition (CVD) techniques were studied as electrode materials for organic oxidation [9,10,11]. Boron-doped diamond (BDD) electrodes have unique properties, such as a very low capacitive background current, a wide potential window, and remarkable physical or chemical stability. Hence, a BDD electrode can be used for many applications, such as wastewater treatment, biosensor and other electrochemical preparation [8,9,10,11]. Marselli *et al.* reported also that the BDD electrode is thought to create large amounts of hydroxyl radical and other active intermediate directly on its surface in the process of anodic polarization [9,11]. The application of biosensor technology for biological samples monitoring purposes [12] is particularly important because this approach would conserve the large amount of foreign exchange that are normally needed for the purchase and maintenance of traditional analytical equipment.

In this study, we propose the development and testing of a biosensor on a BDD platform, which is able to measure L-Phe levels in biological samples, as this will greatly facilitate the measurement and control of dietary L-phenylalanine. The biosensing principle is based on determination of the sensor response to the L-Phe voltammetric method. Cyclic voltammetry is carried out to investigate the activity of BDD film electrodes for L-Phe determination in the solution under different pH and experimental conditions. The oxidation of the response of biosensor to L-Phe has been studied. Tyrosinase (Tyr) is used as a model enzyme for catalysis of

L-Phe. Tyr is applied to the surface of the self-assembled monolayer (SAM) and electrochemical oxidation of L-Phe present in solution is carried out.

In order to improve the superior electrochemical sensors, we have suggested the possibility of using BDD electrode chemically modified with conductive polyaniline (PANI) film doped with poly(vinylsulphonate) (PVS) compounds. The electroactive properties of PANI-PVS allowed preparing non-selectivity sensors provided with a high degree of cross-selectivity and also with a reasonable reproducibility [12,13].

Study of the effect of the operating conditions in the application of L-phenylalanine biosensor as a sensor technology design in which L-phenylalanine levels in biological samples are determined for control of dietary has not been reported in the literature.

### **1.1 Motivation of the study**

The main focus of this project is to exploit the advantages of BDD electrodes and modify them with conductive polymers for development of biosensors for L-phenylalanine (L-Phe) detection. L-Phe is involved indirectly in the production of melanin, the pigment responsible for skin and hair color. Children with phenylketonuria often have lighter complexions than their unaffected siblings. Much of the interest in BDD electrode is due to its unique properties, such as a very low capacitive background current, a wide potential window, and remarkable physical or chemical stability and its interest in applying in the detection of neurotransmitter concentration in mammalian brains, including L-dopa, dopamine, norepinephrine, and epinephrine.

Modification of BDD electrode (diameter: 3.0 mm) with conductive polymers is well established and influenced the basis of the current work. The modifications of polymers were employed on working electrodes such as glassy carbon (GC), platinum (Pt), and gold (Au) [14]. Studies have been performed by voltammetric techniques. Applying similar techniques on BDD electrode will necessitate improved modifications of the polymers due to its unique properties. The features

associated with BDD electrodes are its fast response due to small size, small sample volume required, no deoxygenation of solutions, chemical inerties, and improved detection limits.

The polymer that has been most extensively studied on modified electrodes is Polyaniline (PANI) [4]. It is a conductive polymer with many commercial and technological applications such as electrochromic devices, secondary batteries, electromagnetic interference shielding, and corrosion protection [15-18]. In this work, PANI was doped with polyvinyl sulphonate (PVS) in order to increase the conductivity. The advantage of using the composite PANI-PVS film lies in the electrostatic rejection of anions [19]. Sulfonate ion of the PANI-PVS composite film provides a charged surface for electrostatic interaction between the enzyme and the surface [20].

Exploiting the fact that PANI-PVS is conductive and environmentally stable makes it an ideal candidate to be used as a modified surface in the detection of L-Phe. Its chemical structure also predicts that it is a ligand that can interact within species [21]. An intensive study of PANI is important, since the structure has nitrogen lone pairs with conductive binding sites and five oxidation states due to resonance effects. It is insoluble in many organic solvents and has a complex mechanism [20,22]. The chemical synthesis and characterization of PANI is well established and well documented.

The main goal of this work is to electrochemically polymerization of PANI-PVS composite film immobilized with and without tyrosinase enzyme for use as modifiers on BDD electrode to determine L-Phe levels in biological samples in order to control the dietary L-Phe intake. The main objective of enzyme immobilization on a transducer, for analytical purposes, is to stabilize the biosensor to be used repeatedly over a long period of time.

Two pathways were considered for L-phenylalanine (L-Phe) detection in aqueous solution under mild condition. The first pathway was suggested (see Figure 1.1.A) to use phenylalanine hydroxylase (PAH, EC.1.14.18.1) as an enzyme to catalyze L-phenylalanine (L-Phe) into L-Tyrosine (L-Tyr). Due to the difficult pathway for synthesis of PAH and also is not commercially available, thus a possible alternative mechanism (second pathway, see Figure 1.1B) was used for L-Phe detection that involves tyrosinase (Tyr, EC 1.14.18.1), the enzyme

responsible for the first step in melanin formation. In this step, tyrosinase convert L-Phe into L-Tyr and catalyzed the oxidation of L-tyrosine to L-3,4-dihydroxyphenylalanine (L-dopa) in the presence of the oxygen molecular (see Figure 1.1.B). L-dopa is produced during the first of a series of redox reactions leading to the formation of melanin (see Figure 1.2). L-dopa further drives the reaction by functioning as an alternative substrate for tyrosinase and as a cofactor that stimulates catalytic efficiency. L-Phe is detected and characterized by direct and indirect immobilization of Tyr enzyme onto BDD electrode using potentiometric measurements.

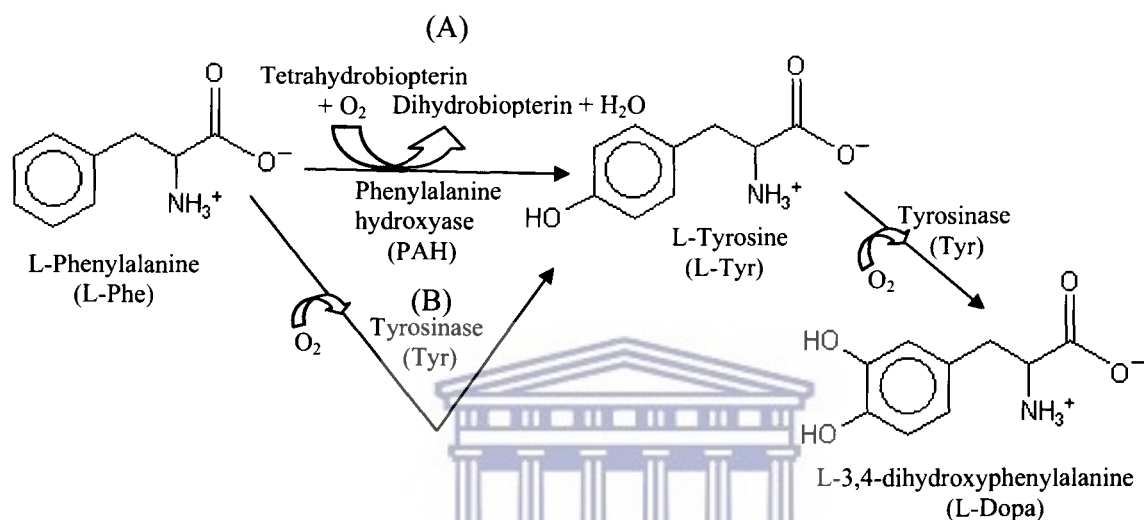


**Figure 1.1.** Pathways for L-phenylalanine detection using: (A) phenylalanine hydroxylase (PAH) and (B) tyrosinase (Tyr), as enzymes.

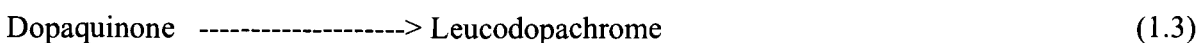
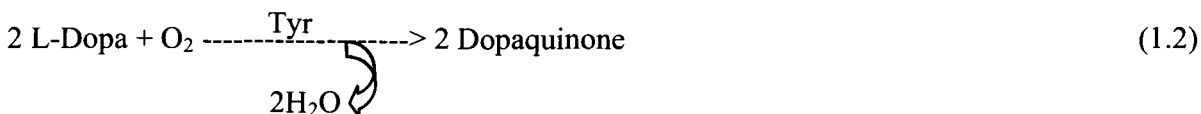
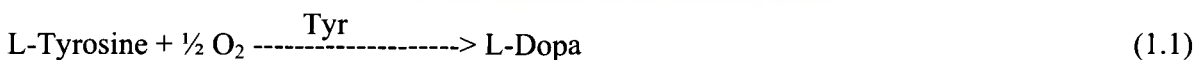


**Figure 1.2.** Catalytic pathways of tyrosinase for L-dopa oxidation (equation 1.1-1.4).

## **1.2 Statement of the problem**

Despite the enormous application potential of PANI, its large scale processability is encumbered by its insolubility in common organic solvents. PANI dissolves only in toxic N-methyl pyrrolidone (NMP) and in strong acids and thus does not render itself to large scale production [23]. Also the fact that PANI decomposes before melting means it cannot be processed by the melt-processing technique. To circumvent this problem several strategies toward more soluble PANI have been adopted. Functionalization of the PANI backbone with more polar molecules [24], co-polymerization of the aniline monomers in the presence of polymeric host stabilizers [25], preparation of PANI blends/composites with other polymers with desirable characteristics have led to more soluble PANI [26]. Also, incorporation of surfactant dopants within the PANI matrix promotes solubility besides enhancing the conductivity and the morphology of the resultant PANI [27]. Despite the above efforts, the processability of PANI is still an issue of concern and a lot of research towards producing more processable PANI is still on going. In this work, we adopt to prepare PANI with stabilizing surfactant dopants, polyvinyl sulphonate (PVS), to improve PANI processability and widen the scope of applicability.

The determination of L-phenylalanine (L-Phe) has important environmental, industrial and clinical implications respectively. The current assay techniques based for these analytes based on volumetric, colorimetric, chemiluminescence and chromatographic analysis are complex, and take long periods of analysis. We aim at producing faster operational devices with reasonable sensitivities.

## **1.3 Aim and objectives**

### **1.3.1 General objectives**

The aim of this present work is to design and characterize a novel biosensor that is highly specific and selective for the detection of the L-phenylalanine (L-Phe), essential amino-acid, in various aqueous media. The study deals with the development of biosensors for potential use in the biological samples diagnostic market.



The biosensor was prepared by incorporating biomolecule (e.g. tyrosinase, Tyr) in the self-assembly processes of L-Phe compounds and electroactive polymers (e.g. polyaniline (PANI) – poly(vinylsulphonate) (PVS)). The biosensor reactivities were modeled using cyclic voltammetric and direct potentiometry techniques.

### 1.3.2 Specific objectives

The specific objectives include:

- i. To monitor the concentration of the L-phenylalanine (L-Phe), essential amino-acid, based compound,  $C_9H_{11}NO_2$  in the aqueous solution and fabricate its self-assembled monolayer (SAM) on interdigitated microsensor electrode (IME) of BDD then characterizing it.
- ii. To evaluate BDD thin film electrodes modified with polyaniline-polyvinyl sulfonate (PANI-PVS) composite film as suitable catalytic sensor platforms for enzyme specific substrate recognition.
- iii. To evaluate the encapsulation of the enzyme tyrosinase (Tyr) by immobilization or drop coating enzyme encapsulation methods in order to minimize the use of binders and stabilizers that may interfere with the enzyme kinetics.
- iv. To assess the tyrosinase enzyme kinetics modeled as typical Michaelis-Menton enzyme-substrate recognition.
- v. To optimize a signal transduction protocol based on the direct potentiometry.
- vi. To evaluate the cost of miniaturization and reproduction of sensor technology for the production of disposable, fast and efficient real time L-phenylalanine sensors for the assaying of biological samples.
- vii. To investigate the effects of PANI-PVS on the Tyr electrocatalytic activity towards the oxidation of L-Phe and to study the interaction between the immobilized Tyr and the L-Phe by UV-Vis Spectroscopy and Fourier transform infrared (FTIR).
- viii. To apply the developed biosensor for the detection of L-Phe in standard solutions and to determine its applicability by analyzing some foodstuff samples contained with L-Phe.

In this study, a simple, efficiency and reliable procedure for preparing Tyr-based biosensor for novel detection of L-phenylalanine is described. Firstly, the PANI films were polymerized on a BDD electrode surface by the electrochemical “soft template” method using PVS as the dopant and structure directing molecule. The use of PVS is important due to the fact that it is known to shift the redox activity of PANI films to a neutral pH environment required during measurements involving the use of enzymes. The heme-protein Tyr was then incorporated onto the electrosynthesized PANI-PVS film and its direct electrochemistry monitored on a BDD electrode. The structured PANI-PVS film was used to provide a suitable micro-environment for Tyr immobilization in order to enhance the direct electron transfer between Tyr and the BDD electrode surface.

#### **1.4 Research hypothesis**

In the recent decade numerous biosensing methods for detection of peptides (e.g. L-phenylalanine, L-tyrosine) have been developed using integrated enzymatic biosensors and immunosensors. Enzymatic determination of peptides is most often based on inhibition of the activity of selected enzymes such as L-phenylalanine hydroxylase, L-phenylalanine dehydrogenase, salicylate hydroxylase, tyrosinase, and tyrosine hydroxylase and pyruvate kinase [4,28,29]. An improvement of detectability levels can be achieved by the use of recombinant enzyme mutants resulting biosensor matrices and data processing with artificial neural networks.

PKU is an autosomal recessive disease caused by mutations in the PAH gene (on chromosome 12 in band 12q23.2) [30]. The mutations result in a complete loss or a variable degree of reduced activity of PAH, leading to an accumulation of L-Phe in the blood and excretion of its metabolite phenylpyruvate in the urine. However, the biochemical basis for the defect was not established until Jervis showed that the liver tissue from normal individuals could convert L-phenylalanine (L-Phe) into L-tyrosine, whereas liver extracts from PKU patients could not [31].



The discovery of this error of metabolism has led to the treatment of PKU patients with a low-phenylalanine diet, resulting in improvements in mental development and behavioral performance [32,33]. This is not done in some developed and developing countries including Southern Africa as the consumers are not aware of the presence of L-phenylalanine-derived products in the market and consume them unknowingly.

It is imperative to monitor the dosage and delivery of L-Phe in the human body. Therefore, there is a strong interest in the development of reliable and rapid sensing analytical methods that can measure the L-Phe levels in biological samples in order to control the dietary L-Phe intake.

### **1.5 Contribution of the work described in this thesis**

The main contribution of this thesis is the development of biosensor for L-phenylalanine (L-Phe) detection. The biosensor will be potentially useful in the biological samples diagnostic market in South Africa. The challenge is to develop a simple and fast L-Phe biosensor based on BDD electrode, which via its applications to dietary phenylalanine-related problems that the biosensor can be found extremely selective and particularly responsive to L-Phe over a wide range of concentration levels intake in the human body in order to promote a better quality of life for all.



UNIVERSITY of the  
WESTERN CAPE

## 1.6 Research framework

In line with the study objectives and the experiment programme, the research framework process is shown on the following Scheme (Figure 1.3).

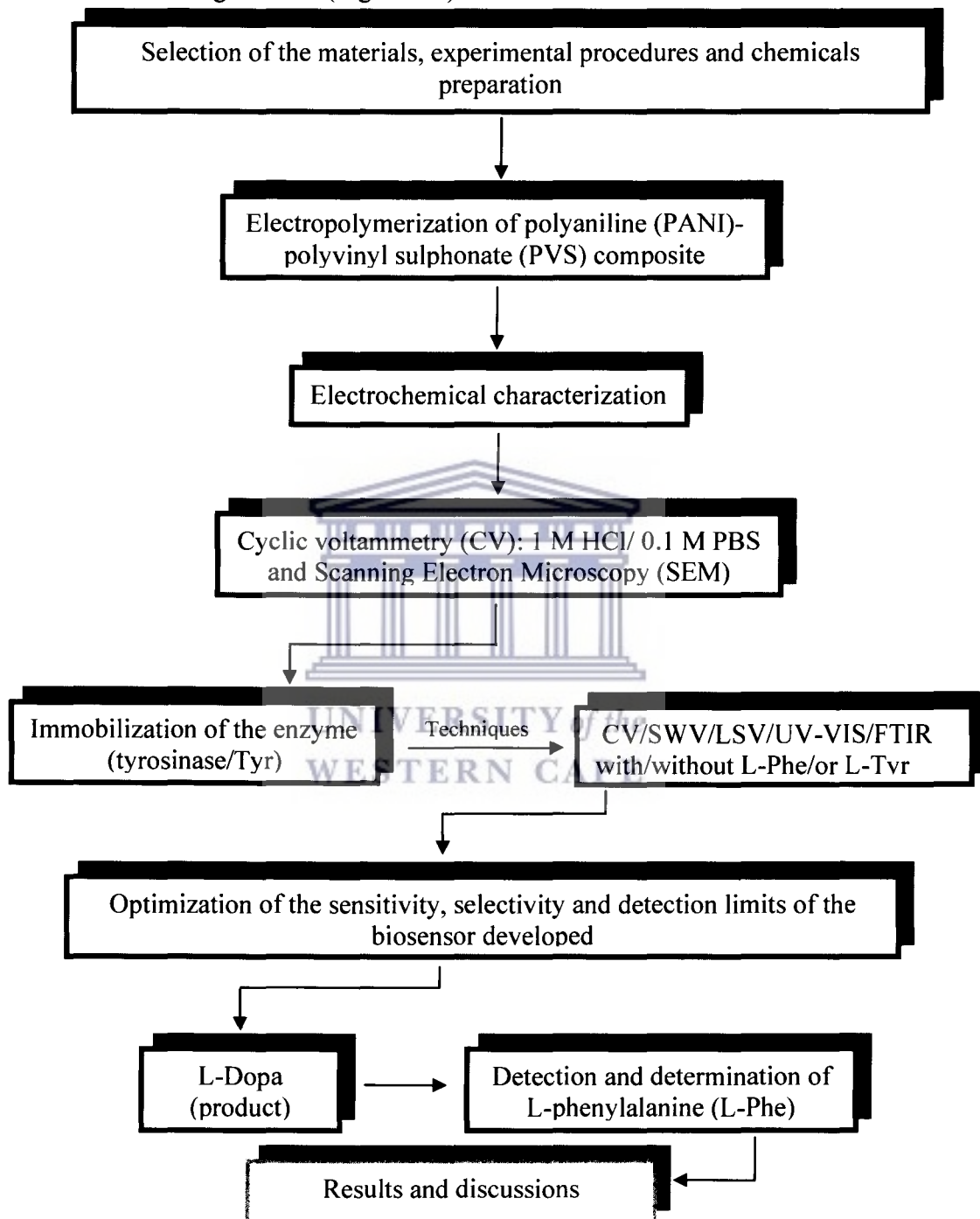


Figure 1.3. Research framework.

## 1.7 Delimitations of the thesis

The main efforts of the thesis involve the following aspects:

- i. Polyaniline (PANI)-polyvinyl sulphonate (PVS) composite films were developed in acidic media. Both electrochemical and physical characteristics of the developed PANI-PVS composites were investigated.
- ii. The electron shuttling ability of the developed composites between a biomolecule and an electrode were demonstrated using Tyr (biomolecule) and BDD electrode in the fabrication of the L-Phe biosensor.
- iii. The developed biosensor was able to determine quantitatively the range of concentration levels of L-Phe in the aqueous solution and real samples.

## 1.8 Proposed “KIMB\*”- mechanisms

“KIMB\*” have proposed mechanisms for L-Phe determination using Tyr/PANI-PVS/BDD and Tyr/BDD, Figures 1.4a and 1.4b, respectively. The point of agreement in the proposed mechanism (Figure 1.4a) is the first step of oxidation of aniline, i.e. the formation of radical cation. This radical gives three different resonance forms. On the basis of the experimental evidence, it was suggested that *p*-aminodiphenylamine is one intermediates in the electrochemical oxidation of aniline. Due to the stiffness of polymer (PANI) backbone, PVS (acidic groups:  $-\text{SO}_3\text{H}$ ) was introduced into the PANI chains to form a so-called “self-doped” PANI, which can maintain its electroactivity in neutral or even basic conditions. The hydrogen binding between adjacent polymeric chains and BDD electrode involve a one-electron transfer step in acidic media. L-Phe was also determined directly without using the mediators (PANI/PVS), Scheme 1.4b. In both methods, the catalytic action of the Tyr (Figure 1.2) begins with the selective hydroxylation of the L-Tyrosine with molecular oxygen ( $\text{O}_2$ ) to yield the L-dopa. L-Phe and L-Tyr were both used as substrates for L-Phe determination in the acidic media. When L-Phe is used as a substrate (Figure 1.1B), the enzyme is able to electrochemically convert L-Phe to L-tyr, followed by the enzyme catalytic oxidation of L-Tyr to form L-dopa (Figure 1.2). Therefore, the activity of the enzyme can be monitored by analyzing the disappearance of L-tyrosine and/or L-Phe as substrates, the appearance of L-dopa as product (Figure 1.4a and 1.4b).

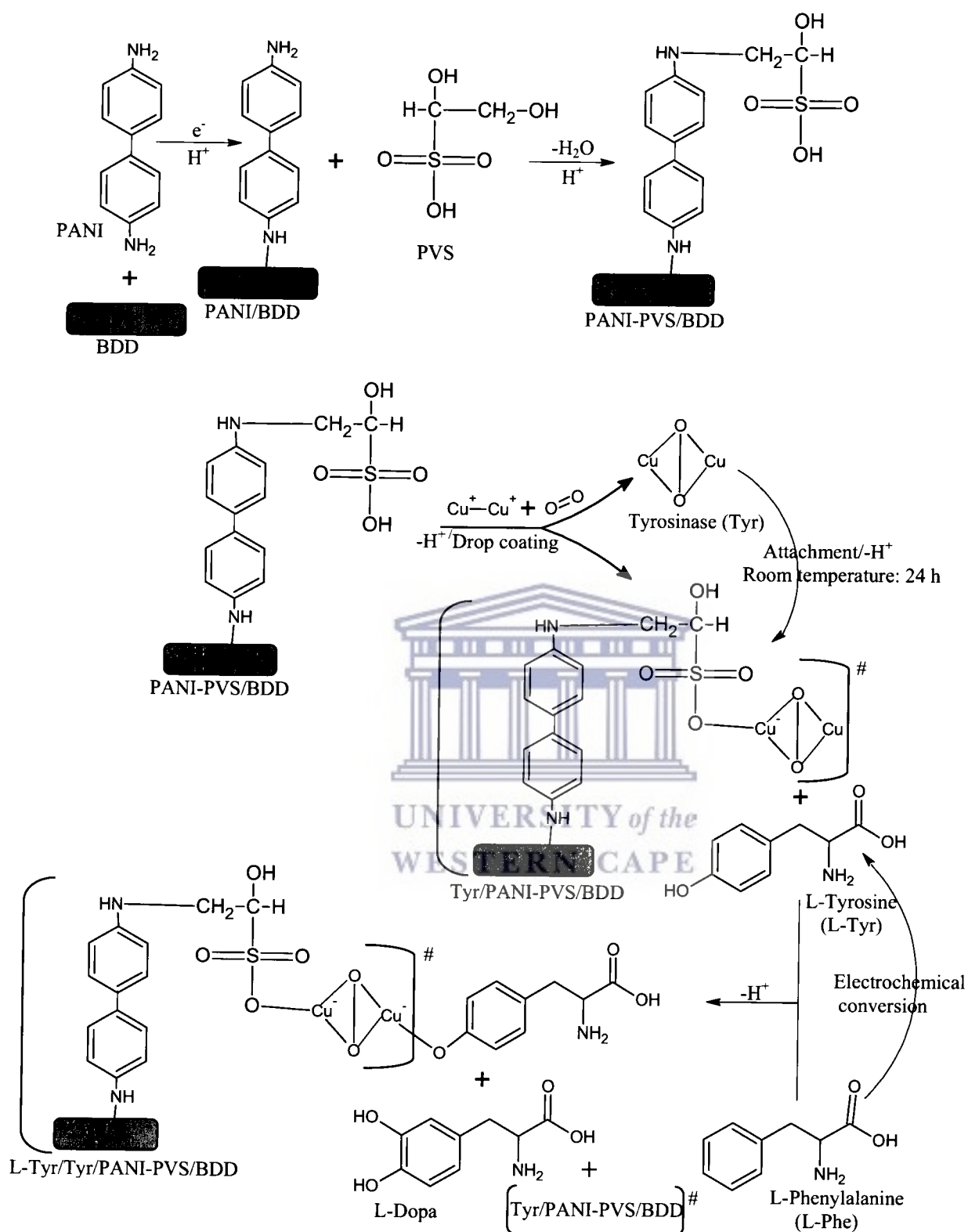


**Figure 1.4a.** Proposed “KIMB\*-1” mechanism for L-Phe detection using Tyr/PANI-PVS/BDD biosensor. “KIMB\*”: Key (K), Iwuoha (I), Mangombo (M), Baker (B).

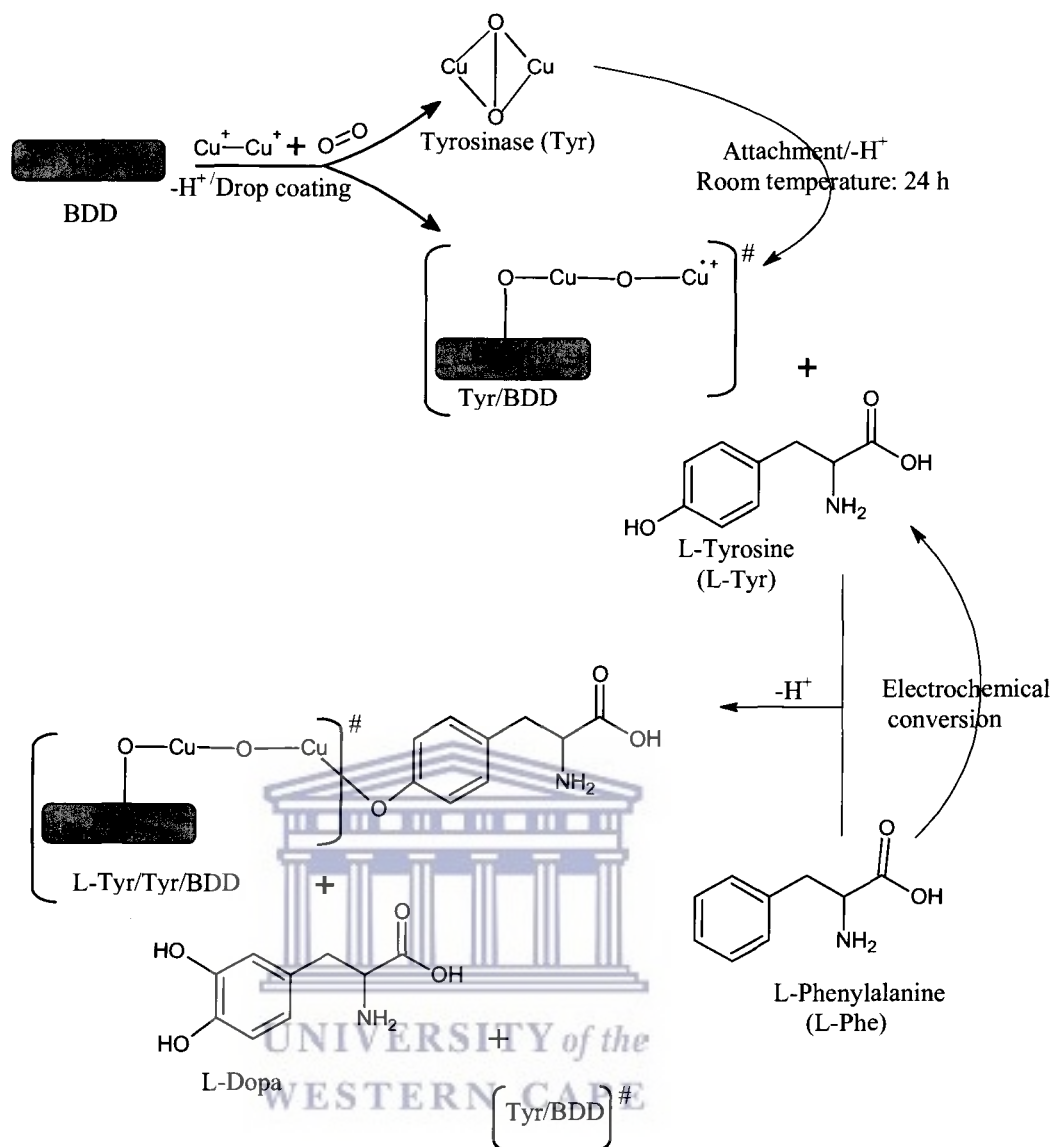


**Figure 1.4b.** Proposed "KIMB\*-2" mechanism for L-Phe detection using Tyr/BDD biosensor. "KIMB\*": Key (K), Iwuoha (I), Mangombo (M), Baker (B).

## 1.9 Overview of the chapters

Chapter 1 introduces the problem of biosensors for L-Phenylalanine determination. Thereafter the motivation of the study, the statement of the problem, aims and objectives are described. The research hypothesis, contributions of the work, research framework and delimitations of the thesis are stated in this chapter.

Chapter 2 discusses the literature review relating to the various aspects of biosensors, biomolecules as well as immobilization techniques. A brief introduction to conducting polymers containing metals, polyaniline and polyvinyl sulfonate is explained, followed by the general aspects of boron-doped diamond electrode, L-phenylalanine and L-tyrosine are highlighted. Characterization methods, mainly cyclic voltammetry, square wave voltammetry, scanning electron microscopy, Ultraviolet-visible (UV-Vis) and Fourier transform infrared (FTIR) are also discussed. In this chapter, the diagram of the biosensor is given.

Chapter 3 covers chemicals, instrumentation and preparation procedures. Scanning electron microscopy characterization and the electrochemistry of the developed composite materials are introduced.

Chapter 4 presents the construction and the development of the biosensor, followed by the discussion of the characterization results of the developed composite.

Chapter 5 presents and discusses the results of biosensor response to standard L-phenylalanine. A given detailed description of the biosensor and its analytical characteristics such as stability, detection limit, response time, linear range and reproducibility are explained.

Chapter 6 shows the applications of the biosensor.

Chapter 7 describes conclusions and recommendation for further study.

## CHAPTER 2

### Literature Review

#### 2.1 Introduction

This chapter is an indication follow up of chapter one. The main focus of this review is related to the various aspects of biosensors, biomolecules as well as immobilization techniques. A brief introduction to conducting polymers containing metals, polyaniline and sulfonate groups is explained, followed by the general aspects of boron-doped diamond electrode, L-phenylalanine and L-tyrosine are highlighted. In this chapter, the diagram of the biosensor is given (Figure 2.1).



#### 2.2 Biosensors

Biosensors can be generally defined as a device that consists of a biological recognition system, often called a bioreceptor, and a transducer. They can also be defined as a subgroup of chemical sensors in which a biologically based mechanism is used for detection of the analyte. Chemical sensors are regarded as miniaturize transducers that selectively and reversibly respond to chemical compounds or ions, yielding an electrical signal, which depends on an analyte concentration [34].

Biosensors are becoming important in a wide range of analysis. They are potentially small, portable, easy to use and capable of providing reliable analytical information continuously. The use of biosensors can offer significant advantages for fast, sensitive and inexpensive monitoring of environment, health and consumer products. Benefits arising from biosensors include efficiency and ability to find applications in many fields. Integrated with new technologies in molecular biology, macro fluids, and nano materials, biosensors have proved to provide selective



identification of target analytes at ultra trace levels. This has found applications in agricultural production, food processing, medical diagnosis and environmental monitoring for rapid, specific, inexpensive, in-field, on-line, and /or real-time detection of pesticides, antibiotics, pathogens, toxins, proteins, nutrilites, odours, microbes, and more in plants, animals, foods, soil, air, and water.

Different biosensor formats have been developed for single target analytes and for broad-spectrum monitoring. Biosensors have nowadays replaced conventional analytical methods of sample analysis, which tend to be complicated, time consuming, expensive and not suitable for *in situ* monitoring [35, 36].

Various biosensors that have been used for detection of peptides are described in literature as follows:

- i. Electrochemical (based on ion-sensitive field effect transistors-ISFET) and optical immune sensors [37].
- ii. Electrochemical biosensors (Amperotric and Potentiometric biosensors)
  - **Amperometric biosensor** - this involves amperometric monitoring of the immobilize of tyrosinase onto the surface of BDD electrodes [38].
  - **Potentiometric biosensor** – this involves potentiometric detection of the degree of inhibition of L-phenylalanine ammonia-lyase.
- iii. Integrated electrochemical enzymatic biosensors and immunosensors.

Clark and Lyons were the first scientists, in 1962, to describe the development of the first enzyme sensor [39] by using the concept of a biosensor. Since then, there have been several activities witnessed in this area of biosensors. Clark used an enzyme called glucose oxidase in a dialysis membrane over an oxygen probe and this devise was called then an enzyme electrode [39]. The enzyme electrode was used in the determination of glucose. Updike *et al* [40] developed an enzyme using electrochemical procedure to design a model that uses glucose oxidase immobilized on a gel to measure the concentration of glucose in biological solutions and in the tissues *in vitro*. The term biosensor emerged from bio-selective sensor [41]. Biosensors can be classified based on the bioreceptor, transduction methods, and sometimes the biorecognition principle. Scheme 3 has shown the typical diagram of a biosensor.



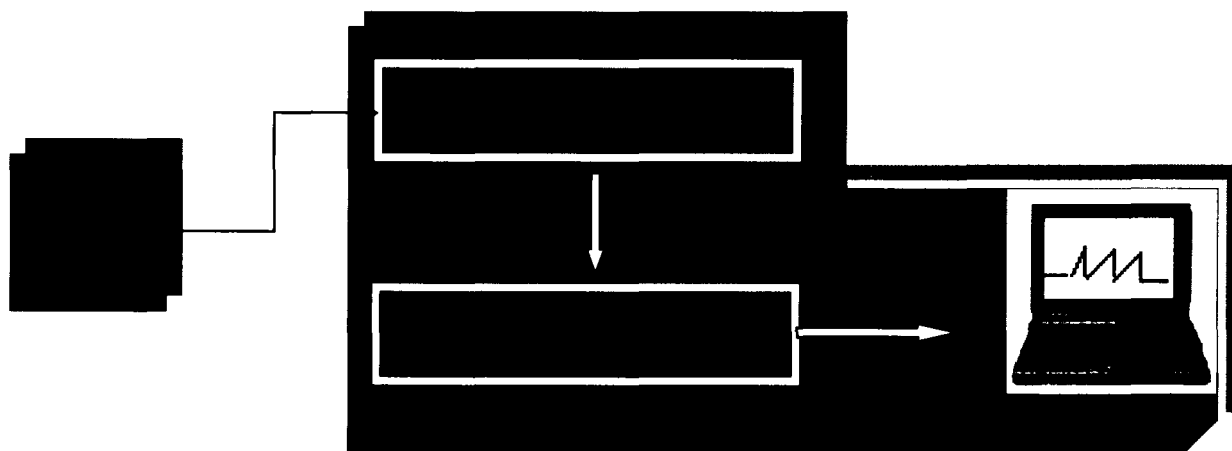


**Figure 2.1:** Typical diagram of a biosensor.

### 2.2.1 Bioreceptors/or biorecognitions

Bioreceptors are the key to specificity for biosensor technology. They are responsible for the biorecognition event which may be catalytic oxidation or reduction of the substrate or binding of the analyte of interest to the sensor for measurement. Common bioreceptors used are enzymes [42, 43-46], antibody [47, 48], DNA [49, 50], whole cell [51] and of recent, peptides [52]. Although the bioreceptor element is the selective part of the biosensor, the overall function of the biosensor is determined by proper combination of the biological receptor element with the transducer with respect to the signal transduction process. Transduction methods used in biosensor include electrochemical, optical, surface plasmon resonance (SPR), thermal, piezoelectric, Quartz crystal microbalance (QCM) [53] and cantilever [54-56]. Electrochemical method of transduction constitutes more than half of the literature on biosensor [57]. The two broad classification of biosensors based on biorecognition principle are catalytic biosensors typical of enzyme bioreceptors and affinity biosensors typical of antibody and protein (peptide). Therefore, a biosensor with electrochemical transduction method and peptide (e.g. L-phenylalanine, L-Phe) as a bioreceptor can be called L-phenylalanine (L-Phe) biosensor (based on bioreceptor) or affinity biosensor (based on biorecognition principle) or electrochemical L-Phe biosensor (based on both the bioreceptor and transducer) - the name used in this writing.

Other biosensors can be named immunosensor (antibody bioreceptor), enzyme biosensor, DNA biosensor and glucose oxidase sensor (using the specific name of the enzyme biomaterial) [49, 50].

Based on the biological specificity-conferring mechanism, biorecognition elements can be classified into biocatalytic recognition elements and biocomplexing or bio-affinity recognition elements. Biocatalytic recognition elements are based on reactions which are catalyzed by macromolecules, present in their original environment, previously isolated or manufactured. This continuous consumption of an analyte(s) is achieved by the immobilized biocatalyst incorporated into the sensor and transient or steady state responses monitored by the integrated detector. The biocatalysts commonly used in this class of biosensors are enzymes (mono or multi-enzyme), whole cells (microorganisms such as bacteria, fungi, eukaryotic cells or yeast) or cell organelles, and tissue (plant or animal tissue slice) [51,57].

More strategies for improving the biosensor performance may be developed when for example several enzymes are immobilized within the same reaction layer. The three possibilities are as follows:

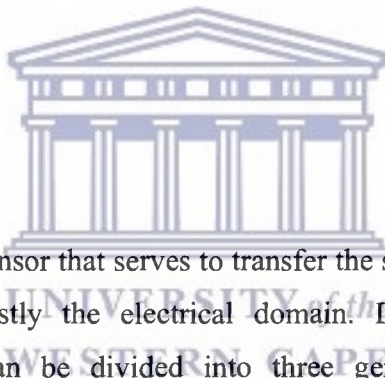
- i. Several enzymes facilitate the biological recognition by sequentially converting the product of a series of enzymatic reactions into a final electroactive form. This allows a much wider range of possible biosensor analytes.
- ii. Multiple enzymes, applied in series, may generate the first enzyme co-substrate and real amplification of the biosensor output signal may be achieved by efficient regeneration of another co-substrate of the first enzyme and
- iii. Multiple enzymes, applied in parallel may improve the biosensor selectivity by decreasing the local concentration of electrochemical interfering substrate.

Enzymes were the first biorecognition elements to be used in biosensors. The product formed from the catalytic reaction is released, thus regenerating the active site. The main advantage of the enzyme based biosensors is the implemented regeneration of the enzyme active site, implying an amplification of the signal concomitantly with an intrinsic reversibility of the sensor. They are suitable to act as recognition elements because of their specificity and availability [57].

Amperometric enzymatic electrodes hold a leading position among the presently available biosensor systems and are more attractive due to their fast response time and high sensitivity [57, 58]. These devices combine the specificity of the enzyme for the recognition of a given target analyte with the direct transduction of the rate of the biocatalytic reaction into a current signal, allowing a rapid, simple and direct determination of various compounds.

In biocomplexing or bio-affinity recognition element, the biosensor operation is based on the interaction of the analyte with macromolecules or organized molecular assemblies that have been either isolated from their original biological environment or engineered. Thus equilibrium is usually reached and there is no further consumption of the analyte by the immobilized biocomplexing agent. These equilibrium responses are monitored by the integrated detector. The biocomplexing reaction itself may in some cases be monitored using a complementary biocatalytic reaction. Steady state or transient signals are then monitored by the integrated detector.

### 2.2.2 Transducers



Transducers are the part of the sensor that serves to transfer the signal from the output domain of the recognition system to, mostly the electrical domain. Depending on the transduction mechanism used, biosensors can be divided into three generations. The first generation biosensors are based on the electroactivity of the enzyme substrate or product whereby the substrate or product of the reaction diffuses to the transducer and causes the electrical response. The second generation biosensors involve utilization of specific soluble mediators (e.g. ferrocene derivatives, ferrocyanide etc.) in order to generate improved response. The drawbacks with the first generation biosensors, such as too high applied potentials, led to the use of mediators, which are redox active molecules that could react with the active site of the enzyme and with the electrode surface, shuttling the electrons between the enzyme and the electrode. The use of soluble mediators made it possible to decrease the applied potential for many redox enzyme-based biosensors. Unfortunately, the uses of soluble redox mediators together with the redox

enzymes facilitate not only the electron transfer between the electrode and the enzyme but also various interfering reactions [58].

The third generation biosensors, also known as reagentless biosensors are based on direct electron transfer between the redox active biomolecule and the electrode surface. In these biosensors, the electron transfer is associated with, or occurs during the catalytic transformation of the substrate to the product. Third generation biosensors usually offer better selectivity, because they are able to operate in a potential range closer to the redox potential of the enzyme itself, becoming less exposed to interfering reactions. Although they present favourable characteristics, only a few groups of enzymes or proteins were found to be capable of interacting directly with an electrode while catalyzing the corresponding enzymatic reaction. This is because the distance between the prosthetic group and the bare electrode surface is often rather too long for direct electron transfer, due to shielding by the protein shell [58].

### 2.2.3 Types of biosensors

Over the past few decades, the design of optimized electrochemical enzyme-based biosensors have drawn increasing attention and enzymes have been immobilized on electrodes to give measurable responses by interacting with the target molecules [59, 60]. A lot of studies have therefore been carried out on the development and optimization of materials to be used as electron transfer interfaces between the redox enzymes and electrodes. The aim in the design of enzymatic biosensors is to provide fast electron transfer processes. In this way, an optimally designed electrode configuration has to ensure that the electron transfer distance between an immobilized redox enzyme and a suitable electrode surface is made as short as possible [58]. An ideal material should be compatible with the enzyme and should provide a suitable interface between the enzyme and the electrode to partly or completely eliminate the denaturation of the enzyme on the electrode surface. Recently, major improvements have been accomplished by modifying the electrode surfaces with matrices such as membranes, surfactant matrix, organic conducting polymers, nanoparticles, silk fibroin film, microcapsule, gels, lipids, hydrogel polymers, carbon, graphite, silica etc. before immobilization of enzymes.

All these matrices have been characterized to improve the micro-environment around the enzymes, provide suitable orientation, shorten the electron transfer distance, enhance sensitivity and stability of the enzyme, and to enhance the direct electron transfer between the immobilized enzymes and the electrodes compared to that on bare electrodes.

Among the matrices used for the incorporation of enzymes, organic conducting polymers present greater advantages due to their good interaction with metallic and carbon conductors. Furthermore, the unique electronic properties of conducting polymers allow direct, efficient and interactive electrical communication between the enzyme redox centre and the electrode surface thus producing a range of analytical signals. The polymers also localize the enzymes close to the electrochemical interface thus minimizing interferences which may lead to undesired side reactions for large background currents. Among the conducting polymers used in fabricating enzymebased biosensors, PANI is considered as the most fascinating and has gained particular popularity due to its electroactivity; favourable storage stability and ease of preparation thus tremendous works have been undertaken in this field. Nevertheless, it has been observed that applications of the conventional PANI and the composite films remain limited by poor sensitivity resulting from the poor diffusion of analyte molecules [61, 62]. However, with recent development in nanoscience and nanotechnology, nanostructured PANI/PVS exhibiting unique properties have extensively been investigated as sensor materials raising hopes that the problems related to interactions between foreign surfaces and biomolecules may soon be solved. One-dimensional nanostructured PANI has been reported to enhance significantly the diffusion of target molecules due to their greater surface area and shorter penetration depth for target molecules than the conventional PANI, and have therefore become alternative materials to improving the sensitivity and response time of biosensors [63]. The conducting polymer materials can be deposited electrolytically from the solution onto a conducting support to provide a three-dimensional matrix for immobilized enzymes where reactants are converted to products [64]. The attractive feature of the direct electron transfer systems is presumably their simplicity of construction. Figure 2.2 illustrates the design of an electrochemical enzyme biosensor incorporating mediators (e.g. conducting polymers).

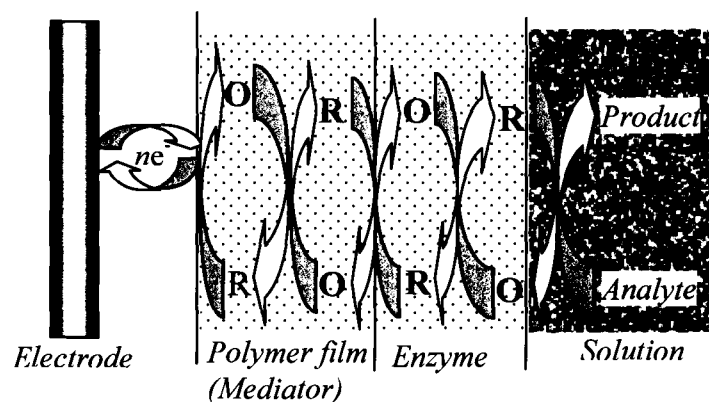


**Figure 2.2.** Typical representation of an electrochemical enzyme biosensor.

Other types of biosensors include resonant biosensors, optical detection biosensors, thermal detection biosensors and ion-selective biosensors. In resonant biosensors, an acoustic wave transducer is coupled with an antibody (bio-element). The mass of the membrane changes when the analyte molecules (antigens) get attached to the membrane. This results in a subsequent change in the resonant frequency of the transducer. This frequency change is measured out. The output transduced signal measured in optical detection biosensors is light. The biosensors may be made based on optical diffraction or electrochemilluminence. In optical diffraction based devices, a silicon wafer is coated with a protein via covalent bonds. The wafer is exposed to UV light through a photomask and the antibodies made inactivated in the exposed regions. The diced wafer chips when incubated in analyte, antigen-antibody binding is formed in active regions, thus creating diffraction grating. This grating produces signal when illuminated with a light source such as laser. This signal can be measured or can be further amplified before measurement for improving sensitivity. Thermal detection biosensors are constructed by combining enzymes with temperature sensors. When the analyte comes into contact with the enzyme, the heat reaction of the enzyme is measured and calibrated against the analyte concentration. The ion-selective biosensors are basically composed of semiconductor field effect transistors. When the ions and the semiconductor interact, the surface electrical potential changes which can be measured.



A number of techniques such as physical adsorption, entrapment, cross-linking between molecules and covalent binding have been used for immobilization of enzymes onto the electrode surfaces. In addition to these conventional methods, sol-gel entrapment, Langmuir-Blodgett (LB) depositions, electropolymerization, self-assembled biomembranes and bulk modification have recently been used [65]. The activity, stability and performance of immobilized enzymes depend upon the surface area, porosity, hydrophilic character of immobilizing matrix, reaction conditions and the immobilization procedure. A common approach for the immobilization of enzymes onto the electrode surfaces is the electrostatic attachment to a previously electropolymerized polymer film on the electrode surface [66]. This immobilization procedure offers numerous advantages over conventional procedures for the design of biosensors in that there is complete coverage of the active surface area; greater control over film thickness and reproducibility and the distribution of the immobilized enzyme can be spatially controlled irrespective of geometry, shape and dimension of the electrode. A series of biosensors have been produced in this way and a variety of enzymes, including galactose oxidase, HRP, glucose oxidase (GOD), sarcosine oxidase, cholesterol oxidase, cytochrome P450, AChE and ascorbate oxidase have been immobilized to a PANI backbone [66-71]. The present work focuses on a similar electrostatic approach for the immobilization of the enzyme Tyr onto the structured PANI-PVS modified BDD electrode.



### 2.3 Enzymes

Enzymes are biocatalysts involved in the performance of metabolic reactions [72]. They are high molecular weight protein compounds, principally made up of amino acid chains linked together by peptide bonds. The catalytic activity of most enzymes is aided by other compounds known as cofactors. The cofactors are mainly co-enzymes, prosthetic groups or metal-ion activators. A coenzyme is non-protein organic substance which is dialyzable, thermostable and loosely attached to the protein part. A prosthetic group is an organic substance which is dialyzable, thermostable and firmly attached to the protein portion whereas metal-ion activators include cations such as  $K^+$ ,  $Fe^{2+}$ ,  $Fe^{3+}$ ,  $Cu^{2+}$ ,  $Co^{2+}$ ,  $Zn^{2+}$ ,  $Mn^{2+}$ ,  $Ca^{2+}$  and  $Mo^{3+}$ .

Enzymes exhibit specificity relative to the reactions they catalyze and this property makes them important diagnostic and research tools. Currently, there exist a large number of enzymes that have been isolated and characterized. These enzymes have been classified according to the type of reaction they catalyze (see Table 2.1).

**Table 2.1.** Classification of the enzyme groups and their type of reaction catalyzed.

Group	Type of reaction catalyzed
Hydrolases	Catalyze cleavage reactions or the reverse fragment condensations. According to the type of bond cleaved, a distinction is made between peptidases, esterases, lipases, glycosidases and phosphatases among others. Examples of this class of enzyme including cholesterol esterase, alkaline phosphatase, glucoamylase, <b>phenylalanine hydroxylase</b> and <b>tyrosinase</b> – catalyze substrate oxidation by molecular oxygen. The reduced product of the reaction in this case is water.
Lingases	Split C-C, C-O, C-N, C-S and C-halogen bonds without hydrolysis or oxidation. The reaction is usually accompanied by the consumption of a high energy compound such as Adenosine triphosphate (ATP) and other nucleoside triphosphates.
Lyases	Non-hydrolytically remove groups from their substrates with the concomitant formation of double bonds or alternatively add new groups across double bonds.
Oxidoreductases	Catalyze oxidation and reduction reactions involving the transfer of hydrogen atoms or electrons.
Transferases	Transfer C, N, P or S containing groups (alkyl, acyl, aldehyde, amino, phosphate or glucosyl) from one substrate to another. They include transaminases, transketolases, transaldolases and transmethyases.

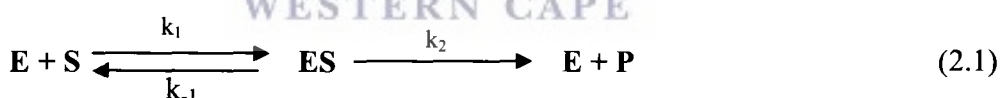


### 2.3.1 Enzyme biosensors

An enzyme biosensor is originated from a combination of a transducer with a thin enzymatic layer, which normally measures the concentration of a substrate. The enzymatic reaction transforms the substrate into a reaction product that is detectable by the electrode. The concentration of any substance can be measured provided that its presence affects the rate of an enzymatic reaction which is especially true for enzyme inhibitors. The signal (current or potential) measured is proportional to the rate-limiting step in the overall reaction.

#### 2.3.1.1 Enzyme kinetics

Enzymes are protein catalysts that speed up the rate of a chemical reaction without being used up in the process. Enzymes can achieve their effect by temporarily binding to the substrate and lowering the activation energy needed to convert it to a product. The rate at which an enzyme works is influenced by several factors such as concentration of substrate molecules, temperature, presence of inhibitors and pH. The study of the rate at which an enzyme works is called enzyme kinetics. The presence of the enzyme ensures the transformation of the substrate into the reaction product according to the following equation 2.1:



where E represents the enzyme, S the substrate and P the reaction product;  $k_1$ ,  $k_{-1}$  and  $k_2$  are the rate constants of the reactions [73]. The Michaelis-Menten kinetics model postulates that enzymatic reactions proceeds through the formation of a transition complex intermediate ES. Once formed, the ES complex either converts to a product or decomposes to the free enzyme and substrate. The Michaelis-Menten model assumes that only a negligible amount of ES complex reverts back to the reactants. According to this model, the hyperbolic relations governing the rate of catalysis and the substrate concentrations are expressed by the equation:

$$v = \frac{V_{max}[S]}{K_m + [S]} \quad (2.2)$$

where  $v$  is the initial rate (moles/time),  $V_{max}$  is the maximum rate of catalysis,  $K_m$  is the apparent Michaelis-Menten constant and  $[S]$  is the substrate concentration. The Michaelis-Menten constant refers to the substrate concentration at which the enzymatic reaction occurs at half the maximum velocity ( $V_{max}/2$ ). The relationship between  $v$  and  $[S]$  in the absence and presence of inhibitors (equation 2.2) is illustrated in Figure 2.3a.

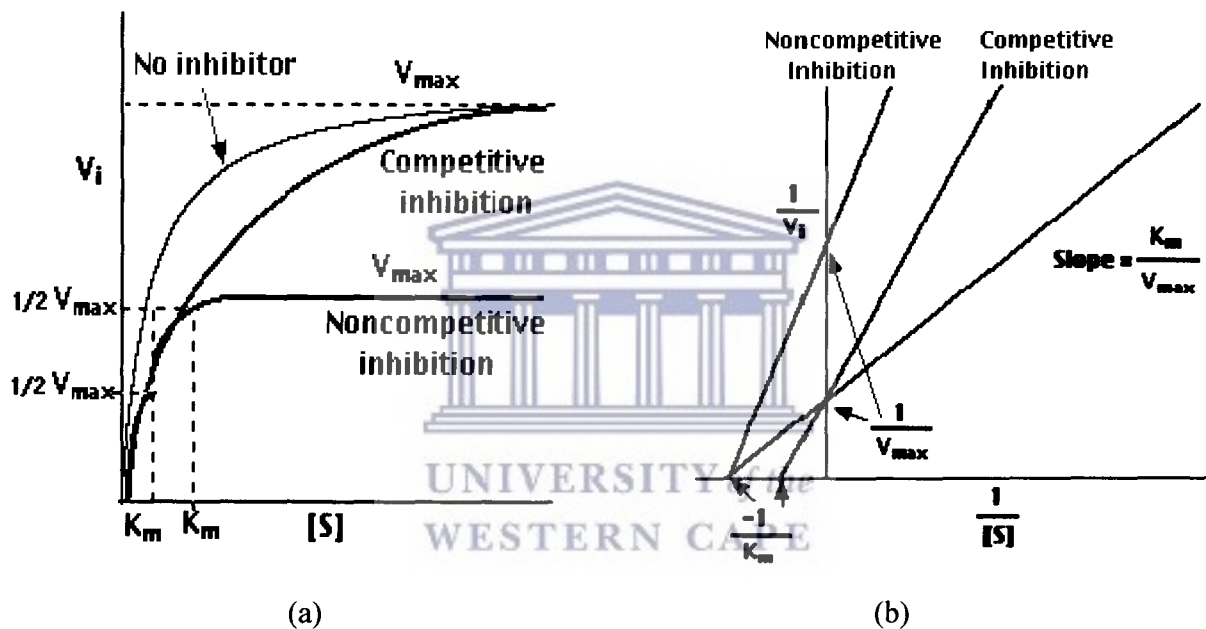


**Figure 2.3.** (a) Variation of the reaction velocity  $v$  with the substrate concentration and (b) Lineweaver-Burk plots for different types of reversible enzyme inhibitors.

When  $[S] \gg K_m$ , a maximum value of the rate constant,  $V_{max}$ , is reached, so that  $V_{max} = k_2 [E_0]$ , and when  $[S] = K_m$ ,  $v = V_{max}/2$ . It is experimentally more convenient to plot the data in a straight line form, and inverting the Michaelis-Menten equation can achieve the equation:

$$\frac{1}{v} = K_m + \frac{[S]}{K_2 [E_0][S]} = \frac{K_m}{V_{max} [S]} + \frac{1}{V_{max}} \quad (2.3)$$

When  $I/v$  is plotted against  $1/[S]$ , a straight line is obtained with a slope of  $K_m/V_{max}$  and a y-intercept of  $1/V_{max}$ ; hence both  $K_m$  and  $V_{max}$  can be obtained. The double reciprocal plot obtained is referred to as a Lineweaver-Burk plot (Figure 2.3b).

In the enzyme based biosensors, the enzyme is retained (immobilized) on the surface of an electrode, mostly a modified electrode while the substrate (analyte) is gradually increased. The signal generated from the catalytic interaction between the enzyme and the substrate is recorded. This implies that the enzyme concentration remains constant while the substrate concentration changes. Under this phenomenon, the reaction velocity increases gradually, and then reaches a maximum when the entire available enzyme is converted to enzyme-substrate complex (equation 2.3). The substrate concentration  $[S]$  at half of the maximum velocity ( $V_{max}/2$ ) allows for an estimation of Michaelis-Menten constant ( $K_m$ ) which gives information about the activity of the enzyme. The equation for this constant is given as (equation 2.4):

$$K_m = \frac{K_1 + K_2}{K_{-1}} \quad (2.4)$$

This is also equal to the substrate concentration at half of the maximum velocity. The rate constants  $K_1$ ,  $K_2$  and  $K_{-1}$  are as explained in equation 2.1. A small  $K_m$  value indicates that the enzyme requires only a small amount of enzyme to become saturated and therefore the maximum velocity is reached at relatively low substrate concentration. A large  $K_m$  indicates that high substrate concentration is needed to achieve maximum reaction velocity. The substrate with the lowest  $K_m$  value upon which the enzyme acts as a catalyst is usually assumed to be the enzymes natural substrate.

### 2.3.1.2 Enzyme inhibition

Enzyme inhibitors are molecules that bind to enzymes thus decreasing their activity. The binding to the immobilized enzyme or the enzyme in solution results in a decrease in biosensor signal. The mode of enzymatic inhibition is variable from one inhibitor to another, and may be

reversible or irreversible. The response of the enzyme sensor provides a continuous measure of the activity of the immobilized enzyme, whether or not its inhibitor is present. Enzyme inhibition can be competitive or noncompetitive. Competitive inhibition is when the substrate and inhibitor compete for binding to the same active site and the degree of inhibition decreases as the substrate concentration increases. When the degree of inhibition increases with the substrate concentration, the inhibition is called “uncompetitive.” In this case, the inhibitors only interact with ES complexes and bind only when the ES is formed. Noncompetitive inhibition is when the inhibitor binds somewhere else on the enzyme molecule reducing its efficiency or activity but does not affect the binding of the substrate. As a result, the extent of inhibition depends only on the concentration of the inhibitor. The kinetic schemes for different kinds of reversible inhibition are presented in Figure 2.4.

To study the type and kinetics of inhibition, Lineweaver-Burk plots for the enzymatic reaction in the presence and absence of inhibitors at their 50 % rate reduction (IC<sub>50</sub>) are plotted using a double reciprocal plot and the values of  $K_m$  and  $V_{max}$  obtained from the plots [74]. Figure 2.3b illustrates an example of Lineweaver-Burk plots in the absence and presence of inhibitors. It is known that noncompetitive inhibitors bind equally well to both E and the complex ES (i.e., they have identical affinities for E and ES). This results in the formation of three complexes ES, EI and ESI, of which only ES can yield the product of enzymatic reaction. The inhibitor is represented by I while  $K_I$  and  $K_I'$  are the dissociation constants for the noncompetitive inhibition. Obviously, the inhibitor is not binding to the same site as S, and this kind of inhibition cannot be overcome by increasing the concentration of the substrate. It also suggests that the inhibitor may be interacting with a site on the enzyme which is not its active site. Noncompetitive inhibition occurs if  $K_I = K_I'$ . In the Lineweaver-Burk plot for non-competitive inhibition (Figure 2.3b), the x-intercept remains the same with or without I. Non-competitive inhibition does not change  $K_m$  (i.e., it does not affect the substrate binding) but decreases  $V_{max}$  (i.e., the inhibitor binding hampers catalysis). On the contrary, a competitive inhibitor does not change  $V_{max}$  but increases the  $K_m$  value [74,75]. The plot for competitive inhibition shows a change in the x-intercept but the y-intercept remains unchanged.

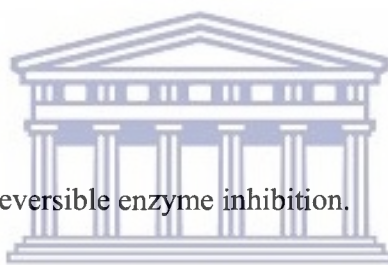
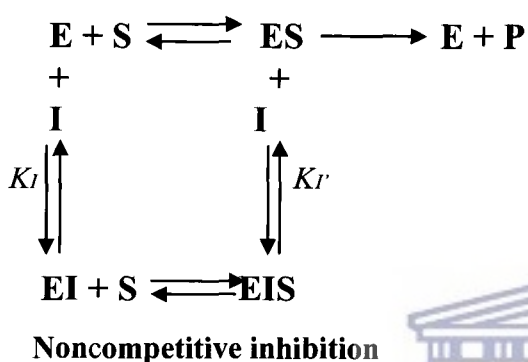
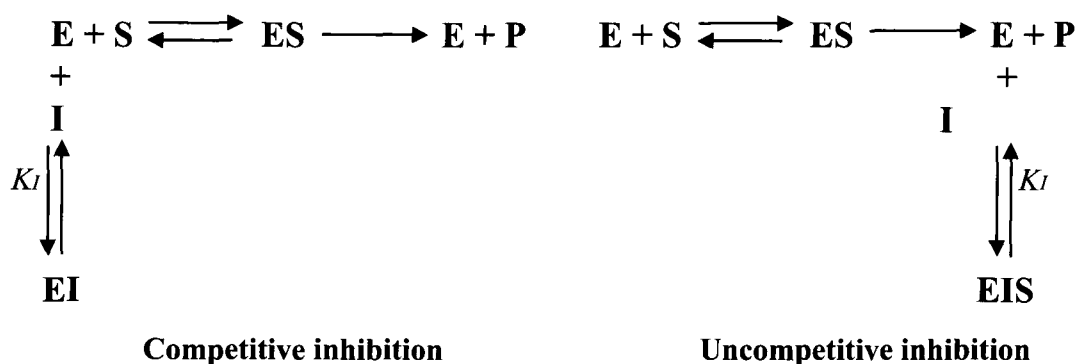


**Figure 2.4.** Kinetic schemes for reversible enzyme inhibition.

All the kinetic equations mentioned above are based on the assumption of homogeneous kinetics of the enzyme-substrate and enzyme-inhibitor(s) interactions. The appropriate parameters of inhibition (i.e.  $K_I$  and  $K_I'$  etc.) indicate the potentialities of an enzyme which could be extended or reduced through the immobilization and incorporation of the enzyme into the membrane material. The immobilization of an enzyme is an indispensable part of the development of biosensors and the multiplicity of application of the enzyme due to immobilization reduces the cost of measurement. The immobilized enzyme is more stable towards extreme working conditions, e.g. high temperature, and can be easily combined with an appropriate sensor in the biosensor assembly [76]. When an enzyme is immobilized, the reaction occurs in the heterogeneous phase because the active sites are in the solid phase and the substrate is in the aqueous phase. The concentration of the substrate varies from one point in the solid support to another, and so the rate of the enzymatic reaction is not the same as that occurring at the solid

surface. During the reaction, a profile of the substrate and product concentrations is established across the support such that the substrate concentration in the active layer is always lower than that in solution. The saturation of the immobilized enzyme therefore requires higher substrate concentrations in the bulk solution than those normally obtained for the enzyme in solution [73].

### 2.3.1.3 Tyrosinase (Tyr) enzyme

Tyrosinase (Tyr), tyrosine hydroxylase, is the common name for an enzyme that is formally termed monophenol monooxygenase and is listed as Enzyme number 1.14.18.1 (E.C. 1.14.18.1). It is also known as cresolase, phenolase, monophenol oxidase and as polyphenol oxidase (PPO) [77]. Enzymes isolated from different sources and measured for their catalytic activity with varying substrates can turn out to be the same protein. Thus, the enzyme Tyr, discovered in animal systems, was named for its action on the amino acid tyrosine, and specifically for its ability to form dopaquinone, an intermediate in the production of melanin. The same enzyme isolated from plant materials had been examined for its ability to oxidase phenolic compounds, and thus the names phenolase, monophenol oxidase and cresolase. Tyr is a copper-containing enzyme of plant and animal tissues that catalyzes the production of melanin and other pigments from tyrosine by oxidation. Of the pigments, melanin is one of the most widely distributed and is found in fungi, bacteria, animals and plants. Tyrosinase (Tyr) is the enzyme responsible for the first step in melanin formation [78]. In this step, tyrosinase catalyzes the oxidation of tyrosine to L-3,4-dihydroxyphenylalanine (L-dopa), Figure 2.5 (i-ii). L-dopa is produced during the first of a series of redox reactions leading to the formation of melanin, which are found in the mammalian eye and brain. L-dopa further drives the reaction by functioning as an alternative substrate for tyrosinase and as a cofactor that stimulates catalytic efficiency. Hence, Tyr catalyzes two reactions: the hydroxylation of monophenols (e.g. L-tyrosine) to *o*-diphenols (e.g. L-dopa) and the oxidation of *o*-diphenols to *o*-quinone, consuming molecular oxygen [79]. These *o*-quinones evolve nonenzymatically to yield several unstable intermediates, which polymerize to render melanins. Quinones are electroactive species that can be electrochemically reduced at low potentials and thus reduction currents obtained serve as good analytical signals for the phenolic



compounds detection [80]. The hydroxylation of L-tyrosine is of considerable importance since it is also the initial step in catecholamine synthesis.

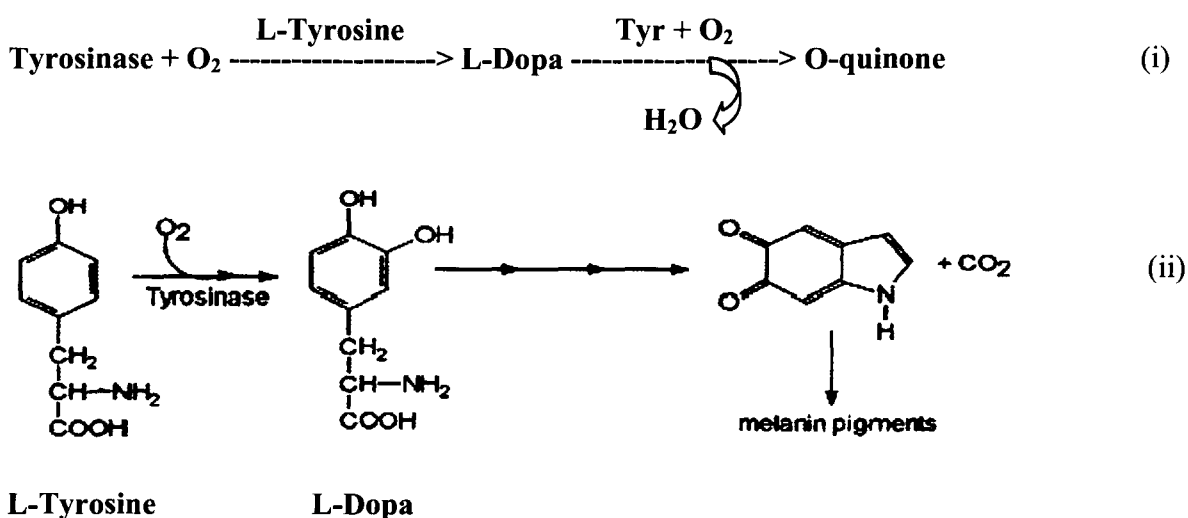


**Figure 2.5.** Tyrosinase pathway for melanin production (i-ii).

Tyrosinase can play a role in neuromelanin formation in the human brain and could be central to dopamine neurotoxicity as well as contribute to the neurodegeneration associated with Parkinson's disease [81]. Some reports have been presented about the amperometric detection of phenol derivatives with tyrosinase-modified electrodes [82-86]. Several groups have investigated tyrosinase-based biosensors for the low potential detection of phenols and catechols in foods, pharmaceuticals and clinical samples [87-91]. Besides the different sources of tyrosinase, a wide variety of matrices, including carbon paste [92], nafion membrane [93], hydrogel [94], graphite [95], conducting polymers [96,97], and biopolymers [98], have been used in the construction of sensor probes. Numerous amperometric biosensors based on the immobilization of Tyr at different electrode material have been described in the literature. Glassy carbon electrodes modified with polymers [99], sol-gel materials [100,101], self-assembled monolayers (SAMs) on gold [102], reticulated vitreous carbon (RVC) [103] and other composite electrodes [104,105] have been used to prepare Tyr electrochemical biosensors. A variety of methods for the immobilization of tyrosinase with an electrochemical transducer have been reported, e.g.,



adsorption [106] or cross-linking [107] on the surface of electrodes, incorporation with a carbon paste matrix [108] or graphite-epoxy composite electrodes [84,109], immobilization in polymer films [110,111] and entrapment in hydrogel [112]. Recently, silica sol-gel [113,114] and alumina sol-gel [115,116] have been applied for the immobilization of tyrosinase for the detection of phenolic compounds.

#### **2.3.1.3.1 Source of tyrosinase**

Tyrosinase (Tyr) is widely distributed in nature in many organisms with slightly different forms (bacteria, plants, insects and animals). In plants, tyrosinase induced pigmentation is responsible for browning of wounded plant parts and is considered to be poisonous to the color quality of plant derived foods and beverages. Tyr is present in some fruits and vegetables, e.g. apple and potato, and is responsible for the dark color produced when cut apple, banana or sliced potato exposed to air [117]. This is due to the conversion of tyrosine to the pigment melanin. This results in huge economical losses because it shortens the shelf life and decreases the quality of raw fruits and vegetables during post-harvest handling and processing [118]. In insects, the enzyme is involved in defensive and developmental processes and for this reason the tyrosinase inhibitors could be used as insect-control agents [119]. In mammals, the final product of tyrosinase activity is melanin, a pigment responsible for the cells of skin, eye, hair color and tumors of early childhood derived from neural crest and characterized by excessive production of L-dopa and dopamine (DA), and in neuroblastomas [120,121,122]. It is produced in melanocytes, cells located in the basal layer of the dermis [123,124]. Albinism is a genetic disease of organisms which fail to produce functional tyrosinase.

### 2.3.1.3.2 Structure of tyrosinase

The structure of tyrosinase (Tyr) is not known, however strong similarities exist between tyrosinase and hemocyanin, which performs the function of oxygen transport in mollusks and arthropods. Tyr is a binuclear copper containing metalloprotein which catalyzes, in the presence of molecular oxygen ( $O_2$ ), two different reactions: the transformation of *o*-mono-phenols into catechols and the oxidation of catechol to *o*-quinone (Figure 2.4). Tyr carries out the oxidation of phenols such as L-tyrosine (L-Tyr) and catechol using dioxygen ( $O_2$ ). This enzyme, product from mushrooms, has an isoelectric point of 4.5 [125] and carries a negative charge for  $pH > 4.5$  in aqueous solution. It has been suggested that there is no common tyrosinase proteins in terms of their structural properties, tissue distribution and cellular location occurring across all species [126,127]. The enzyme found in plant, animal and fungi tissue frequently differ with respect to their primary structure, size, glycosylation pattern and activation characteristics. However, all tyrosinases have in common a binuclear type III copper centre within their active site. Typical example of human tyrosinase, a single membrane spanning transmembrane protein [128], as two copper atoms (Figure 2.6) are each coordinated with three histidine residues; the coordinates for the crystal structure of a *Streptomyces* derived tyrosinase in complex with a so called “caddie protein” [129]. The active site of tyrosinase consists of two copper atoms and three states: 'met', 'deoxy', and 'oxy'. Two copper atoms within the active site of tyrosinase enzymes interact with dioxygen to form a highly reactive chemical intermediate that then oxidizes the substrate. The activity of tyrosinase is similar to catechol oxidase, a related class of copper oxidase. Tyrosinase and catechol oxidases are collectively termed polyphenol oxidases (PPOs).

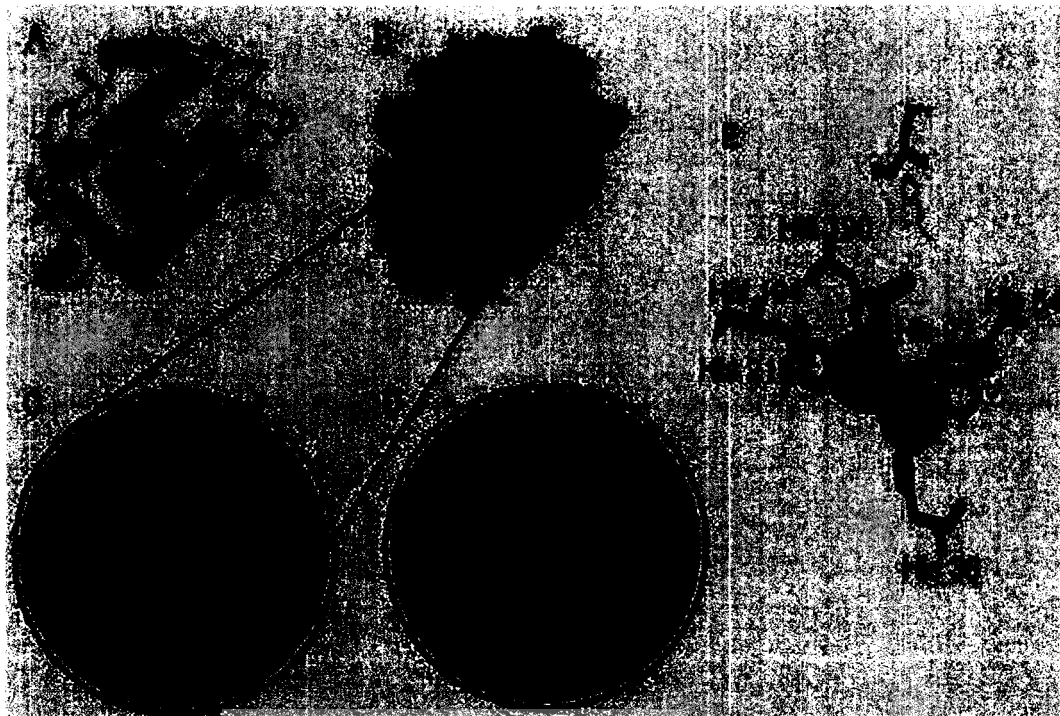


**Figure 2.6.** Model structure of tyrosinase enzyme: (A) – (B) only Tyr molecule has shown, copper atoms are shown in green and in red is the molecular surface. (C) – (D) the active site for the protein sits within a pocket formed on the molecular surface of the molecule. (D) – (E) histidine amino acids are shown as a blue line representation [129].

UNIVERSITY of the  
WESTERN CAPE

### 2.3.1.3.3 Tyrosinase functions

The enzyme Tyr functions as a respiratory shuttle system, a terminal oxidase, in the insects and other animals [130]. L-dopa can serve as the hydrogen carrier to the terminal oxidase and meanwhile, L-tyrosine can act as a reservoir to provide L-dopa to the system (Figure 2.7). Melanins are formed when the system respiratory is perturbed and the reduction of the quinone is inhibited then the shuttle breaks down. Tyr is, functionally, an oxygen oxidoreductase enzyme.

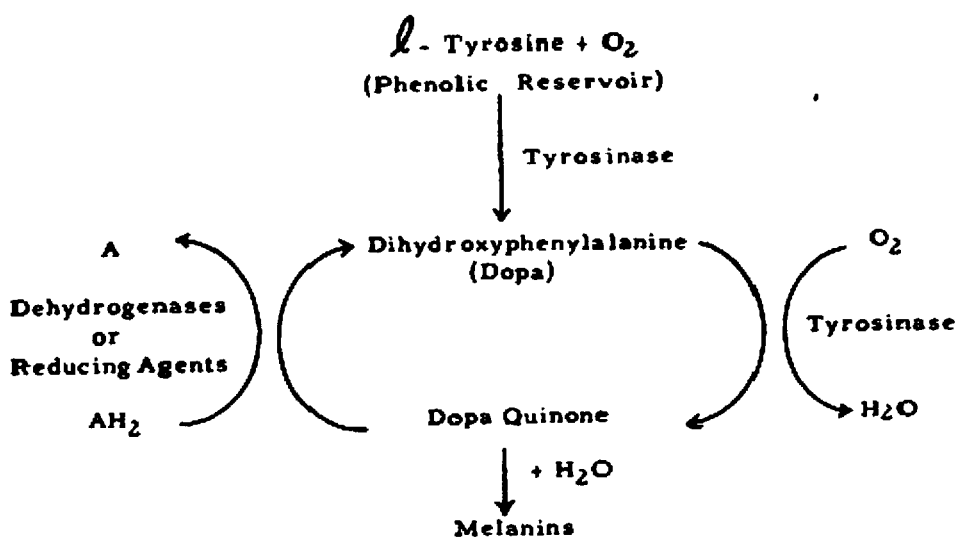


**Figure 2.7.** Tyrosinase pathway for providing L-dopa in the system.

#### 2.3.1.3.4 Reaction mechanisms of tyrosinase

The mechanism involves successive mono-electronic transfers, mediated by a redox active metal ion such Fe<sup>3+</sup> or Cu<sup>2+</sup>. In some cases, non-metallic redox centers may be used by metalloenzymes. Iron and copper are two most familiar redox metals serving biological functions as both can catalyze similar reactions and either copper or iron are found in oxygen carriers, mono-oxygenases, di-oxygenases or oxidases [131]. Prior to the photosynthetic generation of an oxidizing environment, water insoluble copper (I) prevailed and was not biologically available. However, copper can be regarded as a modern bioelement as it became a biological element after iron. Soluble ferrous iron (Fe<sup>2+</sup>) was present in large amounts in the oceans and was used for biological functions. The production of the oxygen molecule (O<sub>2</sub>) by photosynthetic organisms resulted in the oxidation of Cu (I) to soluble Cu (II) and of soluble Fe (II) to insoluble Fe (III). This is indicating the reason why living organisms selected copper then instead of iron. High redox potential for the Cu (II)-Cu (I) system is found in copper enzyme, most of them working between 200 and 1000 mV. This high potential can be used for direct oxidation of certain substrates, easy to oxidize, such as superoxide (in superoxide dismutase) or ascorbate (in ascorbate oxidase) or catechols (in tyrosinase or in lacasses). Figure 2.8 describes the tyrosinase-

copper enzymes for direct oxidation. As copper is more difficult to oxidize than iron (equation 2.5), the Cu (III) redox state might not be biologically relevant.

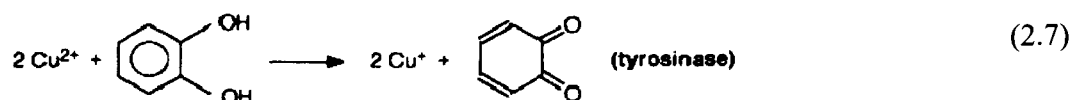
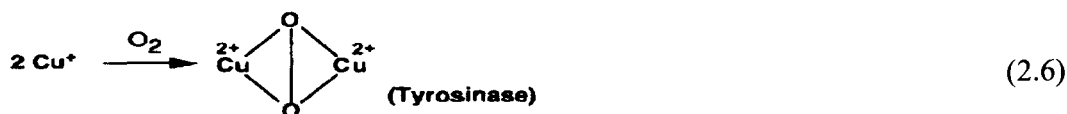
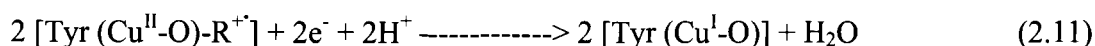
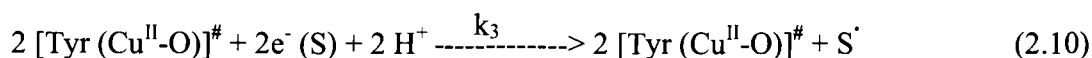
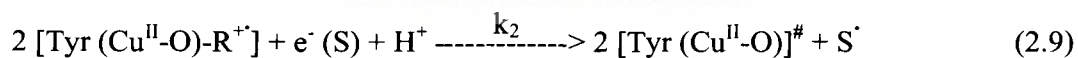
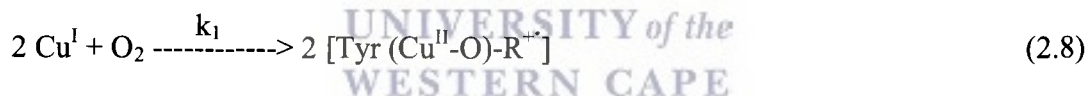


**Figure 2.8.** Direct oxidation by copper enzymes (two metal centers) for a two-electron oxidation.

Tyrosinase (Tyr) is a type III protein containing a binuclear copper active site in which the copper (II) centers are electronically coupled (equation 2.6) [132]. Tyr is a monooxygenase using dioxygen for the ortho hydroxylation of monophenols (monophenolase activity) and also possesses oxidase activities, catalyzing the oxidation of *o*-diphenols to *o*-quinones (catecholase activity) (equation 2.7). As the diphenol product can serve as the two-electron source required for phenol oxidation and as a co-substrate, Tyr is classified as an internal monooxygenase. The reaction can be represented as follows:





The mechanism starts with the binding of oxygen to give rise to the oxygenated form (oxytyrosinase,  $E_{oxy}$ ), equation 2.8, which consists of two tetragonal Cu (II) atoms, each coordinated by two strong equatorial and one weaker axial  $N_{His}$  ligand [133]. The exogenous oxygen molecule is bound as peroxide and bridges the two Cu centers (Figure 2.9) [134]. This electronic structure of side-on bridging would appear to make a significant contribution to the biological function of oxytyrosinase, equation 2.9, when the enzyme catalyzes the oxidation of a substrate (S) via a reaction that involves one-electron oxidation of the heme to form the binding of the substrate (monophenol) to the heme in the Cu (II) state. The enzyme, as an intermediate substance, can be reused in the same solution for two-electron oxidation of the heme for the binding between substrate (diphenol) and the heme in the Cu (II) state (equation 2.10).

The strong  $\sigma^*$  donor interaction results in a less negative peroxide, whereas the  $\pi$  acceptor interaction into the peroxide  $\sigma^*$  orbital greatly weakens the O-O bond, preparing it for cleavage [133,134]. *Met*tyrosinase ( $E_{met}$ ), like the *oxy* form, contains two tetragonal copper (II) ions antiferromagnetically coupled through an endogenous bridge, although hydroxide exogenous ligands other than peroxide are bound to the copper site [135,136]. This derivative can be converted by addition of peroxide to oxytyrosinase, which in turn decays back to *met*tyrosinase when the peroxide is lost (equation 2.10, Figure 2.4). The resting form of tyrosinase, i.e. the enzyme as obtained after purification, is found to be a mixture of  $\geq 85\%$  *met* and  $\leq 15\%$  *oxy* forms [137]. Further more, a half-*met* derivative can be prepared containing the two coppers in a mixed valence oxidation state  $[Cu^I \cdots Cu^{II}]$  and which is EPR detectable [135,136,137]. *Deoxy*tyrosinase ( $E_{deoxy}$ ), by analogy with *deoxy*hemocyanin, has a bicuprous structure  $[Cu^I-Cu^I]$ . Its presence was established in 1938 by Kubowitz [138], who demonstrated the binding of one carbon monoxide per two copper atoms after reduction of the enzyme with catechol (equation 2.11, Figure 2.4).

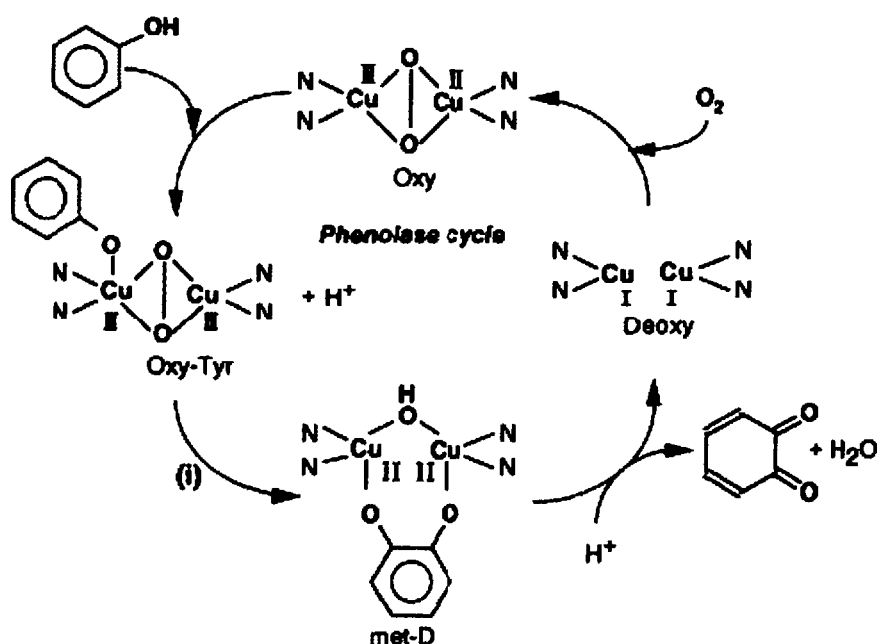


**Figure 2.9.** Catalytic cycle for the oxidation of monophenol and diphenol substrates to *o*-quinones by tyrosinase in the presence of  $O_2$  [123,139].

The monophenolase (i) activity of tyrosinase (Figure 2.10) is generally defined as the first step in the melanization pathway and consists of the *o*-hydroxylation of the monophenol (e.g. L-tyrosine) to *o*-diphenol (e.g. L-dopa) [140-143]. The fact that the hydroxylating activity is expressed in conjunction with the oxidation of the *o*-diphenol to its *o*-quinone (second step in the melanization pathway). This has led some authors to define monophenolase activity as the complete conversion of monophenol to *o*-quinone [144]. Moreover, this activity that distinguishes tyrosinase from other phenol-oxidizing enzymes, such as laccase and peroxidase. The diphenolase activity involves the oxidation of two *o*-diphenols to two *o*-quinones with a concomitant  $4 e^-$  reduction of oxygen molecule ( $O_2$ ), which yields two molecules of water (Figure 2.10).



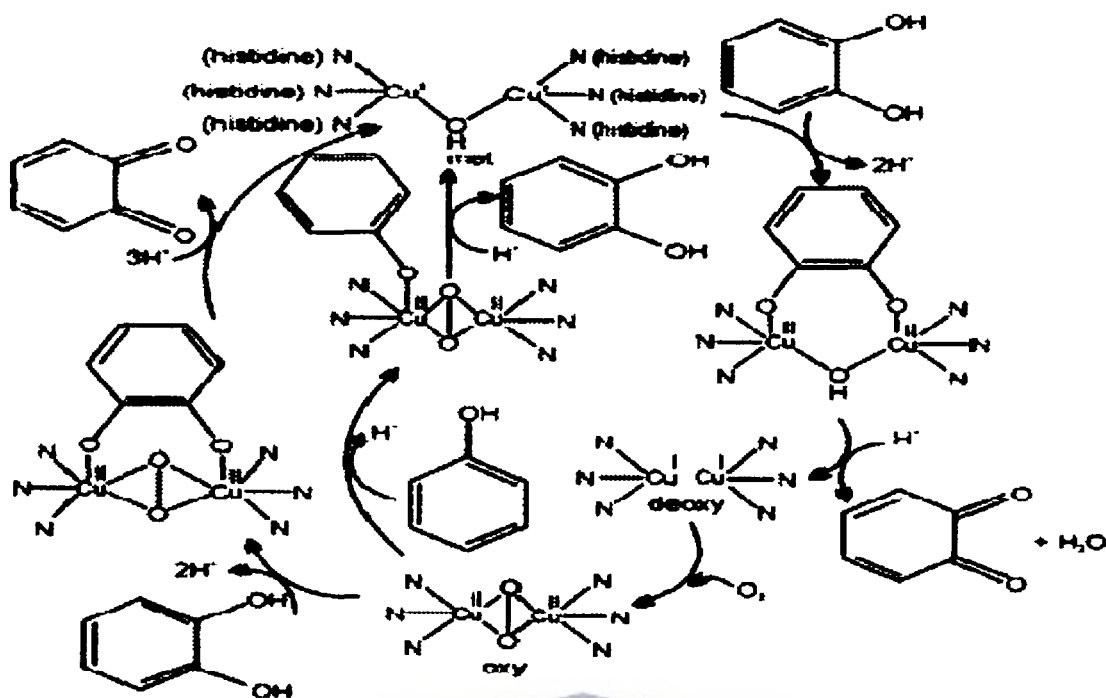


**Figure 2.10.** Mechanism of tyrosinase activity for the oxidation of monophenol and diphenol substrates to *o*-quinones in the presence of  $O_2$  [145].

### 2.3.1.3.5 Kinetics (rate) study of the enzyme tyrosinase (Tyr) reaction

These reactions below (Figure 2.11) are catalyzed by the enzyme tyrosinase in the presence of molecular oxygen. Schemes 1.1 and 1.4 have expressed that L-Phe is electrochemically converted to L-Tyr by the enzyme tyrosinase to form L-dopa. Under appropriate experimental conditions, the reaction rate is monitored by measuring the increase in current when the potential (voltage) is applied in the system, using cyclic voltammetry technique. The UV-vis technique can measure the increase absorbance at specific wavelength that occurs as the reaction proceeds. The rate of the reaction is determined for several different concentrations of substrate (L-Phe or L-Tyr) with the concentration of enzyme (tyrosinase), pH, and temperature held constant for all data sets (runs). For a reaction to obey Michaelis-Menton kinetics, it must proceed by the following equation 2.1, section 2.3.1.1. The reaction studied with L-Phe as a substrate when Tyr

is used as an enzyme (equation 2.8, section 2.3.1.3.4) cannot truly follow this mechanism since L-dopa is not the initial product of the oxidation of L-Phe in the solution.

However, the oxidation of L-tyr by the enzyme Tyr to L-dopa is the rate determining step in the reaction sequence, and subsequent reactions occur very rapidly. Thus, the rate of formation of L-Tyr is almost the same as the rate of formation of L-dopa using L-Phe as a substrate (Figures 1.1 and 1.4).

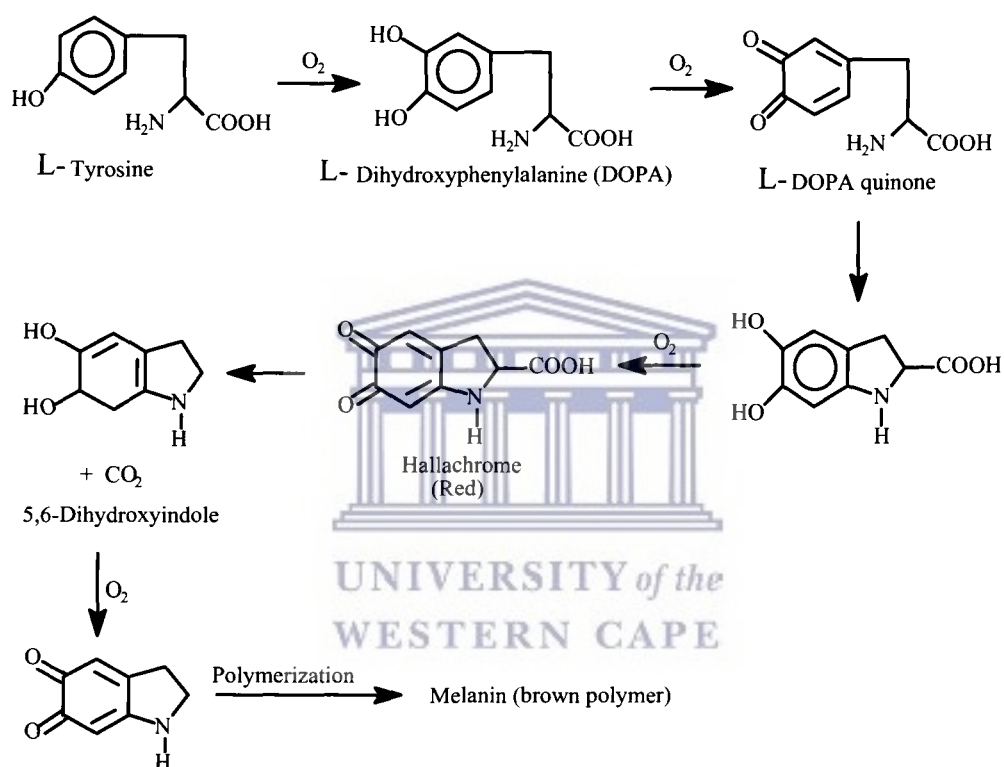


**Figure 2.11.** Catalytic mechanism of tyrosinase enzyme activity for melanin production.

#### 2.3.1.3.6 Tyrosinase (Tyr) inhibition effects

The enzymes function by sterically binding to a substrate. If a molecule interferes with that binding, it will hinder or inhibit the activity of the enzyme. The inhibitory effects of thio-urea and benzoic acid on tyrosinase were characterized as the principal inhibitors, including anisaldehyde (p-methoxybenzaldehyde) which is extract from the seeds of *Pimpinella anisum* known as aniseed and being utilized as a food spice [146]. In addition, ethyl acetate was also found to be an inhibitory activity for tyrosinase enzyme. A number of tyrosinase inhibitors from both natural and synthetic sources that inhibited monophenolase, diphenolase or both of these activities have been identified to date.

### 2.4 Immobilization methods

Immobilization of enzymes retains the enzymes in functionally active form on the electrode surface or a matrix modified electrode. The immobilization matrix may be a membrane, gels, carbon, graphite, silica and polymeric film among others [147]. The immobilization of these protein molecules should be performed under conditions that provide membrane like environment in which all the normal interactions of the proteins are preserved. The method chosen for immobilization of enzymes should therefore prevent loss of enzyme activity by avoiding the change of the chemical nature or reactive groups in the binding site of the enzyme. The achievement of high sensitivity and selectivity requires minimization of nonspecific adsorption and stability of immobilized biomolecules. The control of this step is essential to ensure high reactivity, orientation, accessibility and stability of the surface-confined probe and to avoid nonspecific binding [148]. This statement stresses the importance of a suitable immobilization layer. Since the protection of the active site of the biomolecules involve the incorporation of a protective group that the damage of the active site of the enzyme during the attachment to the electrode may be used with care as the protective group can be removed later on without loss of enzyme activity. The surface on which the enzyme is immobilized is responsible for retaining the structure of the enzyme through hydrogen bonding or the formation of electron transition complexes. These links will prevent vibration of the enzyme and thus increase thermal stability.

The microenvironment of the surface and the enzyme has a charged nature that can cause a shift in the optimum pH of the enzyme up to two units. This can be accompanied by a general broadening of the pH region in which the enzymes may work effectively allowing enzymes that normally do not have similar regions to work together. Several methods have been used and found suitable for retention of the biomolecule on the surface of the electrode. The following immobilization types are found generally in the literature include cross linking, carrier binding and enzyme entrapping. These immobilization chemistries are peculiar to certain electrodes.

#### **2.4.1 Cross-linking**

Cross-linking method involves the intermolecular of the protein, either to other protein molecules or to functional groups on an insoluble support matrix. Cross-linking of an enzyme to itself has been reported to be both expensive and insufficient. This is due to some of the protein material that inevitably acting mainly as a support. This results in relatively low enzymatic activity. Therefore, cross-linking is best used in conjunction with one of the other methods and is considered mostly as a means of stabilizing adsorbed enzymes and also for preventing leakage from polyacrylamide gels. One major advantage of cross-linking as a method of immobilizing is that, very little desorption is likely to occur. This is because the enzyme is covalently linked to support matrix [149,150].

UNIVERSITY of the  
WESTERN CAPE

#### **2.4.2 Carrier-bonding**

Carrier-bonding is the oldest method used for enzyme immobilization on the electrode surface. In this method, the amount of enzyme bonded to the carrier and the activity after immobilization depend on the nature of the carrier [150]. The selection of the carrier depends on the nature of the enzyme itself, particle size, surface area, molar ratio of hydrophilic groups and chemical composition. Increasing the ratio of hydrophilic group may boost the activity of the immobilized enzymes. Polysaccharide derivatives such as cellulose, dextran and agarose are mostly used carriers for enzyme immobilization.

Further subdivisions of carrier bonding such as physical adsorption, covalent bonding and ionic bonding occur depending on the bonding mode of the enzyme.

#### **2.4.2.1 Physical adsorption**

Adsorption is the simplest form for the enzyme immobilization. Adsorption can either be physical or electrostatic. The main advantages of adsorption as an enzyme immobilization method are: (i) there is little or no conformational change of the enzyme or destruction of its active center, (ii) this method can be both simple and cheap, especially if a suitable carrier is found, (iii) this method usually requires no reagents and only a minimum of activation steps are required, (iv) adsorption tends to be less disruptive to the enzymatic protein than chemical means of attachment. This is because the bonding is mainly by hydrogen bonds, multiple salt linkages, and Van der Waal's forces [150]. In this respect, the method bears the greatest similarity to the situation found in natural biological membranes and has used to model such systems. The main disadvantages associated with this method are: (i) the adsorbed enzyme can leak from the carrier during use due to a weak binding force between the enzyme and the carrier, (ii) desorption may also result from changes in temperature and pH, (iii) non-specific adsorption of other protein substances may occur as the immobilized enzyme is being used. If any of these substances happens to be a substrate to the enzyme, then the enzyme activity towards the target analyte is affected. The rate of enzyme activity will be decreased depending on the surface mobility of the enzyme, mobility of the enzyme and the target substrate (analyte).

#### **2.4.2.2 Ionic bonding**

This method relies on the bonding of the enzyme protein to water-insoluble carriers containing ion-exchange residues. Polysaccharides and synthetic polymers are usual carriers in this method having ion-exchange centres. The advantages associated with this method are that, there is little change in the conformation and active site of the enzyme due to the bonding of an enzyme to the carrier, which is easily carried out and the conditions are much milder than those needed for the

covalent bonding method [149,150]. Therefore, immobilized enzymes with high activity are obtained. The forces that bond the protein enzymes to the carriers are much weaker than those in covalent bonding.

### 2.4.2.3 Covalent bonding

Covalent bonding is the most intensely studied method of the immobilization techniques and it involves the formation of covalent bonds between the enzyme and the support matrix (water-insoluble carriers). Two key factors limit the selection of the type of reaction by which a given protein should be immobilized, such as (i) the bonding reaction under which it is carried do not cause loss of enzymatic activity, (ii) the reagents used should preserve the activity site of the enzyme. Several functional groups take part in the bonding of the enzyme to the water-insoluble carriers. These include amino, carboxyl, hydroxyl, imidazole, phenolic, thiol, threonine and indole groups (Figure 2.7). According to the mode of linkage, this method can be further classified into diazo, peptide and alkylation methods. One of the challenges of covalent bonding method of enzyme immobilization is that, the conditions for immobilization are much more complicated and less mild than in the cases of physical adsorption and ionic bonding. Several methods have been devised for prevention of this method as these include: (i) a chemically modified soluble enzyme which covalent linkage to the matrix is achieved by newly incorporated residues; (ii) a reversible covalently linked enzyme-inhibitor complex and (iii) a covalent attachment of the enzyme in the presence of a competitive inhibitor or substrate. Hence, covalent bonding can be brought about by one of the forms as shown below (Figure 2.12). This binding involves the nitrogen from the amino group in the probe Tyr. For the amide bond to be formed there must be a way of activating a carboxylic functional group onto the electrode. In order to increase the yield of the immobilized enzyme, the number of reactive residues of an enzyme can be increased. This increased enzyme reactive residues provide alternative reaction sites to those essential for enzymatic activity. The availability of a wide variety of bonding reactions and insoluble carriers with functional groups can either be capable of covalent coupling or being activated to give such groups to make this method generally applicable.



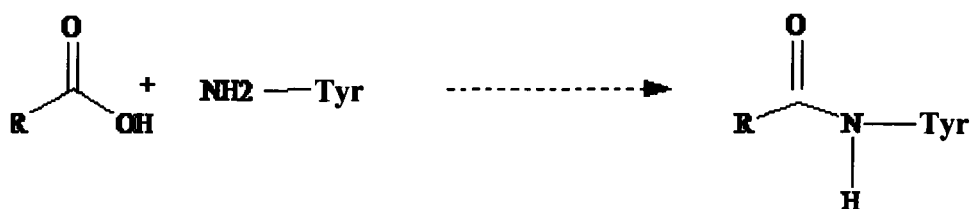


**Figure 2.12.** Typical covalent bonds between Tyr enzyme and activated carboxylic group.

#### 2.4.2.4 Entrapping of enzyme

Entrapment is best achieved when the enzyme is incorporated into conducting polymer films during electrochemical deposition on appropriate electrodes. In this method of immobilization, the enzyme is localized with the lattice of a polymer matrix or a membrane. The enzyme immobilization is done in such a way that the protein is retained within the polymer matrix or the membrane while at the same time allowing penetration of the target analyte (substrate). A solution of the electropolymerizable monomer and an aqueous buffer containing the enzyme is used for the deposition process [147, 150]. Potentiostatic or galvanostatic mode is then used to electrochemically deposit the polymer film, entrapping the enzyme within it. The main advantage of this method of immobilization is that the entrapment of enzymes in conducting polymers provides a facile means for ensuring proximity between the active site of the enzyme and the conducting surface of the electrode with considerable potential for biosensor construction. However, the disadvantage of this method is that it is difficult to retain the activity of the enzyme if the polymer film is electrodeposited on the electrode in highly acidic media. This is because at such a high acidic media, the enzyme would be denatured and render the enzyme inactive. For example, polyaniline which is synthesized either chemically or electrochemically in acidic media in order for it to retain its electroactivity as explained above.



## 2.5 Conducting polymers (CPs)

Conducting polymers (CPs) are polymers that consist of conjugated  $\pi$ -electron backbone responsible for their unusual electronic properties such as electrical conductivity, low energy optical transitions, low ionization potential and high electron affinity [151]. They are characterized by alternating single and double bonds with continuous mobile pi electrons forming a valence band (VB) and conduction band (CB). CPs show almost no conductivity in the neutral (uncharged) state but become electrically conductive upon partial oxidation or reduction, a process commonly referred to as 'doping'. The distinction between these polymers and others is that although they are insulators, doping converts them into intrinsic conductors sometimes with near metal conductivity characteristics.

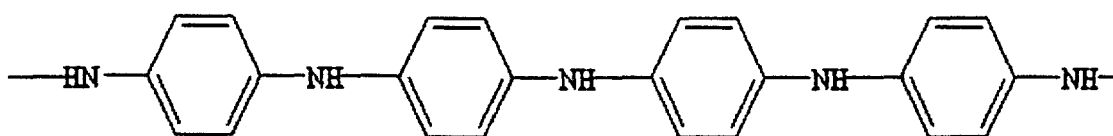
A new class of polymers known as intrinsically conducting polymers (ICPs) or electroactive conjugated polymers has recently emerged. Their intrinsic conductivity results from the formation of charge carriers upon oxidizing (*p*-doping) or reducing (*n*-doping) their conjugated backbone. Such materials exhibit interesting electrical and optical properties previously found only in inorganic systems [152].

CPs are readily oxidized and reduced at relatively low potentials, and the redox process is reversible and accompanied by large changes in the composition, conductivity and colour of the material. A key requirement for a polymer to become intrinsically electrically conductive is that there should be an overlap of molecular orbitals to allow the formation of delocalized molecular wave function. Besides this, molecular orbitals must be partially filled so that there is a free movement of electrons throughout the lattice [153]. This way, charge carriers-electrons or holes-are introduced into the polymer back bone with an effect of converting the supposedly insulators into conductors. Conducting polymers are highly attractive due to their electrical conductivity and the fact that they can be tailor-made to the requirements of the application through modifications in the polymer structure and varying the functional groups in their organic moiety. Many applications of CPs including analytical chemistry and biosensing devices have been reviewed by various researchers [147, 154-160].

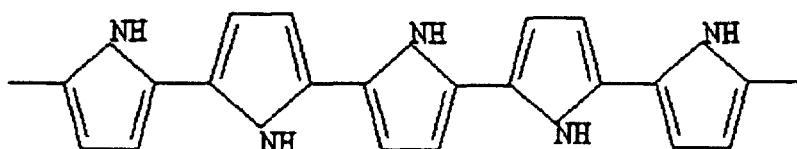
The CPs have widened the possibility of modification of surfaces of conventional electrodes providing new and interesting properties. The common properties desired when CPs are used for biomolecules immobilization is their biocompatibility and redox stability. However, there is always a desire to further optimize a material when targeting a specific application. For biosensors, it is important to tune the hydrophobicity, conductivity, stability, and reactive functionalities in order that the biomolecules can be successfully incorporated and to improve detection limits of the biosensor. In general, manipulation of CP properties such as morphology, porosity, hydrophobicity, mechanical strength, malleability, degradability, redox stability, conductivity etc., can be achieved through chemical means, such as the incorporation of molecules such as dopants or through insertion of functional groups into the CP backbone that may increase conductivity or permit degradation [160].

The current commercial applications of CPs are in thin film transistor, batteries, antistatic coatings, electromagnetic shielding, artificial muscles, light-emitting diodes, gas- and biosensors [69], fuel and solar cells, fillers [161], corrosion protective coatings [162], etc. Generally conducting polymers can be used in electrical, electronic, plastics, medical industries, etc. Among the conducting polymers (CPs), polyaniline (PANI), polypyrrole and polythiophene (Figure 2.13) and their derivatives are the most considered due to a good combination of properties such as good electrical conductivity, facile synthetic processes, environmental stability and good optical and electrochromic properties [163].

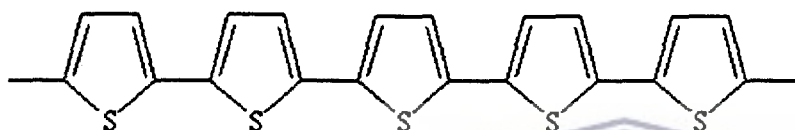
UNIVERSITY of the  
WESTERN CAPE



POLYANILINE



POLYPYROLLE



POLYTHIOPHENE

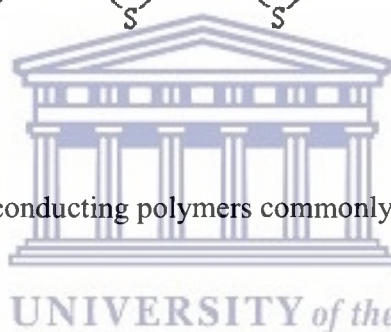


**Figure 2.13.** Structures of some conducting polymers commonly used in biosensors.

### 2.5.1 Historical background of electronically conducting polymers

Research on electrically conducting polymers intensified soon after the discovery of poly(sulphur nitride)  $[(SN)_x]$  in 1975 which becomes superconducting at low temperatures [164]. This has generated renewed interest of the scientific community towards the study and discovery of new conducting polymeric systems. Consequently, the development of aromatic conducting polymers for different applications has received much attention and polyheterocycles, such as polypyrrole (PPy), polythiophene (PTh), polyaniline (PANI), and poly(phenylene vinylene) (PPV) developed in the 1980s, have since then emerged as a class of aromatic conducting polymers that exhibit good stabilities, conductivities, and ease of synthesis [165,166].

## 2.5.2 Synthesis of conducting polymers

Various methods are available for the synthesis of conducting polymers. Conducting polymers can be synthesized either chemically or electrochemically. The most widely used technique is the oxidative coupling involving the oxidation of monomers to form a cation radical followed by coupling to form di-cations and the repetition leads to the polymer. Chemical synthesis is known to permit the scale-up of the polymers, which is currently not possible with electrochemical synthesis. However, electrochemical synthesis is rapidly becoming the preferred general method for preparing electrically conducting polymers because of its simplicity and reproducibility. The advantage of electrochemical polymerization is that the reactions can be carried out at room temperature. By varying either the potential or current with time the thickness of the film can be controlled.

In this procedure, the monomers at the working electrode surface undergo oxidation to form radical cations that react with other monomers or radical cations, forming insoluble polymer chains on the electrode surface. The mechanism of electrochemical polymerization of CPs, using PANI as an example is shown in Figure 2.14. Formation of the radical cation of aniline by oxidation on the electrode surface is considered to be the rate determining step. This is followed by coupling of radicals, mainly *N*- and *para*-forms, and elimination of two protons. The dimer (oligomer) formed then undergoes oxidation on the electrode surface along with aniline. The radical cation of the oligomer couples with an aniline radical cation, resulting in propagation of the chain. It is generally agreed that the mechanism for the chemical/electrosynthetic oxidative polymerisation of the aniline/aniline related monomers is similar. A scheme (Figure 2.14) for the oxidative polymerisation of aniline as proposed by [167,168] is presented below.



be oxidized in the presence of a potential to form reactive radical ion intermediates for polymerization. The common CPs such as PPy, PTh and PANI can be synthesized both chemically and electrochemically. However, several novel conducting polymers with modified monomers are only amenable to chemical polymerization. Electrochemical synthesis has been used to prepare homogeneous and self doped films. Besides this, it is possible to obtain copolymers and graft copolymers [160,168].

### 2.5.3 Applications of conducting polymers

The increasing number of academic, governmental and industrial laboratories throughout the world involved in basic research and assessment of possible applications of conducting polymers show that this area is interdisciplinary in nature. These conducting organic molecular electronic materials have attracted much attention largely because of their many projected applications in solar cells, light weight batteries, electrochromic devices, sensors and molecular electronic devices. Polymeric heterojunctions, solar cells have been fabricated by electrochemical deposition of PPy on n-silicon [169]. Many conducting polymers such as polyacetylene, polythiophene, polyindole, polypyrrole, polyaniline etc. have been reported as electrode materials for rechargeable batteries [170,171,172]. PANI is being used by Hitachi-Maxell for anti-static coating of 4 MB barium ferrite floppy disk [173]. In analytical chemistry the problem of selectivity, particularly at the low analyte concentrations and in the presence of interfering substances is of paramount importance. The development of sensors, which are highly selective and easy to handle opens the door to the problem in analysis. Conducting polymers have enough scope for the development of various sensors. A chemical or biosensor based on conducting polymers also relies on sensible changes in the optical and electrical properties of these materials.

#### 2.5.4 Polyaniline (PANI) as a conducting polymer

Polyaniline (PANI) is one of the most important conducting polymers and probably the oldest known synthetic organic polymer. The detailed study on its structures and properties only began in the 1980s [174]. PANIs have been of particular interest because of their low cost, ease of synthesis, unique redox tunability, good environmental stability, controllable electrical conductivity and interesting redox properties associated with the chain nitrogens. The aniline polymers also exhibit crystallinity and solution- or counterion-induced processability. Furthermore, the electrical properties of PANI can be substantially improved through secondary doping. Now it is generally accepted that PANI is a mixed oxidation state polymer composed of reduced benzenoid units and oxidized quinoid units (Figure 2.15(A)), with the average oxidation state given by  $(1-y)$ . PANI can exist in several oxidation states ranging from the completely reduced *leucoemeraldine base (LEB)* state (Fig.1-1(B)), where  $1-y = 0$ , to the completely oxidized *pernigraniline base (PNB)* state, where  $1-y = 1$ . The half-oxidised ( $1-y = 0.5$ ) *emeraldine base (EB)* state is composed of an alternating sequence of two benzenoid units and one quinoid unit. Each of the above mentioned three forms of PANI is an insulator, although they possess other interesting physical and chemical properties. However, the insulating EB form can be non-redox doped with protonic acids (HA) to yield the *emeraldine salt (ES)* form (also shown in Figure 2.15(B)), which shows a dc conductivity in the metallic regime (ca. 1~5 S/cm) [174]. The conducting ES form can also be obtained through a redox-doping process in acidic conditions from its corresponding reduced LEB form or oxidised PNB form by either a chemical or an electrochemical step (Figure 2.15(B)).



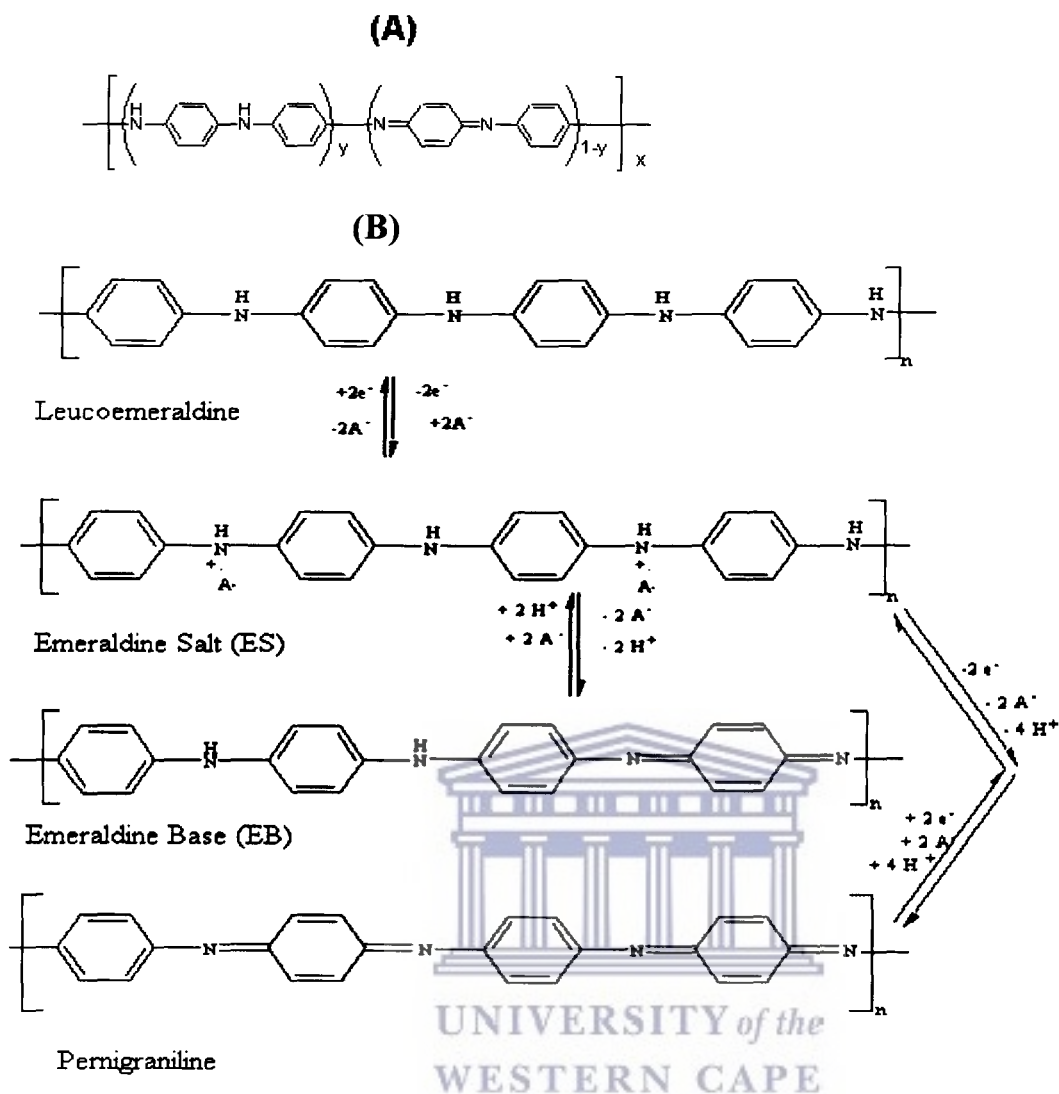
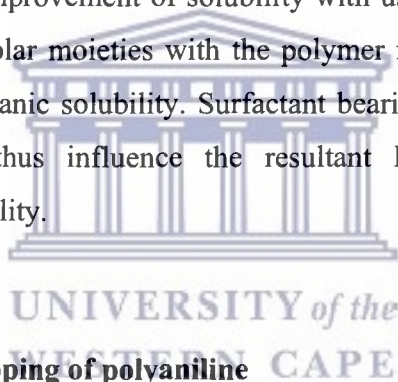


**Figure 2.15.** (A) The general polymeric structure of polyaniline. (B) Oxidation of aniline to polyaniline showing its redox states.

Polyaniline and its derivatives are generally synthesized by chemical or electrochemical oxidative polymerization of the respective aniline monomers in acidic solution, although some other approaches such as plasma polymerization [175,176], electroless polymerization [177], solid-state polymerization [178], biocatalysis [179], enzyme-catalyzed polymerization and photochemically initiated polymerization [180] have also been reported. It has been reported that the formation of polyaniline and its derivatives depend on the reaction conditions such as the type of supporting electrolyte, monomer concentration, applied potential, the type of solvent and

pH of the electrolyte [180,181]. The influence of anions on the electrodeposition of polyaniline and on polyaniline redox reactions has also been extensively described in literature [180,182,183,184]. These factors are known to determine the morphology and properties of the generated polyaniline. The difficult encounter with PANI is its low solubility in common organic solvents with an ultimate restricted processability. Several research studies have been directed towards improving its solubility in organic solvents to enable its utilization for suitable applications [185]. Substituted PANI became an alternative choice to have the desired properties. Incorporation of surfactant dopants within the PANI matrix promotes solubility besides enhancing the conductivity and the morphology of the resultant PANI [186]. Polymerization of a typical dopant, such as poly(vinylsulphonate) (PVS), resulted in soluble conducting polymer. In this case, the substituent groups (sulphonate:  $-\text{SO}_3\text{H}$ ) present in the units of the polymer chain caused decrease in the stiffness of the polymer chain to result in better solubility. The presence of sulphonate - units in the backbone of conducting polymer is expected to improve its solubility and redox characteristics. The improvement of solubility with use of PVS was attributed to the introduction of polar and non-polar moieties with the polymer matrix which promoted solvent compatibility with improved organic solubility. Surfactant bearing sulphonic groups can act as both stabilizers and dopants thus influence the resultant PANI properties in terms of conductivity, stability, and solubility.



#### 2.5.4.1 Conductivity and doping of polyaniline

Conductivity is a measure of electrical conduction and thus a measure of the ability of a material to pass current. Doping is the process of oxidizing (*p*-doping) or reducing (*n*-doping) a neutral polymer and providing a counter anion or cation (i.e., dopant), respectively [159,185]. It is well known that  $\pi$ -conjugated polymeric films or coatings may undergo oxidation and reduction from their electrically neutral, non-conductive state, with the formation of electrochromic, highly conductive *p*- and *n*-doped states. Figure 2.16 attempts to illustrate the concept of *n*- and *p*-doping. This process introduces mobile electronic charge carriers, in the form of charged polarons (i.e., radical ions) or bipolarons (i.e., dications or dianions), into the polymer chain. The attraction of electrons in one repeat-unit to the nuclei in neighbouring units yields charge

mobility along the chains and between chains, often referred to as “electron hopping”. The ordered movement of these charge carriers along the conjugated polymer backbone produces electrical conductivity. Doping of CP can be achieved chemically or electrochemically. Polyaniline has an electronic conduction mechanism that is unique among CPs, because it is doped by both protonation and the *p*-type doping. This results in the formation of a nitrogen base salt rather than the carbonium ion of other *p*-doped polymers. The conductivity of PANI depends on both the oxidation state of the polymer and its degree of protonation. The oxidation state of PANI that can be doped to the highly conducting state is *emeraldine*. Protonic doping in PANI can be achieved through the protonation of the imine nitrogens of the polyemeraldine form of PANI using strong acids [187]. This leads to the production of highly conductive, delocalized, stable polysemiquinone radical cation, the polyemeraldine salt form of PANI. It has also been reported that the conductivity of PANI is dependent on the solvent it is cast from or exposed to. This phenomenon has been referred to as “secondary doping.” The solvent causes a change in the polymer conformation that result in increased conductivity. However, the most significant dependence of the conductivity of PANI is upon the proton doping level. The maximum conductivity occurs when PANI is 50 % doped by protons [180,187]. At doping levels higher than 50 %, some amine sites are protonated, and at levels lower than this some imine sites remain unprotonated. In both instances, delocalization of the charge carriers over the polymer backbone is disrupted, thereby reducing the polymer conductivity.

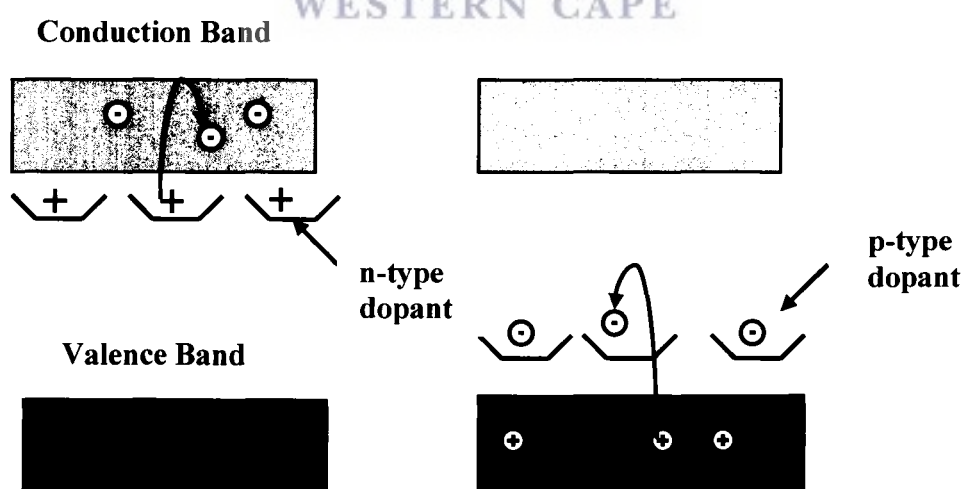
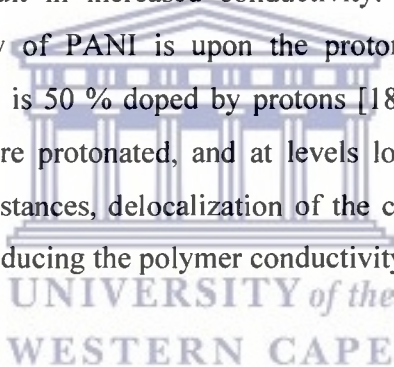


**Figure 2.16.** An illustration of n and p- doping processes respectively.

The first diagram shows electrons flowing from a donor (n-type) dopant to the conduction band (CB). Second diagram shows the acceptor dopant (p-type) receiving electrons from the valence band (CB) leaving positive charges or holes in the polymer backbone.

#### **2.5.4.2 The concept of sulphonated polyaniline (SPAN)**

A different approach to obtain self-doped polyaniline employs electropolymerization of monomers containing anionic groups. From the applied point of view the electrochemical polymerization of cheap, simple aromatic benzoid or nonbenzoid and heterocyclic compounds is of utmost interest. Electrochemical polymerization is preferable than chemical oxidation if the polymeric product is intended to use as a polymer film electrode because the potential control is a precondition of the production of good-quality material and the polymer film is formed at the desirable spot that serves as an anode during the synthesis.

The sulphonated polyaniline (SPAN), a water soluble conducting polymer is interesting because of its unusual electroactive properties, improved processability and potential industrial applications [188,189]. Self-doped polyanilines have more stable and reproducible electrical properties and higher thermal stability than polyaniline (PANI) and showed a pH-independent conductivity from pH 0 to 14 [189,190]. The SPAN polymer has faster electronic, electrochemical, chemical, and optical responses and improved solubility than the parent polymer, polyaniline. The solubility of the SPAN polymer is increased greatly due to the presence of the sulphonic group  $-SO_3H$ . The SPAN polymer is easy to dissolve in basic aqueous solutions in which the polyaniline polymer is insoluble. In addition, due to the electron withdrawing effects of the  $-SO_3H$  group, the SPAN polymer has improved environmental stability over the polyaniline polymer [190]. The process for producing the SPAN comprises reacting the polyaniline polymer with concentrated sulfuric acid. The course of an electropolymerization by potential cycling depends on the experimental conditions (composition of the solution; potential range, particularly the positive limit; potential scan rate; electrode material etc).

### 2.5.5 pH sensitivity and switching properties of polyaniline

Polyaniline undergoes two distinct redox processes as well as pH switching between unprotonated and protonated states [180,191]. The influence of pH on the redox processes of PANI was investigated by MacDiarmid and co-workers [192]. It was found that the potential of the second redox transition shifts cathodically with increasing of pH for 0.12 V/pH. The reason for this behaviour is the release of protons in the redox conversion from emeraldine salt to pernigraniline base. The redox processes are readily observed using cyclic voltammetry. The most conductive form of PANI, *emeraldine salt* occurs between approximately + 0.20 and +0.60 V vs. Ag/AgCl. At less positive potentials, the fully undoped form (*leucoemeraldine*) is much less conductive, as is the fully oxidized form (*pernigraniline*) at higher potentials. If PANI is exposed to potentials higher than the second oxidation process, a third voltammetric response appears upon cycling the potential. This is due to oxidation/reduction of a degradation product [193].

The insoluble degradation products are formed, probably due to chain scission by hydrolysis of amine groups to form benzoquinone and acrylamine terminations. The chemical properties of PANI can be controlled by application of potential, base or acid. Not only do the conductivity and chemical properties of PANI change, the colour of the polymer also changes between each of these states. It is transparent in the reduced state and when oxidized, it changes to green (at ~ +0.2 V) and then to blue upon further oxidation. High colour contrast is usually observed for thick films (> 1  $\mu\text{m}$ ) of PANI but it is achieved at the expense of switching speed [194]. It has been reported that the rate of switching of PANI depends on the electrolyte used (with smaller ions the switching is faster), the solvent employed and the protonation level of the solution while the peak potentials vary with the pH [194,195]. It has also been observed that, when polyelectrolytes are incorporated as dopants in PANI, the switch from conducting to non-conducting material is shifted to very high pH solutions, enabling electrochemistry to be carried out on polyaniline in neutral solutions [195].

Polyaniline can be “switched” by the addition of acids and bases that protonate and deprotonate the base sites within the polymer. This leads to the dependence of the polymer states, and thus

the reactions, upon the pH of the solutions. In solutions of pH greater than 4, PANI loses its electroactivity entirely because the *emeraldine salt*, the only conducting form of the polymer is dedoped to form the insulator *emeraldine base* (EB) [180,195]. The doping reaction of PANI is the same as the one that occurs during polymerization process, and the dedoping reaction is the reverse process. The pH and potential dependencies of conductivity and optical absorption of PANI at 420 nm were reported. Later such investigations were extended to other spectral ranges and also for derivatives of PANI [180,195]. The largest spectral changes due to deprotonation of emeraldine salt are usually observed between pH 5 and pH 8, whereas only small changes are observed between pH 2 and pH 5. Because of hysteresis in the transfer between different forms of PANI, the main spectral changes during decrease of pH are observed between pH 6 to pH 3. This leads to strong limitation of the working range of such sensors [191,193,195]. Polyaniline has been shown to exhibit the same redox behaviour in both aqueous and non-aqueous media [193,195]. However, in organic solvents, the second (more positive) oxidation response is irreversible, due to the lack of protons in such media.

### **2.5.6 Preparation of PANI composites/blends with other copolymers**

Another route towards more processable PANI has been through composite or blend formation. Preparation of polyaniline composites/blends with suitable polymers has been achieved through the in-situ or ex-situ polymerization processes [196]. In the in-situ polymerization process, the polymerization of the monomer (aniline) is carried out in the presence of a polymeric host stabilizer. For instance, the polymerization of aniline monomers in the presence of water soluble polymeric stabilizers such as polyvinyl sulphonate (PVS), polyvinyl pyrrolidone (PVP), polyvinyl alcohol (PVA), polystyrene sulfonic (PSSA), and polyacrylic acid (PAA) has been found to produce water soluble polyaniline composites/ blends [197]. The improved water solubility after co-polymerization is associated with the formation of hydrogen bonding linkages between PANI and the co-polymer thereby enhancing PANI solvation. Figure 2.17 shows an illustration of polyvinyl sulphonate (PVS) copolymer structure.



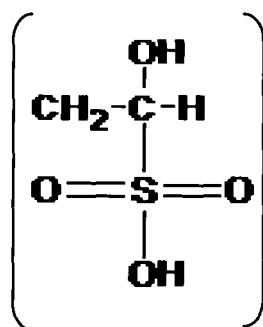


**Figure 2.17.** An illustration of polyvinyl sulphonate (PVS) copolymer structure.

### 2.5.7 Counter-ion induction techniques

Counter-ion induced processability method involves the post synthetic protonic doping of chemically synthesized undoped PANI with suitable functionalized protonic acid dopants. It is therefore a type of secondary doping phenomenon attributable to the expanded coil conformation adopted by doped PANI in a suitable solvent [188,197]. The protonic acids are found to induce the solubility of doped PANI in polar or weakly polar solvents. However, since the counter-ion method is a post synthetic process, this would unnecessarily increase the time required for PANI production.

### 2.5.8 Shortcomings of the solubilization approach

Despite the above efforts to improve the solubility of chemically synthesized PANI, solubility is still an issue of concern. First, complete solubilization of PANI in cheap ordinary organic solvents such as hexane, methanol etc. has not yet being achieved. Furthermore, even with the use of polar solvents, sometimes only partial solubility has been achieved. Second, the introduction of bulky substituent into the PANI backbone has been found to hamper other desirable PANI properties such as conductivity due to increased steric hindrance. For these reasons, a combinational approach is now found more favourable towards more processable



PANI. In such approach, the chemical synthesis of PANI/or PANI derivatives is carried out in the presence of nanostructuring aids which at the same time may have solubilizing properties.

### **2.5.9 Nanostructuring approaches**

The prefix nano is used to represent materials with grain sizes in the order of a billionth of a meter. A composite refers to a material that is made up of two or more constituents which exhibit different physical/chemical properties and which remain separate/distinct within the finished structure. Polyaniline nanocomposites have been prepared for various reasons which include; improving dispersibility (processability), to improve conductivity, to create new smart materials for future technological use. This has been achieved because polyaniline nanocomposites have increased stability and a high surface to volume ratio.

### **2.5.10 Processability**

Since the intractability, i.e., infusibility and insolubility, is the major factor hampering its large scale applications, dispersing of the polymer in common solvents is regarded as one of the most effective approaches to address this problem from both the scientific and technological point of view [198,199]. Accordingly, synthesis of nano-structured PANI, on one hand, is the key step in preparing highly dispersed blend of PANI with other processable polymers, and thus to improve the processability of PANI. On the other hand, nanostructuring will bleed new smart materials for new applications [199]. The fabrication of more dispersible nanosized PANI has been reported by many works [200,201,202,203]. Accordingly, nanostructuring of PANI has mainly been achieved through two processes; the template and the template free processes. Nanostructuring through the template synthesis method involves the placement of suitable nano-pored templates in the polymerisation bath [204]. Polymer deposition within the nano-pores moulds them into nano-shapes. Figure 2.18 displays the structures of two of the most commonly used membranes for the template assisted nanostructuring.

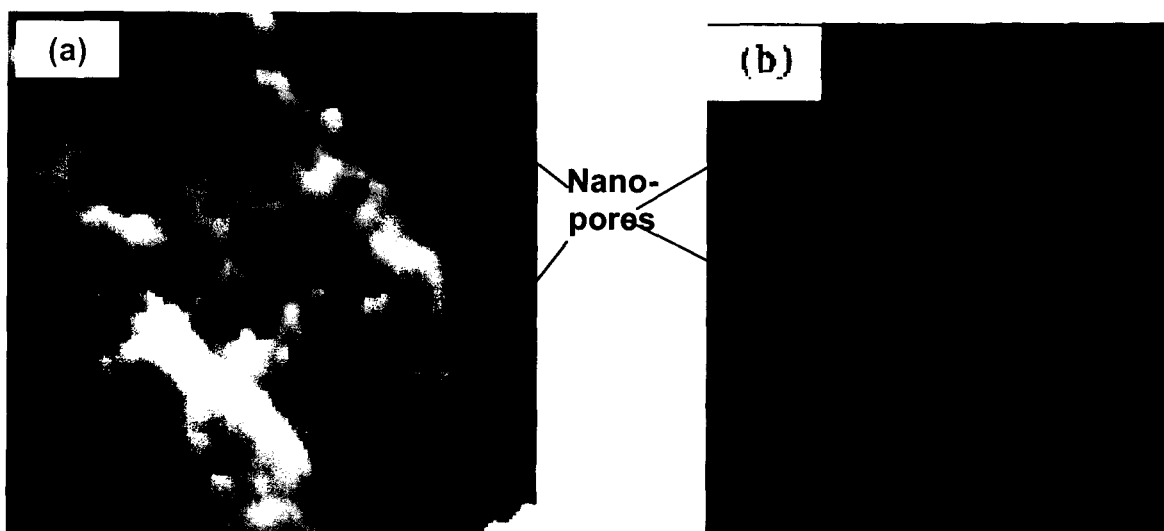


**Figure 2.18.** A poly-carbonate track-etched membrane (PCM) (a) and an anodic alumina membrane (ALM) (b) showing uniformly sized nano-pores within which polymer deposition takes place [204].

Using the template synthesis in anodic alumina pores (ALM), Yang et al., prepared nanosized polyaniline particles which took the rod like shape [204]. The dispersible rods were found to exhibit uniform diameters. The authors discovered that although the resultant materials were in the nano-range and therefore more dispersible, the mechanisms of formation of the resultant nanotubular structures were different. The PANI nanotube formation began in the polymerisation bath before deposition into the membrane pores. For PVS the process began by the adsorption of sulphonate-aniline monomers onto the membranes followed by polymerisation.

Although the template synthesis has been used greatly to obtain dispersible nanosized PANI and that it yields uniformly sized nanostructures (which might be an added advantage), several limitations have been associated with this process. One, the template synthesis demands the post-synthetic removal of template and two; it demands the use of a ‘molecular anchor’ to maintain the nanostructures the shapes which in itself is a challenge and three; the need for the post synthesis template dissolution is limiting in itself because only those templates with a corresponding dissolving solvent can be used [187,205].

Therefore, new approaches towards PANI dispersibility through nanostructurization are now focused on use of ‘inbuilt templates’ or ‘soft templates’ [187,198,205]. The method entails the synthesis of PANI/PANI derivatives in the presence of structure-directing materials such as surfactants, nucleic acids, polyelectrolytes, polyvinyl sulphonate (PVS), sulphonated porphyrins amongst others [198]. Naphthalene sulfonic acid [187], camphor sulphonic acid [163,205], dodecyl benzene sulphonic acid [206] are some of the complex acids with bulky side groups that have been used for the production of one dimensional dispersible PANI. Surfactant molecules in solution exist in micellar form leaving nanoscopic spaces available for monomer polymerization (Figure 2.19).

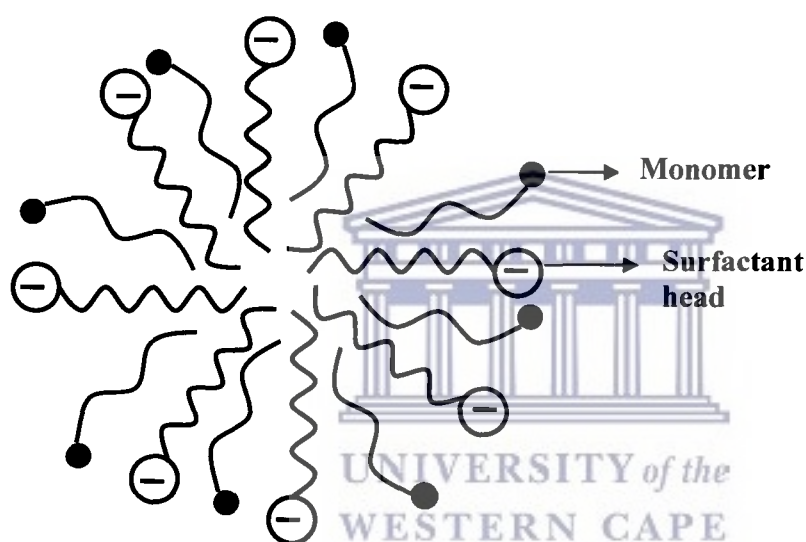


**Figure 2.19.** A schematic diagram showing the micelle-monomer orientation adopted by an anionic-surfactant in a polar solvent during template-free polymerization process.

Surfactants act as soft templates for nanostructurization. Several advantages accompany the use of the ‘soft template’ method to improve processibility. Nanostructurization of PANI leads to increased surface area which boosts its stability and conductivity. Also through the ‘soft template method’, several one dimensional structures taking various forms depending on the nature of template can be obtained.

Besides processability improvement, conductivity and morphology are also improved. By variation of the polymerization bath additives, PANI-composites tailored to suit various applications have been produced. Compared to other methods, the template free method is simple, cheap and is very desirable for the improvement of PANI dispersibility and gives room for the improvement of other properties as well. Although the control of the diameters of the nanostructures is not easily achieved through this method, it is an avenue for the fabrication of many new smart materials (composites) achieved by just varying the contents of the polymerization bath.

### **2.5.11 Electrosynthesis of polyanilines**

Besides the chemical synthetic route, conducting polymers has been prepared through electrosynthetic routes [207,208]. Three electrosynthetic approaches have generally been use namely; potentiostatic, galvanostatic and potentiodynamic techniques. Potentiostatic technique involves the electrodeposition of the polymer on the electrode by the application of constant potential. In galvanostatic methods the polymerisation is achieved by application of a constant current. The cyclic voltammetric technique on the other hand involves sweeping the potential of the electrode to and fro between predetermined potential limits, upon which electrodeposition takes place on the surface of the electrode.

The potentiostatic deposition of optically active polyaniline salts of camphor sulphonic acid have been reported [209]. The chiral PANI-HCSA composites were co-doped with polystyrene sulphonic acid and exhibited great water solubility. The potentiostatically deposited films displayed two redox couples at 0.155 V and 0.515 in HCl, the couples been associated with the oxidation states of polyaniline [210]. Elsewhere, polyaniline-polycarbonate composites were potentiostatically deposited by first dipping the electrode in polycarbonate solution (1 %  $\text{CHCl}_3$ ) followed by the electrodeposition of polyaniline on to the electrode by the application of a constant potential for 12 h. The casting solution consisted of 0.1 M aniline and 0.1 M HCl [211]. The potentiostatic deposition of poly-*o*-methoxyaniline doped with camphorsulphonic acid was carried out on a platinum (Pt) or indium tin oxide (ITO) electrodes by a applying a constant

potential of +0.8 V or 1.1 V respectively. The resultant films were green in nature and chronoamperograms revealed that the electrodeposition process was two phased involving the nucleation and the polymer growth stages [211].

The galvanostatic electrodeposition of polyaniline has been reported [211,212]. Poly-*N*-methylaniline (PNMA) was electrodeposited through potentiostatic and galvanostatic methods [213]. According to these authors, potentiostatic deposition of PNMA could be effected with potentials as low as 0.55 V. However, the resultant polymer dissolved in the electrolytic solution to give a blue coloration which indicated that there was a high tendency to form oligomers. On application of an optimal current density of 2 mA cm<sup>-2</sup> galvanostatically deposited PNMA was a greenish black uniform film with good adhesion which led the authors to conclude that galvanostatic technique was superior to the potentiostatic one. Also, tungsten trioxide based polyaniline films were prepared by the galvanostatic polymerization of aniline in an aqueous HCl solution containing suspended tungsten trioxide particles with the application of a current density of 1 mA cm<sup>-2</sup>. Free standing films were obtained [210,213]. Recently, polyaniline formation through pulse potentiostatic methods (PPM) and pulse galvanostatic methods (PGM) has been reported [214]. But the majority of the works report the electrodeposition of polyanilines using cyclic voltammetry (CV). It has been said that CV produces stable thin homogeneous compact films unlike in the case of both potentiostatic and galvanostatic electrodeposition [182,215]. The electrodeposition of PANI and *N*-alkyl PANI on glassy carbon or quartz glass tin oxide (TO) coated electrodes using, HCl, HClO<sub>4</sub> or DBSA solutions have been reported [216]. According to the authors, the initial polymerisation rate for the aniline monomers was slower than that of the *N*-alkyl monomers but the situation changed beyond 50 cycles. A layer of polyaniline was cast on a platinum electrode on the potentiodynamic mode form solution containing 0.2 M aniline in 1 M HCl between -200 and +1100 potential limits for 10 cycles [68,216]. In this report an initial oxidation of polyaniline occurred at +900 mV followed by the formation of three well formed redox couples characteristic of polyaniline.

### 2.5.12 Factors affecting the electrodeposition processes

A study was conducted to investigate the effect of anions on the electrodeposition of polyaniline. The various effects were marked with peak shifting, decrease in polymerization current as well as in the degradability of the polymer. Of all the anions studied, the PANI-SO<sub>4</sub><sup>2-</sup> system showed the highest degree of degradation followed by PANI-Cl. Slight or no degradation was observed in PANI doped with surfactant anions even at pH 4.0. The presence of surfactant ions stabilized the PANI and the stabilization trend was found to follow DS<sup>-</sup> > DBS<sup>-</sup> > TS<sup>-</sup> where the anions originated from sodium dodecyl sulphate, sodium dodecyl benzene sulphonate, toluene sulphonated surfactants respectively [217]. The authors associated the observed trend to the different surfactant head group charges, distance of anion from PANI positive sites and to the shielding effect of anions on the PANI positive sites. The rate of polymerization may also be affected by the nature of substituent and the position of substituent on the ring. According to Roković et al., [218] on studying the effect of different substituent on the polymerization rate suggested that a substituent in the ortho position leads to longer polymerization rate and decreased molar mass. Anions present on the polymerization bath may affect the monomer oxidation potential and the mechanisms of nucleation because different anions are adsorbed at the electrode.

A comparison between the Cl<sup>-</sup>, HClO<sub>4</sub><sup>-</sup>, HSO<sub>4</sub><sup>-</sup> revealed that the rate of electropolymerization was higher in the Cl<sup>-</sup> than in the presence of either the HClO<sub>4</sub><sup>-</sup> or HSO<sub>4</sub><sup>-</sup>. To justify this trend, the authors argued that the formation of ion pairs between the anilium cations and/or positive charges in the polymer backbone controlled the polymerization rate. The ongoing discussion illustrates the superiority of sulphonated heteronuclear aromatic hydrocarbon doped polyaniline over PANI doped with simple anions such as Cl<sup>-</sup>, SO<sub>4</sub><sup>2-</sup> etc. Faster polymerization rate was observed in the Cl<sup>-</sup> system because the latter formed stronger ion pairs. However, PANI-doped with bulky sulphonic acids is electroactive even at neutral pH a characteristic which is very favourable for biosensor applications since enzymes operate best around their physiological pH usually around pH 7.0.



### 2.5.13 Reported Kinetic parameters on polyaniline systems

The utility of an organic conducting polymer is measured in terms of the rate of electron hopping along the polymer units as well as the rate at which electron transfer occurs across the interface. The calculation of diffusion coefficient ( $D_e$ ,  $\text{cm}^2/\text{s}$ ) and the standard rate constants  $k^0$  ( $\text{cm}/\text{s}$ ) can serve as a useful tool for prediction of polymer value especially for sensor applications. An electrosynthetic PANI film doped with polyvinyl sulfonate (PVS), exhibited a diffusion coefficient value of  $6.46 \times 10^{-8} \text{ cm}^2/\text{s}$  [182]. Polystyrene sulfonic acid doped PANI (PSSA) exhibited a  $D_e$  value of  $8.68 \times 10^{-9} \text{ cm}^2/\text{s}$ . The lower  $D_e$  value of the PANI/PSSA film as compared to that of PANI/PVS was attributed to different electrodeposition conditions, film homogeneity as well as dopant size [68, 182,219]. Langmuir-Schaeffer equation was used to estimate the  $D_e$  value of a glass substrate deposited POMA layer. Diffusion coefficient values of  $2.6 \times 10^{-7}$  and  $1.9 \times 10^{-8} \text{ cm}^2/\text{s}$  were estimated for the nucleation and diffusional controlled growth processes respectively [219]. Nanocomposites of multi-walled carbon nanotubes (MWNTs) embedded in POMA synthesized through the oxidative polymerization process exhibited  $D_e$  values in the range of  $1.78 - 0.75 \times 10^{-8} \text{ cm}^2/\text{s}$  in different supporting electrolytes. Thus in general, the observed  $D_e$  and  $k^0$  are a function of the polymer preparation conditions as well as the exact nature of the polymer. It is expected that substituted polyanilines should exhibit lower  $D_e$  and  $k^0$  than the parent polyaniline so long as the polymers are synthesized under the same conditions. The argument is based on the fact that the presence of substituent in the polyaniline chain causes steric hindrance with consequences of increase interchain distance and a lowered frequency of electron hopping along the polymer chain [220].

### 2.5.14 Spectroscopic determination of the redox states of polyaniline

The common spectroscopic techniques, such as Fourier transform infrared (FTIR) and UV-Vis spectroscopy have been used to provide qualitative indication of the intrinsic redox states of conducting polymers and to predict successful doping [221,222]. It has generally been observed that the FTIR and UV-Vis spectra of unsubstituted PANI are similar to those of substituted PANI though with slight band shifts. Earlier studies suggested that the IR absorption modes at about  $1500 \text{ cm}^{-1}$  and  $1600 \text{ cm}^{-1}$  are associated with aromatic ring stretching assigned the  $1600 \text{ cm}^{-1}$  peak to the quinonoid ring and the  $1500 \text{ cm}^{-1}$  peak to the benzenoid ring [183,222]. The IR



absorption spectrum of *leucoemeraldine* indeed exhibits a very low intensity ratio of the  $1600\text{ cm}^{-1}$ : $1500\text{ cm}^{-1}$  peaks, consistent with the presence of predominantly benzenoid units. On the other hand, *emeraldine base*, which consists of about equal amounts of benzenoid (B) and quinonoid (Q) units, has about equal intensities for the  $1600\text{ cm}^{-1}$  and  $1500\text{ cm}^{-1}$  absorption bands. Furthermore, the IR absorption spectra of *pernigraniline* exhibits an enhanced quinonoid to benzenoid band intensity ratio [223,224]. Another informative peak in the IR absorption spectra of PANI is the weak C-N stretching absorption in QBQ units at about  $1380\text{ cm}^{-1}$ . *Leucoemeraldine* does not absorb at this frequency while *emeraldine* does. The appearance of a small amount of quinonoid imine units in partially oxidized *leucoemeraldine* is accompanied by the appearance of a weak  $1380\text{ cm}^{-1}$  absorption band. However, upon acid protonation of *emeraldine base*, the quinonoid units are believed to be converted to benzenoid units by a proton-induced spin-unpairing mechanism and the absorption band at  $1380\text{ cm}^{-1}$  disappears [225]. In the case of protonated *emeraldine*, the long absorption tail above  $2000\text{ cm}^{-1}$ , which masks the NH stretching vibration in the  $3100\text{-}3500\text{ cm}^{-1}$  region, and the appearance of the intense broad band at about  $1150\text{ cm}^{-1}$ , have been associated with high electrical conductivity and a high degree of electron delocalization in the polysemiquinone forms of the doped PANI [225]. Patil et al. reported the manifestation of the ‘electronic like band’ associated with high conductivity of PANI due to polarons at ca.  $1100\text{ cm}^{-1}$  [221,225]. Table 2.2 summarizes the assignments of IR absorption bands for PANI [226]. For UV-Vis spectroscopy, the lowest energy absorption band for *leucoemeraldine base* (LEB) occurs at ca. 320 nm and may be assigned to the  $\pi\text{-}\pi^*$  electronic transition, i.e., between the valence and conduction bands. For *emeraldine base* (EB), there occurs a similar low wavelength  $\pi\text{-}\pi^*$  band as well as a strong band at ca. 600 nm that has been attributed to a local charge transfer between a quinoid ring and the adjacent imine-phenyl-amine units giving rise to an intramolecular charge transfer exciton ( $\pi\text{-}\pi^*$  quinoid ring) [163,181,211,227]. *Pernigraniline base* (PNB) also exhibits two absorption peaks: a  $\pi\text{-}\pi^*$  band at ca. 320 nm and a band at ca. 530 nm assigned to a Peierls gap transition [181,227]. However, in the presence of dopants, new electronic energy levels are introduced within the polymer sub-gap energies due to more energetically favourable intra-gap transitions [228]. This corresponds to the appearance of polaronic and bipolaronic bands in their spectra and the consequential introduction of charge carrier-electrons or holes within the polymer chain. Protonation of PNB causes a violet-to-blue colour change due to the formation of *pernigraniline*

*salt* (PNS). This change is associated with the loss of the PNB band at 530 nm and the appearance of a strong PNS peak at ca. 700 nm. *Emeraldine salts*, on the other hand typically exhibit three peaks in their “compact coil” conformation: a  $\pi$ - $\pi^*$  (band gap) at ca. 330 nm and two visible region bands at ca. 430 and 800 nm that may be assigned as  $\pi$ →polaron band and polaron→ $\pi^*$  band transitions, respectively [186,205,228]. The appearance of the quinoid  $\pi$ - $\pi^*$  transition band at ca. 600 nm in the spectra of doped PANI is however indicative of incomplete doping [229].

**Table 2.2.** Assignments for FTIR absorption bands for polyaniline

Frequency (cm <sup>-1</sup> )	Assignment
3460	NH <sub>2</sub> asymmetric stretching
3380	NH <sub>2</sub> asymmetric stretching, NH stretching
3310	H-bonded NH stretching
3170	=NH stretching
2930	Impurity or sum frequency
2850	Impurity or sum frequency
1587	Stretching of N=Q=N
1510	Stretching of N-B-N
1450	Stretching of benzene ring
1380	C-N stretching in QBtQ
1315	C-N stretching in QBcQ, QBB, BBQ
1240	C-N stretching in BBB
1160	A mode of N=Q=N
1140	A mode of Q=N+H-B or B-NH-B
1220	C-H in-plane bending of 1,4-ring
1105	
1010	
1115	C-H in-plane bending of 1,2,4-ring
1060	
960	
910	C-H out-of-plane bending of 1,2,4-ring
895	
850	
830	C-H out-of-plane bending of 1,4-ring
740	C-H out-of-plane bending of 1,2-ring
690	
645	Aromatic ring deformation
530	
500	

Abbreviations: B, benzenoid unit; Q, quinonoid unit; t, *trans*; c, *cis*

### 2.5.15 Scanning Electron Microscopy

Different PANI morphology has been reported. Granulated [230], nanotubular, grain like, spherical, nanofibrillar, rodular amongst others [231,232]. According to Wei et al., the resultant morphology is dependent on the synthesis conditions [231]. The variation of the monomer: dopant ratio, synthesis temperature, type of templating molecule, synthesis methodology etc. play a key role towards the determination of the final PANI morphology. By varying the monomer: dopant ratio, [231,232] could manipulate the sizes of the resultant nanoparticles. Huang et al., predominantly produced the nanofibrillar PANI through the interfacial polymerization process [233]. By varying the synthesis temperature, Zhang and Wan, could manipulate the morphologies of the resultant PANI [234]. At a synthesis temperature of about 15 °C, the resultant tubes were thick, short and about 180 nm wide and 0.6 μm in length with intermingled granular structures. However, at 0-5 °C, the tubular structures were 140 nm wide and 3 μm long. The recent interest in nanotubular or nanofibular PANI emanates from the fact that these one dimensional structures are a kind of desirable wire-like material with metallike and controllable conductivity [231,232,234]. It has been shown that aliphatic and heteronuclear aromatic sulphonated acids such as DBSA, NSA, CSA can be utilized reliably to obtain this one dimensional structures [163,231,234,235]. The type, shape and size of dopant type can depend on synthesis conditions. Similar morphologies have been reported for PVS [151].



### 2.5.16 Synthesis of nanostructured polyaniline

The processability and applicability of the synthesized conventional PANI have been mostly hampered by its infusibility or insolubility in organic solvents due to its rigid  $\pi$ - $\pi$  conjugation system. Several strategies have therefore been employed to overcome and improve the solubility of PANI in organic solvents to enable its utilization for suitable applications. Accordingly, synthesis of nanostructured PANI has become the key step in preparing highly dispersed blends of PANI with other processable polymers, and thus the improvement of the processability of PANI. Apart from the physical routes like electrospinning, mechanical stretching, and the doping induced solution route, the chemical approaches adopted for production of one-dimensional nanostructured PANI can be generally categorized into the chemical oxidative way and the

electrochemical oxidative way, just as the ones employed for the synthesis of the conventional PANI powders [162]. The template synthesis method commonly used for the production of one dimensional nanostructured PANI is further subdivided into hard template (physical template) synthesis and soft template (chemical template) synthesis approach according to the solubility of the templates in the reacting media. Non-templated routes for the synthesis of one-dimensional nanostructured PANI such as rapid mixing reaction method, radiolytic synthesis, interfacial polymerization, and sonochemical synthesis have also been reported [236]. Other approaches like combined soft and hard template synthesis are also known.

### **2.5.17 Properties of nanostructured polyaniline**

FTIR and UV-Vis spectroscopy studies have revealed that all PANI nanotubes, nanofibers, nanowires, nanorods, as well as microtubes, have backbone structures similar to that of the conventionally prepared granular PANI [236,237]. In some cases, the Einstein shifts observed in the FTIR and UV-Vis spectra originated from the interaction between the PANI chains and some small molecules, such as ethanol, not from the chemical structures. Conductivity measurement of the hard-template synthesized PANI nanotubules showed that the conductivities decreased with the increase of the diameters, and finally reached the conductivity of the conventional PANI powder [236,237].

UNIVERSITY of the  
WESTERN CAPE

## **2.6 Boron-doped diamond (BDD) thin film electrodes**

### **2.6.1 Introduction**

Diamond is an excellent candidate for electrode material when properly doped resulting in adequate conductivity, as is the case of boron-doped diamond (BDD) thin films [238]. These films have properties such as high stability in the presence of strong oxidizing species, good chemical and electrochemical stability and low background current.

BDD thin films are found to be particularly attractive for electrolysis and electroanalytical applications due to their outstanding properties, which are significantly different from other conventional electrodes, e.g., glassy carbon (GC) or platinum (Pt) electrode [239]. GC is widely used for working electrodes particularly for analytical applications because of its relatively wide potential window in comparison with metal electrodes such as gold (Au) and Pt. The surface of GC, like those of many solid electrodes, may become deactivated as a function of time when it is exposed to the room atmosphere or working solution. BDD electrodes appear to be relatively free from such problems. In addition to original properties of diamond such as hardness, high thermal conductivity and chemical inertness; BDD provides a wide electrochemical potential window in both aqueous and non-aqueous media (-1.35 to 2.3 V/ NHE), very low capacitance, extreme electrochemical stability [240,241] and high potential at which oxygen evolution occurs by water oxidation [242]. These properties make BDD more suitable for electrochemical reactions with compounds that have highly positive standard potentials and which cannot be detected or produced using classical electrode materials.

Although the properties of BDD electrodes make BDD an attractive material, factors such as the dopant concentration, the surface termination, non-diamond carbon impurities and the crystallographic orientation do influence the electrochemical behavior of BDD electrodes [243–246]. The material can be used in electroanalysis and electrolysis. In the electroanalysis, BDD electrodes provide low detection limits for analytes with precision and stability. In the electrolysis, high-current density (1-10 A/cm<sup>2</sup>) observe in solution without any microstructural or morphological degradation, prove as a corrosion-resistant electrocatalyst support, and as an optically transparent electrode for spectroelectrochemical measurements [247,248]. This advanced carbon electrode provides researchers with a material that meets the requirements for a wide range of applications.

## 2.6.2 Carrier mobility of diamond

At room temperature, single-crystal Chemical Vapor Deposition (CVD) diamond displays both the highest electron and hole mobilities at any semiconductor (with wide-bandgap of 5.45 eV), which is clearly an immensely attractive property. Electron and hole mobilities of about  $4500 \text{ cm}^2\text{V}^{-1}/\text{s}$  and  $3800 \text{ cm}^2\text{V}^{-1}/\text{s}$ , respectively, have been reported [259]. Impurity scattering causes the mobility to drop with increasing dopant concentration, therefore, boron-doped diamond can exhibit good hole mobility. In devices where the active region consists of purely inherent diamond, the drop in mobility with dopant concentration is not appropriate as the challenge is to achieve impurity-free material. However, a higher carrier lifetime is an indication of a low impurity and defect concentration and thus an important material quality indicator. Carrier lifetimes of more than 2 microns ( $\mu\text{s}$ ) have been measured in single-crystal CVD diamond [249,250]. In natural diamond, lifetimes of less than a nanosecond are typical.

## 2.6.3 Doping of diamond

Intrinsically, diamond is an insulator. However it can be doped with boron, fluorine or nitrogen, in order to improve its conductivity considerably. Boron doping is readily achieved by adding diborane ( $\text{B}_2\text{H}_6$ ) or trimethyl borate (TMB),  $\text{B}(\text{OCH}_3)_3$ , to the stream or placing boron powder near the edges of the substrate prior to insertion into the CVD chamber [251-255]. With increasing concentration of the doping, the insulator behavior of diamond can change to that of a semiconductor and then into metallic behavior. Two types of doping are possible: positive (p-type) and negative (n-type) [256]. Positive doping consists of substituting some carbons by an atom having a similar size and one less electron than carbon, (*e.g.* boron) [257]. The doping atoms reside at an electronic level just above the valence band of diamond. In the case of negative, doping atom has an extra electron (*e.g.* nitrogen). The boron doping atoms, which are electron acceptors, have free electrons in the dopant band and holes or vacancies in the valence band, to sustain the flow of current [252,257].



The electrical resistivity of BDD films also depends on the doping level in the diamond coating. Next to the doping level, the surface termination is probably the most important issue for controlling the electrochemical behavior. The as-deposited boron-doped diamond surface is hydrogen-terminated with a hydrophobic character; it is stable in air without any apparent degradation for several months. Boron-doped diamond is described as a degenerated semiconductor material with a quite high charge density on its surface due to the boron doping ( $>10^{21}$  boron atoms  $m^{-3}$ ), non diamond ( $sp^2$ ) carbon and surface species. This distribution of charges on its surface promotes the process of electron transfer across the interface between the diamond and the electrolyte [252,257]. The particles deposited onto the diamond surface (graphite) increase the surface charge density until reaching a perfect metallic behaviour. Since a charge transfer occurs onto the deposited particles, the modified diamond electrodes surface can show the electrochemical properties of the deposited material.

#### 2.6.4 Factors influencing the electrochemical behavior of BDD electrodes

The factors that can influence the electrochemical behavior of boron-doped diamond (BDD) electrodes are the crystallographic structure [258,259], the surface functional groups [260-262], the boron doping level [263,264], and the presence of nondiamond amorphous carbon impurities ( $sp^2$ ) [258,265,266]. The preparation conditions and the surface treatment have also a strong effect on the electrochemical behavior of diamond electrodes [261,267,268]. On the other hands, the factors such as boron dopant density, surface termination and cleanliness of the growth process can influence the electrochemical behavior of BDD. In the boron dopant density, the boron dopant levels of ca.  $2 \times 10^{20}$  atoms  $cm^{-3}$  the material undergoes a transition from p-type semiconducting to semi-metallic (characterized by temperature-independent carrier concentration with mainly hopping conduction) [269,270]. At the surface termination, the BDD surface is hydrogen-terminated when using post CVD synthesis. This can be converted to oxygen termination via a variety of means, including oxygen plasma treatment, heating, and cleaning in strong acid [271,272,273]. It has been reported that an oxygen-terminated surface severely inhibits the electron-transfer kinetics for the  $Fe(CN)_6^{3-/4-}$  couple compared to hydrogen terminated [272,274]. Although hydrogen termination has been found to enhance the surface



conductivity of intrinsic diamond, for heavily boron doped films the conversion from hydrogen to oxygen surface termination does not significantly change the surface conductivity [271,275]. In the Cleanliness of the growth process, the CVD process may yield non-diamond carbon, with a fraction of  $sp^2$ -bonded carbon. But at grain boundaries or defects, the activity differs from that of the surrounding BDD material [276].

## **2.6.5 Boron-doped diamond (BDD) electrodes**

### **2.6.5.1 Properties of boron-doped diamond (BDD) electrodes**

The overpotential for oxygen evolution on BDD electrodes, in aqueous acidic solution, creates a potential window sufficiently positive to allow the formation of hydroxyl radicals (i.e.  $\geq + 2.7$  V) [277]. The properties of BDD such as high anodic stability in strongly acidic medium, high oxygen evolution overpotential and formation of hydroxyl radicals produces powerful oxidants with high redox potential for waste water treatment [278]. The electrochemical properties of BDD electrodes towards redox systems in the solution are quite sensitive to prior surface treatments. A decrease in surface conductivity following surface treatments has observed, however, the origin of this effect remains largely controversial. In many papers, a modification of the carrier concentration at the diamond surface was suggested to occur as a result of the treatment [279,280]. Other research groups suggested that surface hydrogen or oxygen terminations may be responsible for the activity of the surface [281,282]. The nature of the surface carriers was not unambiguously defined so far; they could be boron states,  $sp^2$  impurities, or a near-surface hydrogen film promoting electron transfer at the surface. Hydrogen-terminated surface groups could be seen as an electron source in some redox processes. Several redox systems were studied at diamond electrodes in an attempt to correlate the electrochemical response of the electrodes with the surface treatments [283]. As compared to graphite or glassy carbon electrodes, the inertness of BDD (Figure 2.20, typical BDD electrode used in this project) causes very good resistance toward corrosive conditions, which is very useful in electrochemistry (molten salts, batteries, fuel cells) [239,283].

BDD offers several advantages as a substrate for electrochemical modification of metal or metal oxide catalyst, including the nucleation sites on the diamond surface and the catalyst particles. The nucleation sites are randomly distributed due to the inhomogeneous nature of the diamond surface. Whereas, the catalyst particles act as nano or submicro-array electrodes resulting in enhanced signal to background ratios. This is due to the random distribution in the diamond surface [286,287,288]. Such modified electrodes are very attractive for electroanalysis as compared to conventional electrodes (e.g., glassy carbon or platinum electrode) [289]. The quality of conducting diamond films is usually investigated by recording the background cyclic voltammetric (CV) *J-E* curves of the electrodes. The magnitude of the background current, the working potential window and the features of the curves are sensitive to the presence of non-diamond carbon impurities [289,290]. Moreover, high quality diamond film has a flat featureless voltammetric response in the electroanalytical technique. This technique provides a strongly adherent deposit with a lower background current when compared with polished glassy carbon [291].

### 2.6.6 Electrochemical techniques

Anodic polarisation, oxygen plasma oxidation and boiling in strong acid are some of these surface treatment techniques [261,262,266,268,292]. Among all the procedures employed, anodic oxidation is the simplest one. The most evident result of anodic polarization is an improvement in reproducibility of the electrode's response [293]. For this reason anodic oxidation has been widely used as a surface treatment for the electrochemical investigation of diamond electrodes. Significant changes in crystal morphology have not been found, but the chemical changes occurring on the surface during anodic polarization are still almost unknown.

The background currents recorded in the window of the electrolyte stability are higher at untreated diamond electrodes than at prepolarised ones [266,293]. But no specific cause is pointed out to explain this feature. An important effect of the polarization appears to be the elimination of  $sp^2$  species that can be more or less numerous on the diamond surface, depending on the fabrication conditions.

The importance of non-diamond impurities for the electrode's activity is not completely understood as yet. Anodic polarization is expected to modify the diamond surface in terms of chemical composition, wettability and crystal shape. Mild anodic polarization of BDD may lead to an increase in the oxygen/carbon ratio due to the introduction of oxygen-terminated functional groups on the diamond surface [283,294].

The nature of impurities present on the diamond surface is variable and depends on the preparation conditions of the substrate material used. The  $sp^2$  impurities are responsible for the activity during the diamond growth of the electrodes [285,295]. Cyclic voltammetry performed at the potentials of electrolyte stability provides both electrochemical spectrum of the surface redox transitions and measurement of the activity of the electrode surface. The electrochemical response of the electrodes varies as a function of surface treatment. Untreated electrodes can exhibit the highest surface activity. From the measurements, the voltammetric charge can be calculated at different scan rates as the integral of the anodic part of the voltammogram.

In terms of signal transduction via electroanalytical measurements, diamond generally provides significant improvements over conventional carbon electrodes (e.g.,  $sp^2$  carbon), for linear dynamic range, detection limit, response precision, and response stability [296]. Broader application of this new electrode has been limited by the fact that, until recently, there has been no commercial source for the material. There are now at least four commercial units marketing electrically conducting diamond thin-film electrodes. Importantly, the cost is not exorbitantly expensive, as is commonly perceived. Several factors influence the diamond thin-film electrode response (i.e., electrode reaction kinetics): (i) potential-dependent density of electronic states, which is affected by the doping type, level, and distribution, (ii) surface chemistry, (iii) morphology and microstructure, (iv) defect density, (v) nondiamond carbon impurity content, and (vi) double layer structure [295,297].

BDD as substrate electrodes are used in an electrochemical cell either as an anode to oxidize reactants or as a cathode to reduce reactants because of its wide potential window. Examples of reactants that can be treated include chlorides, bromides, organic materials and water. The electrode may be employed for decomposition reactions or other reactions that cannot normally be run on metal electrodes because of the high hydrogen overvoltage on the diamond surface. One example of would be the dehalogenation of organic materials as a reduction reaction at the cathode. The electrode can also be used with an aerated solution to produce peroxide, peroxide radicals and hydroxyl radicals that, in turn, act as a reactant in the decomposition of organic materials not in contact with the diamond electrodes. Oxygen is added at the cathode side to increase the amount of peroxide that is produced. Because of the dimensional stability of the electrode, it may be used with an alternating current (ac) to function cyclically as both an anode and a cathode. An ac signal is desirable for some applications where a prolonged dc current produces undesirable reactions such as a polymerization reaction. On the other hand, the BDD electrodes are also used as cathode materials for the electrochemical reduction of nitrate ions dissolved in high concentrations [298].

Levy-Clement *et al.* reported that at applied potentials between -1.5 and -1.7 V vs. SCE the amount of  $\text{NO}_3^-$  reduced was a constant 10 % and that it was mainly transformed into gaseous products, then it increased to 29 % at -2 V with almost equal parts of nitrite and nitrogenous gas formed, without the production of ammonium [299].

### 2.6.7 Electrochemistry of BDD electrodes

The electrochemical studies of diamond were started more than fifteen years ago with the first paper on the electrochemistry of boron doped polycrystalline diamond published by Pleskov *et al.* in 1987 [300]. The demonstration of the possibility of performing electrochemistry on polycrystalline diamond resulted in considerable interest in electrodes fabricated from this new material. The characteristics of diamond electrodes have been employed in a number of applications [301-305].

### 2.6.7.1 Electrochemical studies of highly BDD in aqueous media

Most electrochemical studies of diamond have been performed on highly boron doped, p-type, and material in aqueous solvents. It has been shown that for simple redox couples in aqueous solution the electrochemical response at a diamond electrode resembles that of a metal electrode [306,307]. Thus any applied potential would be dropped across the Helmholtz layer and reversible electrochemical behaviour observed for simple redox couples. Indeed an accumulation of holes at a hydrogen terminated diamond surface exposed to the atmosphere has been used to explain the enhanced surface conductivity of the material [308,309,310]. Oxygen terminated diamond surface reversible electron transfer occurs at potentials, which Mott-Schottky analysis suggests the surface is in depletion. Impedance studies [311] indicate that electron transfer at an oxygen terminated diamond surface occurs via surface states [312]. It has been postulated that  $sp^2$  carbon surface impurities mediate the charge transfer.

### 2.6.7.2 Electrochemical studies of highly BDD in non-aqueous media

In these studies, it has been reported that diamond electrodes in non-aqueous electrolyte possess an increased potential window, allowing a fifth peak for the reduction of  $C_{60}$  to be observed [313]. Moreover diamond electrodes have been employed in the generation of solvated electrons in ammonia [314].

### 2.6.7.3 Electrochemical studies of moderately BDD in aqueous media

There are limited studies of BDD electrodes. Pleskov *et al.* [315,316] using suprabandgap illumination has performed inconclusive studies on the semiconducting properties of diamond. Rao *et al.* using the same system undertook photocurrent measurements from suprabandgap illumination [317]. The results show some interesting current-voltage responses for semiconductor diamond but Mott-Schottky plots locating the flat band potential are not precise. If the flat band potential is placed as they suggest at approximately at + 4.6 eV versus standard

hydrogen electrode (SHE) the surfaces should exhibit negative electron affinity (NEA). However NEA is observed only at specially pre-treated surfaces [318] or nitrogen doped diamond [319]. Moreover if the flat band is situated as Rao *et al.* propose exchange of the electron for a standard redox couple as ferrocyanide/ferricyanide redox couple should be slow. However a high exchange range at equilibrium and reversible kinetics are observed [320,321].

#### **2.6.7.4 Electrochemical studies of undoped diamond in aqueous media**

There are also limited studies of undoped diamond electrodes. Shakarova *et al.* [322], Zhang *et al.* [323], Rohrer *et al.* [324], Nebel *et al.* [325] and Pereira *et al.* [326] have carried out photoconductivity experiments to determine the energy bands in undoped diamond and its electrical properties. Grain boundaries have been shown to play an important role in the conductivity mechanism. Recently Alvarez *et al.* [327] using red illumination reported similar results in the photoconductivity of undoped diamond. Ramesham *et al.* [328] have studied undoped diamond films using ac impedance. They reported data for the double layer capacitance, solution resistance, film resistance, film capacitance and polarization resistance. Granger *et al.* using undoped diamond has performed flow analysis and liquid chromatography of different organic compounds like azides, chlorpromazine, catecholamines and ascorbic acid [329].

#### **2.6.7.5 Conducting polymer modified BDD electrodes**

A thin layer of a conducting polymer, deposited onto the surface of substrate electrode, is able to enhance the kinetics of electrode process of some solution species. Electronically conducting polymers are extensively conjugated molecules, and it is believed that they possess a spatially delocalized band-like electronic structure. The essential structural characteristic of all conjugated polymers, conventional polymers (*e.g.*, polythiophene, polyaniline, polypyrrole), is their quasi-infinite  $\pi$  system extending over a large number of recurring monomer units. These bands discontinue from the splitting of interacting molecular orbital of the constituent monomer units in a manner reminiscent of the band structure of solid-state semiconductors [330].



The mechanism of conductivity ( $\sigma$ ) is based on the motion of charged defects within the conjugated framework. The charge carriers, either *positive* (p-type) or *negative* (n-type), are the products of oxidizing or reducing the polymer respectively. The conductivity  $\sigma$  of a conducting polymer is related to the number of charge carriers  $n$  and their mobility  $\mu$ :

$$\sigma \propto n \mu$$

where  $\sigma$  is the conductivity ( $1\mu\text{s/cm}$ ),  $n$  is the number of charge carries and  $\mu$  is the mobility ( $1\text{cm}^2/(\text{V}\cdot\text{s})$ ).

Because the band gap of conjugated polymers is usually fairly large,  $n$  is very small under ambient conditions. Consequently, conjugated polymers are insulators in their neutral state and no intrinsically conducting organic polymer is known at this time. A polymer can be made conductive by oxidation (p-doping) and/or, less frequently, reduction (n-doping) of the polymer either by chemical or electrochemical means, generating the mobile charge carriers described earlier. The following overview describes the redox polymers processes in the background of p-type (semiconductor) carriers although the concepts are equally applicable to n-type carriers.

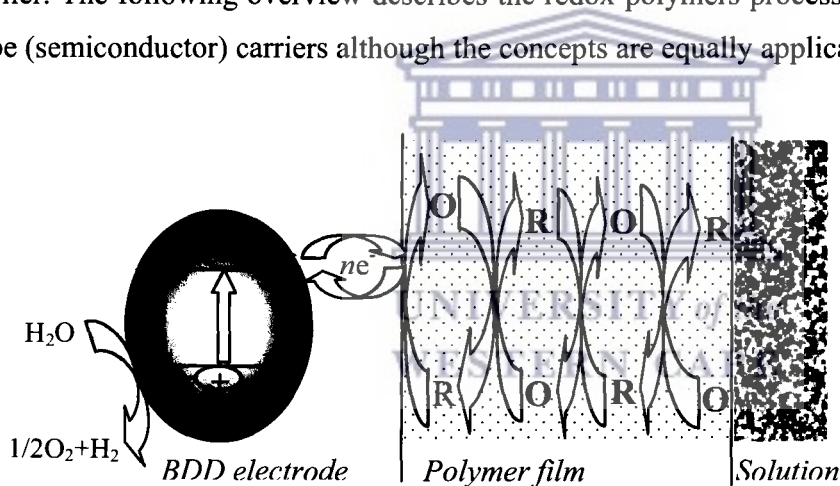


**Figure 2.21.** Redox polymers processes in the background of p-type (semiconductor).

A redox polymer consists of a system where a redox-active transition metal based pendant group is covalently bound to some sort of polymer backbone which may or may not be electroactive (although for synthetic convenience the backbone is frequently formed by the electropolymerization of suitable monomer complexes). A representative example is shown in Figure 2.21.



The common interest of the polymers has been urged by their applicability in the area of chemically modified electrodes [331,332]. One objective of coating electrodes with electroactive polymers is the development of new materials with very active catalytic properties.

The details of charge transport between the BDD electrode and the supported redox sites are a fundamental consideration. Kaufman and coworkers have reported that redox conduction in polymers occurs by the electron transfer process and by self-exchange steps between adjacent redox groups [333,334]. The rate of self-exchange ( $R_{SE}$ ) and electron transfer (ET) processes are connected by the simple relationship  $R_{SE} = k_{ET}C_{ox}C_{red}$ . In the polymer film where the total amount of redox species must be fixed (*i.e.*,  $C_{ox} + C_{red} = C_{tot}$ ) the self-exchange rate will reach a maximum when the concentration of both species is equal, *i.e.*,  $C_{ox} = C_{red}$ , hence maximum conductivity occurs at formal potential ( $E^0$ ).

The sequential self-exchanges which give rise to conductivity through the thickness of the film is depicted in Figure 2.21. Two processes are involved: (i) the charge injection at the polymer-electrode interface, which involves redox sites close to the surface. This is a potential-driven process and conforms to Butler-Volmer kinetics. (ii) The percolation of charge through the film which is driven by concentration gradients and is quantifiable as a quasi-diffusional process [335]. Since electroactive polymers are really mixed conductors, displaying both electronic and ionic conductivity on the electrode surface. This can be predicted from the electron transfer model that as the voltage is increased the reaction rate and therefore the current will increase exponentially. Assuming there are random amounts of (O) and (R) in the solution, the total current flowing  $i$  is the sum of the reductive ( $i_c$ ) and oxidative ( $i_a$ ) currents.

$$i = i_c + i_a = nFk_{red}[O]_o - nFAk_{ox}[R]_o$$

Where  $A$  is the electrode area,  $F$  the faraday constant,  $n$  the number of electrons transferred,  $k_{red}$  and  $k_{ox}$  are the rate constant for the reductive and oxidative steps respectively and  $[ ]_o$  the surface concentration of either (O) or (R). If the rate constant is large, such that any reactant (*i.e.* polymers) close to the interface is immediately converted into products (reduced forms) then the

current will be controlled by the amount of fresh reactant reaching the interface from bulk solution.

Thus movement of reactant in and out of the interface is important in predicting the current flowing. Some models concerning quantitative treatment of electrocatalytic reactions and charge transfer processes within polymer films were a subject of a few reviews [336,337].

## 2.7 Application of BDD electrodes

Recently, there have been many reports on the use of BDD electrodes in the area of waste water treatment [338,339], including electrochemical synthesis [340,341,342]. Depending on the redox analyte that one or more factors can affect BDD electrode reactivity as previously reported by Rodrigo *et al.* [343]. They observed that the electro-oxidation process of aromatic compounds on a BDD electrode resulted in electrode fouling due to the formation of polymeric film on the electrode surface, inhibiting extended use of the electrode [343,344]. BDD electrode can also be applied in electroanalysis and electrolysis. In electrolysis, some applications had been reported [342,345].

BDD electrodes have been used in the biochemistry; especially in the biosensors technology. Only a few BDD-based enzyme electrodes have been reported so far. Troupe *et al.* [346] have developed glucose sensors by connecting BDD to glucose oxidase via ferrocene-based electron transfer relays. Tatsuma *et al.* [347] have reported peroxidase- and heme peptide-modified BDD electrodes, which are responsive to hydrogen peroxide on the basis of direct electron transfer. Rao *et al.* [348] have fabricated mediated alcohol sensors by modifying BDD with alcohol dehydrogenase. However, phenylalanine-modified BDD electrodes have not yet been developed.

BDD has shown high sensitivity, low limit of detection and high stability. Ohnishi *et al.* reported the use of nickel-implanted BDD electrodes for the electrochemical glucose detection [349]. On the other hand, Ushizawa *et al.* have demonstrated that DNA molecules have successfully been immobilized to a variety of diamond substrates using different chemical approaches [350].

Besides DNA linking to diamond surfaces, there are only few reports in the literature dealing with protein-diamond interfaces. Some of the commercial applications of BDD are outlined below:

### **2.7.1 Thermal applications**

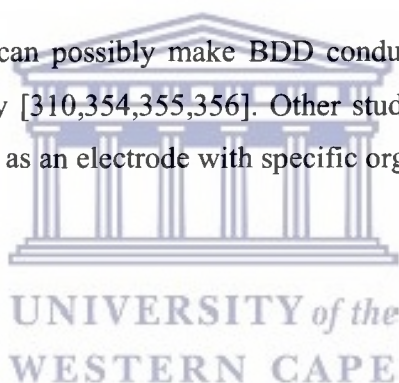
BDD is a material that has the potential of being used as a heat sink for integrated circuits. Its high thermal conductivity and high resistivity coefficient are allowing high-density packing of components, although maintaining low operating temperatures. Some commercial laser diodes and microwave diodes include diamond as a heat sink [351,352,353].

### **2.7.2 Electronic devices**

Producing field emitter devices can possibly make BDD conductive material when combined with its negative electron affinity [310,354,355,356]. Other studies have been concentrated on light emitting devices using BDD as an electrode with specific organic solutions [357].

### **2.7.3 Optical windows**

Boron-doped diamond has a wide range of transparency from deep ultraviolet to the far infrared in the spectrum. BDD can be used as optical material in different ranges of the light spectrum. Several of the materials used for infrared imaging technology e.g. ZnSe, are too soft and require outer coatings for protection and reinforcement. BDD emerges as an optimal material for a coating. It gives the strength and resistance, which ZnSe requires in the commercial device. An alternative route is the use of free standing diamond, *i.e.*, diamond as both detector and protection [358]. Free standing diamond is transparent and very resistant but it has some drawbacks, not least that it can only be deposited in planar shapes.



#### **2.7.4 Abrasives**

For more than 30 years diamond has been used as a material to abrade, cut and polish. Mainly it has been applied in heavy duty machinery in industry to cut, drill and polish materials. Nowadays as the price of diamond synthesis has decreased it is being used in less demanding environments as protective material in gloves and clothes and in specific surgery material like dental drills and scalpels [359,360].

### **2.8 L-phenylalanine (L-Phe)**

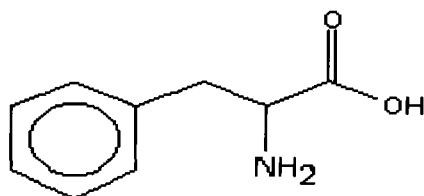
#### **2.8.1 Introduction**

Phenylalanine exists in two forms, L-Phenylalanine (L-Phe) and D-Phenylalanine (D-Phe). There is also a mixed form, DL-Phenylalanine (DLPA) that can be created in the laboratory. L-Phenylalanine is considered as an essential protein amino acid because the body cannot produce or synthesize it. It is called indispensable (essential amino acids) and must be supplied through the diet or by supplementation. A healthy diet that includes meat, fish, eggs, cheese and milk can help supply L-phenylalanine to the body to meet its physiological demands. Therefore, it is necessary for proper muscle, enzyme and hormone formation.

L-Phe can be converted in the body to L-tyrosine (L-Tyr), which in turn is used to synthesize two important neurotransmitters - dopamine and norepinephrine. It is available in three different forms - L-, D- and DL-. The L- form is the most common and the type in which it is incorporated into the body's proteins. The D- form acts as a painkiller and the DL- a combination of the two. However, this nutrient could prove of benefit to people suffering from Parkinson's disease, tiredness, depression, busy with alcohol withdrawal, rheumatoid arthritis, osteo-arthritis and vitiligo [361,362].

L-Phe is marketed as a nutritional supplement and used by some for its putative antidepressant activity. L-phenylalanine is also known as beta-phenylalanine, alpha-aminohydrocinnamic acid,

(S)-2-amino-3- phenylpropanoic acid and alpha-amino-beta-phenylpropionic acid. It is abbreviated as either Phe or by its one-letter abbreviation F. The molecular formula of L-phenylalanine is C<sub>9</sub>H<sub>11</sub>NO<sub>2</sub>, and its molecular weight is 165.19 daltons. L-phenylalanine is an aromatic amino acid with the following structural formula:



L-phenylalanine (L-Phe)

Because L-Phe is involved indirectly in the production of melanin, the pigment responsible for skin and hair color, children with phenylketonuria often have lighter complexions than their unaffected siblings. There is a characteristic "mousy" odor that results from the accumulation of phenylacetic acid. This odor may be detected on their breath, skin, and urine if the condition has not been treated immediately from birth or if foods containing L-phenylalanine are consumed. Provided you eat enough protein, you are likely to get enough L-phenylalanine for your nutritional needs. There is no nutritional need for D-phenylalanine [361,362].

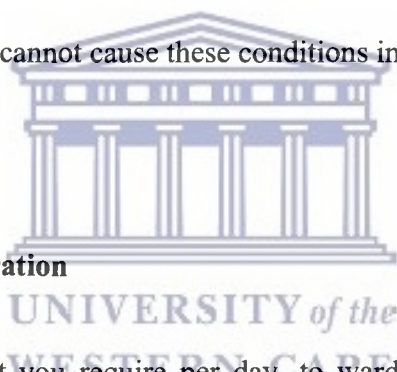
L-phenylalanine is required for elevating the mood since it is so closely involved with the nervous system, as well as help with memory and learning and has been used as an appetite suppressant. People suffering from Parkinson's disease, it is DLPA (or the D- or L-form alone) is used to treat depression and the D form may also be helpful in the treatment of Parkinson's disease and chronic pain in both osteo-arthritis and rheumatoid arthritis with mixed results increases blood levels of norepinephrine, epinephrine and dopamine - all three required for neurotransmission [363].

### **2.8.2 Deficiency of L-phenylalanine**

L-Phenylalanine deficiency can lead to a number of symptoms, including slowed growth, apathy, muscle loss, lethargy, edema, skin lesions as well as liver damage and weakness. However, excessive amounts can cause hypertension and/or migraine headaches. Patients already taking antidepressants should not supplement with phenylalanine. Women who are lactating should also avoid it. A deficiency in diet would only occur with an extremely low protein intake.

There are several rare inborn metabolic disorders that result in an accumulation of L-phenylalanine in the bloodstream [364]. The most commonly known is phenylketonuria (PKU). PKU is caused by a deficiency or absence of phenylalanine hydroxylase (PAH; phenylalanine 4-monooxygenase, EC 1.14.16.1), the enzyme necessary for converting L-phenylalanine into another amino acid. All children are tested at birth for these genetic defects [365]. Treatment consists of a diet low in L-phenylalanine.

Consumption of L-phenylalanine cannot cause these conditions in individuals who are not born with this enzyme deficiency.



### **2.8.3 Dosage and administration**

The dosage is the minimum that you require per day, to ward off serious deficiency of this particular nutrient. Otherwise, the amount of L-phenylalanine to be taken depends on the condition being treated. For depression, some practitioners recommend 1-4 grams daily; for attention deficit disorder, 0.5 grams; and for Parkinson's disease, 0.5-2.0 grams. In the therapeutic use of this nutrient, the dosage is usually increased considerably, but the toxicity level must be kept in mind [366].

The daily dosage is unknown but supplements are taken at about 14 mg per kilogram of body weight per day - which would translate to about 980 mg for a 70 kg male, but since it has powerful mood altering effects, only use under medical supervision.



L-phenylalanine supplements as well as DL-phenylalanine supplements are available in the nutritional supplement market place. Those who use L-phenylalanine supplements typically use 500 milligrams to 1.5 grams daily.

#### **2.8.4 Overdosage**

There are no reports of L-phenylalanine overdosage in the literature.

#### **2.8.5 Toxicity and symptoms of high intake**

Toxicity is rare in dietary intake but large amounts in supplement form may play destruction with your blood pressure and cause headaches, nausea and heartburn. Large amounts of this nutrient may also cause nerve damage. Some people cannot metabolize phenylalanine and should not take supplementation of this amino acid. There are no known signs of toxicity from L-phenylalanine [366].

#### **2.8.6 Food sources of L-phenylalanine (L-Phe)**

L-Phe is found in proteins of all life forms. Dietary sources of the amino acid are principally derived from animal and vegetable proteins [362]. Vegetables and juices contain small amounts of the free amino acid. The free amino acid is also found in fermented foods such as yogurt and miso. The alternative sweetener aspartame is a dipeptide of L-phenylalanine, as is the methyl ester, and L-aspartic acid.

L-Phe is also found in a variety of sources, including almonds, avocados, bananas, brown rice, cheese, corn, eggs, fish, lima beans, peanuts, pumpkin seeds, sesame seeds and soy products [362]. It is sold as a supplement in tablet or capsule form.



### **2.8.7 Actions**

L-phenylalanine is marketed as a nutritional supplement and used by some for its putative antidepressant activity. It may also, when used in conjunction with UVA irradiation, have antivitiligo activity [367].

### **2.8.8 Mechanism of action**

In addition to being involved in protein synthesis, L-phenylalanine is the precursor of L-tyrosine (Figure 1.1A). The conversion of L-phenylalanine to L-tyrosine is via the enzyme L-phenylalanine hydroxylase (PAH). It is this enzyme that is virtually absent in those with the inborn error of metabolism phenylketonuria (PKU).

### **2.8.9 Indications and usage**

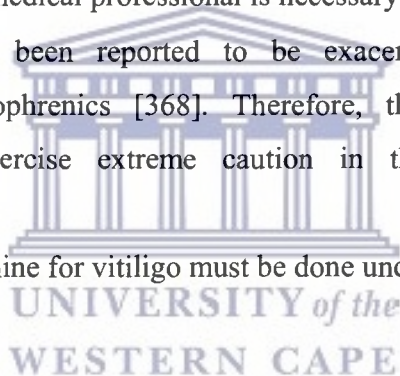
L-phenylalanine acts as an analgesic and antidepressant. It also acts as an appetite suppressant by administering the release of an intestinal hormone that signals the brain to feel satiated after eating. As an analgesic, it has been shown to decrease back pain, toothaches, and pain associated with migraine headaches. It has also been used to treat attention deficit disorder, fatigue, Parkinson's disease and premenstrual syndrome. It is best not to take your phenylalanine supplement at the same time as a high-protein meal, as it may not be absorbed well. It may also be useful in the treatment of vitiligo. There is some evidence that L-phenylalanine may exacerbate tardive dyskinesia in some schizophrenic patients and in some who have used neuroleptic drugs [368].

### **2.8.10 Contraindications**

L-phenylalanine is contraindicated in those with phenylketonuria and with those taking non-selective monoamine oxidase (MAO) inhibitors. L-phenylalanine is also contraindicated in those hypersensitive to any component of an L-phenylalanine-containing supplement.

### **2.8.11 Precautions**

- Pregnant women and nursing mothers should avoid supplementation with L-phenylalanine.
- People suffering from anxiety attacks, high blood pressure, diabetes and phenylketonuria, should not take it. DLPA supplements may interact with certain antidepressants or stimulants. Consulting a medical professional is necessary.
- Tardive dyskinesia has been reported to be exacerbated after ingestion of L-phenylalanine by schizophrenics [368]. Therefore, those with schizophrenia and hypertension should exercise extreme caution in the use of supplemental L-phenylalanine.
- Make use of L-phenylalanine for vitiligo must be done under medical supervision.



### **2.8.12 Adverse reactions**

L-phenylalanine will exacerbate symptoms of phenylketonuria if used by phenylketonurics. L-phenylalanine was reported to exacerbate tardive dyskinesia when used by some with schizophrenia [368].

### 2.8.13 Recommendations

L-phenylalanine has recorded negative interactions with several drugs and it is not recommended that they be used together including the following drugs such as antipsychotic drugs, levodopa, monoamine oxidase inhibitors (MAOIs), and selegiline. For all these drugs and supplements, it is necessary to consult a health care professional before use [365,367].

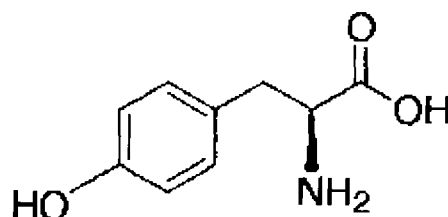
## 2.9 L-tyrosine (L-Tyr)

L-tyrosine is a nonessential amino acid (protein building block) that the body synthesizes from L-phenylalanine, another amino acid. L-Tyrosine is important to the structure of almost all proteins in the body. It is also the precursor of several neurotransmitters, including L-dopa, dopamine, norepinephrine, and epinephrine. L-tyrosine, through its effect on neurotransmitters, may affect several health conditions, including Parkinson's disease, depression, and other mood disorders [369].

Studies have suggested that L-tyrosine may help people with depression [370]. Preliminary findings indicate a beneficial effect of L-tyrosine, along with other amino acids, in people affected by dementia, including Alzheimer's disease [371]. Due to its role as a precursor to norepinephrine and epinephrine (two of the body's main stress-related hormones), L-tyrosine may also ease the adverse effects of environmental, psychosocial, and physical stress [371,372,373]. L-tyrosine is converted by skin cells into melanin, the dark pigment that protects against the harmful effects of ultraviolet light. Thyroid hormones, which have a role in almost every process in the body, also contain tyrosine as part of their structure.

People born with the genetic condition phenylketonuria (PKU) are unable to metabolize the amino acid L-phenylalanine. Mental retardation and other severe disabilities can result. While dietary L-phenylalanine restriction prevents these problems, it also leads to low L-tyrosine levels in many (but not all) people with PKU. L-Tyrosine supplementation may be beneficial in some

people with PKU, though the evidence is conflicting [374]. L-tyrosine is an aromatic amino acid with the following structural formula:



L-Tyrosine

## 2.10 Phenylketonuria (PKU)

PKU is a genetic disorder affecting the degradation pathway of L-phenylalanine [375]. There are two ways in which a patient may be affected by the disorder: Classical and non-classical PKU.

- **Classical PKU** is characterized as a lack or absence of the degradation enzyme phenylalanine hydroxylase (PAH). This type of PKU can manifest itself in varying degrees of severity.
- **No-classical PKU** is characterized by an error in the degradation pathway due to a lack in either impaired regeneration of tetrahydrobiopterin (THB or BH<sub>4</sub>) or impaired synthesis of THB.

UNIVERSITY of the  
WESTERN CAPE

### 2.10.1 Signs and symptoms effects

In PKU the inability for L-phenylalanine to be degraded leads to a toxic buildup of L-phenylalanine. PKU can manifest itself in many forms depending on the severity of the genetic mutation. The signs and symptoms of the disease include: mental retardation, behavioral or social problems, seizures or tremors, rocking, hyperactivity, stunted growth, eczma, microcephaly, a musty odor on the breath, skin or urine, fair skin and blue eyes, and vomiting. Symptoms develop from the lack of specific amino acids that are necessary proteins for development and neurotransmitters [376].

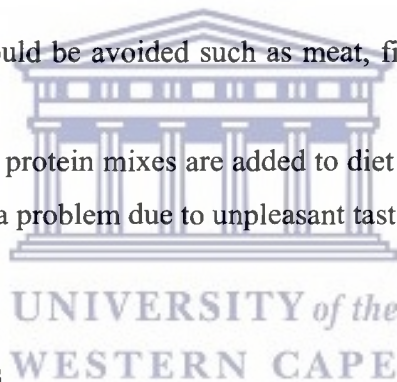
The symptoms manifest themselves throughout life depending on the amount L-phenylalanine consumed in the diet. However, there are two times in life where there is major risk for long lasting symptoms. During childhood development untreated PKU can lead to life long debilitations. Second, it is also vital that pregnant individuals who suffer from PKU strictly adhere to a treatment plan. Not doing so will lead to permanent symptoms in the child.

### **2.10.2 Nutritional therapy**

A low L-phenylalanine (L-Phe) diet is normal treatment for PKU. Also, increased L-tyrosine (L-Tyr) supplementation is necessary since L-Phe is a precursor for L-Tyr synthesis.

### **2.10.3 Precautions**

- Food high in proteins should be avoided such as meat, fish, poultry, eggs, cheese, milk, dried beans, and peas.
- Supplemental phenyl-free protein mixes are added to diet to ensure enough protein in the diet. Compliance is often a problem due to unpleasant taste of the protein mix.



### **2.10.4 Maternal PKU effects**

Maternal PKU is a condition in which a high level of L-Phe in a mother's blood causes mental retardation in her child when in the womb. A woman who has PKU and is not using a special low-phenylalanine diet will have high levels of L-Phe in the blood. Her high L-Phe levels will cross the placenta and affect the development of her child. The majority of children born from these pregnancies is mentally retarded and have physical problem, including small head size (microcephaly) and congenital heart disease. Most of these children do not have PKU [376].

### **2.10.5 Recommendations**

In patients with non-classical PKU, adding BH<sub>4</sub> has been recommended as an additional and not replacement form of treatment [376]. Women who are pregnant should remain on the phenyl-free diet to prevent abnormally high L-phenylalanine levels in the developing fetus.

### **2.11 Conclusion and future trends**

The documented health effects and the occurrence of large amounts of L-phenylalanine in biological samples (i.e. blood) and foodstuffs raise particular concern in view of the anticipated human exposure to this nutrient, which eventually passes into the brain causing nerve damage, mental retardation or other neurological problems. Generally, the levels of this nutrient are not adequately monitored in biological samples and foodstuffs since the methods of its analysis are complex and costly and cannot be applied on a regular basis. The review indicates that biosensors can meet the need for continuous monitoring of L-phenylalanine to replace or complement the intermittent analytical techniques due to their low cost of analysis, ease of operation, high sensitivity and minimization of sample pre-treatment. Biosensors have undergone rapid development over the last few years due to the combination of new bioreceptors with the ever-growing number of transducers and materials for transducer modification. By combining the use of electronically conducting polymers with immobilized enzymes and by making use of the particular properties of conducting polymers, it is possible to develop biosensors with enhanced performances. Great progress in this field has shown that the modification of electrode surfaces using proper matrices provide a favourable micro-environment for the enzyme to exchange its electrons directly with the underlying electrode and thus affords a new opportunity for the detailed study of the enzyme electrochemistry and its direct electron transfer. Despite the vast amount of research conducted on biosensors, their use is still against many unresolved technical problems and a number of factors such as sensitivity, selectivity, miniaturization for in-vivo applications, integration of signal processing steps on a chip, building of arrays for more complex pattern recognition analysis, biocompatibility, stability and response time still require investigation. Currently, the research is focused on improving biosensor sensitivity through the



use of nanostructured materials as mediators. Nanostructured PANI is one of the most promising candidates for the development of nanobiosensor due to their high surface area, versatile synthesis approaches, high conductivity, as well as the controllable chemical and physical properties by oxidation and protonation, and the good environmental stability. Although various kinds of synthesizing methods have been established, preparation of one-dimensional nanostructured PANI with controllable morphologies and sizes, especially well oriented arrays on a large scale is still a major challenge and therefore new synthetic methods are required.



## CHAPTER 3

### Electrochemical techniques

This chapter describes the principles of the electrochemical techniques utilized in the preparation and characterization of the polyanilines doped with polyvinyl sulphonated (PANI-PVS), the principles governing electrode processes and various electroanalytical techniques employed mainly cyclic voltammetry (CV), square wave voltammetry (SWV) and Linear sweep voltammetry (LSV). Ultra violet-visible (UV-Vis) spectroscopy, scanning electron microscopy (SEM), and Fourier transform infrared (FTIR) spectroscopy are also studied. Detailed research methodology and general experimental procedures for the electrochemical synthesis of nanostructured conducting polymer, biosensor construction, characterization and application of the developed biosensor for the determination of L-phenylalanine are discussed.

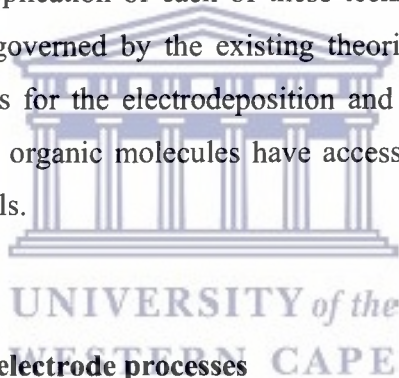
#### 3.1 Reagents and materials

The reagents hydrochloric acid (HCl) ( $\geq 32\%$ ), sulfuric acid ( $\text{H}_2\text{SO}_4$ ), disodium hydrogen phosphate (98 %) and potassium dihydrogen phosphate (99 %) were purchased from Sigma-Aldrich (Cape Town, South Africa) and were of analytical grade. The enzyme tyrosinase (E.C. 1.14.18.1, binuclear type III copper centre, 5370 units  $\text{mg}^{-1}$ ) was obtained from Sigma-Aldrich, South Africa and refrigerated at  $-20\text{ }^\circ\text{C}$ . Stock solutions of tyrosinase (Tyr) were prepared by dissolving 4.5 mg in 1.0 mL phosphate buffer (pH 6.2). The stocks were refrigerated at  $-20\text{ }^\circ\text{C}$  and fresh enzyme solutions prepared prior to experiments. 0.2 M Aniline (Sensor Lab, Chemistry Dept./UWC, South Africa) was distilled before use, 15 mg/ml polyvinyl sulphonated (PVS) was obtained from Sigma-Aldrich and fresh solutions of L-phenylalanine (L-Phe) and L-tyrosine (L-Tyr) were diluted and prepared daily from their stocks. Deionized water ( $18.2\text{ M}\Omega\text{ cm}$ ) purified by a Milli-QTM system (Millipore) was used as reagent water for aqueous solution preparation.

Phosphate buffer solution (0.1 M, pH 7.2) was prepared from anhydrous disodium hydrogen phosphate and potassium dihydrogen phosphate monohydrate. Phosphate buffer solution of 0.1 M was prepared by dissolving 3.549 g of disodium hydrogen phosphate and 3.4023 g of potassium dihydrogen phosphate separately in 250 mL deionized water, then mixing the salt solutions according to Henderson-Hasselbalch equation to obtain the required pH values. The phosphate buffer solution (PBS) was refrigerated at 4 °C. All chemicals used were Analytical grade.

### 3.2 Principles of the electrochemical techniques used

The major techniques used for the preparation and/or characterization of the PANI-PVS were electrochemical in nature. Cyclic voltammetry (CV) and square wave voltammetry (SWV) techniques were utilized. The application of each of these techniques and their choice for the preparation of PANI-PVS was governed by the existing theories of electrode processes. The ability to utilize these techniques for the electrodeposition and characterization of PANI-PVS was based on the fact that these organic molecules have accessible frontier molecular orbitals with well defined formal potentials.



### 3.3 Principles governing electrode processes

An electrode process is a heterogeneous reaction occurring at the electrode-electrolyte interface. The rate of electrode process is dependent upon the mass transfer rate at which the analytes are brought to the electrode surface, the electrodynamics of electron transfer across the interface, chemical reactions preceding or following electron transfers as well as various other surface reactions. The net rate of a heterogeneous electrode process can be presented by the equation 3.1 below:

$$\text{Rate (mol s}^{-1}\text{cm}^{-2}) = i / n F A \quad (3.1)$$

Where  $F$  and  $A$  are the Faraday constant ( $C \text{ mol}^{-1}$ ) and the area of the electrode respectively. The observed current ( $i$ ) is a function of all the electrode processes and is limited by the more sluggish reactions (rate determining step) [377]. In particular, the mass transfer issue is a function of three components namely: migration, diffusion and convectional effects. The mass transfer of the analyte species to an electrode is governed by the Nernst-Planck equation [378]:

$$J_i(x) = -D_i \frac{\partial C_i(x)}{\partial x} - \frac{z_i F}{RT} D_i C_i \frac{\partial \Phi(x)}{\partial x} + C_i v(x) \quad (3.2)$$

Where  $J_i(x)$  is the flux of species  $i$  ( $\text{mol s}^{-1} \text{ cm}^{-2}$ ) at distance  $x$  from the surface,  $D_i$  is the diffusion coefficient ( $\text{cm}^2/\text{s}$ ),  $\partial C_i(x)/\partial x$  represents the concentration gradient at a distance  $x$ ,  $\partial \Phi(x)/\partial x$  is the potential gradient. The parameters  $z_i$  and  $C_i$  are the charge and the concentration ( $\text{mol cm}^{-3}$ ) respectively where  $v$  is the velocity ( $\text{cm/s}$ ) in which a volume element in solution moves in the direction along the distance ( $x$ ).

The three terms at the right hand side of the equation 3.2 represent the three components of mass transfer. Hence, the electrode reactions can be tailored to simplify the complications related to mass transfer. For organic conducting polymers for instance, keeping the monomer concentration very low compared to the concentration of the supporting electrolyte nullifies the migration effect [379]. Also carrying out the electrodeposition/electrochemical characterisation under quiescent (unstirred) conditions eliminates the conventional contribution [377,379]. This way the Nernst-Planck equation collapses to only the diffusion term (first term). Under the circumstances, the rate at which flux is transported to the electrode surface becomes the rate determining step and its movement is governed by Fick's laws of diffusion so long as the working electrode (WE), which is kept at right-angles to the incoming flux. Other factors that might affect the overall observed current such as the IR drop are minimized by placing the reference electrode at close proximity to the working electrode and through use of IR compensation modes in the instruments. Simplification of the electrode processes during the preparation of PANI-PVS, quiescent (unstirred) conditions were adopted and it was always ensured that the WE was always in a vertical position.

### **3.4 Electroanalytical techniques employed**

The detection method widely employed in this study involves the combination of enzymatic biosensors with electrochemical techniques such as cyclic voltammetry (CV), square wave voltammetry (SWV) and Linear sweep voltammetry (LSV). Generally, electrochemical techniques are based on the transformation of chemical information into an analytically useful signal. This section describes the instrumentation, the electrochemical techniques as well as the enzyme biosensors employed in this study and its principles of operation. The other techniques used include scanning electron microscopy (SEM), ultra violet-visible (UV-Vis) and Fourier transform infrared (FTIR) spectroscopy.

#### **3.4.1 Instrumentation**

The basic components of a modern electroanalytical system for voltammetric and amperometric measurements are a potentiostat, a computer, and the electrochemical cell. The potentiostat plays the role of applying accurate and controlled potential and monitoring the current produced. The most widely used potentiostats are assembled from discrete integrated-circuit operational amplifiers and other digital modules. In many cases, especially in the larger instruments, the potentiostat package also includes electrometer circuits, analog-to-digital converter (ADC) and digital-to-analog converter (DAC), and dedicated microprocessors with memory. In the computer-controlled instruments, the properties of the modulation and the waveform are under software control and can be specified by the operator. The most commonly used waveforms are linear scan, differential pulse, and square wave. The use of micro- and nanometre-size electrodes has made it necessary to build potentiostats with very low current capabilities. Microelectrodes routinely give current responses in the pico- to nanoampere range. High-speed scanning techniques such as squarewave voltammetry require very fast response times from the electronics. These diverse and exacting demands have pushed potentiostat manufacturers into providing a wide spectrum of potentiostats tailored to specific applications.

The electrochemical cell, where the electrochemical measurements are carried out, consists of a working (indicator) electrode, a reference electrode, and usually a counter (auxiliary) electrode. In general, an electrode provides the interface across which charge can be transferred or its effects felt. Because the working electrode is where the reaction or transfers of interest takes place, whenever we refer to the electrode, we always mean the working electrode. The reduction or oxidation of a substance at the surface of a working electrode, at the appropriate applied potential, results in the mass transport of new material to the electrode surface and the generation of current. The three electrodes are presented in Figure 3.1 and are described below:

- i. **Working electrode** – this is the electrode at which the redox of the analyte or the electrochemical phenomena being investigated takes place. The commonly used materials for working electrodes include platinum, gold and glassy carbon;
- ii. **Reference electrode** – this is the electrode whose potential is known and is constant. Its potential is taken as the reference, against which the potentials of the other electrodes are measured. The most commonly used reference electrodes for aqueous solutions are the saturated calomel electrode (SCE) and silver/silver chloride electrode (Ag/AgCl);
- iii. **Auxiliary electrode** – it serves as a sink for electrons so that current can be passed from the external circuit through the cell. Reactions occurring at the auxiliary electrode surface are unimportant as long as it continues to conduct current well. To maintain the observed current, this electrode will often oxidize or reduce the solvent or bulk electrolyte though the reactions occur over short periods of time and rarely produce any appreciable changes in bulk concentrations. Most often the auxiliary electrode consists of a metallic foil or thin platinum wire, although gold and sometimes graphite have also been used.



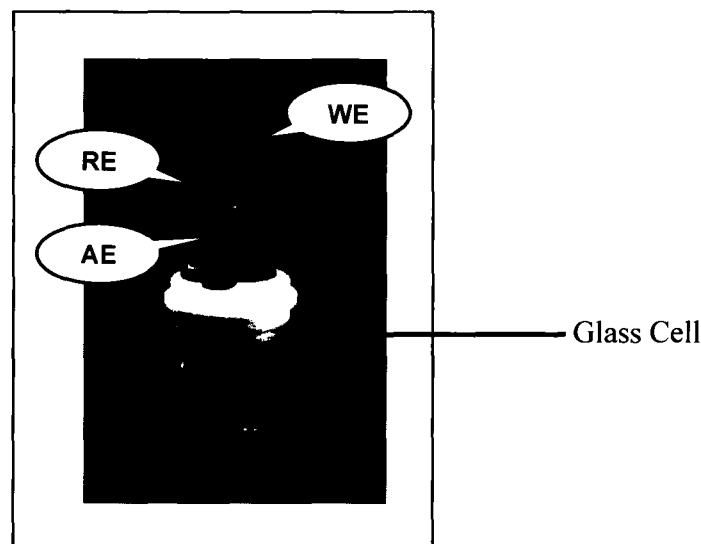


**Figure 3.1.** A typical electrochemical cell consisting of three electrodes: WE = working electrode, RE = reference electrode and AE = auxiliary electrode

Other solid or metal electrodes are commonly used as working electrode are carbon, platinum, gold, graphite and diamond (Figure 3.2). Electrodes based on carbon are currently in widespread use in voltammetric technique, primarily because of their broad potential window, low background current, rich surface chemistry, low cost, chemical inertness and suitability for various sensing and detection application. It includes glassy carbon electrode (GCE), carbon paste electrode (CPE), chemically modified electrode (CME) and screen-printed electrode (SPE). The glassy carbon electrode is the most commonly used carbon electrode in electroanalytical application. Recent review articles covering the early stages and the development of the research into applications of diamond electrodes share the excitement of a completely new tool now available to electrochemists [380-384]. Due to the limited benefits of  $sp^2$ -carbon rich diamond compared to other forms of graphitic carbon, most work in electroanalysis with diamond to date has been carried out with high quality boron-doped diamond (BDD) electrodes.



**Figure 3.2.** A typical commonly electrodes used as working electrode: carbon, platinum, gold, graphite and diamond electrodes, respectively.

Voltammetric techniques also utilize microelectrodes with the size of electrode radius much smaller than the diffusion layer thickness as the working electrode. It is constructed from 5 different materials such as platinum, gold, palladium, silver and iridium. The diameter of microelectrodes is smaller to enhance mass transport of analyte to the electrode surface due to smaller electrode than the diffusion layer. Hence, increasing signal-to-noise ratio and measurement can be made in highly resistive media due to decrease of the ohmic drop that results when the electrode size reduced [385,386,387].

Figure 3.3 illustrates the setup for the electroanalytical system used in this study. The cyclic voltammetry (CV) and square wave voltammetry (SWV) measurements were performed using a potentiostat BAS 100B/W electrochemical analyzer from Bioanalytical Systems, Inc. (West Lafayette, IN) with a conventional three-electrode system consisting of boron-doped diamond (BDD) (3.0 mm diameter for disk electrode) as the working electrode, platinum wire as the auxiliary electrode, and Ag/AgCl (saturated 3 M NaCl) as the reference electrode. Prior to experiments, the bare BDD electrodes were polished with aqueous slurries of 0.05  $\mu\text{m}$  alumina powder, rinsing with distilled water after polishing. The polished electrode was then sonicated in water and absolute ethanol. The auxiliary electrode was cleaned by burning in a flame for several minutes and the Ag/AgCl electrode was cleaned by rinsing with copious amounts of distilled

water. All potentials were quoted with respect to Ag/AgCl. The potentiostat was computer-controlled therefore the experimental modes were selected from the software and specified during its operation. Phosphate buffer solution (0.1 M PBS, pH 7.2) was used as the supporting electrolyte except for the pH dependent experiments which were performed in PBS at various pH values. All experiments were carried out under aerobic conditions and at room temperature.

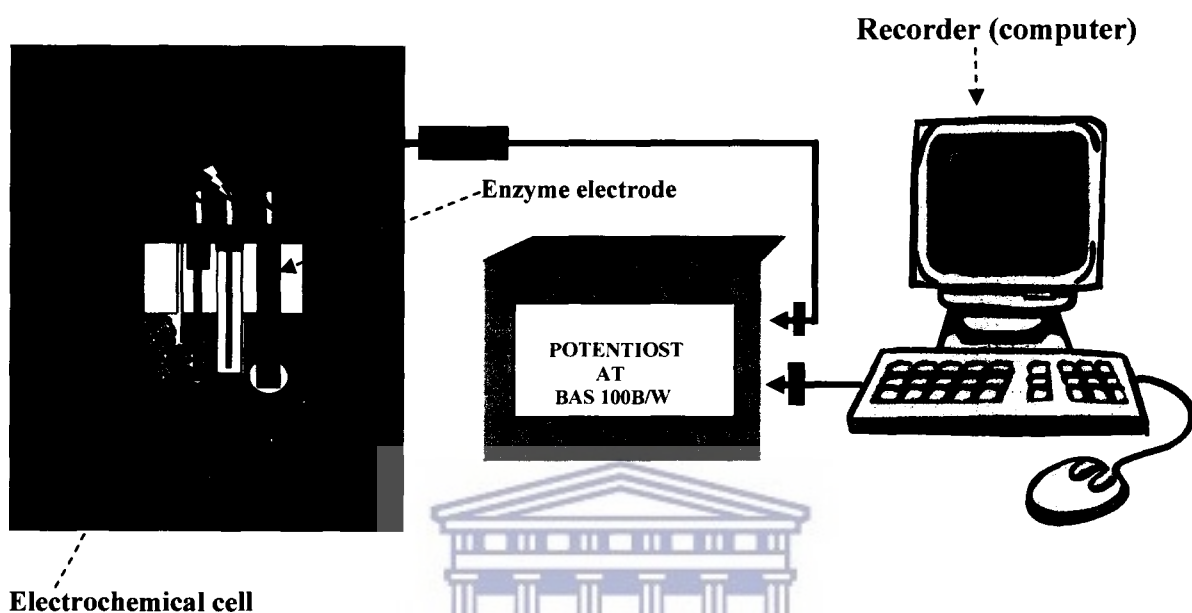


**Figure 3.3.** A typical electroanalytical system used for the electrochemical measurements.

UNIVERSITY of the  
WESTERN CAPE

### 3.4.2 Cyclic voltammetry

Cyclic voltammetry represents the most versatile and useful technique for performing electrochemical measurements. In cyclic voltammetry the execution signal is a linear potential scan with a triangular waveform that sweeps the potential of the working electrode back and forth between two designated values called switch potentials. The triangle returns at the same speed and permits the display of a complete voltammogram with oxidative and reductive waveforms one above the other as shown in Figure 3.4.

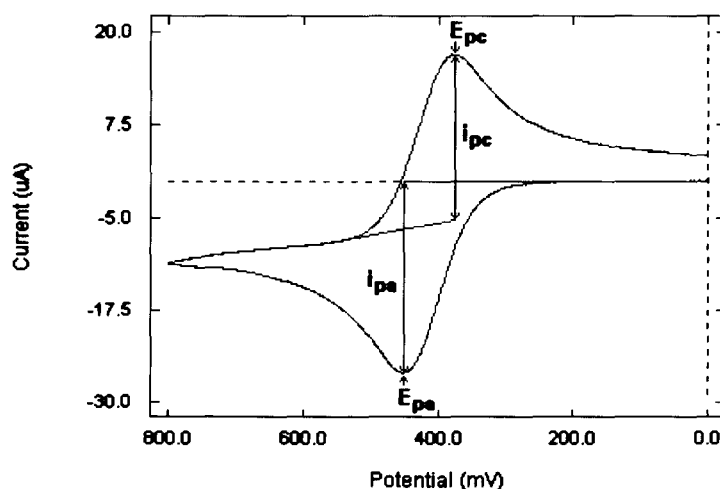


**Figure 3.4.** An E-I curve (voltammogram) demonstrating the most important parameters associated with cyclic voltammetry.

The common characteristics of all voltammetric techniques is that they involve the application of a potential ( $E$ ) to an electrode and the monitoring of the resulting current ( $I$ ) flowing through the electrochemical cell. In many cases, the applied potential is varied or the current is monitored over a period of time ( $t$ ). Thus all voltammetric techniques can be described as some function of  $E$ ,  $I$ , and  $t$ . They are considered as active techniques (as opposed to passive techniques such as potentiometry) because the applied potential forces a change in the concentration of an electroactive species at the electrode surface by electrochemically reducing or oxidizing it.

During cyclic voltammetry measurement, the potential is ramped from an initial potential,  $E_i$ , by switching potential at the end of its linear sweep, the direction of the potential scan is reversed, usually stopping at the initial potential  $E_i$  (or it may commence an additional cycle) [381]. The potential is usually measured between the reference electrode and the working electrode and the current is measured between the working electrode and the auxiliary electrode, also known as the counter electrode. This data is then plotted as current versus potential as shown in Figure 3.4. The forward scan produces a current peak for any analytes that can be reduced (or oxidized depending on the initial scan direction) through the range of the potential scanned. The current increases as the potential reaches the reduction potential of the analyte, but then decreases as the

concentration of the analyte is depleted close to the electrode surface. If the redox couple is reversible, then reversing the applied potential makes it reach a potential that re-oxidizes the product formed in the first reduction reaction, thus producing a current of reverse polarity from the forward scan [381]. The oxidation peak usually has the same shape as that of the reduction peak. As a result, the information about the redox potential and the electrochemical reaction rates of compounds can be obtained. For instance, if the electronic transfer at the surface is fast and the current is limited by the diffusion of species to the electrode surface, then the current peak will be proportional to the square root of the scan rate. Figure 3.5 is an example of a cyclic voltammogram for protonic mineral acid doped polyaniline showing the potential regions for the various oxidation/reduction processes.

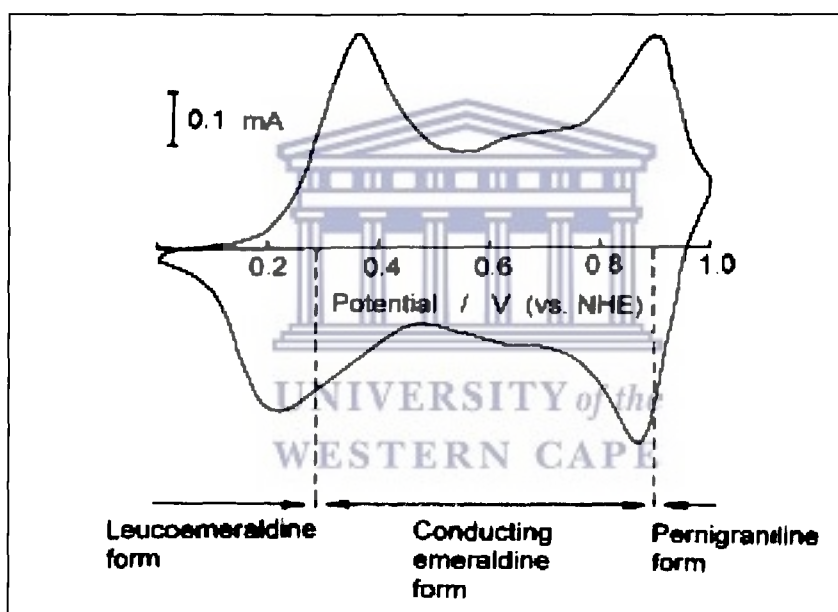


**Figure 3.5.** A typical cyclic voltammogram for polyaniline doped with a strong acid showing the potential regions for redox state inter-conversions.

### 3.4.2.1 Characteristics of reversible systems

In cyclic voltammetry, the important parameters are the peak potentials ( $E_{pc}$ ,  $E_{pa}$ ) and peak currents ( $I_{pc}$ ,  $I_{pa}$ ) of the cathodic and anodic peaks, respectively. If the electron transfer process is fast compared with other processes (such as diffusion), the reaction is said to be electrochemically reversible, and the peak separation is (equation 3.3):

$$\Delta E_p = |E_{pa} - E_{pc}| = 2.303 RT / nF \quad (3.3)$$

Thus, for a reversible redox reaction at 25 °C with  $n$  electrons  $\Delta E_p$  should be  $0.0592/n$  V or about 60 mV for one electron. In practice this value is difficult to attain because of such factors as cell resistance. Irreversibility due to a slow electron transfer rate results in  $\Delta E_p > 0.0592/n$  V, greater, say, than 70 mV for a one-electron reaction. The diagnostic tests for electro-reversibility are listed in Table 3.1.

**Table 3.1.** Diagnostic tests for the electrochemical reversibility of a redox couple, carried out by cyclic voltammetry

1.  $|I_{pa} / I_{pc}| = 1$
2. The peak potentials,  $E_{pc}$  and  $E_{pa}$ , are independent of the scan rate  $v$
3. The formal potential ( $E^{0'}$ ) is positioned midway between  $E_{pc}$  and  $E_{pa}$ , so  
$$(E^{0'}) = (E_{p,a} + E_{p,c}) / 2$$
4.  $I_p$  is proportional to  $v^{1/2}$
5. The separation between  $E_{pc}$  and  $E_{pa}$  is  $0.0592/n$  V for an  $n$ -electron couple (i.e.  $\Delta E_p = |E_{pa} - E_{pc}| = 0.0592/n$  V)

For a reversible reaction, the concentration is related to peak current by the Randles–Sevcik expression, equation 3.4, at 25 °C [381,382]:

$$I_p = 2.69 \times 10^5 n^{3/2} A C D^{1/2} v^{1/2} \quad (3.4)$$



where  $I_p$  is the peak current in amperes,  $n$  is the number of electrons transferred,  $A$  is the electrode area ( $\text{cm}^2$ ),  $D$  is the diffusion coefficient ( $\text{cm}^2 \text{s}^{-1}$ ),  $C$  is the concentration in  $\text{mol cm}^{-3}$ , and  $\nu$  is the scan rate in  $\text{V/s}$ . Cyclic voltammetry is carried out in quiescent solution to ensure diffusion control. A three-electrode arrangement is used. The utility of cyclic voltammetry is highly dependent of the analyte being studied. The analyte has to be redox active within the experimental potential window. It is also highly desirable for the analyte to display a reversible wave. A reversible wave is displayed when an analyte is reduced or oxidized on a forward scan and is then re-oxidized or re-reduced in a predictable way on the return scan as shown in Figure 3.3. For a multi-oxidation state electroactive species like PANI and its derivatives, several redox couples are recorded in the voltammogram and the critical potentials at which these limiting currents occur are related to the standard electrode potentials for the specific chemical system (see Figure 3.5). Electrochemical reactions sometimes show non-reversible or quasi-reversible waves with deviation from the above reversibility behaviours.

#### 3.4.2.2 Characteristics of quasi-reversible systems

A cyclic voltammogram is useful in diagnosing quasi-reversibility or irreversibility from the shape of the  $i$ - $E$  curve. For quasi-reversible systems for instance, the peak -to - peak separation  $\Delta E_p$  is greater than the  $59/n$  mV recommended for reversible systems. The cathodic and anodic peak currents differ in magnitude i.e.  $I_{pc} / I_{pa} \neq 1$  and the peak current  $I_p$  increases unproportionally to the square root of the scan rate ( $\nu^{1/2}$ ). It has been shown that most conducting polymers systems show reversibility at low scan rates but the behaviour transits to quasi-reversibility at higher scan rates. At this high scan rates therefore, the shapes of the quasi-reversible voltammograms for the organic conducting polymers are functions of the scan rate  $\nu$ , the standard rate constant  $k^0$ , the transfer coefficient  $\alpha$ , and the switch potential ( $E_\lambda$ ) and  $\Psi(E)$  (a kinetic parameter). The effect of the switch potential on the shapes of quasi-reversible systems is easily eliminated by keeping the switch potential at least  $90/n$  mV beyond the last cathodic peak [378]. It has also been shown that most quasi-reversible systems exhibit  $\alpha$  values in the range  $0.3 \leq \alpha \leq 0.7$ . This way the observed waves are independent of the transfer coefficient  $\alpha$  and depend only on the kinetic parameter  $\Psi(E)$ . From well established  $\Delta E_p / \Psi(E)$  tables

established by Nicholson, the peak currents  $I_p$  and the heterogeneous rate constants for the quasi-reversible systems can be determined by use of the equation 3.5 [378]:

$$i = F A D^{1/2} C_O^* f^{1/2} v^{1/2} \Psi(E) \quad (3.5)$$

Where  $F$  is the Farady,  $A$  is area of the electrode ( $\text{cm}^2$ ),  $D$  is the diffusion coefficient ( $\text{cm}^2/\text{s}$ ),  $f$  is equal to  $F/RT$  and  $\Psi$  is the kinetic facility dependent on  $\Delta E_p$ .

The heterogeneous rate constant for the quasi-reversible systems can then be obtained by use of the equation 3.6 below:

$$k^0 = \frac{\Psi(E) \cdot [D \cdot \pi \cdot v \cdot n F / RT]^{1/2}}{(D_O/D_R)^{\alpha/2}} \quad (3.6)$$

For  $D_O = D_R = D$ , it has been established that the  $k^0$  ( $\text{cm}^2/\text{s}$ ) for quasi-reversible systems lie in the range:  $0.3v^{1/2} \geq k^0 \geq 2 \times 10^{-5} v^{1/2}$

The CV was employed for the synthesis of the polymer and to investigate the redox processes and the electrochemical properties of analytes in solution.

UNIVERSITY of the  
WESTERN CAPE

### 3.4.2.3 Estimating the surface concentration of a redox couple

The shapes and general appearance of cyclic voltammograms is significantly affected by the adsorption of one species or both. The location of the peak potential  $E_p$  relative to the formal potential  $E^{0'}$  depends on the strength of the adsorption. When oxidized species (O) is strongly adsorbed, the wave is displaced towards negative potentials beyond the position of a reversible wave is expected to occur and vice versa [378]. Although the equations for solution species as discussed previously still hold, adsorption demands the choice of adsorption isotherms and therefore additional parameters thus complicating the situation (equation 3.7).

Based on the applications of the linearized Langmuir adsorption isotherms, it has been shown that the current component in a cyclic voltammogram where either oxidized (O) or reduced species (R) or both are adsorbed is given by [378]:

$$i_p = n^2 F^2 v A \Gamma^* / 4RT \quad (3.7)$$

Where  $\Gamma^*$  ( $\text{mol cm}^{-2}$ ) refers to the surface concentration of the adsorbed species and the other parameters have their usual meaning.

Under these circumstances, the peak current is proportional to the scan rate  $v$ , and a plot a Brown Anson plot (plot of peak current versus scan rate) is useful for the determination of the surface concentrations ( $\Gamma^*$ ) of the adsorbed species. Another approach towards the determination of the surface concentration of the adsorption is based on the fact that the area under the oxidation/reduction wave ( $nFA \Gamma^*$ ) is equivalent to the charge  $Q$  (coulombs) passed during oxidation/reduction [388]. Then the surface concentration for either the oxidized or reduced species is given by the equation 3.8 below:

$$\Gamma^* = Q / nFA \quad (3.8)$$

where  $Q$  is the charge in coulombs; other parameters have their usual meaning.

### 3.4.3 Square wave voltammetry (SWV)

Square voltammetry is a highly sensitive technique with detection limits as low as 10 nM. Its ability to eliminate background currents and speedy operation allows it for use in the study of many kinds of electrode kinetics. In square wave voltammetry, the excitation signal is a symmetrical square pulse of amplitude  $E$  superimposed on a staircase wave form (Figure 3.6) of step height  $\Delta E$  [389]. The observed net current is the difference between the forward/reverse currents and corresponds to the analyte's redox potential. The magnitude of the peak current is proportional to the concentration of the electroactive species in solution.

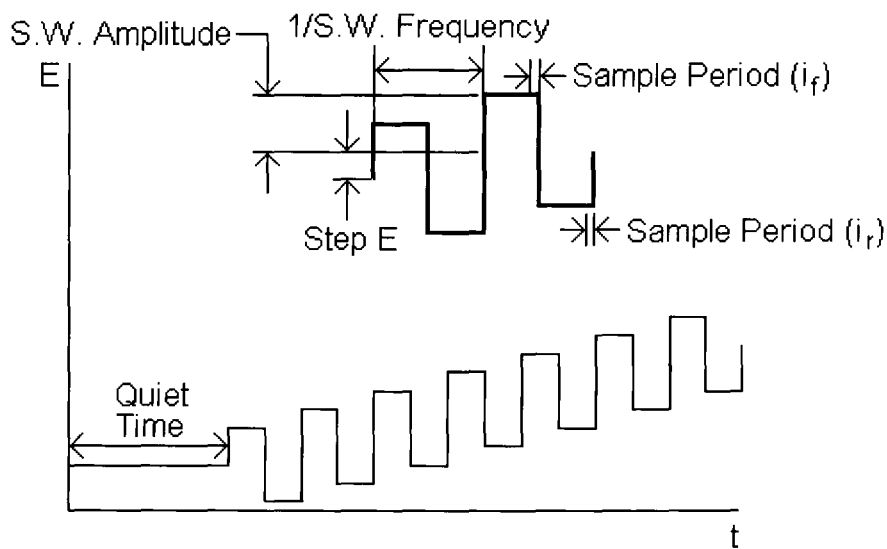


**Figure 3.6.** Potential wave form for square wave voltammetry.

#### 3.4.4 Linear sweep voltammetry (LSV)

In linear sweep voltammetry (LSV) a potential applied to a working electrode is swept from a lower limit to an upper limit over time and the resultant current is measured as the output signal. In a typical linear sweep voltammogram, the potential range is scanned starting at the initial potential (corresponding to a point where no current flows through solution) and ending at the final potential (Figure 3.7).

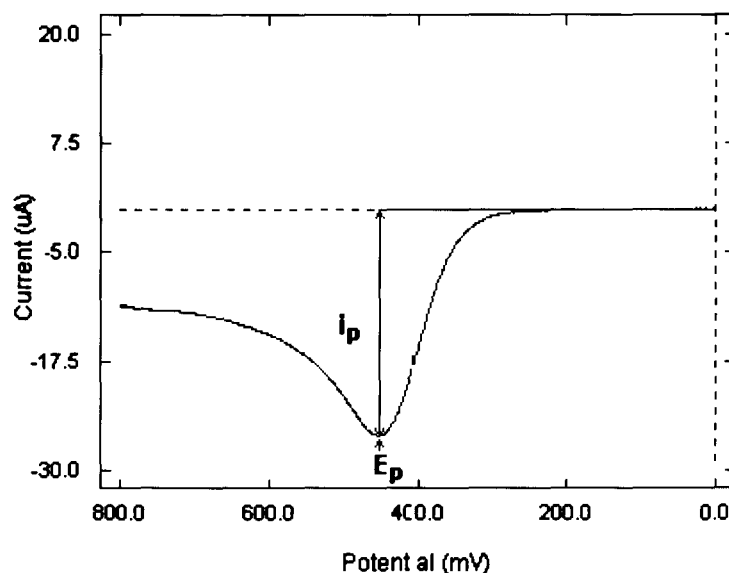


**Figure 3.7.** Typical linear sweep voltammogram for anodic sweep.

The current flow from the solution species back to the electrode and occurs in the opposite sense to the forward sweep but otherwise the behaviour can be explained in an identical manner. Yet, for the reversible electrochemical reaction the CV recorded has certain well defined characteristics, such as:

i) the voltage separation between the current peaks is:

$$\Delta E = E_p^a - E_p^c = 59/n \text{ (mV)}$$

ii) the positions of peak voltage do not alter as a function of voltage scan rate.

iii) the ratio of the peak current is equal to one

$$i_p^a/i_p^c = 1$$

iv) the peak currents are proportional to the square root of the scan rate:

$$i_p^a \text{ and } i_p^c \propto \sqrt{v}$$

### 3.4.5 Electrochemical enzyme biosensors

Most electrochemical biosensors make use of the existing transducers, the instrumentation and techniques already associated with them. The transducers can be connected to a millivoltmeter for potentiometric measurements, or to a potentiostat for amperometric or voltammetric measurements (see Figure 3.3). The system is then connected to a recorder which monitors the biosensor signal and progression of its response curve towards steady state. The principle modifications are mostly made to the part of the transducer where the enzyme is to be immobilized. An enzyme biosensor is usually constructed by immobilization onto the electrode surface a thin enzymatic layer, which measures the concentration of a substrate. The enzymatic reaction transforms the substrate into a reaction product that is detectable by the electrode. The enzyme biosensors therefore require a recording system to decode the signal produced during the enzymatic reaction. The signal (current) measured is usually proportional to the concentration of analyte in the solution. The enzymes used in these systems do require periodical renewal to maintain their optimal activity.



#### 3.4.5.1 Principles of operation

A schematic representation of an enzyme biosensor setup used in this study is given in Figure 3.7. The sensitive BDD electrode surface is in contact with an enzymatic layer incorporated in PANI-PVS composite films, and it is assumed that there is no mass transfer across this surface. The external surface of the enzymatic layer is immersed in a solution containing the substrate or analyte under investigation. The substrate or analyte migrates towards the interior of the layer and is converted into reaction products when it reacts with the immobilized enzyme. In order to achieve rapid equilibrium of concentrations, the polymer film and the enzymatic membrane must be as thin as possible. The solution must also be well stirred to ensure constant supply of the analyte and proper mixing of the solution when the analyte is introduced. In summary, the steps during the operation of an enzyme electrode are as follows:

- i. Transport of the substrate or analyte from the bulk of the solution towards the enzymatic layer;
- ii. Diffusion of the substrate or analyte within this layer, accompanied by the enzymatic transformation of the substrate or analyte into reaction product. Diffusion is the movement of a species down a concentration gradient and it occurs whenever there is a chemical change at an electrode surface;
- iii. Migration of the product towards the BDD electrode surface. Migration is the movement of charged species due to a potential gradient, and it is the mechanism by which charge passes through the electrolyte. For the electroactive species, the forces leading to migration are purely electrostatic, and hence the charge can be carried by any ionic species in the solution [390];
- iv. Conversion of the concentration of the product at this interface into an electrical signal by the BDD electrode;
- v. Amplification, measurement and decoding of the signal (current or potential) by an appropriate electronic unit.

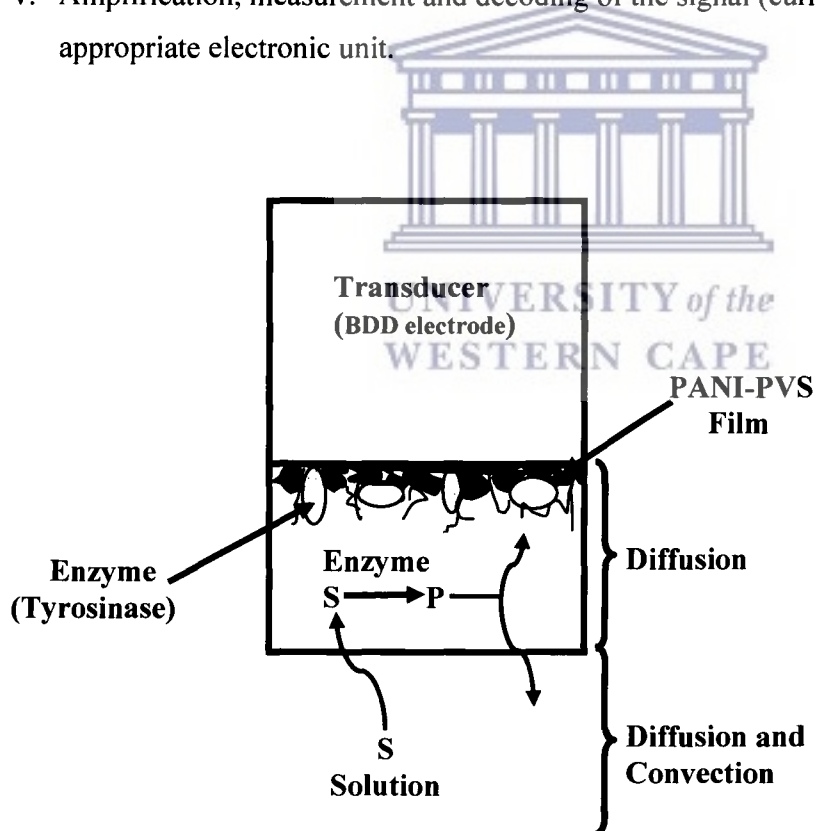


**Figure 3.8.** Schematic representation of the diffusion of the substrate S and the product P in the enzymatic layer on a transducer.



### 3.4.5.2 Practical aspects

Once the biosensor has been conceived and constructed, it can be installed in a number of different ways according to the objective required. It may be simply immersed into the sample medium, placed in a cell into which the sample is injected, or integrated into an automated system. Specific application of an enzyme biosensor requires precise information about its response time, the range and the reproducibility of its calibration curve, its detection limit, and any other parameters that determine the stability of its response. Appropriate experiments were therefore conducted to optimize the enzyme biosensor parameters.

#### 3.4.5.2.1 Response time

The response time of a biosensor is the time taken for it to reach a steady state where it is no longer possible to detect any variation in the signal. The response time is very difficult to evaluate precisely in steady state so the  $t_{98}$  value corresponding to the time taken to reach 98% of the sensor response is often used instead of the response time [73]. In practice, the transducer does not transform a chemical signal into an electric one immediately, but requires a certain time, which depends on the transducer used. It is reported that stirring the sample medium or using forced convection reduces the response time of a biosensor since it favors the movement of the substrate or analyte towards the active enzymatic membrane [73].

#### 3.4.5.2.2 Biosensor calibration

A biosensor can be calibrated by varying the substrate concentration as shown in Figure 3.8. The biosensor has a linear range for L-Phe concentrations between  $1.0 \times 10^{-5}$  M and  $3.0 \times 10^{-5}$  M. The curve flattens out on both sides of the linear zone. The upper plateau corresponds to high concentrations of L-Phe ( $[S] \gg Km$ ), a situation which saturates the active sites of the enzyme while the lower plateau corresponds to the detection limit of the transducer. The important part of the curve is usually the linear range where variation in substrate concentration gives a

variation in the current. The slope of the curve in the linear zone corresponds to the sensitivity of the biosensor because it expresses a variation in the signal obtained as a function of the analyte concentration.

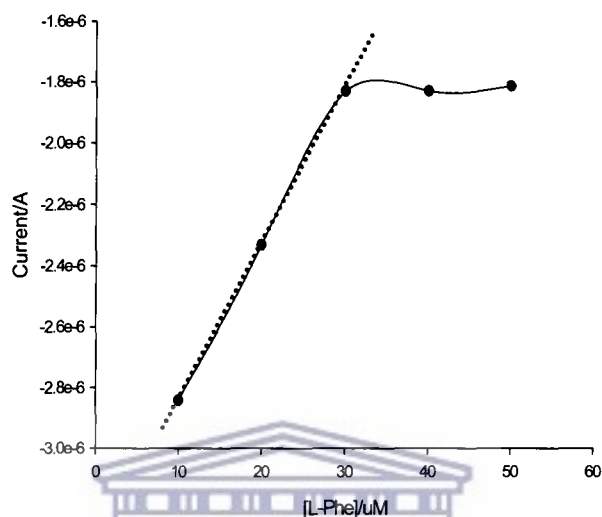


**Figure 3.9.** Calibration of an amperometric enzyme electrode for L-phenylalanine.

### 3.5 Electrochemical procedures

#### 3.5.1 Electrochemical activation and cleaning of BDD electrodes

A BDD disk microelectrode, prior to the use in electrochemical experiments, was activated by repeated cycling the potential in vigorously stirred (to remove gas bubbles) aqueous 1 M  $\text{HNO}_3$  solution between -200 and +1500 mV until a stable signal is detected for 15 cycles at scan rate of 50 mV/s (versus Ag/AgCl). This kind of pretreatment is introducing surface hydroxyl groups at the BDD electrode surface. The hydroxyl ( $\text{OH}^-$ ) terminated BDD electrode was then further modified by deposited PANI-PVS films in aqueous solution. This is followed by drop coating a solution tyrosinase enzyme dissolved in PBS buffer onto the active electrode surface. The

cleaning processes were applied each time when the modified electrode was used for subsequent study; polished with slurries of 0.05  $\mu\text{m}$  alumina, rinsed with doubled distilled water, sonicated with pure ethanol/or water for 3 minutes and then cycled in 1 M  $\text{HNO}_3$  at scan rate of 50 mV/s (versus Ag/AgCl) to ensure that a consistent BDD surface had been prepared and ready to be used.

### **3.5.2 Electrochemical synthesis and characterization of polyaniline doped with polyvinyl sulphonate (PANI-PVS)**

Polyaniline doped with polyvinyl sulphonate (PANI-PVS) films were synthesized in both 1 M  $\text{H}_2\text{SO}_4$  and 1 M HCl aqueous solutions of distilled 0.2 M aniline and 15 mg/ml PVS (Sigma-Aldrich) using potentiostatic method at room temperature in one compartment, three electrode glass cell. PANI-PVS films were deposited on the BDD microelectrode by cyclic voltammetry (CV) method. The potential was cycled between  $-200$  and  $+1200$  mV at a scan rate of  $50 \text{ mV s}^{-1}$  (versus Ag/AgCl) for 10 cycles. The modified BDD electrode was used as a working electrode. The electrolyte solutions were prepared in distilled water. The applied current density  $1 \text{ mA/cm}^2$  and the pH of the electrolytes ( $\text{pH} < 1$ ) were kept constant during synthesis of composite film. After preparation, the polymer deposited electrode was rinsed thoroughly in distilled water, dried in room temperature and then used for subsequent characterization. The same electrochemical synthesis procedure was employed for the deposition of the polymer on screen-printed BDD electrode for SEM analysis.

### **3.5.3 Multi-scan rate studies on the electrochemical behaviour of electrodeposited PANI-PVS**

#### **3.5.3.1 Characterization of PANI-PVS in H<sub>2</sub>SO<sub>4</sub> and HCl**

The characterization of the polyaniline doped with polyvinyl sulphonate was carried out by performing multi-scan rate cyclic voltammetry. The polymer modified electrode was placed either in degassed 1 M H<sub>2</sub>SO<sub>4</sub> or 1 M HCl solution. The potential of the working electrode was then cycled between -200 and +1200 mV potential limits and multi-scan rate voltammograms recorded at scan rates of 5–200 mV s<sup>-1</sup>. This procedure was repeated for all the other electrodeposited PANI-PVS composite films.

#### **3.5.3.2 Characterization of the polymer composites in phosphate buffer solution (PBS)**

The characterization of the polymer-modified electrodes in phosphate buffer was similar to that done in 1 M HCl. However voltammograms were recorded between -200 and +1200 mV potential limits. Measurements were done in phosphate buffer pH 7.2. Square wave measurements were done as previously described. It was deemed necessary to perform composite characterization in phosphate buffer in order to verify their electroactivity and therefore validate their usefulness for biosensor construction.

### **3.5.4 Preparation and characterization of the enzyme biosensor**

Test enzyme employed for the biosensor construction (see Figure 3.9) in this project was tyrosinase (Tyr) (E.C. 1.14.18.1, binuclear type III copper centre, 5370 units mg<sup>-1</sup>). The enzyme was immobilized by drop coating on composite PANI-PVS film onto BDD electrode. The drop coating enzyme solution was prepared as 4.5 mg/ml 0.01 M phosphate buffer (pH 6.2) of which an aliquot of 5 µL was immobilized onto the PANI-PVS film electrode surface allowed to dry in air at room temperature (25 °C) for 24 hours. This kind of immobilization results in a greater

physical and chemical stability of the catalytic material due to the attachment formed between polymers and enzyme. In this case, the active sites of the enzyme could be more accessible for the enzymatic reaction. The biosensor (Tyr/PANI-PVS/BDD) electrodes were rinsed with de-ionized water to remove any loosely bound enzyme, and stored in buffer solution (pH 6.8) at 4 °C when not in use. The resultant biosensor was then applied to the measurement of L-phenylalanine (L-Phe). The same procedure for immobilization of Tyr onto the surface of PANI-PVS modified screen-printed BDD electrodes was used for SEM analysis. The electrochemical behaviour of the biosensor (Tyr/PANI-PVS/BDD) electrodes was investigated by CV in the potential range between -200 and +1200 mV. The characterization of the biosensor was carried out in 0.1 M PBS at various scan rates. Other biosensor parameters such as stability and sensitivity were investigated and optimized. All experiments concerning use of enzymes were carried out in an air-conditioned atmosphere. This was necessary because enzymes are easily denatured in harsh conditions e.g. high temperatures, pH outside their physiological pH limits.

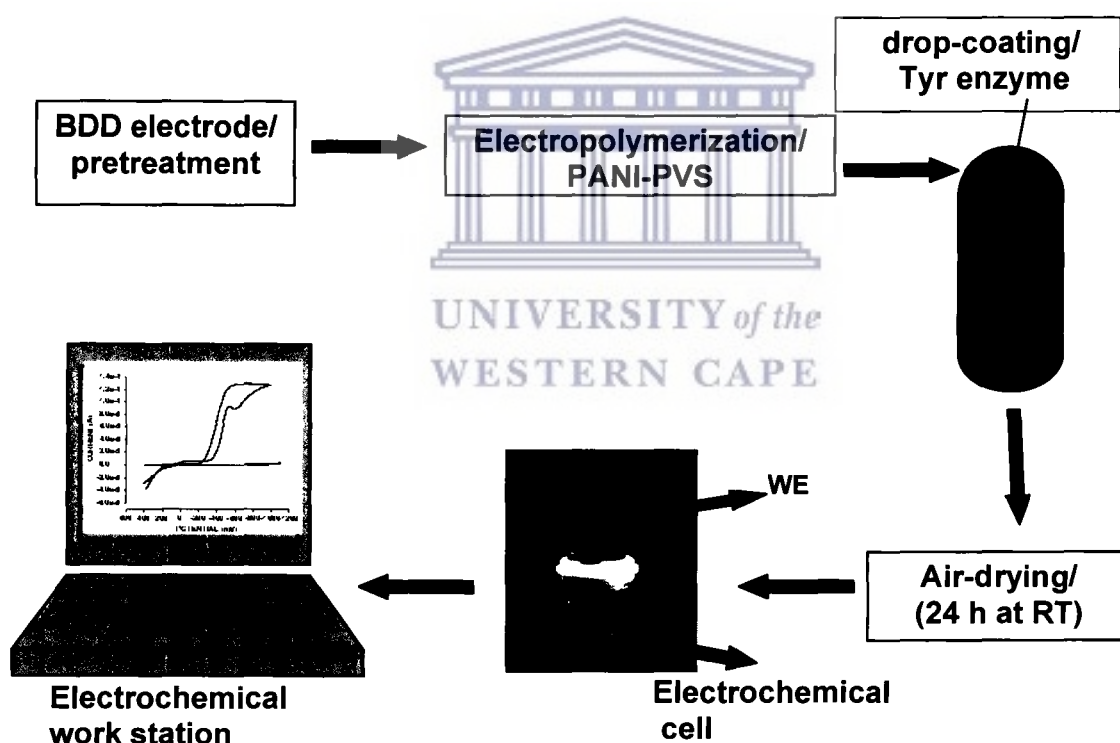


**Figure 3.10.** A scheme of the steps followed during the preparation of enzyme electrodes and ultimate biosensor construction.

### 3.5.5 Electrochemical measurements

The cell used for the electrocatalytic oxidation of L-phenylalanine (L-Phe) consisted of Tyr/BDD and Tyr/PANI-PVS/BDD biosensors respectively as the working electrodes, platinum wire as counter electrode and Ag/AgCl as reference electrode. Cyclic voltammetry was used to measure the responses of the Tyr/BDD and Tyr/PANI-PVS/BDD biosensors to the substrate L-Phe before and after adding its standard solutions at controlled room temperature of 25 °C. The enzyme biosensor constructed was immersed into the cell in 0.1 M PBS (pH 7.2), 0.2 M L-Phe standard solutions were each time added and connected to the instrumentation for the electrochemical measurements, therefore, voltammetric detections were performed. A magnetic stirrer was used for 60 seconds to stir the solution at 750 rpm after injection of the substrate then the solutions left to stand still before the voltammograms were recorded. The response of the biosensor electrode was measured in a quiescent solution and recorded.

The oxidation current generated is proportional to the concentration of L-Phe standard solution and it is a measure of the activity of the immobilized enzyme. L-tyrosine was used as substrate in this study to serve as a reference for L-3,4-dihydroxyphenylalanine (L-dopa) production and its biosensor response was also measured in a quiescent solution and recorded. All cyclic voltammograms (CVs) were performed at 50 mV s<sup>-1</sup>. Linear sweep voltammetry (LSV) and Square wave voltammetry were used to measure the responses of the biosensor to L-Phe and the square wave voltammetry was carried out using a step potential of 50 mV, a frequency of 15 Hz, and amplitude of 50 mV.

### 3.6 Graphing and data analysis

After collecting the data in an experimental setup using BAS Programs, OriginLab and SigmaPlot 8.0 software were used for graphing and data analysis.

### 3.7 Determination of the limit of detection (LOD)

The limits of detection (LOD) for the biosensor towards the substrate were calculated as shown below (equation 3.9):

$$LOD = \frac{3 \times \text{Standard Deviation (S.D) of replicate analysis of the Blank}}{\text{Sensitivity}} \quad (3.9)$$

Sensitivity is defined as the slope of the linear calibration curve of the biosensor. In the case of determination of analytes that are inhibitors of an enzymatic activity, the limit of detection can also be defined as the concentration of the inhibitor required to obtain 10-20% of inhibition considering the error of the measurements [391,392].





## CHAPTER 4

### Synthesis and characterization of Polyaniline Doped with Polyvinyl sulphonate (PANI-PVS)

#### 4.1 Introduction

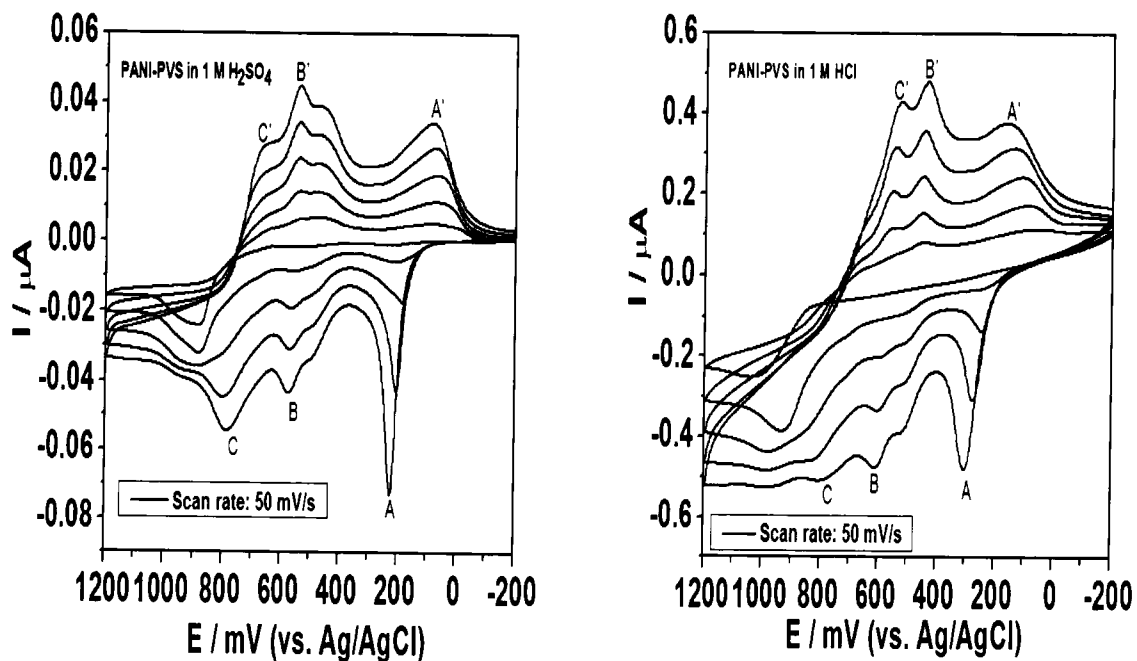
As mentioned earlier, PANI and its derivatives have been studied extensively since its discovery in the 1980s. The interest in this material and its derivatives is mainly due to their interesting electrical and optical properties together with its chemical tunability, ease of derivatization, processability into fibres and films, as well as its stability. It has generally been agreed that the chemical/electrochemical oxidative polymerization of monomers of substituted aniline is similar to that of the parent (unsubstituted) aniline and that the properties of substituted PANIs including their nanostructures are similar to those of the parent PANI [183]. During the past two decades, PANI has been synthesized and its chemical and physical properties studied extensively under different conditions, and tremendous advances in the chemistry, electrochemistry, physics, and processing of PANI have been achieved. However, solubility of PANI has been of concern and studies are now directed towards the improvement of its solubility. In light of this, attention is now diverted to synthesis of derivatized, doped or nanostructured PANI materials which are believed to produce soluble and more processable PANI for various applications including biosensor applications. Although PANI is generally regarded to have three main stable oxidation states, i.e. *leucoemeraldine base (LEB)* form, *emeraldine base (EB)* form and the *pernigraniline base (PNB)* form, each of the above insulating base forms can be transformed into the corresponding *emeraldine salt (ES)* form either by redox doping or non-redox doping (see chapter 2).

In this study, the electrochemical synthesis of nanostructured (nanofibers, nanoparticles and nanotubes) polyaniline (PANI) was achieved by the soft-template ('template-free') method in absence and presence of a structure directing molecule, polysulphonate (PVS). The polyelectrolyte PVS acted as a dopant and a structure-directing molecule providing the template

for the production of the nanostructured materials. Firstly, the properties of the synthesized PANI and PANI-PVS films in acidic and neutral conditions were investigated in order to lay a good foundation for the subsequent studies of the properties of PANI-PVS film in neutral conditions and its potential biosensor application. The electropolymerization and doping properties of PANI-PVS films were investigated by a combination of electrochemical techniques such as cyclic voltammetry (CV) and spectroscopic techniques such as UV-Vis spectroscopy and Fourier transform infrared (FTIR) and the results are presented in this chapter. In addition, scanning electron microscopy (SEM) was used to investigate the morphology of the polymers and for estimation of their sizes. The undoped PANI was used as a reference to study the effect of doping and to ascertain if doping indeed took place.

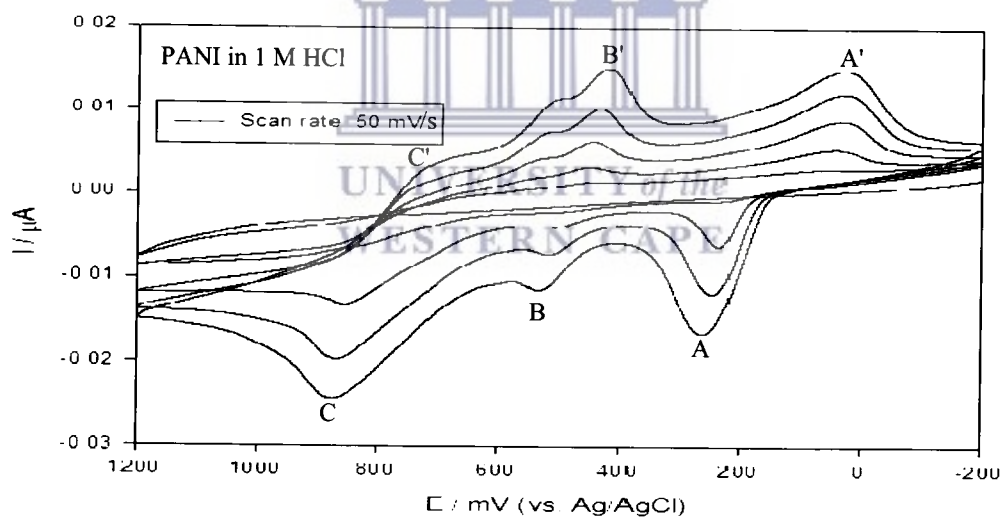
## 4.2 Electrochemical synthesis and characterization of PANI-PVS

Electrochemical polymerization of the monomer aniline on BDD electrode surface in absence and presence of the polyelectrolyte PVS was achieved by cycling the potential repeatedly between -200 and +1200 mV at a scan rate of  $50 \text{ mV s}^{-1}$  (cf. chapter 3, section 3.5.2). The cyclic voltammograms for the electrodeposition of PANI and PANI-PVS films on the BDD electrode surfaces are shown in Figure 4.1(i-iii). The electrodeposition of PANI on the BDD electrode surface (Figure 4.1(iii)) proceeds via a radical cation mechanism (cf. chapter 2, section 2.5.2). Two pairs of redox peaks centred at ca. 170 mV (a/a') and 550 mV (c/c'), corresponding to transition from leucoemeraldine to emeraldine and emeraldine to pernigraniline states respectively, were observed for both the doped PANI (PANI-PVS) and the undoped PANI [162]. This indicates the presence of discrete electroactive regions in the films. The origin of another pair of redox peaks observed at ca. 400 mV (b/b') for both PANI-PVS and PANI is much more complex and it can be attributed to many different intermediates and degradation products (cross-linked polymer, benzoquinone, etc.) [193,392].



(i)

(ii)

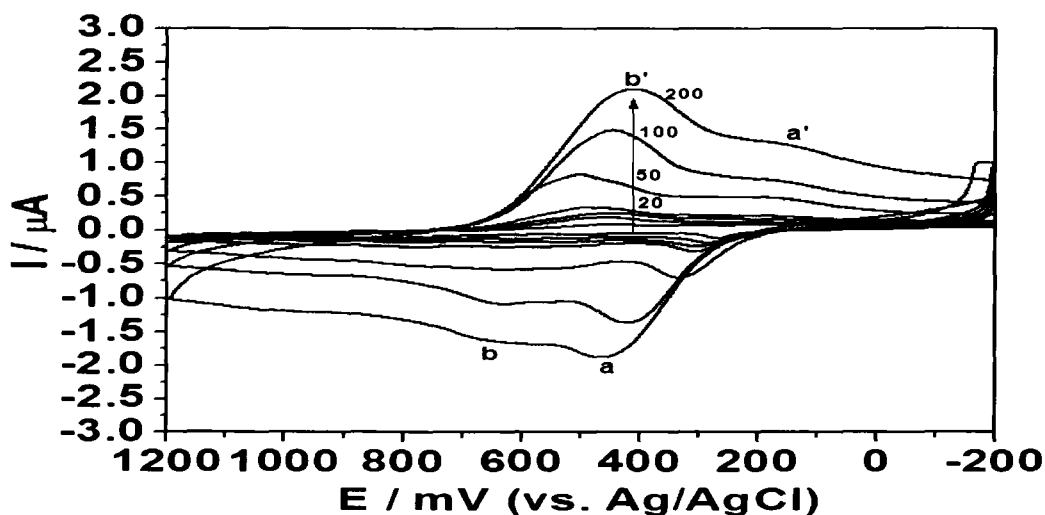


(iii)

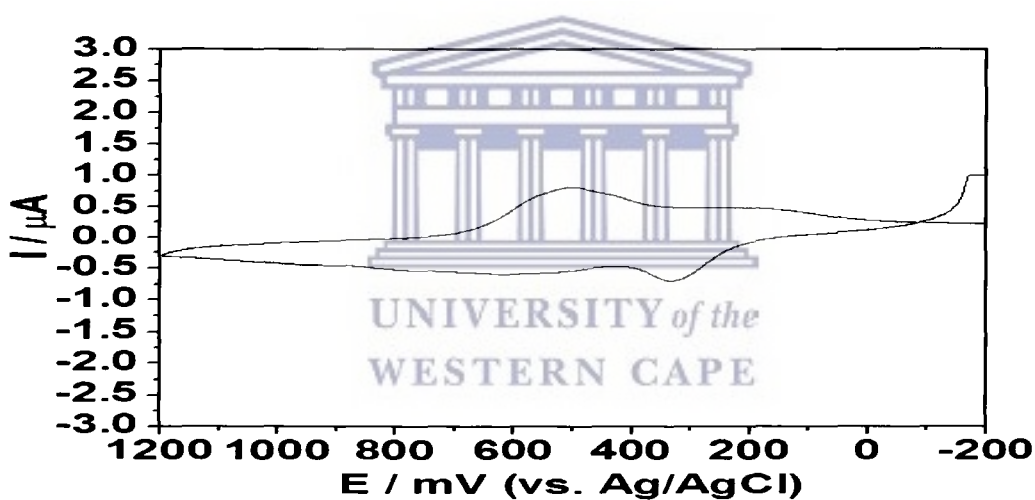
**Figure 4.1.** Cyclic voltammograms for electrochemical synthesis of (i) PANI-PVS in 1M H<sub>2</sub>SO<sub>4</sub>, (ii) PANI-PVS in 1 M HCl and (iii) PANI in 1 M HCl, using scan rate of 50 mV s<sup>-1</sup>.

However, by comparing the cathodic peaks (this peak corresponds to the reduction process of the conducting emeraldine to the insulating leucoemeraldine) in both voltammetric profiles (Figures 4.1(i) and (ii)), a higher current is observed in Figure 1(ii) and this increases the reactivity of the polymer backbone due to electron affinity. Therefore, the growth of PANI-PVS film is favoured more in the HCl than in H<sub>2</sub>SO<sub>4</sub>. It is evident that there are other factors affecting the PANI-PVS film electrode in H<sub>2</sub>SO<sub>4</sub>. To understand this paradoxical behaviour, PANI-PVS films growth on BDD electrode in both supporting electrolytes were further analyzed by scanning electron microscopy (SEM), Figure 4.6.

The PANI-PVS film electrodeposited on BDD electrode was further characterized by cyclic voltammetry (CV) in 1.0 M HCl at different scan rates and in 0.1 M PBS (pH 7.2) at a scan rate of 5 mV/s and the results are shown in Figure 4.2. Only two pairs of redox peaks occurred at approximately +200 mV (a/a', corresponding to the transformation of leucoemeraldine base to emeraldine salt) and at approximately +500 mV (b/b', corresponding to transformation of emeraldine salt to pernigraniline salt) [71] can be observed for the PANI-PVS modified electrode in 1.0 M HCl (Figure 4.2(iv)). It was also observed that the peak currents increased with increase in scan rates while the redox peaks that correspond to incorporation of degradation products disappeared. These results confirm that PANI-PVS film was successfully attached onto the BDD electrode surface. PANI being a PANI derivative, it reflects features and properties similar to those of PANI. The voltammogram for PANI-PVS film in 0.1 M PBS (Figure 4.2(v)) showed that it exhibited good electroactivity at pH 7.2 and within the potentials closer to 0 mV which is the potential range mostly employed for studies of direct electron transfer of enzymes. This makes PANI-PVS a perfect candidate for use as a mediator in enzyme biosensors. Broad redox peaks, with a large peak separation ( $\Delta E_p = E_{pa} - E_{pc}$ ) of +200 mV, are observed for PANI-PVS film in 0.1 M PBS which may be attributed to the superposition of two redox processes usually observed for PANI in strong acidic solutions (such as those in Figure 4.2(iv)), i.e., a doping/dedoping and a deprotonation/protonation process. At low pH values, two separate redox peaks can clearly be seen (Figure 4.2(iv)). The redox peak at the low potential corresponds to the doping/dedoping process, while the one at higher potential corresponds to the deprotonation/protonation process which is highly pH dependent.



(iv)

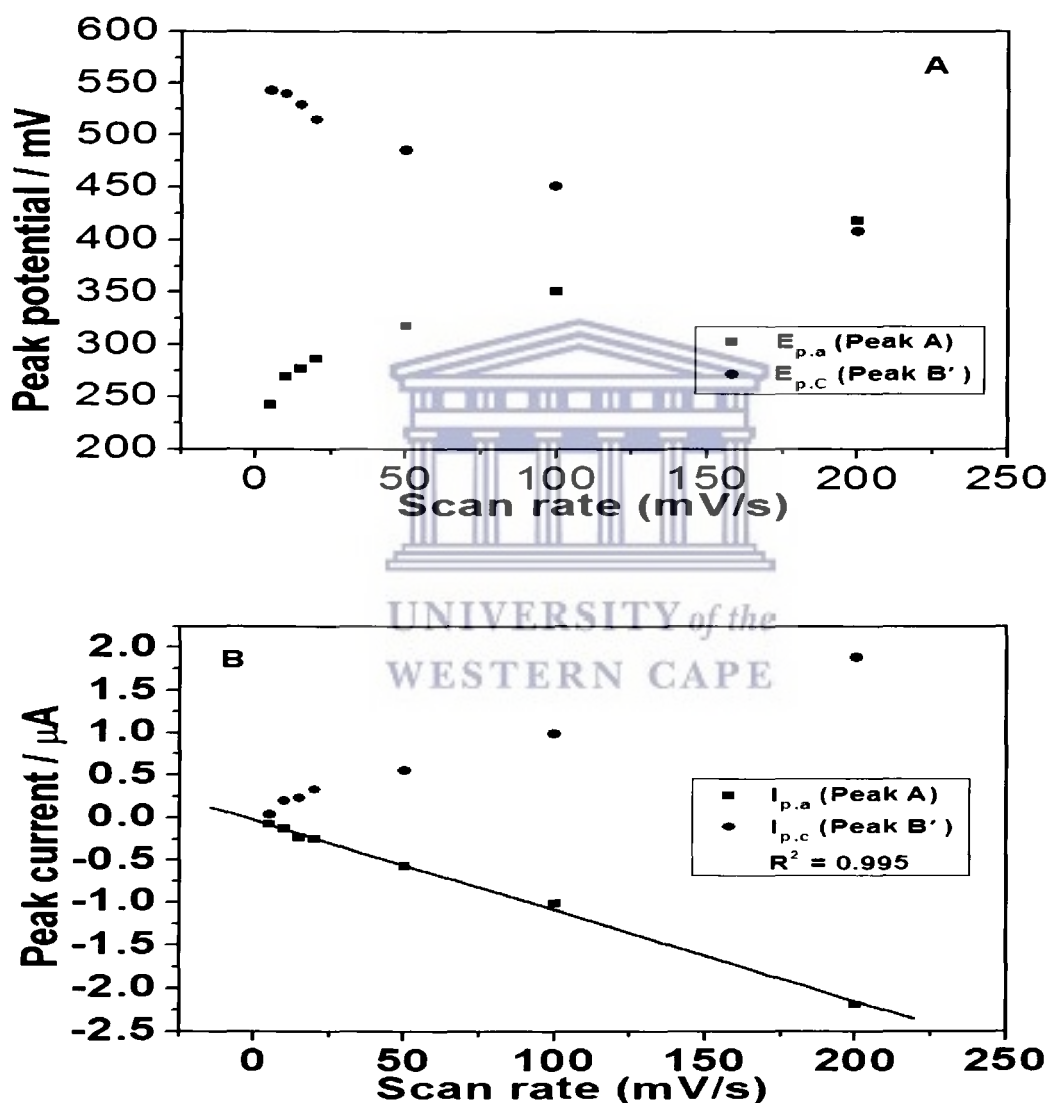


(v)

**Figure 4.2.** Cyclic voltammograms of PANI-PVS film electrodeposited on BDD in (iv) 1 M HCl solution at scan rates between 5-200  $\text{mV s}^{-1}$  and (v) 0.1 M PBS (pH 7.2), scan rate of 5  $\text{mV s}^{-1}$ .

The increasing amplitude of the redox peaks with repeated potential scans was observed (Figure 4.2(iv)), indicating that the polymer was deposited at the BDD surface and was conducting. This electrosynthesized PANI film played two roles when used in these biosensor systems. Firstly, it behaved as an electron mediator, transferring electrons between the immobilized enzyme and the

electrode surface. Secondly, it served as a point of attachment for the protein (e.g. tyrosinase). Moreover, this increasing in the amplitude of the redox peaks (Figure 4.2(iv)) may confirm that the diffusion of electrons was taking place along the polymer chain (Figure 4.3A). The dependence of peak currents of anodic peak *I* on the scan rate indicated that we have a thin film of surface-bound conducting electroactive polymer, undergoing rapid reversible electron transfer reaction (Figure 4.3B).



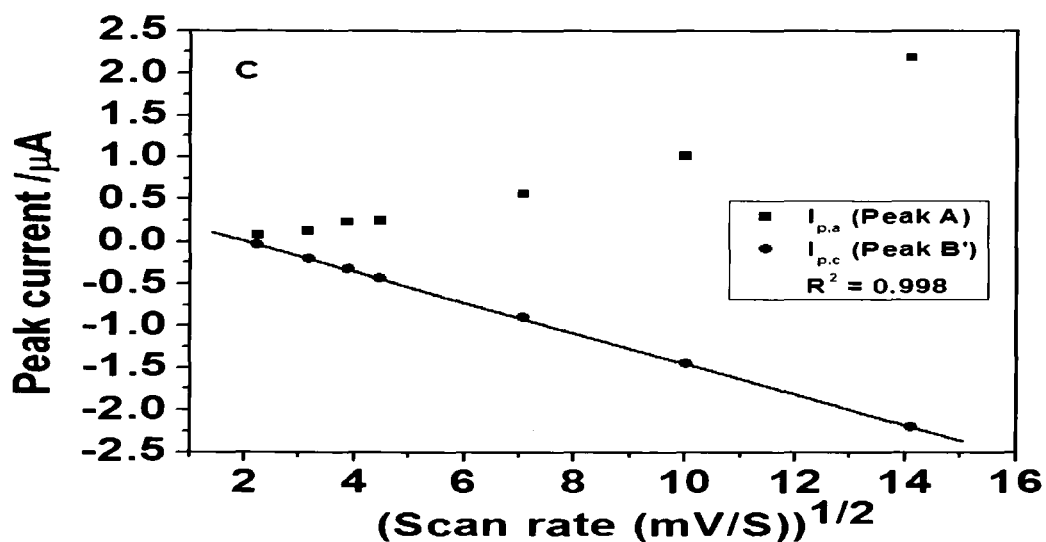


**Figure 4.3.** The plots obtained after the electropolymerization of PANI-PVS at BDD electrode (PANI-PVS/BDD electrode): (A) peak potentials ( $E_p$ ) versus scan rate, (B) peak currents ( $I_p$ ) versus scan rate and (C) peak currents ( $I_p$ ) versus square root of the potential scan rate. The values of  $E_p$  and  $I_p$  were effectively calculated from peaks a and b' of PANI-PVS/BDD electrode at different scan rates (see Figure 4.2(iv)), where  $I_{p,a}/I_{p,c} = 0.995$ .

Figure 4.3C illustrates the dependence plot of the cathodic peak current ( $I_{p,c}$ ) as a function of the square root ( $v^{1/2}$ ) of the potential scan rate (correlation coefficient,  $r^2 = 0.998$  and slope 0.1058) for the PANI-PVS film. This shows an indication of the diffusion-controlled of the cathodic peak current arising from the electron propagation through the polymer chain. The surface concentration of the adsorbed electroactive PANI-PVS film can be estimated from the plot of current versus potential (Figure 4.2(i)) using Brown-Anson model. The Randel-Sevcík equation was used to determine the rate of electron transport (i.e., diffusion coefficient of the electrons,  $D_e$ ) within the polymer.  $D_e$  can be evaluated from the slope of the straight line obtained from the  $I_{p,a}$  versus  $v^{1/2}$  plot (Figure 4.3C). The calculated results have shown in Table 1.



**Table 4.1.** Kinetic parameters of the PANI-PVS composite film in 0.1 M PBS (pH=7.2)

Variable	Symbol	Result
Peak separation	$\Delta E_p$	$129 \pm 5$ mV
Surface concentration of polymer film	$\Gamma^*$	$1.86 \times 10^{-7}$ $\text{mol cm}^{-2}$
Diffusion coefficient	$D_e$	$6.51 \times 10^{-8}$ $\text{cm}^2 \text{s}^{-1}$

The diffusion coefficient ( $D_e$ ) value is found to be  $6.51 \times 10^{-8} \text{ cm}^2 \text{ s}^{-1}$  for PANI-PVS film. This value is in agreement with the value ( $6.46 \times 10^{-8} \text{ cm}^2 \text{ s}^{-1}$ ) that has been reported previously in the literature [151] concerning a similarity of the electroactive polymer film characteristics in 1M HCl solution. Thus,  $D_e$  value depends on the density and homogeneity of the film as well as other conditions for growing the polymer. Nevertheless, the inclusion of the ionic co-polymer PVS has shown to increase the conductivity of the PANI film.

#### 4.3 Optimization of the stability of BDD surface electrode for electropolymerization of PANI-PVS in 1 M HCl

A well-defined reproducible voltammogram for the electropolymerization of PANI-PVS in 1 M HCl was obtained (Figure 4.4). The BDD electrode exhibited excellent electrochemical stability for the measurements performed at different times, which indicated strong bonding of PANI-PVS with BDD.

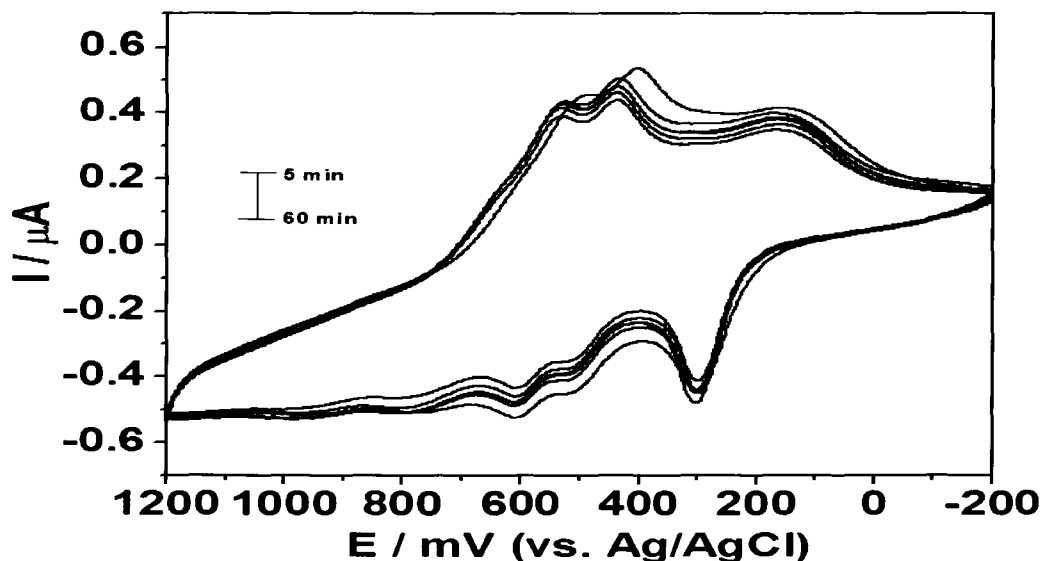


**Figure 4.4.** CV of stability BDD/PANI-PVS in 1 M HCl with measurements performed at different time (from 5-60 min), at scan rate of  $50 \text{ mV s}^{-1}$ .

#### 4.4 Characterization of PANI-PVS films using UV-Vis spectroscopy

The UV-Vis spectroscopy is a common technique that is used to give qualitative indication of the intrinsic redox states of conducting polymers. In this study, UV-Vis has been used to give an indication of the redox state of PANI-PVS and to study the changes that occur as a result of doping. The electropolymerized PANI and PANI-PVS films were dissolved in N,N-dimethylformamide (DMF) and subjected to UV-Vis analysis. The UV-Vis spectra are presented in Figure 4.5.

Differences in the positions of absorption bands are observed when UV-Vis spectrum of undoped PANI is compared with that of PANI-PVS. The UV-Vis spectrum of PANI-PVS film shows only one peak in the region ca. 493 nm due to the polaron  $\rightarrow \pi^*$  band transition for emeraldine salt form of PANI. This confirms the effective doping of PANI during electropolymerization. Michira also observed the same kind of behaviour for PDMA doped with

naphthalene sulfonic acid (NSA) in which only one polaron band appeared at ca. 780 nm [237]. This polaron band is a diagnostic test for the conformation of the PANI chains [393]. The undoped PANI on the other hand displays also the same behaviour for a strong band at ca. 493 nm that is characteristic of emeraldine base. This can be attributed to a local charge transfer between a quinoid ring and the adjacent imine-phenyl-amine units giving rise to an intramolecular charge transfer exciton [182,394].

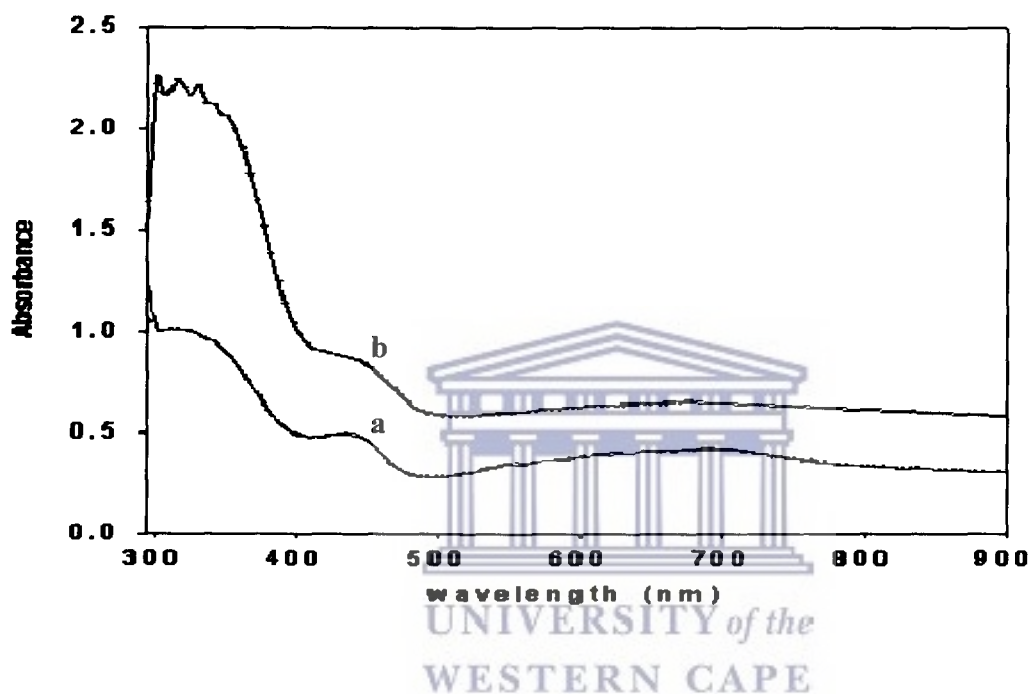
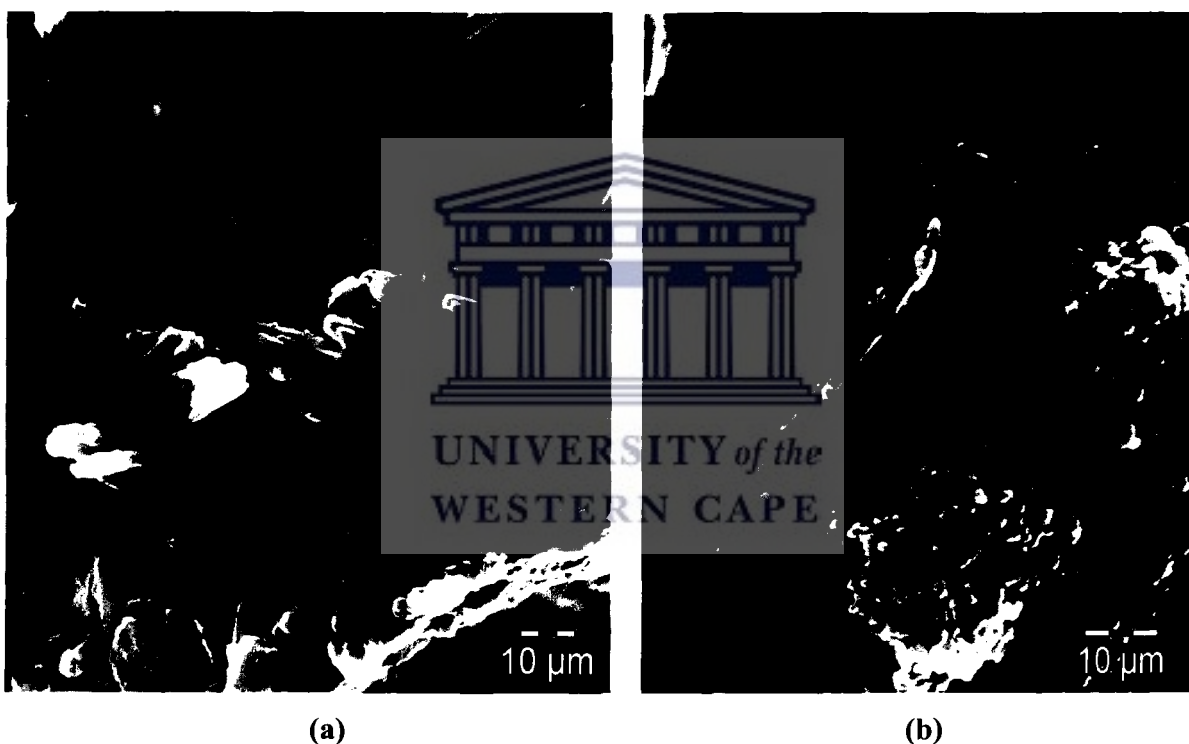


**Figure 4.5.** UV-Vis spectra of a) PANI and b) PANI-PVS films.

#### 4.5 Characterization of PANI-PVS films using SEM

The chemical and electrochemical synthesis of PANI and PANI derivatives result in different kinds of morphologies depending on the synthesis conditions such as the nature of dopant, solvent used, synthesis temperature, the type of template used, the monomer: dopant ratio, synthetic route used etc. One-dimensional nanostructured PANI have mostly been synthesized by the use of hard and soft templates either chemically or electrochemically. On the contrary, the PANI nanoparticles can be synthesized chemically or electrochemically without employing

templates. The scanning electron microscopy (SEM) images of the electrosynthesized PANI and PANI-PVS films are shown in Figure 4.6. The SEM image of the PANI film synthesized by the electrochemical “no-template” method i.e. without employing any template is shown in Figure 4.6a. ‘Flower-like’ microfiber aggregates with diameters less than 200 nm are observed on the image. The SEM image of PANI synthesized by the electrochemical “soft template” method (PANI-PVS), employing the polyelectrolyte PVS to act as a structuredirecting molecule shows globular morphology with buds of polymer having diameters less than 100 nm. As observed, there is a change in morphology when PVS is incorporated into PANI (Figure 4.6b) indicating that PVS played a role in directing the structure and morphology and aligning the monomers to form more ordered structures.



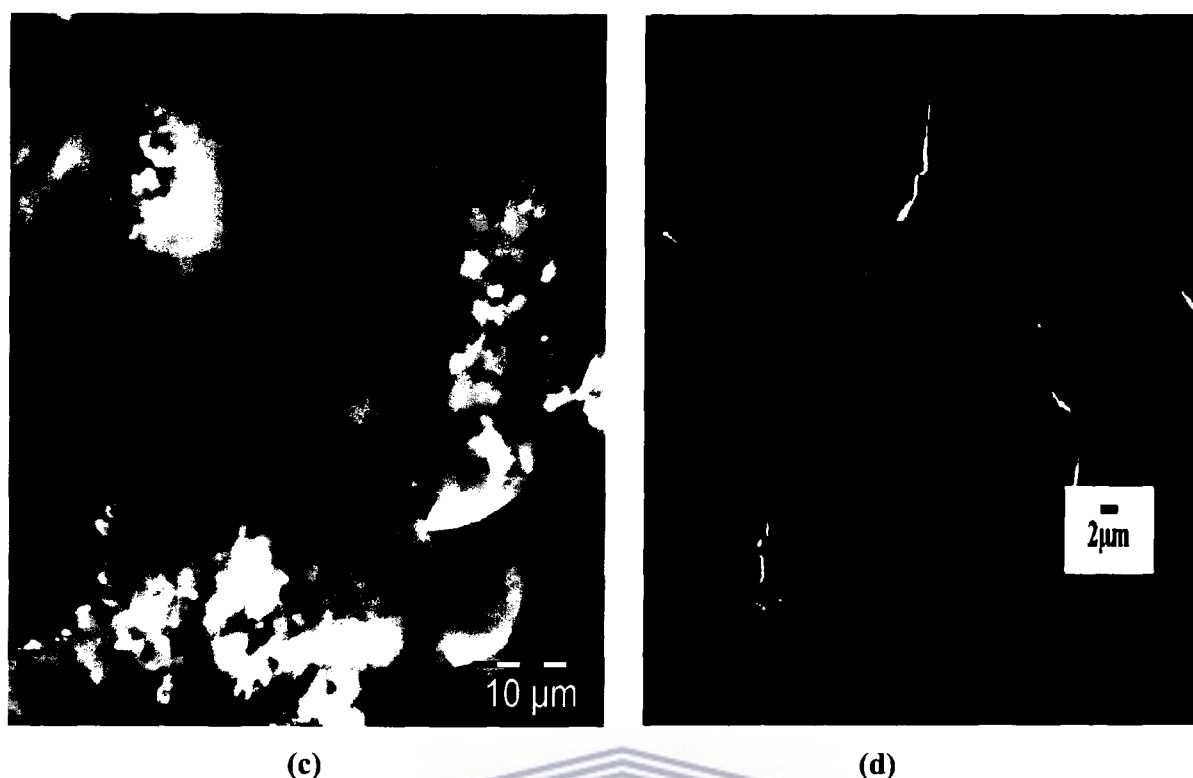


**Figure 4.6.** SEM image of (a) PANI and (b) PANI-PVS in 1 M HCl; (c) PANI-PVS in 1 M H<sub>2</sub>SO<sub>4</sub> and (d) bare electrode (BDD without modification).

PANI-PVS was also electrochemically synthesized in 1 M H<sub>2</sub>SO<sub>4</sub> as stated in section 4.2. As follows from the resulting micrographs (Figure 4.6b and c) when compared with the unmodified electrode (Figure 4.6d), the samples have different morphological structure. The SEM micrograph of PANI-PVS in H<sub>2</sub>SO<sub>4</sub> (Figure 4.6c) demonstrates a porous layered structure, whereas PANI-PVS in HCl (Figure 4.6b) shows a granular porous structure. This feature could explain the higher currents observed on the voltammetric profiles for this electrode (Figure 4.1b). These observations demonstrate different supporting electrolytes may yield conductive polymers with different morphological structure even when the same synthesis method and the same monomer are used. The morphology of the polymers is influenced by the electrolyte type. In this study, the growth rate of a PANI-PVS film in hydrochloric acid (HCl) is more favoured than that in sulphuric acid (H<sub>2</sub>SO<sub>4</sub>). It means that the granular morphology of a porous structure favors a higher rate of polymerization of aniline. Due to all these factors the SEM micrograph of PANI-PVS in HCl is more granular and porous than in other supporting electrolyte, H<sub>2</sub>SO<sub>4</sub>.

#### 4.6 Conclusions

Nanostructured PANI-PVS materials were successfully prepared by the electrochemical “soft template” method in which PVS acted as a dopant and provided the template for the synthesis of the nanomaterials. The results indicate that when PVS is used as a polyelectrolyte, it can direct the synthesis of both nanotubes and nanoparticles with diameters less than 100 nm. The microscopic technique revealed that the PANI-PVS materials exhibited properties similar to those of the parent doped PANI (unsubstituted) and they have backbone structures similar to that of the conventionally prepared granular doped PANI. Successful electrochemical doping was confirmed by the spectroscopic techniques as The nanostructured PANI-PVS materials synthesized by the electrochemical ‘soft template’ method also presented highly attractive features such as ease of synthesis, high solubility in N,N-dimethylformamide, good structural stability and conductivity in neutral pH which are suitable for their application as biosensor materials.



## CHAPTER 5

### Tyr/PANI-PVS Biosensor characterization and Optimization

#### 5.1 Introduction

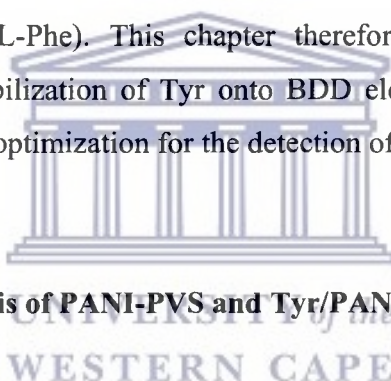
The direct electron transfer between an electrode and a redox enzyme is very important for the fundamental studies and the construction of biosensors. However, because of the unfavorable orientation of the enzyme on the bare electrode surface or the adsorption of impurities that denature it, the enzyme often exhibits sluggish electron transfer at conventional electrode surfaces. As discussed earlier (cf. chapter 2, section 2.3), modification of the electrode surface using suitable compatible matrices are known to provide a favorable micro-environment for the protein to exchange its electrons directly with the underlying electrode and thus the study of enzyme electrochemistry can be achieved. Hence, a suitable mediator has been used to realize the direct electron transfer of Tyr at an electrode surface. Tyrosinase (Tyr) is an important heme-containing enzyme (type III protein) that has a binuclear copper active site in which the copper (II) centers are electronically coupled [395]. Tyrosinase possesses oxidase activities, catalyzing the oxidation of *o*-diphenols to *o*-quinones (catecholase activity) [396]. Nevertheless, direct electrochemistry of Tyr at boron-doped diamond (BDD) electrode has been discussed in this study.

Nanostructured conducting polymers and in particular, PANI and PANI derivatives have attracted much more attention with this regard in recent years especially in biological and chemical researches because of their biocompatibility. It is well-known that the nanostructured polymers possess interesting features including high electrical conductivity, stability, improved processability and solubility in a variety of solvents which are superior to those of the parent polymers. On the other hand, they can act as tiny conduction centers to facilitate electron transfer between the enzyme and the electrode surface. They are also known to provide a suitable micro-environment for enzyme immobilization during biosensor construction enabling direct communication between the immobilized enzyme and the electrode surface.



In most cases, biosensors have been constructed by electrodeposition of nanostructured polymers onto the electrode surface, followed by drop coating attachment of the enzymes to the polymer layers.

In this study, the interesting features of the nanostructured PANI-PVS materials synthesized by the “soft template” method, such as ease of synthesis, good structural stability, conductivity in aqueous media at neutral pH and high solubility in N,N-dimethylformamide were investigated for their possible application as mediators in the construction of Tyr/PANI-PVS biosensor. After their electrodeposition on BDD electrode surface, the model enzyme Tyr was immobilized by the drop coating attachment method resulting to an enzyme biosensor, Tyr/PANI-PVS. The direct electron transfer of Tyr on nanostructured PANI-PVS matrix was then investigated and the biosensor parameters were characterized by cyclic voltammetry (CV), as well by spectroscopic techniques such as UV-Vis spectroscopy and FTIR. Finally, the biosensor operating parameters were studied, optimized and then applied for the evaluation of its electrocatalytic activity for the oxidation of L-phenylalanine (L-Phe). This chapter therefore presents the results for the characterization of direct immobilization of Tyr onto BDD electrode and the Tyr/PANI-PVS biosensor as well as those for its optimization for the detection of L-phenylalanine.



## **5.2 Spectroscopic analysis of PANI-PVS and Tyr/PANI-PVS films**

### **5.2.1 UV-Vis spectroscopy**

The rationale behind the use of the UV-Vis spectroscopy technique as a spectroscopical signature for conductivity [397] relies on the fact that doped polymers are structurally modulated and their electronic spectra display additional absorption bands associated with the existence of polarons/bipolarons. The latter bands are delocalization charge defects in the polymer whose presence converts the polymer into an intrinsic conductor. It is now well known that the electronic spectra of undoped polyanilines are basically made up of two absorption bands. A band at ca. 320 nm due to the  $\pi$ - $\pi^*$  transition of the benzoid rings and another at ca. 600 nm assigned to the  $\pi$ - $\pi^*$  of the quinonoid structures [398,399]. In addition to these bands, doped

polyanilines are characterized by additional bands at ca. 420 and 800 nm associated with the polaron/bipolaron states in the polymer. The latter states are new electronic energy levels created within the polymer sub-gap energies during the polymer /dopants interactions.

However, the UV-Vis spectroscopy is therefore an effective means for monitoring the possible changes of the Soret band in the heme group region. The position of the Soret band of the heme provides information regarding the tertiary structure of heme proteins; especially with regards to conformational changes in the heme region [400,401]. The UV-Vis spectra were recorded on a Nicolet Evolution 100 Spectrometer (Thermo Electron Corporation, UK). After electrodeposition of doped or undoped PANI-PVS and immobilization of Tyrosinase (Tyr) onto the PANI-PVS (in the case of Tyr/PANI-PVS films), the samples were placed in 4 cm<sup>3</sup> quartz cuvettes and their UV-Vis spectra recorded. The choice of the quartz cuvettes was because they are transparent both in the UV and the visible regions and therefore freely allowed the passing of the optical light. Free L-Phe sample was dissolved in 0.2 M HCl, pH 0.25 and its spectrum recorded. The spectra were recorded in the region of 200-600 nm. The spectra obtained were then scrutinized and compared to verify the absorption bands of the L-Phe as well as those of the polymers.

Figure 5.1 shows the UV-Vis spectra of free Tyr in PBS (pH 7.2) and that of Tyr/PANI-PVS film in PBS-DMF mixture. The Soret band for free Tyr appears at 409 nm with high absorbance while for Tyr/PANI-PVS it is slightly shifted to 415 nm. The slight shift in the Soret band for Tyr/PANI-PVS and the decrease in its absorbance may be due to the interaction between PANI-PVS film and Tyr during immobilization. Such interactions do not destroy the structure of the biomolecules, thus the results are an indication that Tyr was successfully attached and retained its biological activity after immobilization on PANI-PVS modified electrode. The spectrum of PANI-PVS film does not show any absorption near absorption wavelength of Tyr, thus the band of Tyr/PANI-PVS at 415 nm is entirely due to the Tyr Soret band. This leads to the conclusion that the nanostructured PANI-PVS film provides a suitable microenvironment for the immobilization of Tyr and can be used as a mediator to aid its direct electron transfer on the BDD electrode surface.

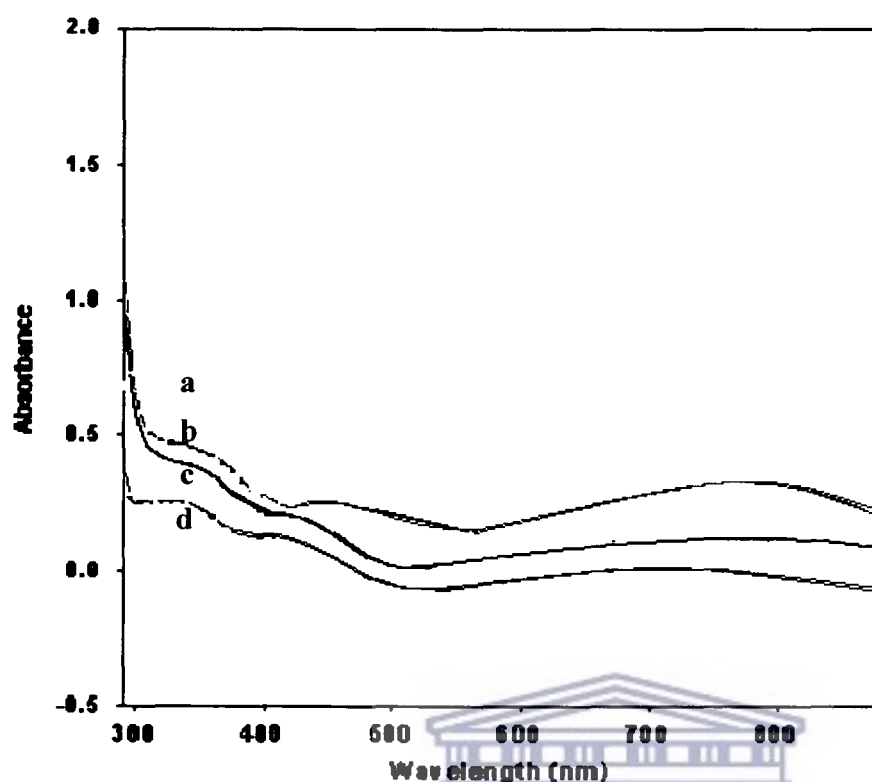


**Figure 5.1.** UV-Vis spectra for a) PANI in DMF, b) PANI-PVS films in PBS-DMF solution, c) Tyr/PANI-PVS in PBS-DMF solution and d) Tyr in PBS (pH 7.2).

UNIVERSITY of the  
WESTERN CAPE

## 5.2.2 Fourier transform infrared (FTIR) spectroscopy

The FTIR spectroscopy has been used extensively to identify the various functional groups in the polymer. Yet, the shapes and positions of the amide I and amide II infrared absorbance bands of proteins provide detailed information regarding the secondary structure of peptide backbone chain  $-(C=O)-NH-$  in both naturally occurring and artificial proteins [402,403]. The FTIR spectra were recorded on a PerkinElmer Spectrum 100, FT-IR spectrometer. The specimen were prepared by first electrodepositing doped or undoped PANI on the BDD electrode surface, then immobilizing Tyr onto PANI-PVS (in the case of Tyr/PANI-PVS films), followed by scrapping them gently from the electrode surface. The spectra of the specimen were recorded in the region

380-4000  $\text{cm}^{-1}$  directly without mixing with KBr. The spectra obtained were used to identify the various functional groups in the polymer as well as those in the backbone chain of L-phenylalanine.

The amide I band (1700-1600  $\text{cm}^{-1}$ ) is caused by C=O stretching vibrations of the peptide linkages. The amide II band (1620-1500  $\text{cm}^{-1}$ ) results from a combination of N-H in plane bending and C-N stretching vibrations of the peptide groups [404]. These two amide bands are sensitive markers for protein conformational changes. The sensitive technique widely used to probe into the secondary structure of the proteins is FTIR spectroscopy. Studies have shown that when enzymes are immobilized on substrates by electrostatic forces, there is usually a little change in their FTIR spectra [405,406]. In this study, FTIR spectroscopy has been employed to probe into the secondary structure of Tyr in order to evaluate its interaction and compatibility with the PANI-PVS film. The FTIR spectra for the free Tyr and that of Tyr/PANI-PVS film are presented in Figure 5.2. The results indicated that Tyr did not denature and its integral structure was not altered during its immobilization onto PANI-PVS/BDD electrode. This conclusion was verified by comparing the FTIR spectra of free Tyr with that of the Tyr/PANI-PVS film. Free Tyr showed an IR signal at 1643  $\text{cm}^{-1}$  for amide I band, and another one at 1528  $\text{cm}^{-1}$  for amide II band (Figure 5.2c), whereas the amide I band for Tyr/PANI-PVS film appeared at 1642  $\text{cm}^{-1}$  and the amide II band at 1530  $\text{cm}^{-1}$  (Figure 5.2b). It was observed that PANI-PVS did not show absorbance in the amide I and amide II band regions as those of Tyr and Tyr/PANI-PVS (Figure 5.2a). The IR peaks at 1642 and 1530  $\text{cm}^{-1}$  for Tyr/PANI-PVS film were thus attributed to those of amide I and II bands of Tyr indicating that the nanostructured PANI-PVS film provided a biocompatible environment for Tyr immobilization enabling it to retain its integral structure.

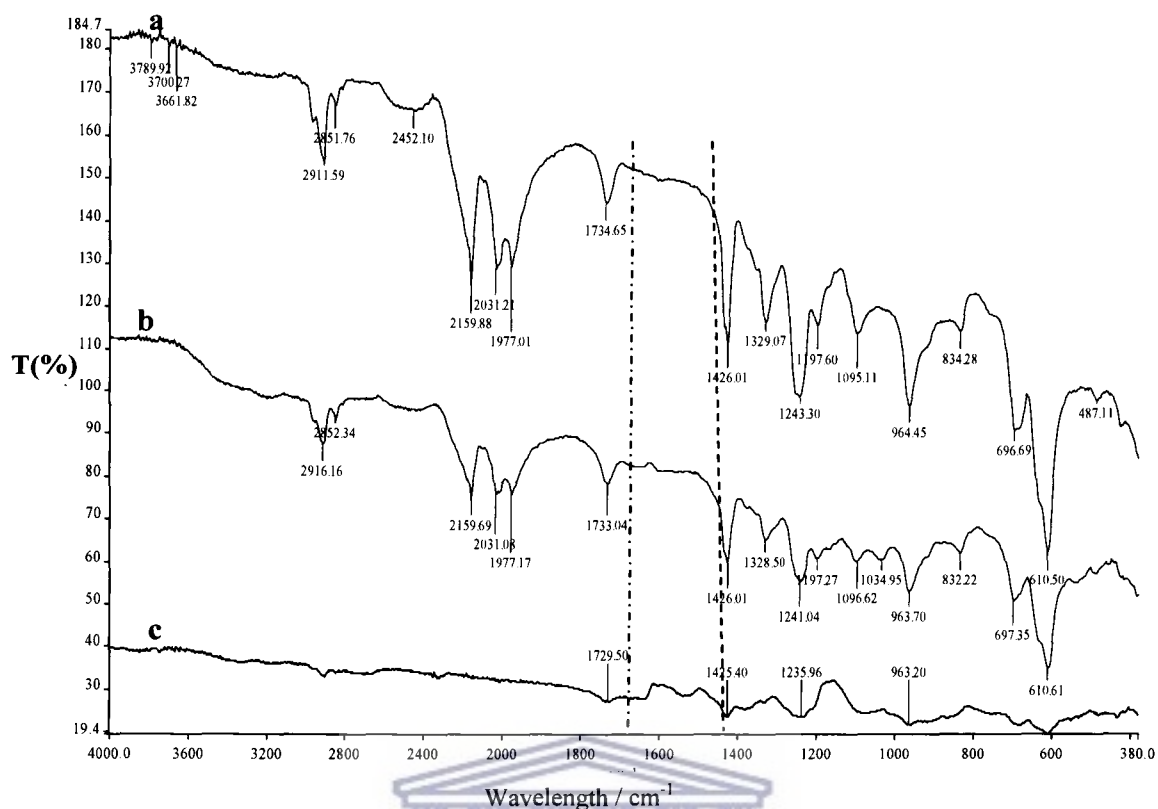


**Figure 5.2.** FTIR spectra of (a) PANI-PVS film, (b) Tyr/PANI-PVS film and (c) free Tyr.

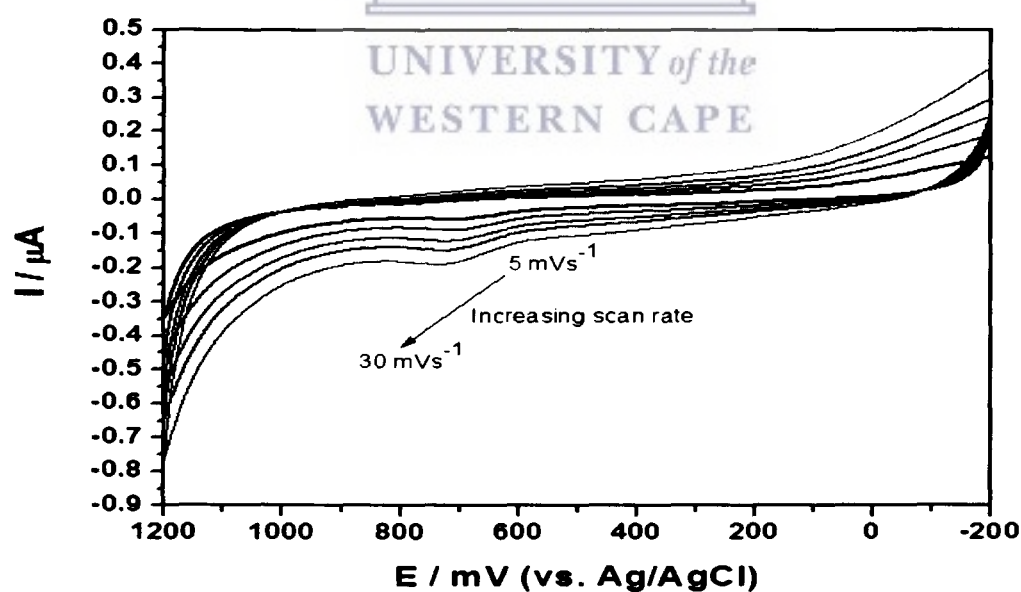
### 5.3 Direct electrochemistry of Tyrosinase (Tyr) and electrochemical characterization of the Tyr/BDD biosensor

#### 5.3.1 Immobilization and characterization of Tyrosinase (Tyr) onto BDD electrode

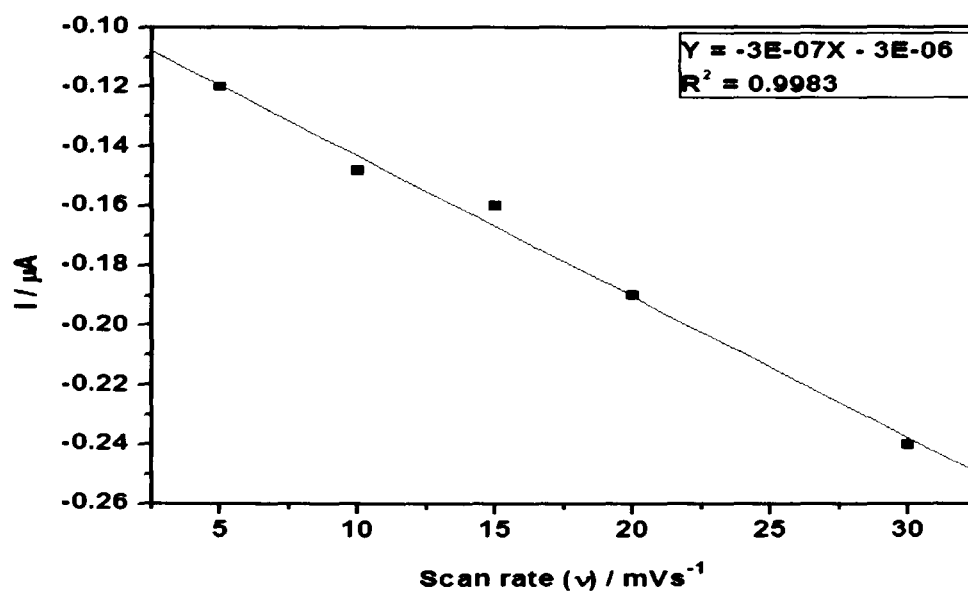
Various methods have been reported for the immobilization of Tyr on different suitable substrates. These reports have employed conventional electrode materials as substrates, such as glassy carbon [407,408], graphite-epoxy resin [84], gold [409] and other materials [410,411,412], etc. However, Tyr-based electrochemical biosensors on some substrates suffer from low stability and significant inhibition of enzyme by reaction products; both factors deteriorate electrode characteristics in phenolic compounds determination. One of the causes of poor stability is desorption of enzyme from electrode materials.

Therefore, the search for reliable methods or electrode substrates that would be a strong and efficient bonding of tyrosinase is still interesting.

In this study after ascertaining that Tyr was successfully immobilized on BDD electrode surface and that it did not denature during this process, the developed Tyr/BDD biosensor was subjected to characterization by cyclic voltammetry (CV). The cyclic voltammograms of Tyr/BDD biosensor in PBS (pH of 7.2) at various scan rates (5-30  $\text{mV s}^{-1}$ ) are shown in Figure 5.3a. It was observed that the anodic peak potential ( $E_{pa}$ ), in PBS, shifted positively with increasing scan rate while the reverse cathodic peak potential ( $E_{pc}$ ) in the CV is either diminished or completely absent which is indicative of an electron transfer reaction coupled to a catalytic process. This suggests that the Tyr enzyme was immobilized onto BDD surface. The anodic peak currents increased linearly and were directly proportional to the scan rates (Figure 5.3b), consistent with thin layer electrochemical behavior [407]. It suggests that a single protonation accompanies the single electron transfer between the BDD electrode and the heme Cu (II) of Tyr. Thus, the redox reaction between the Tyr and the BDD electrode surface is a single electron transfer process. The value estimated for the number of electrons,  $n = 1$ , was therefore used to calculate the surface concentration of electroactive Tyr at BDD electrode surface.



(a)



(b)

**Figure 5.3.** (a) Cyclic voltammograms of Tyr/BDD biosensor in 0.1 M PBS (pH 7.2) and (b) The plot of anodic peak current versus scan rates in 0.1 M PBS (pH 7.2).

The surface concentration ( $\Gamma^*$ ) of the adsorbed electroactive Tyr film can be estimated by integration of the peaks of the cyclic voltammograms of the biosensor (Figure 5.3a) and using Faraday's law according to the equation 3.9 below [413]:

$$I_p = n^2 F^2 \nu A \Gamma^* / 4RT \quad (3.9)$$

where  $I_p$  is the oxidation peak current,  $n$  is the electron transfer number,  $F$  is the Faraday constant (96493 C/mol),  $A$  denotes the geometric area of the working electrode ( $\text{cm}^2$ ),  $\nu$  is the scan rate (V/s),  $T$  is the temperature in Kelvin and  $R$  is the gas constant ( $8.314 \text{ J mol}^{-1} \text{ K}^{-1}$ ).

Scanning electron microscopy was used to characterize the morphology of PANI and PANI-PVS film. The images were acquired using either a Gemini LEO 1525 Model or a Hitachi X-650 analyzer employing the secondary electron (SE) mode with interchangeable accelerating voltages of 25 kV. In order to prepare the samples for viewing, clearly labeled (on the underside)



aluminium stubs were covered with conducting glue. The samples were then sparingly sprinkled on to the stubs. The sample containing stubs were held with a pair of forceps and knocked on the sides to remove excess polymer leaving behind an evenly spread layer. The samples were then sprayed with a thin layer of gold under vacuum. Viewing was done at different magnifications to display the morphology of the composites both in the micro and nano- ranges. The resultant images were compared to show the morphological influence of the different dopants used. Equation 5.1 illustrates the variation of peak currents with scan rates (Figure 5.3b). Considering that the integrated oxidation peak of the cyclic voltammogram for the biosensor =  $4.6213 \times 10^{-6}$  A,  $\nu = 0.01$  V/s,  $T = 295\text{K}$ ,  $A = 0.071$  cm<sup>2</sup>, and  $n=1$ , the surface concentration ( $\Gamma^*$ ) of the electroactive Tyr at BDD electrode surface was estimated to be  $6.86 \times 10^{-9}$  mol cm<sup>-2</sup>. This suggests that Tyr films were immobilized on the BDD electrode surface (Figure 5.4).



**Figure 5.4.** SEM images obtained from the surfaces of (a) bare electrode and (b) tyrosinase-modified BDD electrode.

### 5.3.2 Detection of L-phenylalanine (L-Phe) using Tyr/BDD biosensor

In an attempt to verify the conversion of L-phenylalanine to L-dopa during the electrochemical and subsequent enzyme oxidation steps, UV-Vis spectroscopy was employed. The UV-Vis absorption maxima for L-phenylalanine and L-tyrosine were confirmed at 213 nm and 256 nm respectively, based on absorbance of standard solutions prepared in the PBS buffer (Figure 5.5).

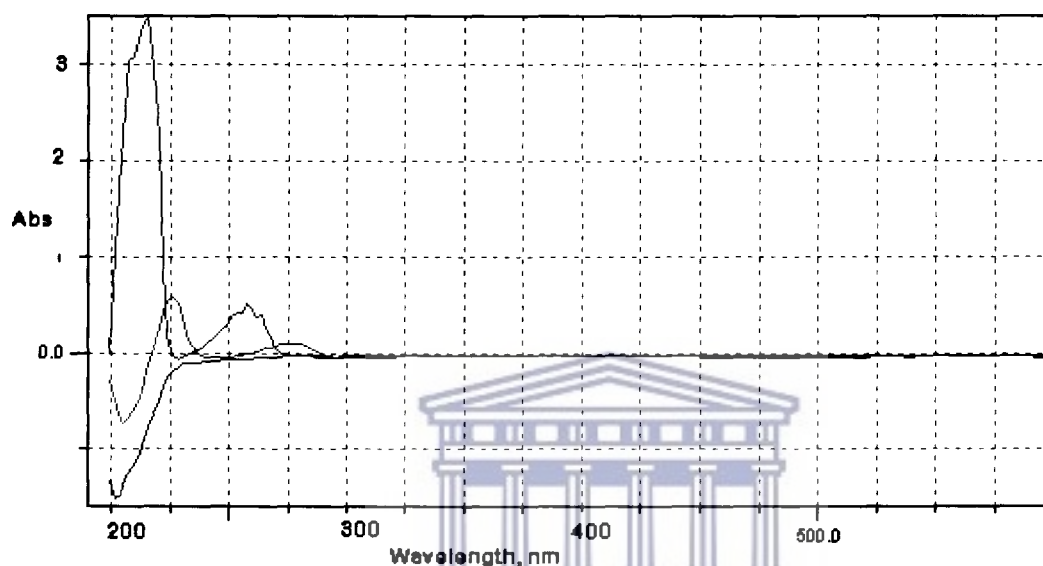


**Figure 5.5.** UV absorption for L-phenylalanine (grey), L-tyrosine (pink) and PBS only (red).

A 3 mL solution of PBS to which 20  $\mu\text{L}$  aliquots of L-phenylalanine (0.2 M) was added, was analysed by linear sweep voltammetry between 0 and 1000 mV at a sweep rate of 50  $\text{mV s}^{-1}$ . The electrochemical oxidation of L-phenylalanine produced an increase in peak current with each addition at around 800 mV (Figure 5.6). The peak was identified as L-dopa based on the biological oxidation (scheme 1.4a) in which L-phenylalanine is first converted to L-tyrosine and then to L-dopa. UV-Vis absorption measurements were performed after oxidation of 60, 120 and 160  $\mu\text{L}$  of L-phenylalanine respectively. A sharp peak at wavelength 204 nm showed increasing absorbance values in keeping with L-phenylalanine oxidation trend (Figure 5.7). The final sample was spiked with an L-phenylalanine standard to observe the difference in absorbance peaks of starting material and oxidation product (L-dopa) (Figure 5.8).

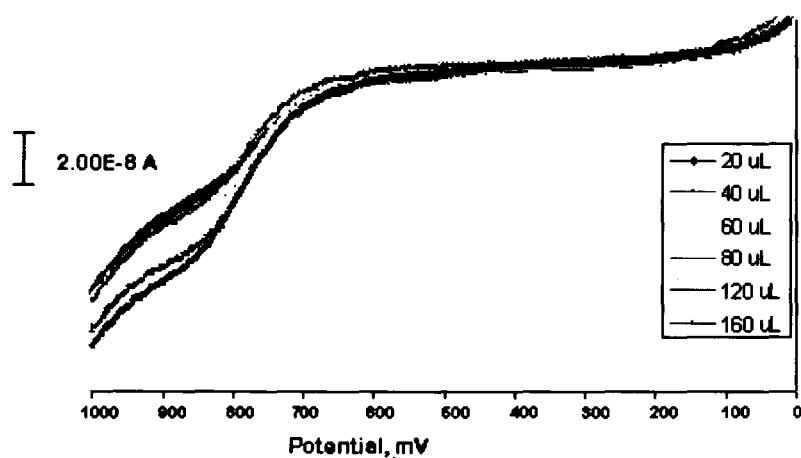


**Figure 5.6.** Linear sweep voltammetry of 20–160  $\mu\text{L}$  (1.32 - 10.66 mM) L-phenylalanine oxidation, scan rate of  $50 \text{ mV s}^{-1}$ .

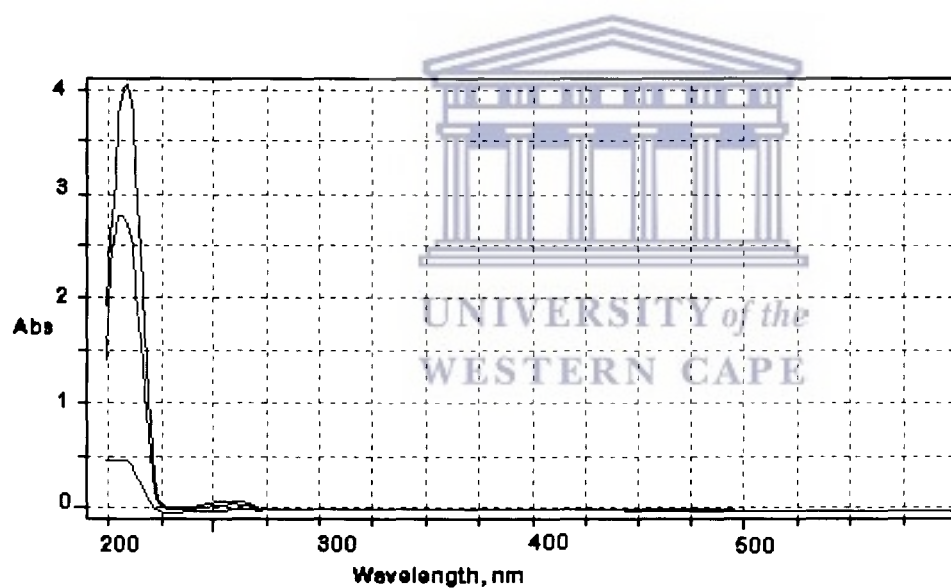


**Figure 5.7.** UV-Vis absorption measured after oxidation of 60  $\mu\text{L}$  (red), 120  $\mu\text{L}$  (green) and 160  $\mu\text{L}$  (blue) of L-phenylalanine standard added.

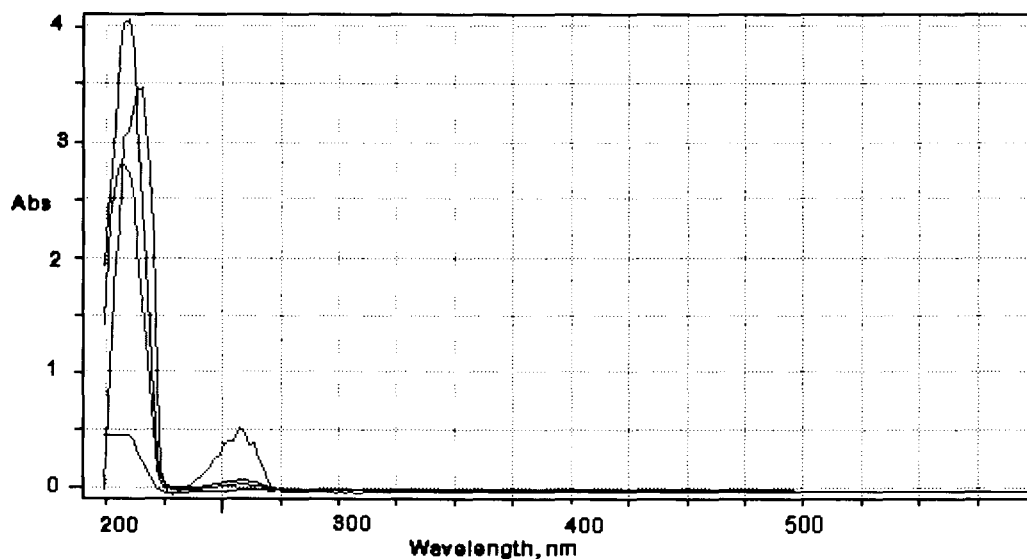
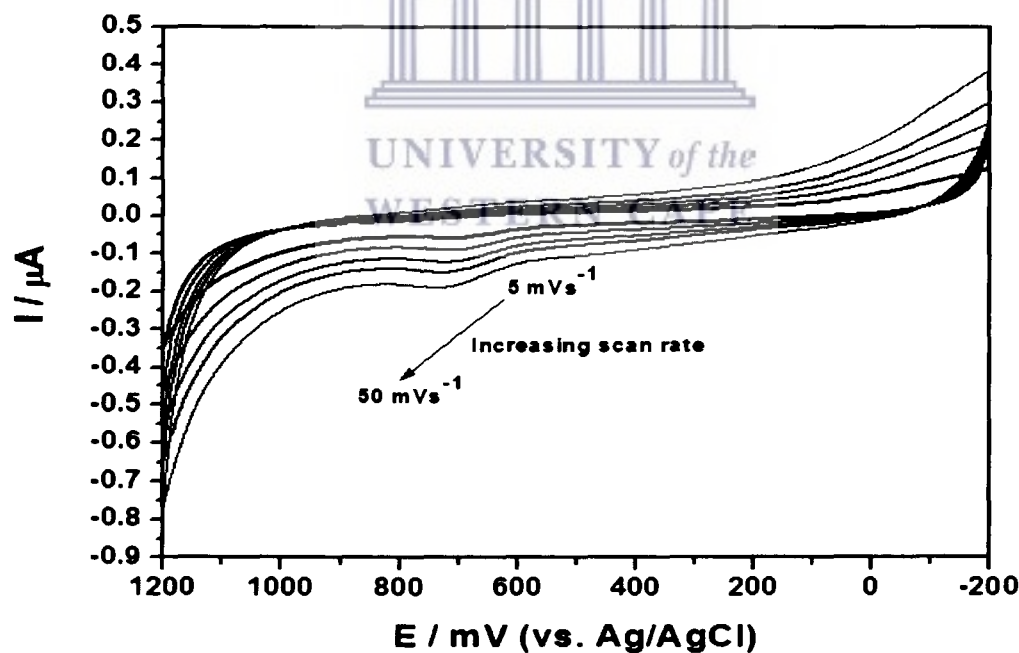


**Figure 5.8.** UV-Vis absorption of L-phenylalanine standard (in PBS) overlapped with absorption of L-dopa.

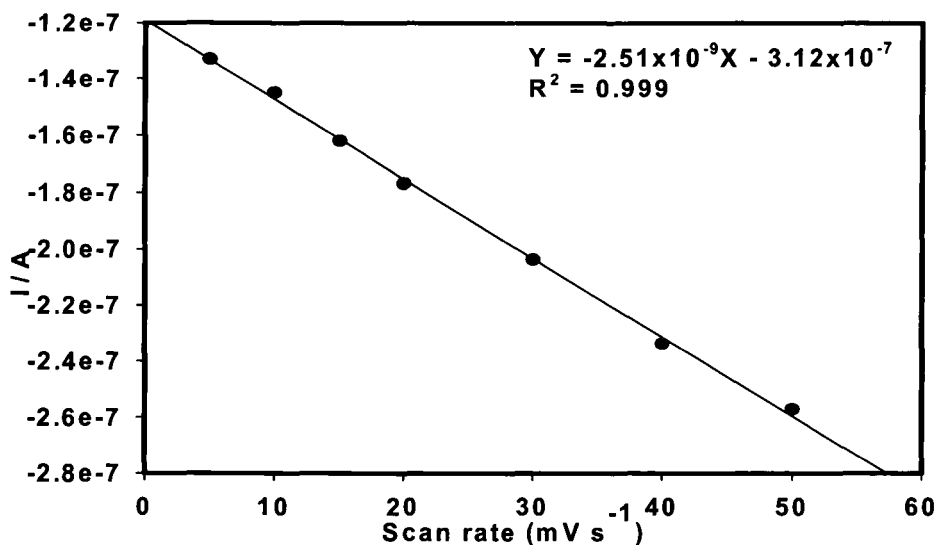
#### 5.4 Direct electrochemistry of Tyrosinase (Tyr) and electrochemical characterization of the Tyr/PANI-PVS biosensor

Considering that Tyr was successfully immobilized on PANI-PVS and that it did not denature during this process, the developed Tyr/PANI-PVS biosensor was subjected to characterization by cyclic voltammograms (CV). The cyclic voltammograms of Tyr/PANI-PVS biosensor in PBS (pH of 7.2) at various scan rates ( $5\text{-}50\text{ mV s}^{-1}$ ) are shown in Figure 5.9a. It was observed that the anodic peak potential ( $E_{pa}$ ), in PBS, shifted positively with increasing scan rate while the reverse cathodic peak potential ( $E_{pc}$ ) in the CV is either diminished or completely absent which is indicative of an electron transfer reaction coupled to a catalytic process. This suggests that the materials onto which the enzymes are immobilized play a major role in determining the resulting features of the biosensor. The anodic peak currents increased linearly and were directly proportional to the scan rates (Figure 5.9b), consistent with thin layer electrochemical behaviour [404,414]. It suggests that a single protonation accompanies the single electron transfer between the PANI-PVS/BDD electrode and the heme Cu (II) of Tyr. Thus, the redox reaction between the Tyr and the BDD electrode surface through the mediator PANI-PVS is a single electron transfer

process. The value estimated for the number of electrons,  $n = 1$ , was therefore used to calculate the surface concentration of electroactive Tyr in the PANI-PVS film. For thin layer electrochemical behaviour like that exhibited by Tyr, the surface concentration ( $\Gamma^*$ ) of its electroactive species in the mediator or promoter used can be deduced by integration of the peaks of the cyclic voltammograms of the biosensor (Figure 5.9a) and using Faraday's law according to the following equation 5.1, section 5.3, which exhibits the variation of peak currents with scan rates (Figure 5.9b). Yet, taking into account that the integrated oxidation peak of the cyclic voltammogram for the biosensor =  $4.8975 \times 10^{-7}$  A,  $\nu = 0.01 \text{ V s}^{-1}$ ,  $T = 295\text{K}$ ,  $A = 0.071 \text{ cm}^2$ , and  $n=1$ , the surface concentration of the electroactive Tyr in the PANI-PVS film ( $\Gamma^*$ ) was estimated to be  $7.268 \times 10^{-10} \text{ mol cm}^{-2}$ . Hence, both calculated value for Tyr/PANI-PVS/BDD biosensor and Tyr/BDD electrode implies that multiple layers of Tyr were immobilized on the nanostructured PANI-PVS film as well as BDD electrode surface when Tyr was coated directly on the electrode surface. Nevertheless, the ability of the PANI-PVS to maintain electroactivity and conductivity in neutral media means it can play as effective electron transfer mediators for the construction of biosensors.



(a)



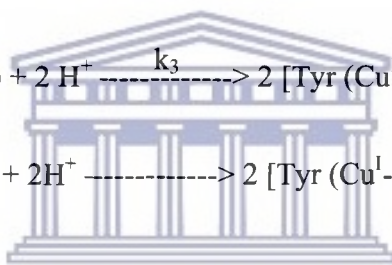
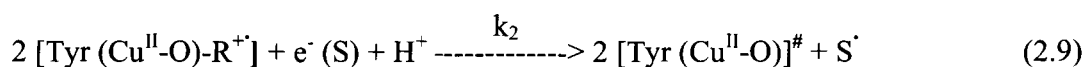
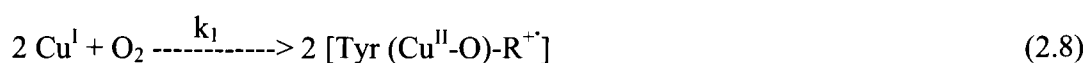
(b)

**Figure 5.9.** (a) Cyclic voltammograms of Tyr/PANI-PVS biosensor in PBS (pH 7.2) and (b) The plot of anodic peak current versus scan rates in PBS (pH 7.2).

It is well known that enzymes are pH sensitive and operate best around their physiological pH. The physiological pHs for the Tyr enzyme have been reported to be 6.8-7.2. In view of this a multi-scan rate study was performed in phosphate buffer (Figure 5.9a), the CV observed indicates that the PVS was still electroactive even in neutral and/or slightly basic media. Ideally, undoped polyaniline is pH sensitive and loses electroactivity beyond pH 4. It means the incorporation of sulphonic groups into the PANI matrices stabilizes the polymers allowing them to maintain electroactivity even at neutral pH. This is because the bulky sulphonic groups cannot easily diffuse out of the polymer matrices once incorporated. Thus the successful doping of PVS is expressed by the fact that the polymers maintained their electroactivity even at a pH 7.2. However, the polyleucoemeraldine peak was very distinct but slightly shifted to lower potentials.

## 5.5 Investigation of the electrocatalytic activity of the Tyr/PANI-PVS biosensor

The electrocatalytic activity of the Tyr/PANI-PVS biosensor for the oxidation of L-phenylalanine (L-Phe) was investigated by cyclic voltammetry. Figure 5.10 shows the CV responses of Tyr/PANI-PVS biosensor to L-Phe in PBS (pH 7.2) at 50 mV s<sup>-1</sup>. It was observed that when 0.3, 0.5 and 0.7 of μM L-Phe were successively added into the PBS solution, the biosensor showed remarkable increase in response (increasing in current peak with increasing in concentration) and anodic peak currents indicating that the immobilized Tyr retained its bioelectrocatalytic activity and was not denatured [76,132]. The electrocatalytic process can be expressed as follows (cf. chapter 2, section 2.3.1.3):



The direct (mediatorless) heterogeneous electron transfer from the bare electrode surface to the active site of the enzyme (equation 2.11) is usually hampered by its low rate resulting from the deep burying of the electroactive groups within the protein structure due to unfavourable orientations of the molecules at the electrode surface and the long electron transfer distance between the electrode surface and the active site of Tyr [415]. In the presence of nanostructured PANI-PVS film, the heterogeneous direct electron transfer in equation 2.11 can be carried out at a reasonable rate. This results in an increasing current, which is then correlated to the increasing concentration of L-phenylalanine in solution. Figure 5.11 illustrates the proposed catalytic cycle of Tyr immobilized on PANI-PVS film.



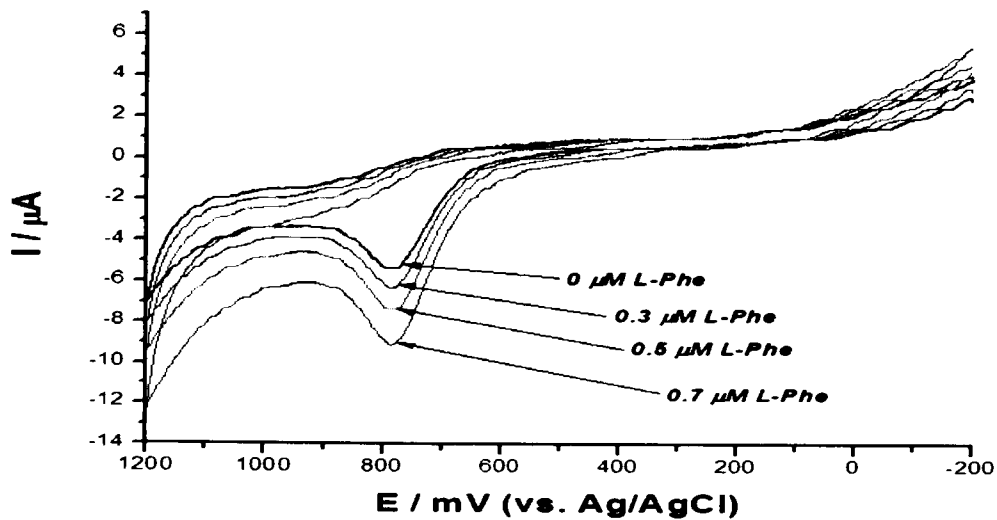


**Figure 5.10.** Cyclic voltammograms of Tyr immobilized on PANI-PVS biosensor in response to different concentrations of L-Phe (0.3, 0.5 and 0.7  $\mu\text{M}$ ) in PBS (pH 7.2), scan rate of  $50 \text{ mV s}^{-1}$ .

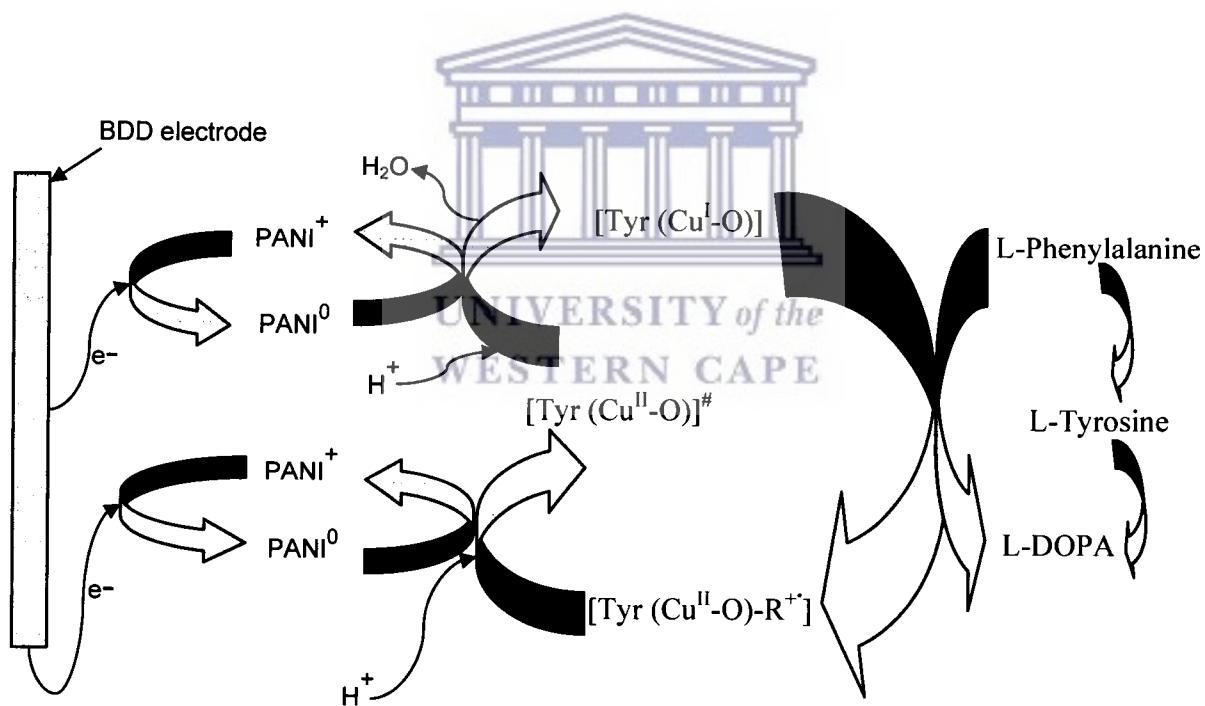


**Figure 5.11.** The proposed catalytic cycle for the Tyr/PANI-PVS biosensor in aerobic medium. PANI<sup>0/+</sup> are the PANI-PVS bound redox sites.

It has been reported that the oxidation of phenol [416,417] as substrate starts at a potential close to the formal potentials of  $\text{Cu}^{\text{II}}/\text{Cu}^{\text{I}}$  in the active centre of Tyr, which were determined by potentiometric studies to be in the range between 200 and 1000 mV (vs. SCE, pH 6.8-7.2) (see chapter 2, section 2.3.1.3.4.). In this study, the oxidation of L-phenylalanine occurred at an anodic peak potential around 800 mV (Figure 5.10) which is within the range of the formal potential obtained from other studies. This confirms that the immobilized Tyr was responsible for the oxidation of L-phenylalanine. Hence, the peak potential around 800 mV was selected as the optimized monitoring potential and was applied throughout this study when a magnetic stirrer was used to introduce convection into the solution.

As expected for the study of cyclic voltammograms of Tyr immobilized on PANI-PVS biosensor in response to different concentrations of L-Phe (0.3, 0.5 and 0.7  $\mu\text{M}$ ) in PBS (pH 7.2), at scan rate of  $50 \text{ mV s}^{-1}$ , no reduction peaks were observed at a tyrosinase-modified PANI-PVS/BDD electrode, only an oxidation peak, Figure 5.10, (cf. Chapter 1, section 1.1, equation 1.1).

However, Liu *et al.* have demonstrated the reduction peaks of other phenol derivatives, such as 4-chlorophenol and dopamine (o-diphenol) at the enzyme electrode [115]. The reduction peaks observed were attributed to the direct reduction of the enzymatically-produced quinone, in the presence of the oxygen molecular, at enzyme electrode surface. The steps of the enzymatic reaction on the BDD electrode surface were shown as follows (5.1-5.3):

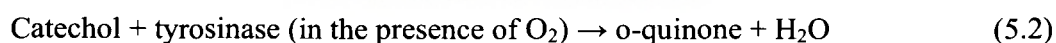
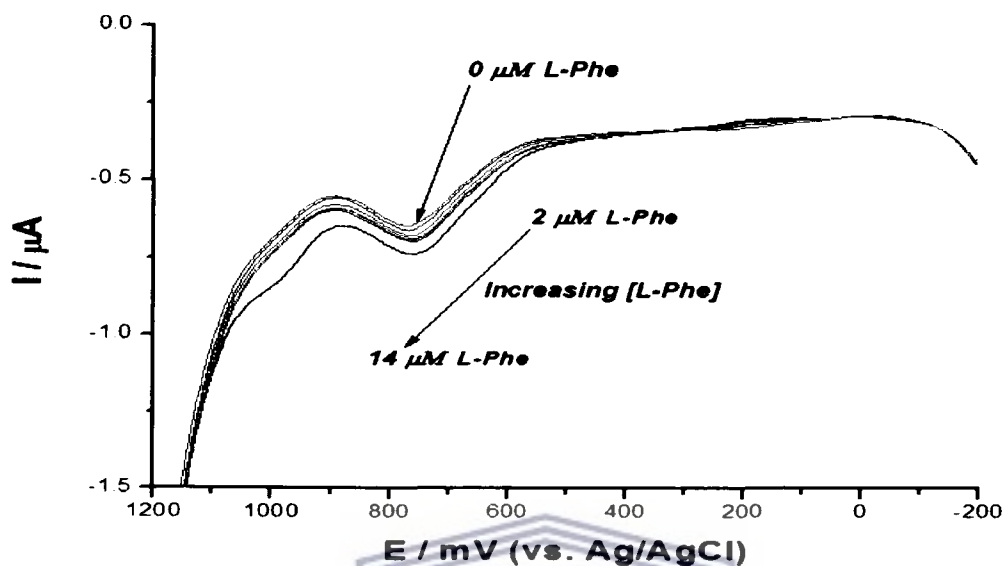
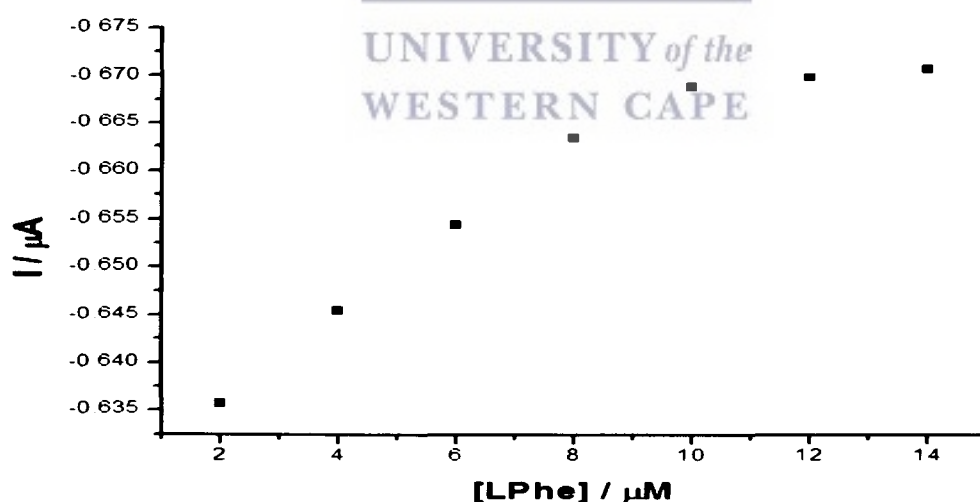


Figure 5.12 shows the typical square wave voltammogram (SWV) responses of the Tyr/PANI-PVS biosensor to successive additions of L-Phe into PBS (pH 7.2). Calibration curves are presented. Catalytic characteristics of the biosensor and increase in current illustrated in Figure 5.13 were observed for successive additions of L-Phe into the electrolyte solution. A linear range from 2–8  $\mu\text{M}$  was observed for the biosensor ( $r = 0.999$ ,  $n = 6$ ), with a sensitivity of  $5.99 \text{ Amol}^{-1} \text{ dm}^3$  and a detection limit of  $1.0 \times 10^{-3} \mu\text{M}$  (based on equation 3.7) when low enzyme loading of 5  $\mu\text{L}$  (26.85 units) of 4.72 mg/ mL (5370 units) buffer solution of Tyr was used (Figure 5.14).

The detection limit achieved by the Tyr/PANI-PVS biosensor was lower; this indicates that the PANI-PVS materials played a role in enhancing the sensitivity and response of the biosensor due to their nano-sizes.



**Figure 5.12.** Biosensor responses to successive addition of L-Phe in PBS, scan rate of  $50 \text{ mVs}^{-1}$ .



**Figure 5.13.** Calibration curve for the Tyr/PANI-PVS biosensor responses to different concentration of L-Phe (2-14  $\mu\text{M}$ ).

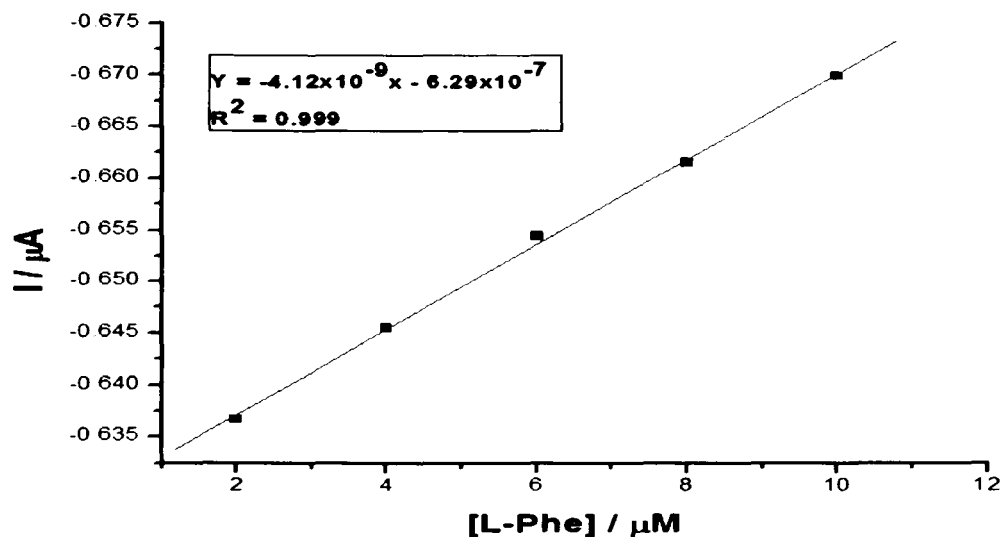


**Figure 5.14.** Calibration plot for the Tyr/PANI-PVS biosensor to the different concentration in the linear range between 2-10 μM.

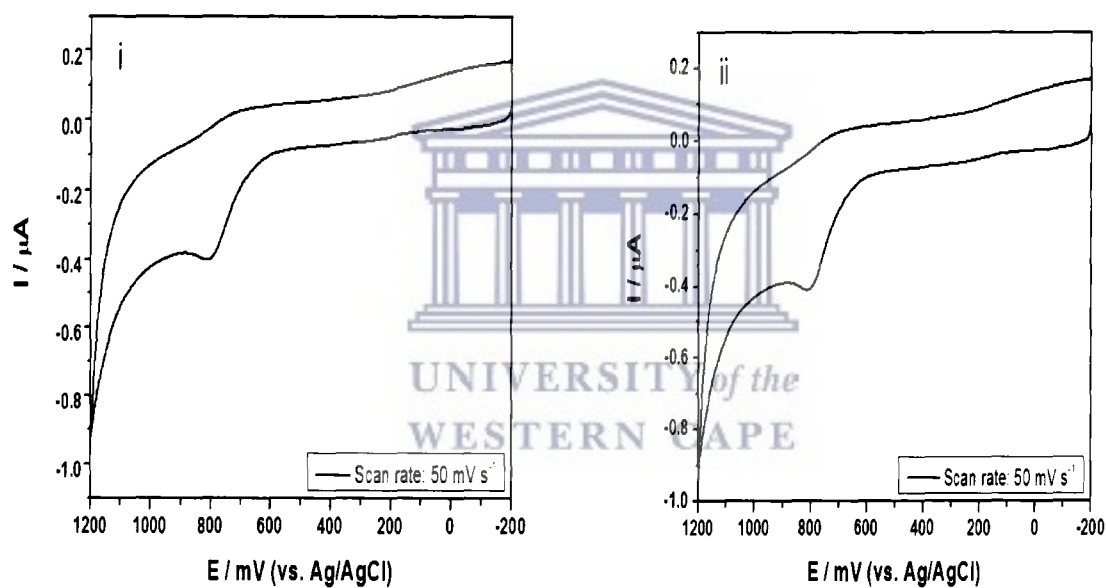
### 5.6 Response time of the Tyr/PANI-PVS biosensor

The response time of this biosensor was estimated as the time taken to reach 98 % of its steady state peak current before each addition of L-Phe. The response time of the Tyr/PANI-PVS biosensor was estimated to be  $20 \pm 5.0$  s ( $n = 6$ ).

### 5.7 Reproducibility and stability of the Tyr/PANI-PVS biosensor

Tran-Minh reported that the stability of the enzyme sensor increases with the enzyme concentration [73,417]. When the membrane contains more active enzyme, the biosensor is more stable and has a longer lifetime. In this study, the long-term stability of the Tyr/PANI-PVS film was investigated by evaluating the response of the same biosensor (stored at 4 °C and at room temperature of 25 °C in PBS) to 0.2 M L-Phe.

The biosensor showed good response and there was no significant change in its catalytic activity during repetitive measurements over a period of one week. In addition, the biosensor could be used to perform several potentiodynamic measurements with many additions of L-Phe such as those of Figures 5.9 and 5.12, with a decrease in current response by only 5 % of the original value after one week. The stability of this biosensor is good with more than 85 % of its initial activity reserved after continuously using one hour (Figure 4.4). The stable electrocatalytic activity and sensitivity of the Tyr/PANI-PVS/BDD biosensors used in this study was certainly facilitated by the good mediating capabilities of the conducting PANI-PVS films capable of fast electron transfers. The biosensor has proved good efficiency measurements over a period of one month. Yet, no significant change was observed in terms of response (Figure 5.15).



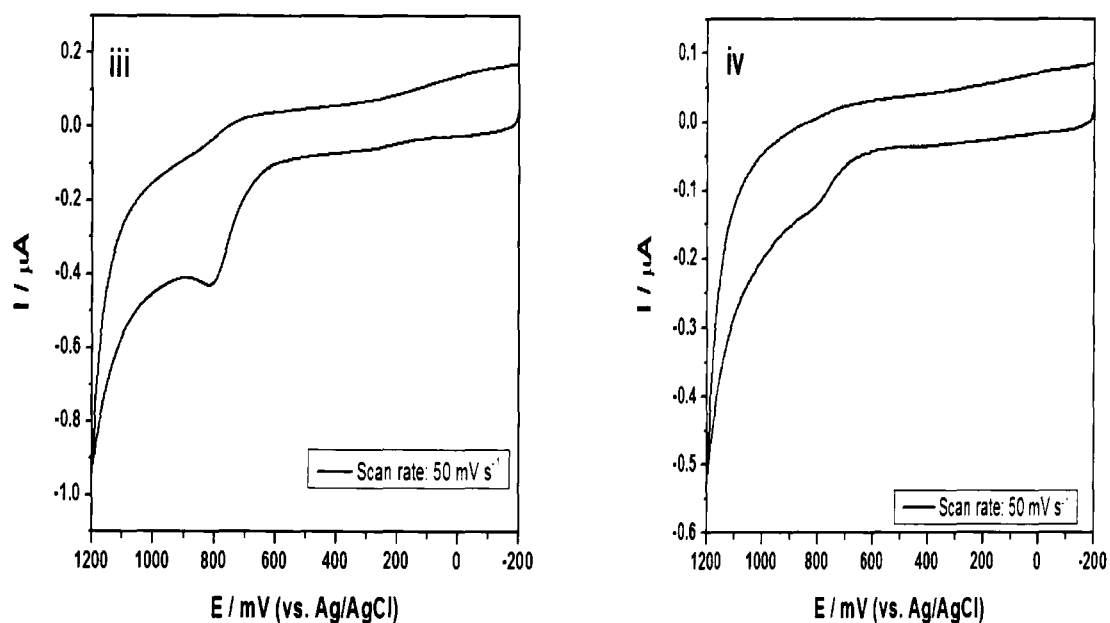
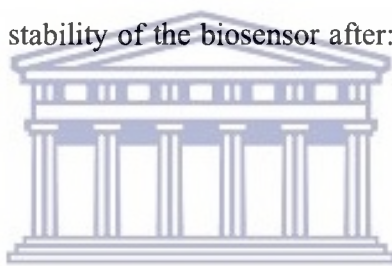


**Figure 5.15.** Reproducibility and stability of the biosensor after: i) one week, ii) two weeks, iii) three weeks and iv) four weeks.



UNIVERSITY of the  
WESTERN CAPE

## 5.8 Conclusions

The PANI-PVS film showed to be an attractive material for immobilization of Tyr, promoting its direct electron transfer on boron-doped diamond (BDD) electrode. The UV-Vis and FTIR results indicated that the enzyme Tyr immobilized on PANI-PVS film retained its bioelectrocatalytic activity towards the oxidation of L-Phe and was not denatured. This proves that the immobilization procedure used in this study allows for the construction of stable enzyme membranes. It also demonstrates that the PANI-PVS film provided a suitable-microenvironment for immobilization of Tyr and is therefore suitable for the construction of Tyr/PANI-PVS biosensor for the detection of the phenol compounds. The high sensitivities achieved with this biosensor can allow sensitive detection of the selected phenol compounds at low concentrations.

## CHAPTER 6

### **Application of Tyr/PANI-PVS Biosensor for the detection of phenol compounds**

#### **6.1 Introduction**

After the Tyr/PANI-PVS biosensor was constructed and optimized, some studies for the detection of phenol compounds were performed to verify its applicability as effective biosensor. It was placed into a three-electrode electrochemical cell into which the analytes and samples of interest were determined. The electrodes were connected to a computer-controlled potentiostat and the substrates employed were L-phenylalanine and L-tyrosine (L-Tyr). The biosensor response to its natural substrate, L-tyrosine, was compared to its response to L-phenylalanine using voltammetric methods and the results obtained were modelled as Michaelis-Menton non-competitive enzyme binding. The biosensor was also applied to commercially available pharmaceutical preparations to assess its performance in real sample analysis. The response of the biosensor with L-Phe and the phenol compounds was measured by investigating its biocatalytic activity towards the oxidation of the substrates. This chapter presents the results of analysis of L-Phe, L-Tyr and some phenolic compounds by Tyr/PANI-PVS biosensor employing cyclic voltammetry (CV), square wave voltammetry (SWV) and Linear sweep voltammetry (LSV) techniques as well as the UV-Vis spectroscopy technique. Both potentiodynamic techniques were used to confirm the formation of L-3,4-dihydroxyphenylalanine (L-dopa) as the oxidation product at an oxidation potential of 803 mV at the biosensor compared to 746 mV at the bare BDD electrode. The potential range chosen was suitable in all experiments to avoid further oxidation of L-dopa to quinone. The UV spectroscopy confirmed the formation of L-dopa as oxidation product and was measured as an absorption peak in the range between 200 – 600 nm. L-Phe and L-dopa were investigated by using the BDD electrode (polished only). CV and differential pulse voltammograms (DPV) were recorded in 0.1 M HCl using 100  $\mu$ L of 0.2 M L-Phe/L-dopa solutions prepared in 0.2 M HCl and distilled water, respectively.



## 6.2 Fabrication of the Tyr/ PANI-PVS biosensor

Prior to fabrication, a commercial boron-doped diamond (BDD) electrode (Windsor Scientific) was activated in 1M HNO<sub>3</sub> by repeated cycling the potential between -200 and +1500 mV versus Ag/AgCl at scan rate of 50 mV s<sup>-1</sup> for 15 cycles. In this way surface hydroxyl groups (OH<sup>-</sup>) were introduced at the surface of the BDD electrode. The OH<sup>-</sup> terminated BDD electrode was then further modified by the enzyme/polymer. In this biosensor format, electrochemically as-synthesized PANI-PVS was constituted in a suitable solvent and then followed by immobilization of the tyrosinase enzyme thus tuning the sensor for L-Phe sensing. The preformed enzyme could either be drop-coating or inoculation onto the active PANI-PVS/BDD electrode surface area (0.0177 cm<sup>2</sup>, diameter 3 mm) as a working electrode followed by drying method gave rise to a stable enzyme/polymer layer and was predominantly used. The drop coating enzyme solution was prepared as 4.7 mg/ml (5370 units) in 0.01 M PBS buffer (pH 6.2) of which an aliquot of 5 μL (26.85 units) was drop coated onto the electrode surface and allowed to dry in air at room temperature for 24 hours. The resultant biosensor was then applied to the measurement of L-phenylalanine. The biosensor was cleaned by polishing with aqueous slurries of 0.05 μm alumina and rinsing was done after polishing for reuse in the following experiment.

## 6.3 Experimental conditions

A standard three electrode electrochemical cell was used in all experiments with a starting cell volume of 10 mL to study the electrocatalytic behaviour of the Tyr/PANI-PVS biosensor. The working electrode was tyrosinase/PANI-PVS modified BDD electrode, the reference electrode was Ag/AgCl 3M Cl<sup>-</sup> (BASi, LaFayette) and the counter electrode was a 5 cm Pt wire (Sigma Aldrich). All solutions were prepared using MilliQ UHQ water (resistivity 18Ω). All chemicals used were Analytical grade.

The UV/vis absorbance measurements were recorded at room temperature on a UV/VIS 920 spectrometer (GBC Scientific Instruments, Australia) using a specially designed quartz cell with pathlength 1 cm.

#### 6.4 Detection of L-Tyrosine (L-Tyr) using the Tyr/PANI-PVS/BDD biosensor

The responses of Tyr/PANI-PVS biosensor to L-3,4-dihydroxyphenylalanine (L-dopa) in subsequent concentrations of L-Tyrosine (L-Tyr) standard solutions were investigated by cyclic voltammetry (CV) in the same potential window as before (cf. chapter 3, section 3.5.5) and the results are illustrated in Figure 6.1. The voltammograms depict the catalytic currents resulting from the coupling of the electro-oxidation of the PANI-PVS films to the catalytic oxidation of L-Tyr. The currents produced at any particular potential depend on the concentration of L-Tyr present in the solution. That is the PANI-PVS films are functioning as electron-transfer mediators between the BDD electrode and the Tyr biomolecule. Increase in anodic peak currents assigned to L-DOPA (at around 800 mV) was clearly observed after each 20  $\mu$ L addition of L-tyrosine into PBS (Figure 6.1). The increase in the current of the peak at around 800 mV demonstrates an effective electrocatalytic oxidation of L-Tyr on the BDD electrode. The ongoing sensor results were based on the assumptions that the Tyr redox catalytic sites were diffusional. It was also assumed that the polymer-PANI-PVS-Tyr sensors were thin homogeneous films in which the L-Tyr oxidation charge is propagated along the polymer chain by fast electron reactions involving the reduced and oxidized forms of the polymers [185]. This way, for a substrate limited kinetic case, the expression for the steady state current ( $I$ ), simplifies to the electrochemical Michaelis-Menten equation [188] given by (equation 6.1):

$$I = I_{\max} [\text{L-Tyr}] / ([\text{L-Tyr}] + K_m^{\text{app}}) \quad (\text{equation 6.1})$$

Where  $I$  is the observed catalytic current,  $I_{\max}$  is the steady state current for the biosensor, and  $[\text{L-Tyr}]$  is the bulk solution concentration of L-Tyr. Figure 6.2 represents the calibration plot for the various sensors response to different concentration of L-Tyr as fitted into the Michaelis – Menten equation. An evaluation of the linear range and limit of detection for the biosensor modelled as Michaelis-Menton non competitive enzyme binding, established the linear range for the biosensor as from 2-10  $\mu$ M ( $r = 0.999$ ,  $n = 6$ ) and the limit of detection as  $1.0 \times 10^{-2}$   $\mu$ M. The apparent Michaelis-Menten constant ( $K_m^{\text{app}}$ ) of the immobilized tyrosinase was 2.83  $\mu$ M. Sensitivity:  $3.53 \text{ Amol}^{-1} \text{ dm}^3$ .

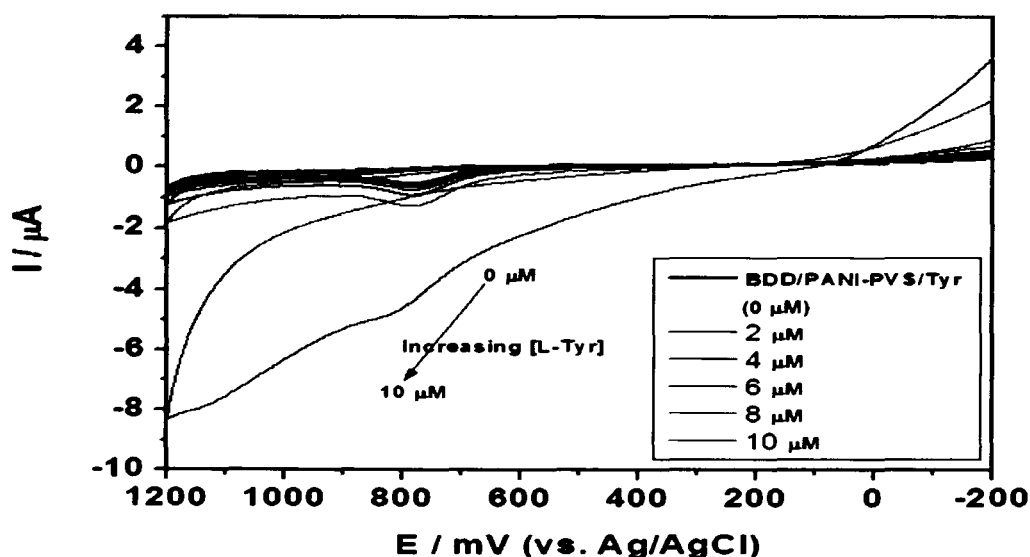


**Figure 6.1.** Cyclic voltammograms of the increasing L-tyrosine concentration (0-10  $\mu\text{M}$ ) using Tyr/PANI-PVS/ BDD biosensor in 0.1 M PBS (pH 7.2), scan rate: 50 mV/s, aerobic condition.

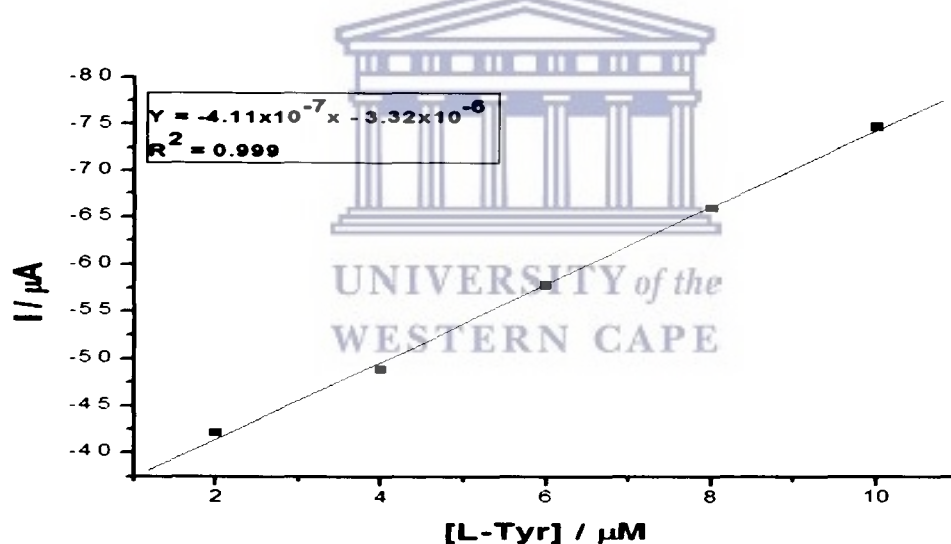


**Figure 6.2.** Calibration plot for the Tyr/PANI-PVS biosensor to the different concentration of L-tyrosine in the linear range between 2-10  $\mu\text{M}$ .

Figure 6.3 shows the square wave voltammetric (SWV) results of the electrochemical behaviour of the Tyr/PANI-PVS biosensor to the different concentration of L-Tyrosine (0-10  $\mu\text{M}$ ) recorded in phosphate buffer pH 7.2 at scan rate of 50 mV/s. The sensitivity was 100  $\mu\text{A/V}$  and potential

measured against an Ag/AgCl was between -200 and 1200 mV. All Tyr experiments were conducted under aerobic conditions. The existence of well formed oxidative peaks observed at around 800 mV was an indication that of L-3,4-dihydroxyphenylalanine (L-dopa) produced in the solution (Fig. 6.3).

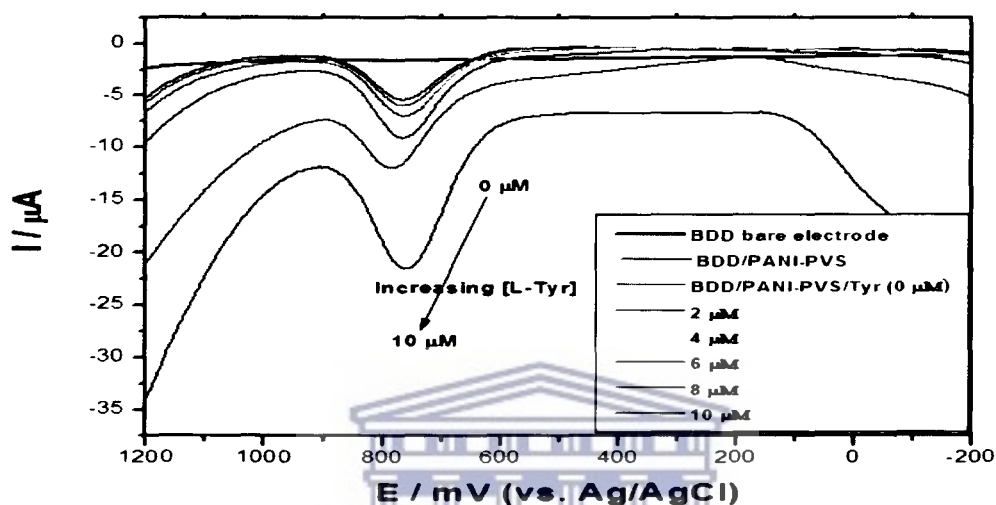


**Figure 6.3.** Square wave voltammetry (SWV) of the increasing L-tyrosine concentration (0-10  $\mu\text{M}$ ) using Tyr/PANI-PVS/BDD biosensor in 0.1 M PBS, pH=7.2, scan rate:  $\text{mV s}^{-1}$ , aerobic condition.

### 6.5 Detection of L-Phenylalanine (L-Phe) using the Tyr/PANI-PVS/BDD biosensor

In a similar experiment consecutive additions of L-phenylalanine (20  $\mu\text{L}$ ) was added to the electrolyte solution (0.1 M PBS, pH 7.2) and oxidized by the Tyr/PANI-PVS modified BDD biosensor (Figure 6.4). Tyr immobilized at modified BDD interface, converts L-Phe into L-tyrosine (L-Tyr), followed by the oxidation of L-Tyr to form L-3,4-dihydroxyphenylalanine (L-Dopa) in the presence of the molecule of oxygen. The immobilization of the redox enzyme (Tyr) was performed by electrostatic attachment involving the reducing of the modified BDD in phosphate buffer solution (pH 7.2) at potentials range from -200 mV to + 1200 mV at scan rate

of  $50 \text{ mV s}^{-1}$ . Cyclic voltammetry (CV) of L-Phe oxidation showed a quasi-reversible process since the oxidation potential at around  $800 \text{ mV}$  was assigned to the formation of L-dopa and confirmed subsequently by UV/vis spectroscopy. The anodic peak current showed a linear increase with scan rate in the low range, which illustrates that the oxidation of L-Phe at the biosensor interface is a diffusion-controlled process (Figure 6.5). The linear increase was observed in the concentration range between  $2 - 10 \text{ }\mu\text{M}$  ( $r = 0.999$ ,  $n = 6$ ) and the relative standard deviation (R.S.D) of  $5 \%$  was obtained. The detection limit was found to be  $1.0 \times 10^{-2} \text{ }\mu\text{M}$ . The apparent Michaelis-Menten constant ( $K_m^{\text{app}}$ ) of the immobilized tyrosinase was calculated to be  $1.39 \text{ }\mu\text{M}$  and the sensitivity was  $7.19 \text{ Amol}^{-1}\text{dm}^3$  (Figure 6.6).

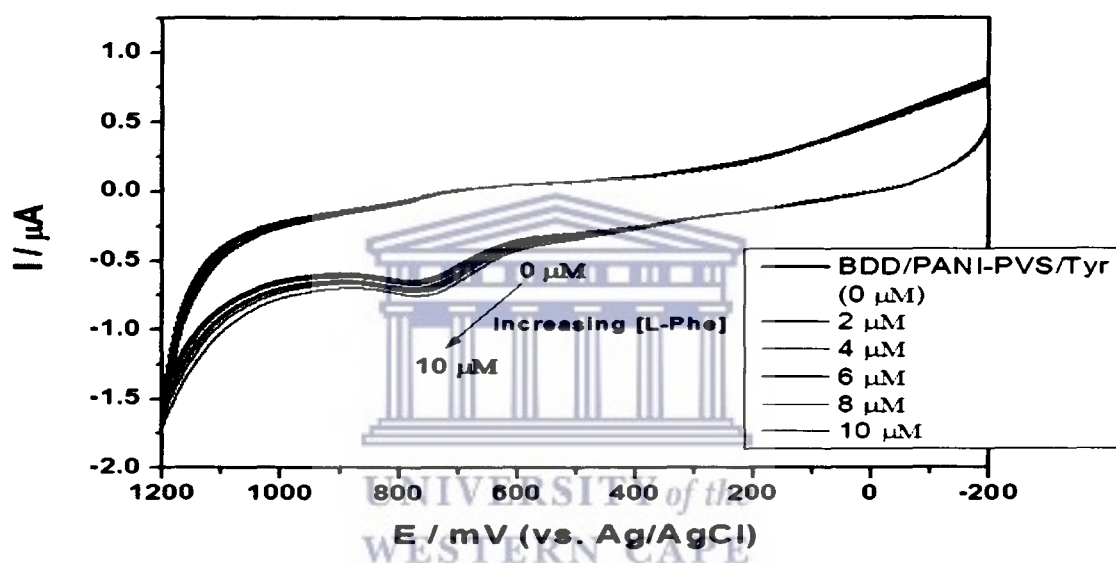


**Figure 6.4.** Cyclic voltammograms of the increasing L-Phe concentration ( $0-10 \text{ }\mu\text{M}$ ) using Tyr/PANI-PVS/BDD biosensor in  $0.1 \text{ M PBS}$ ,  $\text{pH}=7.2$ , scan rate:  $50 \text{ mV s}^{-1}$ , aerobic condition.

The cyclic voltammetric responses of the Tyr/PANI-PVS/BDD biosensor to different concentrations of L-Phe show one anodic peak, ( $E_{\text{pa}} = 803 \text{ mV}$ ). The anodic peak current increased as the concentration of the L-Phe substrate increased, confirming the activity of the immobilized Tyr. The reproducibility of this method was very good and evaluated by plotting different calibration curves using their slopes to determine the relative standard deviation (R.S.D). The low R.S.D of  $5\%$  (duplicate measurements) obtained for the biosensor

demonstrates that its response was highly reproducible. Therefore, it was observed that the same biosensor could be further applied for the analysis of real samples.

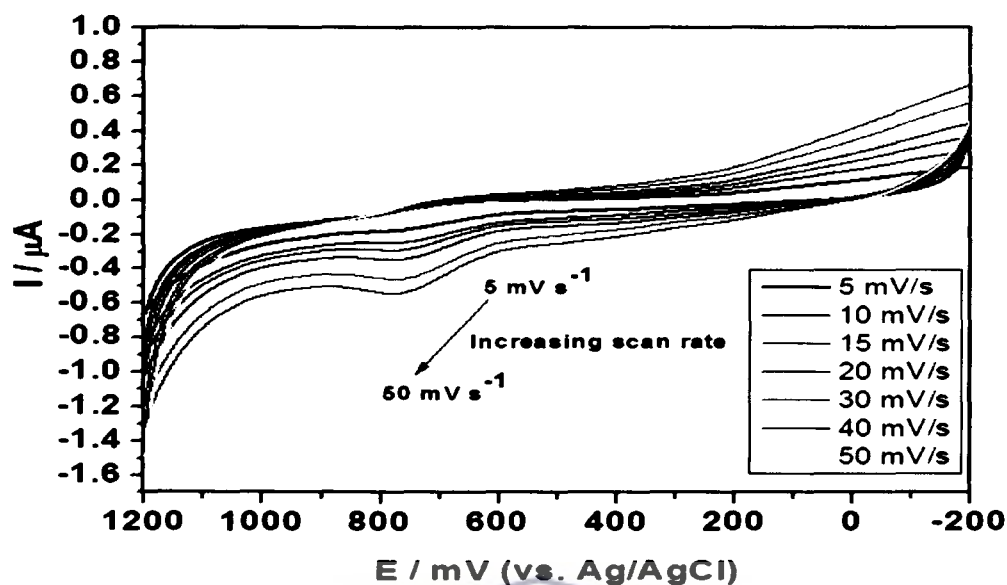


**Figure 6.5.** Influence of scan rates on oxidation peak current of L-Phe using Tyr/PANI-PVS/BDD biosensor in 0.1 M PBS (pH 7.2). The CV has shown the increasing current with the increasing scan rate (5-50  $\text{mV s}^{-1}$ ).

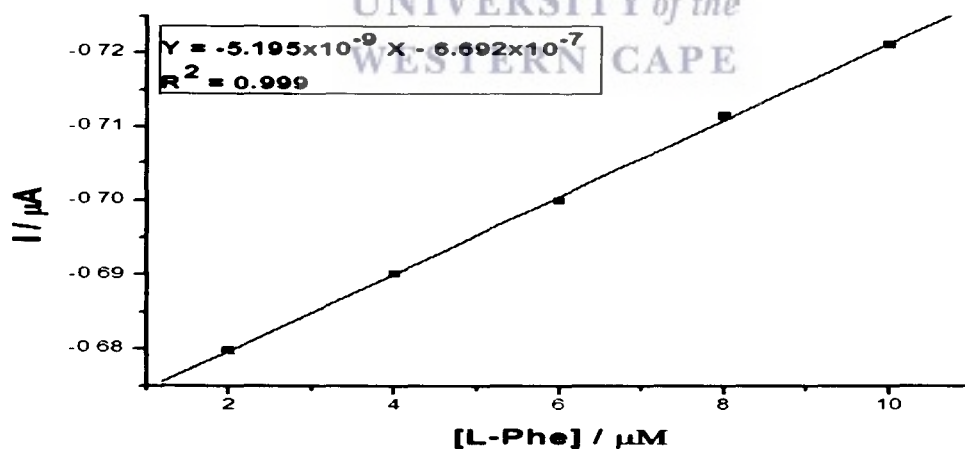


**Figure 6.6.** The relationship between response potential and L-Phe concentration for Tyr/PANI-PVS/BDD biosensor in 0.1 M PBS (pH 7.2). Linear range: 2-10  $\mu\text{M}$ .

In order to measure the conversion of L-Phe as the formation of L-dopa, the linear sweep voltammograms (LSV) was used as a technique. The potential range of the linear sweep was extended from 0 to 1000 mV. During this potential sweep the L-phenylalanine is oxidised to L-tyrosine, electrochemically and subsequently to L-dopa by the enzyme tyrosinase. The only increasing peak observed during the linear sweep was that of L-dopa, which indicates that the tyrosinase formed was immediately converted to L-dopa (Figure 6.7). UV/vis spectroscopy was employed to verify the conversion of L-Phe to L-dopa. The UV/vis absorption maxima for L-phenylalanine and L-tyrosine were confirmed at around 213 nm and 256 nm respectively, based on absorbance of standard solutions prepared in the PBS buffer (Figure 6.8).

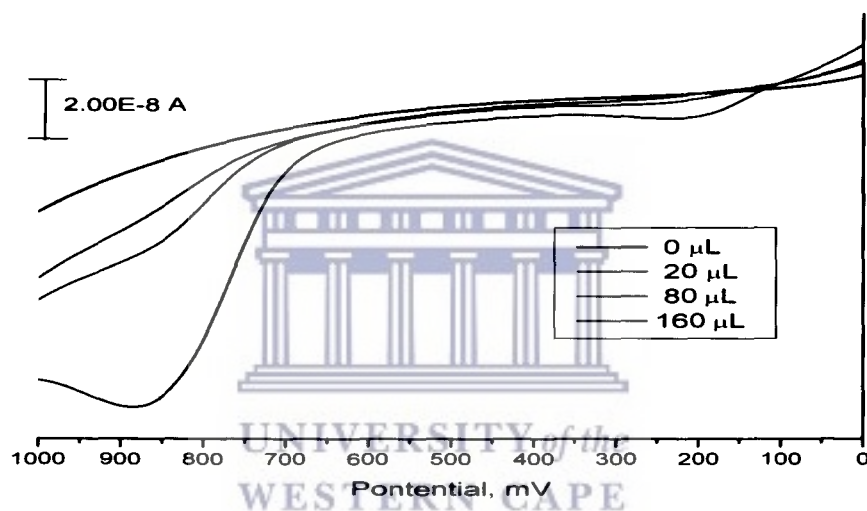


**Figure 6.7.** Linear sweep voltammetry (LSV) for the conversion of L-Phe (0-10.66 mM) to the formation of L-dopa using Tyr/PANI-PVS/ BDD biosensor in 0.1 M PBS (pH 7.2).



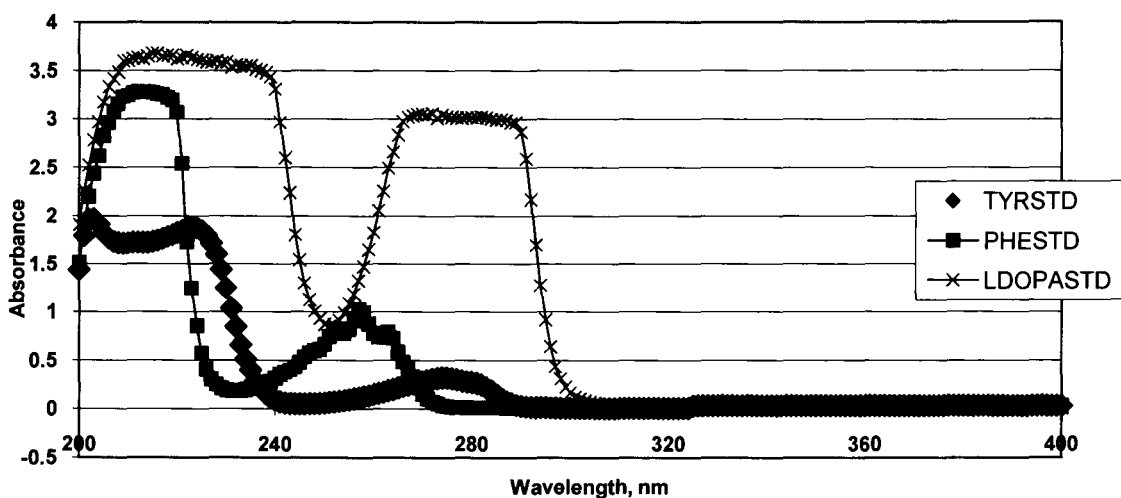


**Figure 6.8.** UV-Vis absorption for L-Phe STD (pink), L-Tyr (dark blue) and L-dopa (light blue).

The performance of the method was verified using similar conditions. The peak was assigned as L-dopa based on the biological oxidation (scheme 1.4a) in which L-phenylalanine is first converted to L-tyrosine and then to L-dopa. UV-Vis absorption measurements were performed after oxidation of 160  $\mu$ L of L-phenylalanine (10.66 Mm). A sharp peak at wavelength 204 nm showed the absorbance value for L-phenylalanine oxidation assigned to the production of L-dopa (Figure 6.9).

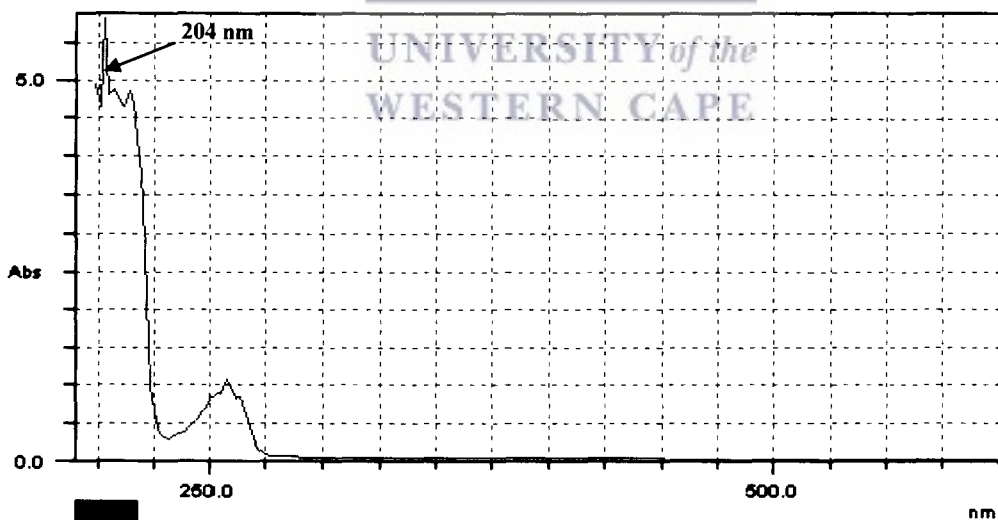


**Figure 6.9.** UV-Vis absorption measured after oxidation of 160  $\mu$ L of L-phenylalanine standard added using Tyr/PANI-PVS/ BDD biosensor in 0.1 M PBS (pH 7.2).

To find evidence for tyrosinase immobilization on the PANI-PVS film, the FTIR spectra has been recorded (Figure 6.10). It was reported that the bands at about 1643 and 1528  $\text{cm}^{-1}$  are corresponding to amide I and II respectively (see figure 5.2). Yet, it was observed that the FTIR spectra recorded after the contact of the immobilized Tyr with the L-Phe, as L-Phe was electrochemically converted to L-tyrosine (PANI-PVS/Tyr-L-Tyr), showed the disappearance of amide I band of Tyr (Figure 6.10). This indicates the covalent binding of the substrate to the enzyme. Since the amide I band is attributed to C=O stretching vibration of peptide linkage in the Tyr backbone, the binding by the substrate suggests that it coordinated with the oxygen atoms in the C=O groups of Tyr through its  $^+\text{NH}_2$  group, forming a complex of Tyr-substrate. The formation of this complex is therefore responsible for the conformational changes of Tyr. The 1326  $\text{cm}^{-1}$  band was observed and was ascribed to the C=N stretching vibration of the oxidized polymer. Appearance of the C=N bond is however connected with deprotonation of the polyaniline ring in acidic medium during the redox process. Similar phenomenon may be observed in the spectra of PANI-PVS with immobilized tyrosinase at neutral medium (see Figure 6.10), thus suggesting the proton exchange at the polyaniline ring during the redox process. This proton exchange is facilitated by the presence of the  $\text{NH}_3^+$  groups of amino acid residues of the polymer-bound tyrosinase onto BDD matrix.

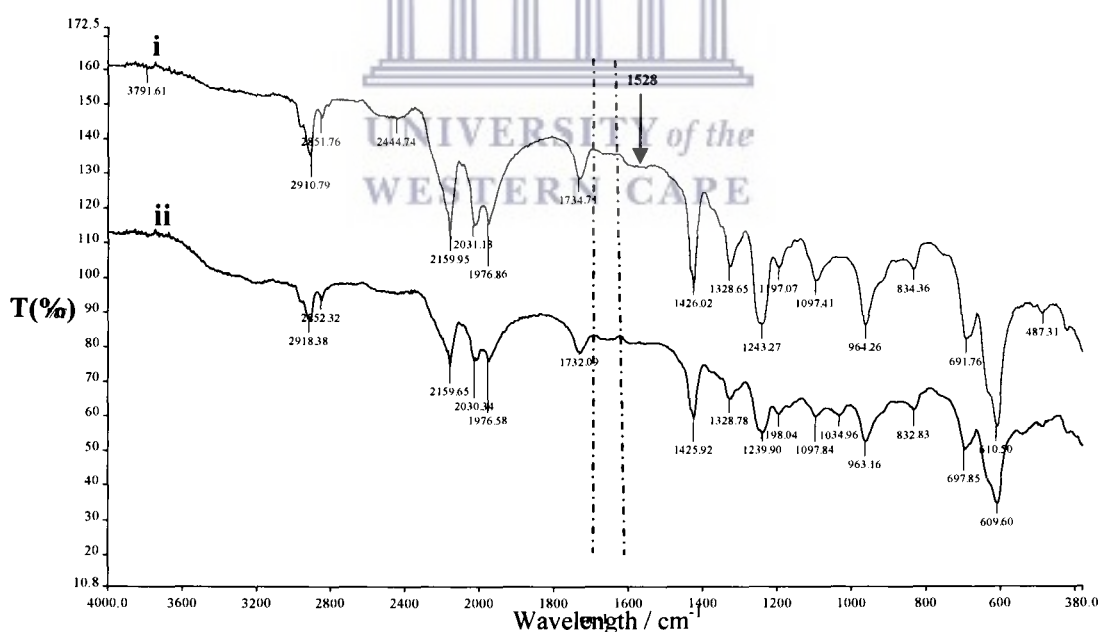


**Figure 6.10.** FTIR spectra of (i) the immobilized Tyr/PANI-PVS film with L-Phe and (ii) Tyr/PANI-PVS film in 0.1 M PBS (pH 7.2).

Other interesting study was carried out to evaluate the results for simultaneous determination of L-Phe and L-dopa at BDD electrode. In this way, differential pulse voltammetry (DPV) was performed aiming to develop a new analytical method. Figure 11 displays the cyclic voltammograms of L-Phe and L-dopa in 0.1 M HCl. As can be seen at the surface of the BDD electrode, no redox peak for L-Phe was observed due to the slow electron transfer rate for oxidation of L-Phe at the unmodified electrode. In this case, the modification of the electrode is therefore required. However, it was observed that the oxidation and reduction of L-dopa is electrochemically reversible at the surface of the electrode according to scheme 1.2. The cathodic peak potential ( $E_{pc}$ ) shifted negatively while anodic peak potential ( $E_{pa}$ ) shifted positively at scan rate of  $50 \text{ mV s}^{-1}$ . The effect of potential scan rate on the redox response of L-dopa was investigated in the range between  $5\text{-}50 \text{ mV s}^{-1}$  (not shown). A linear relationship between the redox peak current and the square root of scan rate was found for L-dopa as follows:

$$I_{p,a} (\mu\text{A}) = -3.8 v^{1/2} (\text{mV/s}) + 0.845 (R^2 = 0.998)$$

$$I_{p,c} (\mu\text{A}) = 1.8 v^{1/2} (\text{mV/s}) + 0.387 (R^2 = 0.996)$$

Hence, the plot of  $I_{p,a}$  and  $I_{p,c}$  for L-dopa versus square root was linear. The linear relationship between peak currents and square root of scan rates is indicative that the oxidation currents were diffusion-controlled, which is the ideal case for quantification measurements for adsorption of L-dopa on the electrode surface. These phenomena have proved the determination of L-phenylalanine in the aqueous media and real samples.

UNIVERSITY of the  
WESTERN CAPE

Additionally, eventhough the peaks for L-Phe are not evident in CV as discussed previously, the differential pulse voltammograms of L-Phe (Figure 12) has showed excellent improvement in redox peak currents according to Scheme 1.4. (see chapter 1), which explains that in the first step of the oxidation by the enzymatic reaction, L-Phe is converted electrochemically to L-Tyr followed by the oxidation of L-Tyr to form L-dopa. In other word, the interactions involving Tyr and L-Phe were indicated that the Tyr electrocatalytic activity for the oxidation of L-Phe by coordinating with the oxygen atoms of the carbonyl groups in the peptide chain of Tyr formed a complex which led to the obstruction of the electron transfer of Cu (II) in the phenolase cycle of its heme group, and thus a reduction in Tyr/PANI-PVS biosensor response. Terminated by the chosen potential range (at around  $800 \text{ mV}$ ) in order to avoid further oxidation of L-dopa to quinone.

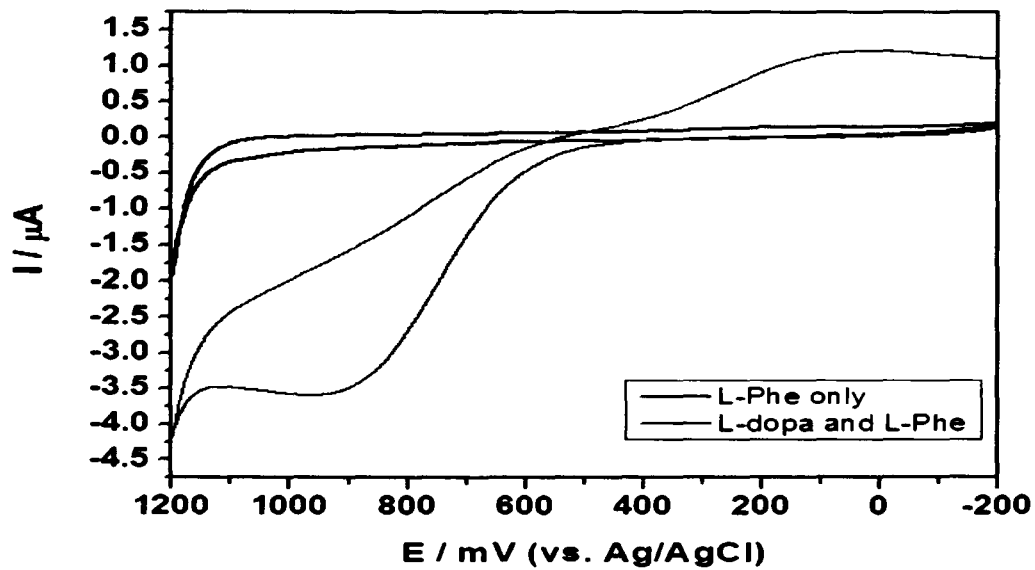


**Figure 11.** Cyclic voltammograms of L-Phe (0.1 M) and mixed L-dopa with L-Phe (0.1 M) using BDD electrode in 0.1 M HCl, scan rate:  $50 \text{ mV s}^{-1}$ .

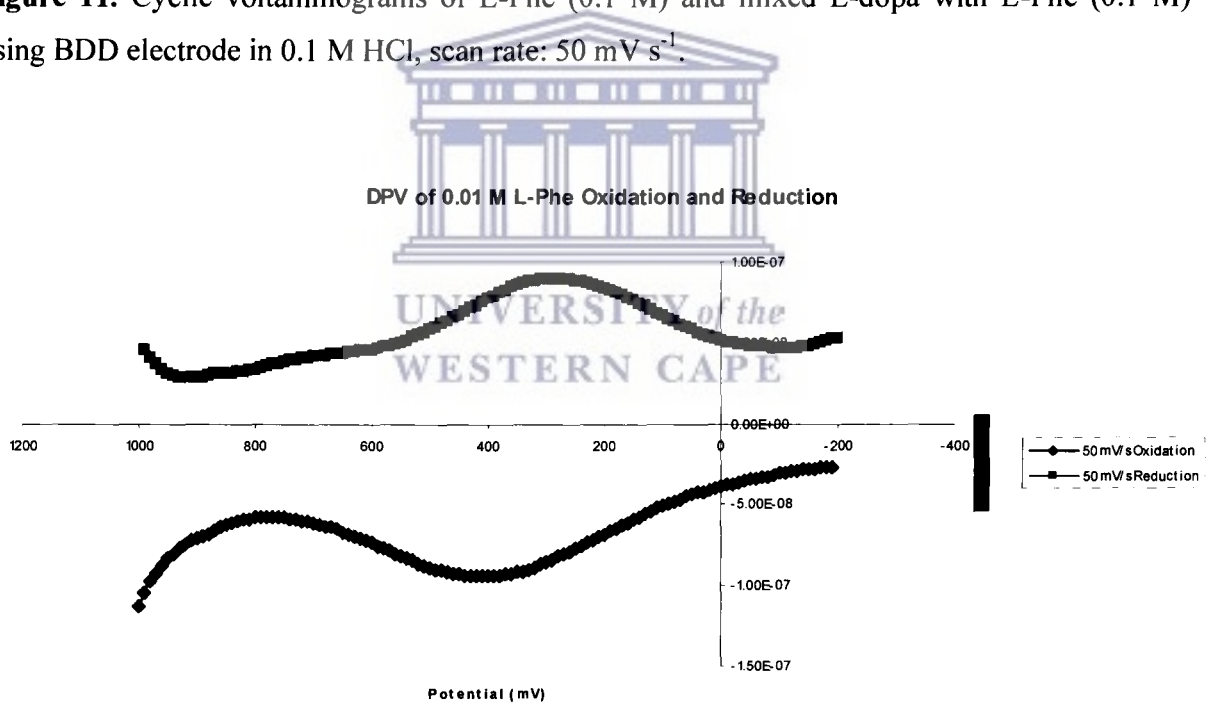


**Figure 12.** Differential pulse voltammograms of L-Phe (0.1 M) solution using BDD electrode in 0.1 M HCl, scan rate:  $50 \text{ mV s}^{-1}$ .

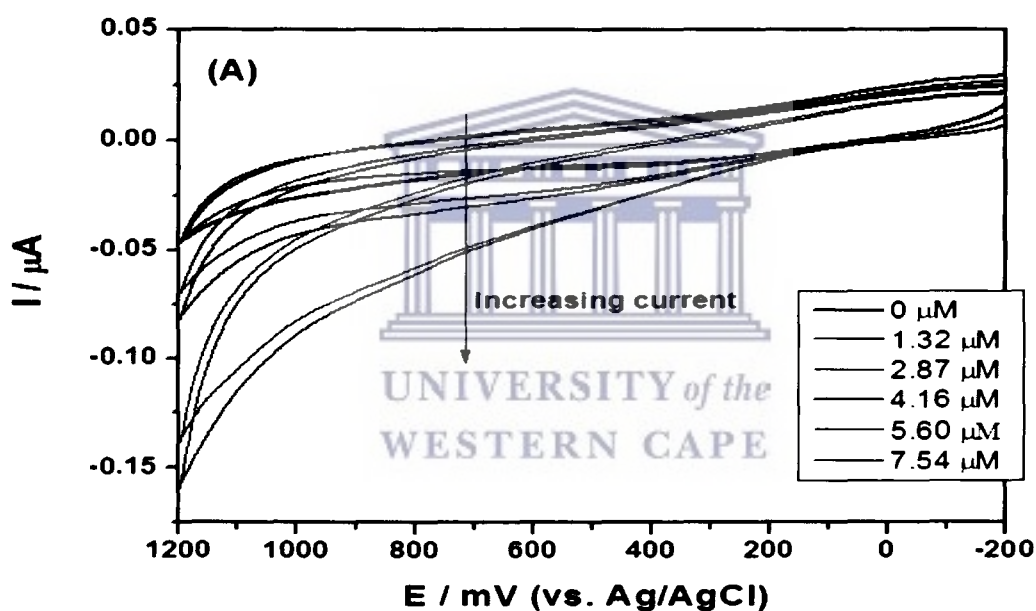
Figure 12 shows the differential pulse voltammetric responses of the BDD electrode to the L-Phe (0.1 M) and a  $\Delta E_p = 57$  mV, potential shift towards more positive values. This indicates the presence of a catalytic reduction process coupled to an electrode transfer reaction at the electrode. This is also confirmed by the increase in anodic current  $I_{p,a}$  as the scan rate increased (not shown). The anodic peak current (around 400 mV) linearly increases with the square root of scan rate in the low range, suggesting that the oxidation of L-Phe on the BDD electrode is a diffusion-controlled process. It also reveals that there is no diffusion limitation at the surface of the electrode.

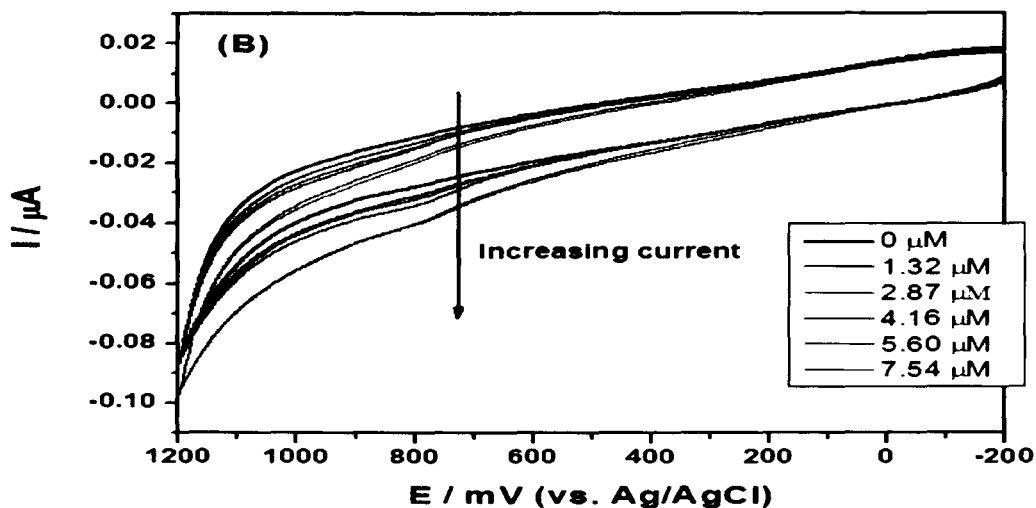
## 6.6 Application of Tyr/PANI-PVS biosensors

### 6.6.1 Electrochemical study of real samples using Tyr/PANI-PVS/BDD biosensor

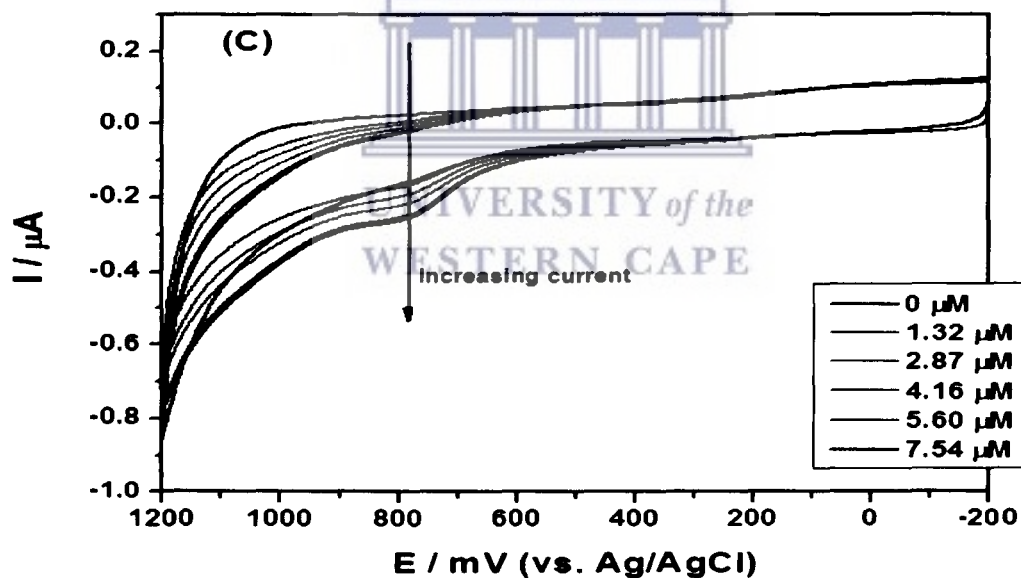
The Tyr/PANI-PVS/BDD biosensor was applied to the analysis of real samples in order to assess its analytical performance. Two samples were selected based on the classification on the packaging as 'products containing L-phenylalanine'. The first sample was an effervescent flu tablet (Schedule status, S2) and the second an artificial sweetener. Duplicate samples were prepared. Each sample was weighed and dissolved in 250 mL of 0.1 M HCl until complete dissolution was obtained. In the case of the artificial sweetener the L-phenylalanine was present as a dipeptide and the sample required heating to release the free L-phenylalanine. The samples were filtered and stored until analysis. Quantification of peak current of sample analysis was done using calibration curve for L-phenylalanine. The catalytic response of the biosensor to L-phenylalanine in the samples was observed as a proportional increase in current (Figure 6.13 and 6.14 respectively) upon successive additions (20  $\mu$ L) of analyte to 10 mL of PBS (pH 7.2) in the cell. The quantitative evaluation of L-phenylalanine in these samples was based upon the calibration curve for standard L-phenylalanine in PBS (Figure 6.6) and the results for the duplicate sample analysis are shown (Table 1).

Note that the electrooxidation of phenolics components of real samples (the cathode part of voltamperogram) is irreversible, that is, the substances oxidized during the electrochemical reaction were not then reduced. It is known that electroactive compounds, e.g. L-phenylalanine, contained in solution (including polyphenolic compounds) are oxidized on electrodes during electrochemical analysis; moreover, at a certain value of the potential, the current is sometimes directly proportional to the concentration of the substance in solution. It is impossible to calculate the precise concentration of electroactive substances (L-phenylalanine) in real samples, as the solution contains a mixture of substances with various structures. Therefore, the results shown in Table 1 were evaluated from the calibration curve for standard L-phenylalanine.





**Figure 6.13.** Cyclic voltammograms of effervescent flu tablet-T1 (A) and flu tablet -T2 (B) using Tyr/PANI-PVS/BDD biosensor in 0.1 M PBS (pH 7.2), scan rate:  $50 \text{ mV s}^{-1}$ , aerobic condition.





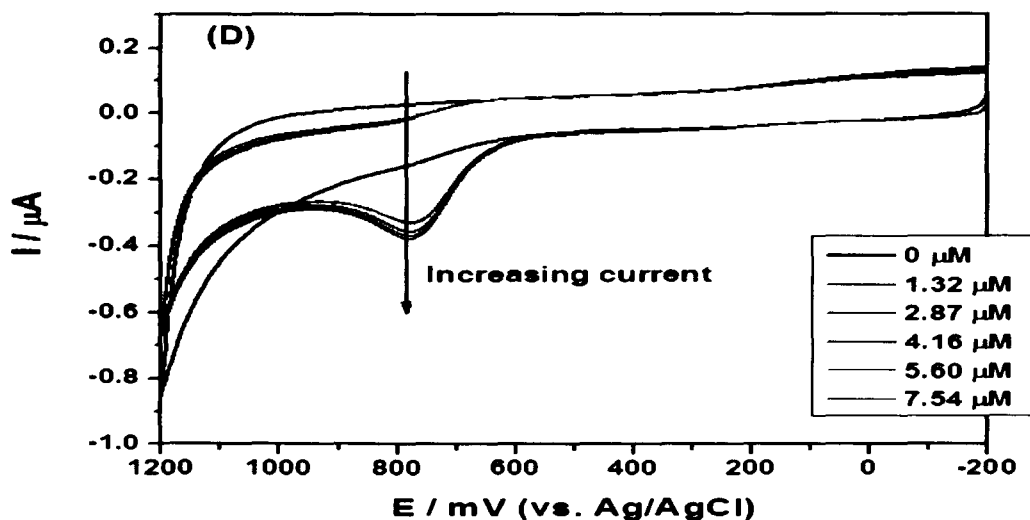


**Figure 6.14.** Cyclic voltammograms of sugar-S1 (C) and sugar-S2 (D) using Tyr/PANI-PVS/BDD biosensor in 0.1 M PBS (pH 7.2), scan rate: 50 mV s<sup>-1</sup>, aerobic condition.

**Table 6.1.** Mass % of L-phenylalanine in selected pharmaceutical preparations.

Sample	starting mass (g)	average concentration (± 0.01/ μM)	mass % L-Phe (%)
Effervescent flu tablet –T1	4.1089	0.1815	9.12
Effervescent flu tablet –T2	3.9741	0.1836	9.51
Sugar – S1	0.8890	0.1105	25.66
Sugar – S2	0.7876	0.1083	28.40

### 6.6.2 Determination of L-Phe in biological sample using Tyr/PANI-PVS/BDD biosensor

Yet, to assess the matrix effect of complex biological media and real sample, the Tyr/PANI-PVS/BDD biosensor was used in the presence of lipoprotein (human plasma) and lemonade (soft drink) samples. The lipoprotein (human plasma) was prepared as 1 mg/ml in 0.01 M PBS buffer (pH 6.2) of which 20 μL aliquots of lipoprotein was added in 0.1 M PBS buffer (pH 7.2) and analysed by cyclic voltammetry between -200 and +1200 mV at a scan rate of 50 mV s<sup>-1</sup>.

The lemonade (soft drink), purchased in the shop, and was used without further dilution. Electrochemical measurements were performed in an electrochemical cell of a three electrode configuration. The Tyr/PANI-PVS/BDD biosensor developed showed an excellent selectivity for the responses of lipoprotein and lemonade samples in the presence of L-phenylalanine. As shown in Figures 6.15 and 6.16, respectively, the electrochemical oxidation of L-Phe in both samples produced an increase in peak current with each addition of an aliquot into system, which resulted from the enzymatic reaction catalyzed by the tyrosinase on the enzyme electrode. The increase in current, at a fixed scan rate of  $50 \text{ mV s}^{-1}$ , was observed as L-phenylalanine is first converted to L-tyrosine and then to L-dopa (scheme 1.4a). This enzymatic reaction was attributed to the direct reduction of the enzymatically-produced L-dopa at enzyme electrode surface (cf. Chapter 1, section 1.1 and equation 1.1). The selectivity determination of lipoprotein and lemonade in the presence of L-Phe is feasible at this enzyme modified PANI-PVS/BDD electrode.

The evaluation of L-phenylalanine in these samples was based upon the calibration curve for standard L-phenylalanine in PBS (Figure 6.6). Figure 14 showed increase in the current with increase in concentration for lipoprotein (A) and lemonade (B). Table 2 presents the response characteristics of the enzyme electrode, including linear range, low detection limit, and correlation coefficient for both samples. Moreover, the detection limits were calculated according to the formula mention in chapter 3, section 3.7 (equation 3.9). A negligible matrix effect on electrochemical response by lipoprotein (human plasma) and lemonade (soft drink) confirms the biocompatibility of composite and its suitability for working in complex biological media and real sample. Thus, the forgoing results demonstrated that the new composite biopolymeric matrix can be applied successfully for the immobilization of tyrosinase and the subsequent fabrication of electrochemical biosensor for L-phenylalanine detection.

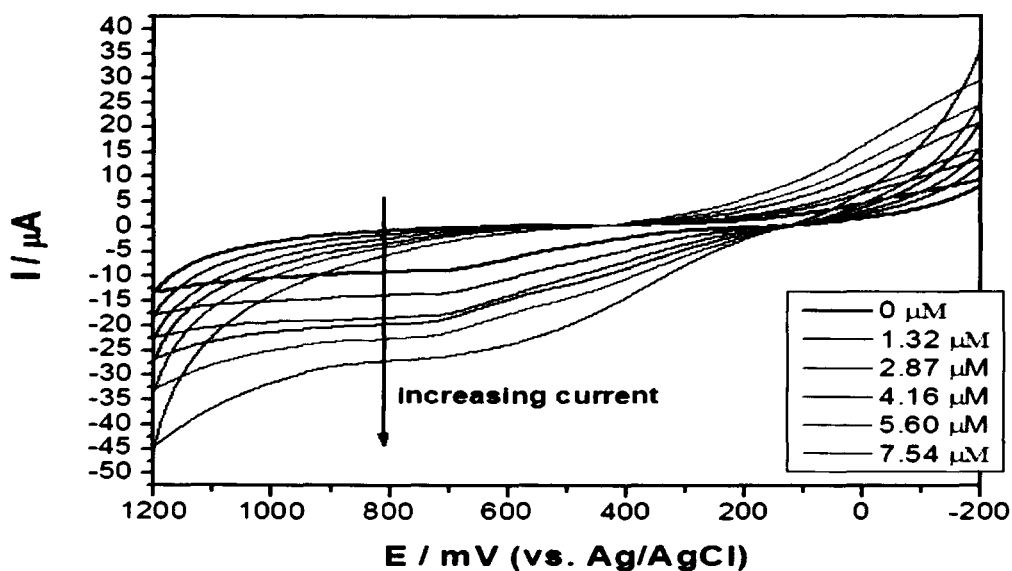


**Figure 6.15.** Cyclic voltammograms of lipoprotein (human plasma) sample using Tyr/PANI-PVS/BDD biosensor in 0.1 M PBS (pH 7.2), scan rate:  $50 \text{ mV s}^{-1}$ , aerobic condition.

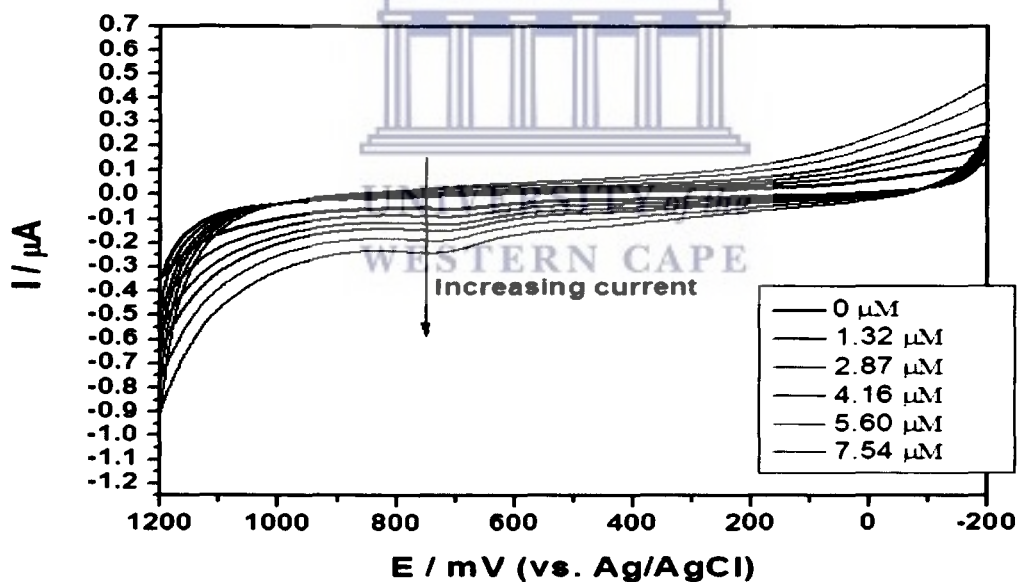


**Figure 6.16.** Cyclic voltammograms of lemonade (soft drink) sample using Tyr/PANI-PVS/BDD biosensor in 0.1 M PBS (pH 7.2), scan rate:  $50 \text{ mV s}^{-1}$ , aerobic condition.

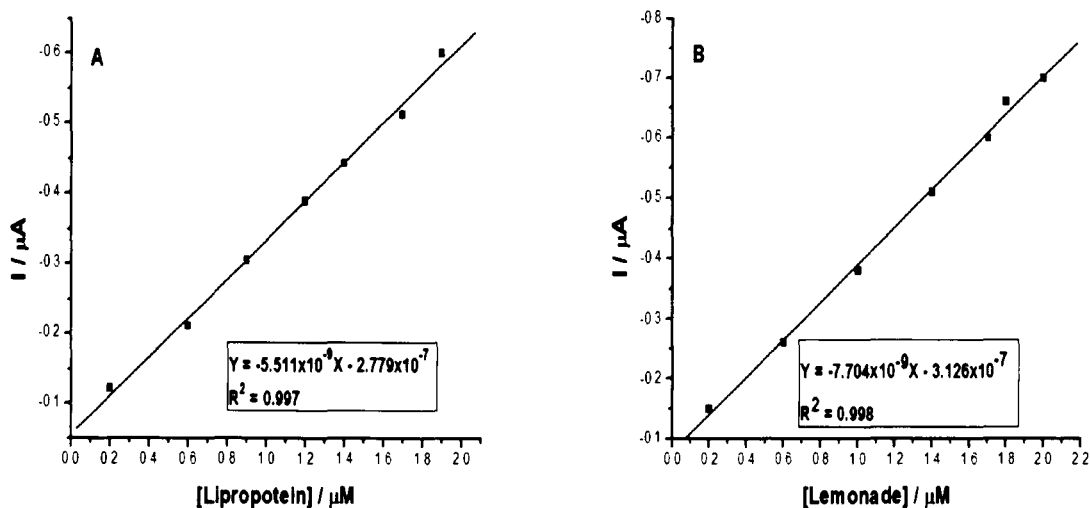


**Figure 6.17.** Calibration plots of currents versus concentration of (A) lipoprotein (human plasma) and (B) lemonade (soft drink).

The increase in the value of the oxidation current with increasing concentration of lipoprotein (A) and lemonade (B) in the solution results in the increased concentration of L-dopa during the enzymatic reaction (CVs were not shown). The variation of oxidation current obtained for the Tyr/PANI-PVS/BDD biosensor indicating linearity as 0.2-20  $\mu\text{M}$  for lipoprotein (human plasma) and 0.2-22  $\mu\text{M}$  for lemonade (soft drink), Figure 17. It appears that the Tyr/PANI-PVS/BDD biosensor provides a biocompatible environment to Tyr enzyme, and PANI-PVS films act as an electron mediator resulting in an accelerated electron transfer between tyrosinase and BDD electrode.

**Table 6.2.** Response characteristics of the biosensor in the presence of lipoprotein (human plasma) and lemonade (soft drink).

Sample	linear range ( $\pm 0.1 \mu\text{M}$ )	detection limit ( $\pm 0.1 \mu\text{M}$ )	coefficient correlation ( $R^2$ ) at n = 6
Lipoprotein (human plasma)	0.2 – 20	$1.0 \times 10^{-3}$	0.997
Lemonade (soft drink)	0.2 – 22	$1.0 \times 10^{-3}$	0.998

Considering the electrocatalytic reaction for the detection of L-phenylalanine by the Tyr immobilized on the electrode surface (step 1, equation 2.8), it is expected that L-phenylalanine is electrochemically converted to L-tyrosine followed by the oxidation of L-tyrosine to L-dopa. Tyrosinase would bind to compound in step 1 (equation 2.8) thus tyrosine encountering its electro-oxidation to the initial active state of tyrosinase ( $\text{Cu}^{\text{II}}$ ), Figure 6.18. This is result a continuously reaction in the cycle and the electron transfer of  $\text{Cu}^{\text{II}}$  leading to the Tyr electrocatalytic activity for the oxidation of L-tyrosine to produce L-dopa at the PANI-PVS/BDD electrode surface (step 2, equations 2.9-2.11). A similar behavior is expected for compounds which contained L-phenylalanine and the same reactive functional groups as L-tyrosine.

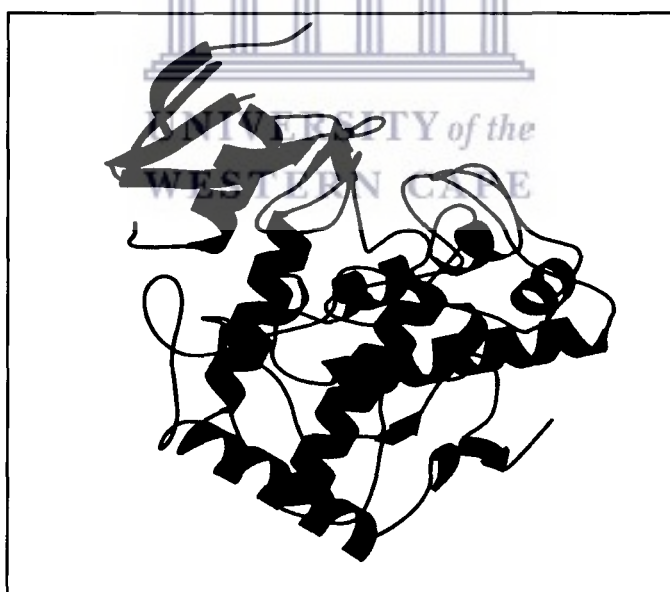
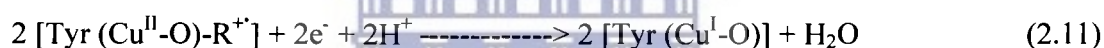
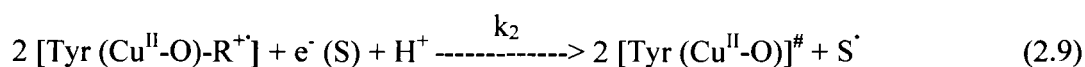
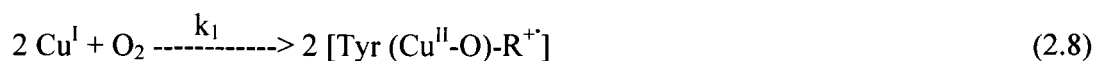


**Figure 6.18.** Model structure of tyrosinase enzyme showing copper atoms (in green), the active site for the protein sits.

## 6.7 Discussion

Numerous amperometric biosensors based on the immobilization of tyrosinase at different electrode material have been described in the literature. Glassy carbon electrodes modified with polymers [99], sol-gel materials [100,101], self-assembled monolayers (SAMs) on gold [102], reticulated vitreous carbon (RVC) [103] and other composite electrodes have been used [104,105]. However it is relatively uncommon to approach biosensor construction by direct immobilisation of tyrosinase. In a related study highly boron-doped diamond (BDD) electrodes were modified covalently with tyrosinase for the determination of estrogenic phenol derivatives and glutaraldehyde was employed as cross-linker. No further matrix for immobilization of the enzyme was employed. These electrodes were applied to a flow injection system, and the lower detection limit for bisphenol-A was  $10^{-6}$  M [418]. In another study where the enzyme tyrosinase was entrapped in a composite biopolymer matrix the  $K_m^{\text{app}}$  for L-tyrosine as substrate was found to be 0.01  $\mu\text{M}$ , with a detection limit of  $1 \times 10^{-2}$   $\mu\text{M}$  [419].

The apparent  $K_m^{\text{app}}$  values obtained from Lineweaver–Burk plots in this study were found to be  $2.83 \pm 0.01$   $\mu\text{M}$  and  $1.39 \pm 0.01$   $\mu\text{M}$  respectively, for L-tyrosine and L-phenylalanine as substrates. The detection limit for L-tyrosine was  $1.0 \times 10^{-2}$   $\mu\text{M}$  and for L-phenylalanine was  $1.0 \times 10^{-2}$   $\mu\text{M}$ . The sensitivity of the biosensor towards L-tyrosine as a substrate was  $3.53 \text{ Amol}^{-1} \text{ dm}^3$  compared to  $7.19 \text{ Amol}^{-1} \text{ dm}^3$  for L-phenylalanine. These biosensor kinetic parameters speak of a highly sensitive biosensor design, which may be largely attributed to the simplistic design of the biosensor and the absence of matrix effects impeding signal transduction.

The correlation between electrochemical response for L-phenylalanine standard analysis and real sample analysis is evidence that the biosensor is selective and sufficiently sensitive in its recognition of L-phenylalanine as alternative substrate, in the absence of L-tyrosine. The influence of other interferents in the selective detection of L-Phe by the tyrosinase biosensor has not yet been investigated. UV/vis analysis indicates the formation of an oxidation product with a sharp absorption peak (204 nm) clearly separated from the absorption maximum of the L-Phe standard (213 nm). The chemical structure of L-Phe and L-dopa differ by the presence of two hydroxyl groups on the benzene ring of L-dopa only and it is therefore plausible that their

UV/vis absorptions will be within close proximity. The UV/vis absorbance wavelength of L-dopa is strongly affected by pH and nature of absorption medium [27].

The L-Phe concentration as measured in real samples was difficult to control, since the packaging of both samples carry the Food and Drug Administration (FDA) warning of phenylalanine (Phe) content, but no indication of the quantity of Phe. However the mass/mass percentage for the flu tablets translates to a mass of  $\pm 300$  mg Phe per tablet, well below the daily recommended dose of Phe as nutritional supplements 1000-2000 mg per adult per day. Yet, the low detection limit found for lipoprotein ( $1.0 \times 10^{-3} \pm 0.1 \mu\text{M}$ ) and lemonade ( $1.0 \times 10^{-3} \pm 0.1 \mu\text{M}$ ) indicating that the new composite biopolymeric matrix can be applied successfully for the immobilization of tyrosinase and the subsequent fabrication of electrochemical biosensor for L-phenylalanine detection.





## CHAPTER 7

### Conclusions and Recommendations

#### 7.1 Conclusions

We have demonstrated a simple tyrosinase modified BDD biosensor design through covalent bonding of the enzyme with activated BDD electrode surface. L-tyrosine and L-phenylalanine were used as substrates. The detection and quantification of the L-tyrosine and L-phenylalanine have been achieved using the developed Tyr/PANI-PVS biosensor. The detection principle was based on measurement of the oxidized response of the biosensor occurring as a result of the catalytic activity of Tyr immobilized on composite film PANI-PVS onto BDD electrode. The tyrosinase biosensor was able to catalyse L-Phe to L-dopa efficiently and completely. The stability of this biosensor is good with more than 85 % of its initial activity retained after 24 hours. The biosensor was evaluated up to one month. The biosensor showed a linear response to L-tyrosine and L-phenylalanine in the concentration range 2 – 10  $\mu\text{M}$  ( $r = 0.999$ ,  $n = 6$ ). The detection limit for L-tyrosine was  $1.0 \times 10^{-2}$   $\mu\text{M}$  and for L-phenylalanine was  $1.0 \times 10^{-2}$   $\mu\text{M}$ . The low detection limit found indicating that the new composite biopolymeric matrix can be applied successfully for the immobilization of tyrosinase and the subsequent fabrication of electrochemical biosensor for L-phenylalanine detection.

UV-Vis spectroscopy confirmed the existence of the absorbance value (at wavelength 204 nm) for L-phenylalanine oxidation assigned to the production of L-dopa (Figure 6.9). Thus spectroscopic studies suggested that electrochemically synthesized PANI in the presence of PVS was electroconductive. The shifting of the quinoimine bands for the benzene and quinoid units in the FTIR of electrochemically synthesized PANI-PVS to lower wavenumbers was indicative of successful doping. It was observed that the FTIR spectra recorded after the contact of the immobilized Tyr with the L-Phe, electrochemically converted to L-tyrosine, (PANI-PVS/Tyr-L-Tyr) showed the disappearance of amide I band of Tyr (Figure 6.10). This was an evidence of the binding of the enzyme with participation of the phenol groups of the substrate. Though UV-Vis

and FTIR studies were not conducted for the real samples, the fact that polymer growth was observed marked by the increasing peak currents with scan rates was indicative of their conducting nature. Scanning electron microscopy showed the granular porous morphology of PANI-PVS film indicating that the electrosynthesized PANI-PVS could be used for electromediation purposes in biosensor construction where the PANI-PVS is expected to provide an electronic link between the biomolecule redox center and the electrode.

The apparent Michaelis-Menten constant ( $K_m^{app}$ ) calculated for the Tyr/PANI-PVS biosensor in the presence of L-tyrosine and L-phenylalanine were found to be 2.83  $\mu\text{M}$  and 1.39  $\mu\text{M}$ , respectively. The low  $K_m^{app}$  values obtained for the Tyr/PANI-PVS biosensor indicate strong binding to Tyr by the substrates. The sensitivity of the biosensor towards L-tyrosinase as a substrate was 3.53  $\text{Amol}^{-1}\text{dm}^3$  compared to 7.19  $\text{Amol}^{-1}\text{dm}^3$  for L-phenylalanine. The L-Phe content of effervescent flu tablets determined using this biosensor was 9.10 % and 9.51 % (m/m) and that of an artificial sweetener containing L-Phe as a dipeptide before hydrolysis, was 25.66 % and 28.40 % (m/m). The developed biosensor was also used for the determination of L-phenylalanine in lipoprotein (human plasma) and lemonade (soft drink). The biosensor has shown the linearity from 0.2 to 20  $\mu\text{M}$  for lipoprotein (human plasma) and 0.2 to 22  $\mu\text{M}$  for lemonade (soft drink). The detection limit was found to be  $1.0 \times 10^{-3} \pm 0.1 \mu\text{M}$  for both lipoprotein and lemonade.

The biosensor exhibited high sensitivity for L-Phe detection, very good reproducibility and with a relative standard deviation (R.S.D) of 5 % (duplicate measurements) was obtained. The low R.S.D obtained for the biosensor demonstrates that its response was highly reproducible. It was observed that the same biosensor could be further applied for the analysis of real samples. The development of this method is a step forward in the analysis of L-Phe at residue levels such as those occurring in the environment. The detection limit obtained for L-Phe by the Tyr/PANI-PVS biosensor was found to be lower. Therefore, the biosensor is sufficient in providing high sensitivity for determination of L-Phe in real samples at residue levels.

The biosensor method also demonstrated its simplicity, ease of construction, rapidity, sensitivity, and low-cost compared to the conventional analytical techniques corroborating that it can effectively be applied for environmental surveillance of these compounds containing L-Phe at residue levels on a regular basis. The granular porous morphology of PANI-PVS film provided a suitable micro-environment for the immobilized Tyr and acted as a mediator enhancing the heterogeneous direct electron transfer rate of Tyr. The composite film materials can act as tiny conduction centers to facilitate electron transfer between the enzyme and the electrode surface. The high stability of the Tyr/PANI-PVS film was due to the electrostatic attachment procedure used for the immobilization of the enzyme and the incorporation of the dopant PVS into the polymer matrix.

## 7.2 Recommendations

One of the foremost problems encountering PANI application in large scale processes has been its insolubility, infusibility and intractability. It is thus suggested that the incorporation of sulphonic groups could provide a solution to this problem.

The results indicate that the Tyr/PANI-PVS/BDD biosensor is sensitive enough to detect the L-phenylalanine at low concentrations. However, in order that the biosensor can be fully applied for the detection of this L-phenylalanine in samples containing complex matrices, further optimization and selectivity studies would be required. A follow up procedure should include (i) the studies of interfering species in the analyte solutions when sampling real samples, (ii) the investigation of other PANI modified BDD platforms for the biosensor and (iii) the transfer of technology to screen printed electrode formats for preparation of portable biosensor for on site monitoring. The application of Tyr/PANI-PVS biosensor should be extended to analysis of other biological samples such urine, saliva, blood etc.

## References

1. Kroger, S., Turner, A.P.F., Mosbach, K., Haupt, K., (1999). Imprinted polymer-based Sensor system for herbicides using differentialpulse voltammetry on screen-printed electrodes. *Anal. Chem.* 71, 3698–3702.
2. Levi, R., McNiven, S., Piletsky, S.A., Cheong, S.H., Yano, K., Karube, I., (1997). Optical detection of chloramphenicol using molecularly imprinted polymers. *Anal. Chem.* 69, 2017–2021.
3. Pei J, Tian F. and Thundat T., (2004). Glucose Biosensor Based on the Microcantilever. *Anal. Chem.* 76, 292–297.
4. Bergmeyer ed. (1985). "L-Phenylalanine and L-Tyrosine", *Methods of Enzymatic Analysis* 8, 405-411.
5. Hirokazu Koyama, (1984). "A simple and rapid enzymatic determination of L-phenylalanine", *Clinica Chimica Acta* 136, 131-136.
6. Wendel & Keffler, (1990). "A new approach to the newborn", *Clinica Chimica Acta* 192, 165-170.
7. Ryan S, Scriver CR., (2003) Jan 24. Phenylalanine Hydroxylase Deficiency. *Gene Reviews*. Accessed 2003, March 13.
8. McKusik VA., (1966-2003). Phenylketonuria (#261600). Accessed on OMIM database, 2003, March 13.
9. Marselli, B.; Garcia-Gomez, J.; Michaud, P.-A.; Rodrigo, M. A.; Comninellis, Ch.,(2003). *J.Electrochem. Soc.*, 150, D79.

10. Martínez-Huitle, C. A., Ferro, S., De Battisti, A., (2004). *Electrochim. Acta*, 49, 4027.
11. Martínez-Huitle C.A., Quiroz M.A., Comninellis Ch., Ferro S., De Battisti A, (2004). *Electrochim. Acta*, 50, 949.
12. Iwuoha, E.I. and Smyth, M.R., (1996). "Application of polymers in Electroanalytical Chemistry". In *Electroactive Polymers Electrochemistry, Part II: Methods and Applications*, ed.M.E.G. Lyons, Plenum Press, N.Y., 297-328.
13. Iwuoha E.I, Smyth M.R, (1996). Polymer-based amperometric biosensors, in: M.E.G. Lyons (Ed.), *Electroactive Polymer Electrochemistry*, Plenum Press, New York, 297–325.
14. Stejskal J., Sapurina I., (2005). *Pure Appl. Chem.* 77, 815.
15. Gerard M, Chaubey A, Malhotra B.D., (2002). *Biosensors. Bioelectron.* 17, 345.
16. Mu,S.C., Chen C, Wang J, (1997). *Synth. Met.* 88, 249.
17. Kraljić,M; Mandić,Z; Duić, L.j., (2003). *Corr. Sci.* 45, 181.
18. Bernard M.C., Hugot-Le Goff,A., Joiret S.,Phong,P.V., (2001). *Synth. Met.* 119, 283.
19. Naoi K., Lien M.M., and Smyrl W.H., (1991). *J. Electrochem. Soc.*138, 440.
20. Newman J.D., White S.F., Tothier I.E., and Turner A.P.F., (1995). *Anal. Chem.* 67 4594.
21. Ngamna O., Morrin A., Moulton S.E., Killard A.J., Smyth M.R., and Wallace G.G., (2005). *Synth. Met.*, 153, 185.

22. Bartlett P.N., and Wang J.H., J.H., (1996). *J. Chem. Soc., Faraday Trans. 92*, 4137.
23. Triotsky V. I., Berzina T. S., Fontana M. P., (2002). *Langmuir- Blodgett Assemblies with Patterned Conductive Polyaniline Layers. Material Science and Engineering:C*, 22:239-244.
24. Chandrakanthi R. L. N., Careem M.A., (2002). *Preparation and Characterisation of CDS and Cu<sub>2</sub>S nanoparticle/polyaniline Composite Films. Thin Solid Films*, 471: 51-56.
25. Mirmohseni A., Wallace G. G, (2003). *Preparation and characterisation of processable electroactive polyaniline- polyvinyl alcohol composite. Polymer*, 44:3523-3526.
26. Pud A., Ogurstov N., Korzhenko A., Shapoval G., (2003). *Some aspects of preparation methods and properties of polyaniline blends and composites with organic polymers. J. Progress in Polymer Science*, 28:1701-1753.
27. Wei Z., Zhang Z., Wan N., (2002). *Formation mechanism of self-Assembled polyaniline micro/nanotubes. Langmuir*, 18: 917-921.
28. Hirokazu Koyama, (1984). "A simple and rapid enzymatic determination of L-Phenylalanine", *Clinica Chimica Acta* 136, 131-136.
29. Wendel & Keffler, (1990). "A new approach to the newborn", *Clinica Chimica Acta* 192, 165-170.
30. Eisensmith, R. C. & Woo, S. L., (1991). *Phenylketonuria and the phenylalanine hydroxylase gene. Mol.Biol. Med.* 8, 3-18.
31. Jervis, G. A., (1953). *Phenylpyruvic oligophrenia deficiency of phenylalanine-Oxidizing system. Proc. Soc Expt. Biol. Med.* 82, 514-515.

32. Bickel, H., Gerrard, J. & Hickmans, E. M., (1954). The influence of phenylalanine Intake on chemistry and behavior of a phenylketonuria child. *Acta Paediatr. Scand.* 43, 64-77.
33. Woolf, L. I., Griffiths, R. & Moncrief, A., (1955). Treatment of phenylketonuria with a diet low in phenylalanine. *Brit. Med. J.* 1, 57-64.
34. Hulanicki, A.; Glab, S., and Ingman, F., (1989). IUPAC discussion paper commission, V.1
35. Evtugyn, G.A.; Budnikov, H.C.; Nikolsyaka, E.B., (1998). Sensitivity and selectivity of electrochemical sensors for inhibition determination. *Talanta* 46, 465-484
36. Kukla, A.L.; Kanjuk, N.I.; Starodub, N.F; Shirshov, Y.M., (1999). Multienzyme electrochemical sensor array for determination of heavy metal ions. *Sensors and Actuators B* 57, 213-218.
37. Huang, T; Warsinke, A.; Kuwana, T.; and Scheller, F.W., (1998). Determination of L-phenylalanine based on an NADH-Detecting biosensor. *Analytical Chemistry*, vol.70, no.5, 991-997.
38. Zhi, J.F.; Zhou, Y.L.; and Tian, R.H., (2007). Amperometric biosensor based on Tyrosinase immobilized on a BDD. *Biosensors and Bioelectronics* 22, 822-828.
39. Clark, L.C Jr. Lyons, C, (1962). Electrode systems for continuous monitoring in cardiovascular surgery. *Annals of the New York Academy of Sciences* 102, 29-45.
40. Updike, S.J.; Hicks, G.P., (1967). The enzyme electrode, a miniature chemical transducer using immobilised enzyme activity. *Nature* 214, 986-988.



41. D'Orazio, P., (2003). Biosensors in clinical chemistry. *Clinica Chimica Acta* 334, 41-69.
42. Somerset V.S, Klink M.J., Baker P.G.L., Iwuoha E.I., (2007). Acetylcholinesterase-polyaniline biosensor investigation of organophosphate pesticides in selected organic solvents *Journal of Environmental and Health Part B* 42, 297-304.
43. Updike S.J., Shultz M., Ekman B., (1982). Implanting the glucose electrode: problem, progress, and alternative solutions. *Diabetes Care* 5, 207- 212.
44. Iwuoha E.I., Smyth M.R., (2003). Reactivities of organic phase biosensors: 6. Square-wave and differential pulse studies of genetically engineered cytochrome P450<sub>cam</sub> (CYP101) bioelectrodes in selected solvents. *Biosensors and Bioelectronics* 18, 237-244.
45. Iwuoha E., Ngece R., Klink M., Baker P., (2007). Amperometric responses of CYP2D6 drug metabolism nanobiosensor for sertraline: a selective serotonin reuptake inhibitor. *IET Nanobiotechnology* 1, 62 - 67.
46. Zejli H., Cisneros J.L.H.H.d., Rodriguez I.N., Liu B., Temsamani K.R., Marty J.L., (2008). Phenol biosensor based on Sonogel-Carbon transducer with tyrosinase alumina sol-gel immobilization. *Analytica Chimica Acta* 612, 198-203.
47. Gore M.R., Szalai V.A., Ropp P., Yang I.V., Silverman J.S., Thorp, H.H., (2003). Detection of Attomole Quantities of DNA Targets on Gold Microelectrodes by Electrocatalytic Nucleobase Oxidation *Analytical Chemistry* 75, 6586-6592.
48. Owino J.H.O., Ignaszak A., Ahmed A.A., Baker P.G.L., Alemu H., Ngila J.C., Iwuoha, E.I., (2007). Modelling of the impedimetric responses of an aflatoxin B1 immunosensor prepared on an electrosynthetic polyaniline platform. *Analytical and Bioanalytical Chemistry* 388, 1069.

49. Drummond T.G., Hill M.G., Barton J.K., Electrochemical DNA sensors, (2003).  
Nature Biotechnology 21, 1192-1199.
50. Lucarelli F., Tombelli S., Minunni M., Marrazza G., Mascini M., (2008).  
Electrochemical and piezoelectric DNA biosensors for hybridisation detection.  
Analytica Chimica Acta 609, 139-159.
51. Bontidean I., Mortari A., Leth S., Brown N.L., Karlson U., Larsen M.M.,  
Vangronsveld J., Corbisier P., Csöregi E., (2004). Biosensors for detection of  
mercury in contaminated soils. Environmental Pollution 131, 255-262.
52. Zhi, J.F., Zhou Y.L., and Tian R.H., (2007). Amperometric biosensor based on  
Tyrosinase immobilized on a BDD. Biosensors and Bioelectronics 22, 822-828.
53. Nakamura H., Karube I., (2003). Current research activity in biosensors. Analytical  
and Bioanalytical Chemistry 377, 446-468. 55. 31.
54. Carrascosa L.G., Moreno M., Álvarez M., Lechuga L.M., (2006). Nanomechanical  
biosensors: a new sensing tool. TrAC Trends in Analytical Chemistry 25, 196-  
206.
55. McKendry R., Zhang J., Arntz Y., Strunz T., Hegner M., Lang H.P., Baller  
M.K., Certa U., Meyer E., Guntherodt H.-J., Gerber C., (2002). Multiple label-free  
biodetection and quantitative DNA-binding assays on a nanomechanical cantilever  
array. Proceedings of the National Academy of Sciences USA 99, 9783-9788.
56. Raiteri R., Grattarola M., Butt H.-J., Skládal P., (2001). Micromechanical  
cantilever-based biosensors. Sensors and Actuators B: Chemical 79, 115-126.
57. D'Orazio, P., (2003). Biosensors in clinical chemistry. Clinica Chimica Acta 334, 41  
69.

58. Freire R. S., Pessoa C. A., Mello L. D., & Kubota, L. T., (2003). Direct electron transfer: An approach for electrochemical biosensors with higher selectivity and sensitivity. *J. Braz. Chem. Soc.*, 14, 230-243.
59. Liu S. Q., & Ju H. X., (2002). Renewable reagentless hydrogen peroxide sensor based on direct electron transfer of horseradish peroxidase immobilized on colloidal gold-modified electrode. *Anal. Biochem.* 307 , 110–116.
60. Tang J. L., Wang B. Q., Wu Z. Y., Han X. J., Dong S. J., & Wang, E. K., (2003). Lipid membrane immobilized horseradish peroxidase biosensor for amperometric determination of hydrogen peroxide. *Biosens. Bioelectron.* 18, 867-872.
61. Collins G. E., & Buckley L. J., (1996). Conductive polymer-coated fabrics for chemical sensing. *Synth. Met.*, 78, 93–101.
62. Huang J. X., & Kaner R. B. (2004). A general chemical route to polyaniline nanofibers. *J. Am. Chem. Soc.* 126, 851-855.
63. Zhang D., & Wang, Y., (2006). Synthesis and applications of one-dimensional nanostructured polyaniline: An overview. *Mater. Sci. Eng., B* 134 , 9-19.
64. Zhang S., Wright G., & Yang Y., (2000). Materials and techniques for electrochemical biosensor design and construction. *Biosens. Bioelectron.* 15, 273–282.
65. Rodriguez-Mozaz S., Lopez de Alda M. J., Marco M. -P. & Barcelo D., (2005). Biosensors for environmental applications: Future development trends. *Pure Appl. Chem.* 76, 723-752.
6. Grennan K., Killard A. J., Hanson C. J., Cafolla A. A., & Smyth M. R., (2006). Optimisation and characterisation of biosensors based on polyaniline. *Talanta* 68, 1591–1600.

67. Iwuoha E. I., Leister I., Miland E., Smyth M. R., & Fágáin C. O., (1997). Reactivities of organic-phase biosensors. I. Enhancement of the sensitivity and stability of amperometric peroxidase biosensors using chemically modified enzymes. *Anal. Chem.* 69, 1674-1681.
68. Mathebe N. G., Morrin A., & Iwuoha, E. I., (2004). Electrochemistry and scanning electron microscopy of polyaniline/peroxidase-based biosensor. *Talanta* 64, 115-120.
69. Morrin A., Ngamna O., Killard A. J., Moulton S. E., Smyth M. L., & Wallace G., (2005). An amperometric enzyme biosensor fabricated from polyaniline nanoparticles. *Electroanalysis* 17, 423-430.
70. Somerset V. S., Klink M. J., Baker P. G. L., & Iwuoha E. I., (2007). Acetylcholinesterase-polyaniline biosensor investigation of organophosphate pesticides in selected organic solvents. *J. Environ. Sci. Health., Part B*, 42, 297-304.
71. Songa E. A., Waryo T., Jahed N., Baker P. G. L., Kgarebe B. V., & Iwuoha E. I., (2009). Electrochemical Nanobiosensor for Glyphosate Herbicide and its Metabolite. *Electroanalysis*, DOI: 10.1002/elan.200804452 [In Press].
72. Copel J.A., Grannum P.A., Hobbins J.C., (1991). Interventional procedures in obstetrics. *Seminars in Roentgenology* 26, 87-94.
73. Tran-Minh C., (1993). *Biosensors*. London: Chapman & Hall.
74. Sariri R., Sajedi R. H., & Jafarian V., (2006). Inhibition of horseradish Peroxidase by thiol type inhibitors. *J. Mol. Liq.*, 123, 20-23.

75. Amine A., Mohamed H., Bourais I., & Palleschi G., (2006). Enzyme Inhibitionbased biosensors for food safety and environmental monitoring. *Biosens. Bioelectron.*, 21, 1405-1423.
76. Evtugyn G. A., Budnikov H. C., & Nikolskaya E. B., (1998). Sensitivity and selectivity of electrochemical enzyme sensors for inhibitor determination. *Talanta*, 46, 465–484.
77. Zawistowski J., Biliaderis C. G., and Eskin N. A. M., (1991). Polyphenol oxidase. In: *Oxidative Enzymes in Foods* (D. S. Robinson and N. A. M. Eskin, eds.). Elsevier, London, pp. 217-273.
78. Ogawa M., Perdigao N. B., Santiago M. E., and Kozima T. T., (1984). On physiological aspects of black spot appearance in shrimp. *Bull. Jpn. Soc. Sci. Fish.* 50, 1763-1769.
79. Kazandjian R., Klibanov R.A., (1985). Regioselective oxidation of phenols catalyzed by polyphenol oxidase in chloroform, *J. Am. Chem. Soc.* 107, 5448–5450.
80. Rivas G., Solis V., (1991). Indirect electrochemical determination of L-tyrosine using mushroom tyrosinase in solution, *Anal. Chem.* 63, 2762–2765.
81. Xu Y., Stokes A. H., Freeman W. M., Kumer S. C., Vogt B. A., and Vrana K. E., (1997). Tyrosinase mRNA is expressed in human substantia nigra. *Mol. Brain Res.* 45, 159-162.
82. Zhang J., Li B., Xu G., Cheng G., Dong S., (1999). *Analyst* 124 699.
83. Wang J., Lu F., David L., (1994). *Analyst* 119, 455-458.
84. Cosnier S., Innocent C., (1992). *J. Electroanal. Chem.* 328, 361.

85. Adeyolu O., Iwuoha E.I., Smyth M.R., Leech D., (1996). *Analyst* 121, 1885.
86. Ortega F., Domínguez E., (1993). *J. Biotechnol.* 31, 289.
87. Mannino S., Cosio M., (1994). Organic-phase enzyme biosensor for moisture determination in Food products, *Analyst* 119, 2001–2003.
88. Wang J., Chen L., (1995). Hydrazine detection using a tyrosinase based inhibition biosensor, *Anal. Chem.* 67, 3824–3827.
89. Xiaoya H., Zongzhou L., (1995). Determination of cyanide using a tyrosinase Amperometric biosensor with catechol as substrate, *Analyst* 120, 1555–1557.
90. Dennison M, Hall J., Turner A., (1995). Gas-phase microbiosensor for monitoring phenol vapor at ppb levels, *Anal. Chem.* 67, 3922–3927.
91. Kiba N., Suzuki H., Furusawa M., (1993). Flow-injection determination of L-tyrosine in serum with immobilized tyrosinase, *Talanta* 40, 995–998.
92. Caruso C., Vieira I., Filho O., (1999). Determination of epinephrine and dopamine in pharmaceutical formulations using a biosensor based on carbon paste modified with crude extract of cara root *Dioscorea bulbifera*, *Anal. Lett.* 32, 39–50.
93. Furbee J, Thomas C., Kelly R., Malachowski M., (1993). Mediated electrochemical reduction of cytochrome c and tyrosinase at perfluorosulfonated ionomer coated electrodes, *Anal. Chem.* 65, 1654–1657.
94. Daigle F., Leech D., (1997). Reagentless tyrosinase enzyme electrodes: effects of enzyme loading, electrolyte pH, ionic strength, and temperature, *Anal. Chem.* 69, 4108–4112.

95. Nistor C., Emneuso J., Gorton L., Ciucu A., (1999). Improved stability and altered selectivity of tyrosinase based graphite electrodes for detection of phenolic compounds, *Anal. Chim. Acta* 387, 309–326.
96. Arslan A., Kiralp S, Toppare L., Yagci Y., (2005). Immobilization of tyrosinase in polysiloxane/polypyrrole copolymer matrices, *Intl. J. Biol. Macromol.* 35, 163–167.
97. Christophe V., Silvia F., Canh T., (2003). Amperometric tyrosinase based biosensor using an electrogenerated polythiophene Wlm as an entrapment support, *Talanta* 59, 535–544.
98. Aihua L., Itaru H, Haoshen Z., (2005). Electrochemical biosensor based on protein–polysaccharide hybrid for selective detection of nanomolar dopamine metabolite of 3,4-dihydroxyphenylacetic acid (DOPAC), *Electrochem. Commun.* 7, 233–236.
99. Vedrine C., Fabiano S., Tran-Minh C., (2003). *Talanta* 59, 535.
100. Yu J., Liu S., Ju H., (2003). *Biosens. Bioelectron.* 19, 509.
101. Wang B., Zhang J., Dong S., (2000). *Biosens. Bioelectron.* 15, 397.
102. Campuzano S., Serra B., Pedrero M., Manuel de Villena F.J., J.M. Pingarron J.M., (2003). *Anal. Chim. Acta* 494, 187.
103. Pena N., Reviejo A.J, Pingarron J.M., (2001). *Talanta* 55, 179.
104. Serra B., Jimenez S., Mena L., Reviejo J., Pingarron J.M., (2002). *Biosens. Bioelectron.* 17, 217.



105. Onnerfjord P., Emneus J., Marko-Varga G., Gorton L., Ortega F., Dominguez E., (1995). *Biosens. Bioelectron.* 10, 607.
106. Yaropolov A.I., Kharybin A.N., Emneus J., Marko-Varga G. and Gorton L., (1995). *Anal. Chim. Acta* 308, 137.
107. Tillyer C.R. and Gobin P.T., (1991). *Biosens. Bioelectron.* 6, 569.
108. Rogers K.R., Becker J.Y. and Cembrano J., (2000). *Electrochim. Acta* 45, 4373.
109. Önnerrfjord P., Emnéus J., Marko-Varga G., Gorton L., Ortega F. And Domínguez E., (1995). *Biosens. Bioelectron.* 10, 607.
110. Cosnier S. and Popescu I.C., (1996). *Anal. Chim. Acta* 319, 145.
111. Wang J., Lin Y. and Chen Q., (1993). *Electroanalysis* 5, 23.
112. Deng Q., Guo Y.Z. and Dong S.J., (1996). *Anal. Chim. Acta*, 319, 71.
113. Li J., Chia L.S., Goh N.K. and Tan S.N., (1998). *Anal. Chim. Acta* 362, 203.
114. Wang B.Q., Zhang J.Z. and Dong S.J., (2000). *Biosens. Bioelectron.* 15, 397.
115. Liu Z.J., Liu B.H., Kong J.L. and Deng J.Q., (2000). *Anal. Chem.* 72, 4707.
116. Liu Z.J, Deng J.Q. and Li D., (2000). *Anal. Chim. Acta* 407, 87.
117. Pawelek J.M. and Korner A., (1982). *Am. Sci.* 70, 136-145.

118. Perez-Gilbert M. and Garcia-Carmona, F., (2000). Characterization of catecholase and cresolase activities of eggplant polyphenol oxydase, *J. Agric. Food Chem.* 48, 695-700.
119. Kramer K. J., and Hopkins T.L., (1987). Tyrosine metabolism for insect cuticle tanning, *Arch. Insect Biochem. Physiol.* 6, 279-301.
120. Hearing V. J., Tsukamoto, K., (1991). Enzymatic control of pigmentation in mammals. *FASEB J.* 5,2902-2909.
121. Ross R. A., Biedler J. L., (1985). Presence and regulation of tyrosinase activity in human neuroblastoma cell variants in vitro. *Cancer Res.* 45,1628-1632.
122. Slack R., Lach B., Gregor A., al-Mazidi H., Proulx P., (1992). Retinoic acid- and staurosporine-induced bidirectional differentiation of human neuroblastoma cell lines. *Exp. Cell Res.* 202,17-27.
123. Spritz R.A., and Hearing V. J. Jr., (1994). Genetic disorders of pigmentation, *Adv. Hum. Gent.* 22, 1-45.
124. Perez- Bernal A., Munoz-Perez, M. and Camacho, F., (2000). Management of facial hyper-pigmentation, *Am. J. Clin. Dermatol.* 1, 261-268.
125. Gerritsen Y.A.M., Chapelon C.G.J., Wichers H.J., (1994). *Phytochemistry* 35, 573.
126. Mayer, AM, (2006). "Polyphenol oxidases in plants and fungi: Going places? A review". *Phytochemistry* 67: 2318-2331. PMID 16973188.

127. Jaenicke, E and Decker, H., (2003). "Tyrosinases from crustaceans form hexamers". *Biochem. J.* 371: 515-523. PMID 12466021.
128. Kwon B. S., Haq A. K., Pomerantz S. H. and Halaban R., (1987). Isolation and sequence of a cDNA clone for human tyrosinase that maps at the mouse c-albino locus. in *Proceedings of the National Academy of Sciences*. Volume 84, pages 7473-7477.
129. Matoba Y, Kumagi, T. et al (2006). "Crystallographic evidence that the dinuclear copper center of tyrosinase is flexible during catalysis". *J. Biol. Chem.* 281 (13): 8981-8990. PMID 16436386.
130. Sussman, A. S., (1949). The functions of tyrosinase in insects. *Quart. Rev. Biol.*, 24: 328-341.
131. Holm, R.H., Kennepohl, P., Solomon, E.I. (1996). *Chem. Rev.* 96, 2239.
132. Lerch, K., (1987). *Life Chem. Rep.* 5, 221-234.
133. Solomon, E.I. and Lowery, M.D., (1993). *Science* 259, 1575-1581.
134. Eickman, N.C., Himmelwright, R.S. and Solomon, E.I., (1979). *Proc. Natl. Acad. Sci. USA* 76, 2094-2098.



135. Himmelwright R.S., Eickman, N.C., LuBien, C.D., Lerch, K. and Solomon, E.I., (1980). *J. Am. Chem. Soc.* 102, 7339-7344.
136. Solomon E.I., (1981). In *Copper Proteins* (Spiro, T.G., eds.), Vol. III, pp. 41-108, Wiley-Interscience, New York.
137. Jolley R.L., Evans L.H., Makino N. and Mason H.S., (1974). *J. Biol. Chem.* 249, 335-345.
138. Kubowitz F., (1938). *Biochem. Z.* 299, 32-57.
139. Wilcox D.E., Porras A.G., Hwang Y.T., Lerch K., Winkler M.E. and Solomon, E.I., (1985). *J. Am. Chem. Soc.* 107, 4015-4027.
140. Hearing V.J. and Tsukamoto K., (1991). *FASEB J.* 5, 2902-2909.
141. Korner A.M. and Pawelek J., (1982). *Science* 217, 1163-1165.
142. Mason H.S., (1956). *Nature* 177, 79-81.
143. Robb D.A., (1984). In *Copper Proteins and Copper Enzymes* (Lontie, R., ed.), Vol. II, pp. 207-241, CRC Press, Boca Raton, CA.
144. Naish-Byfield S. and Riley P.A., (1992). *Biochem. J.* 288, 63-67.
145. Lerner A., and Fitzpatrick T.B., (1950). *Physiol. Rev.* 30, 91-123.
146. Kubo I., Kinoshita H., and Yokokawa Y., (1994). Tyrosinase inhibitors from *Anacardium occidentale* fruits. *J. Nat. Prod.* 57, 545-551.
147. Gerard M., Chaubey A., Malhotra B.D., (2002). Application of conducting polymers to biosensors. *Biosensors and Bioelectronics* 17 345-359.

148. Sassolas A., Bouvier B.D.L, Blum L.J., (2008). DNA Biosensors and Microarrays. *Chemical Reviews* 108, 109-139.
149. Tillyer C.R. and Gobin P.T., (1991). *Biosens. Bioelectron.* 6, 569.
150. Rogers K.R., Becker J.Y. and Cembrano J., (2000). *Electrochim. Acta* 45, 4373.
151. Iwuoha E. I. and Smyth M., (1996). Polymer-based amperometric biosensors, In: *Electroactive Polymer electrochemistry, Part 2 , Methods and Applications*, Michael E.G. Lyons, Plenum Press, NewYork, USA, chapter 11, 297-328.
152. Duke, C. B., & Schein, L. B., (1980). Organic solids: Is energy-based theory enough? *Phys. Today*, 33 , 42–48.
153. Bloor D., & Movaghar B., (1983). Conducting polymers. *IEEE Proceedings*, 130, 225–232.
154. Wring, S. A., & Hart, J. P., (1992). Chemically modified carbon-based electrodes and their application as electrochemical sensors for the analysis of biologically important compounds. *Analyst*, 117, 1215–1229.
155. Schuhmann, W., (1995). Conducting polymers and their application in amperometric biosensors. *Mikrochim. Acta*, 121, 1–29.
156. Trojanowicz M., & Krawczyk T. K., (1995). Electrochemical biosensors based on enzymes immobilized in electropolymerized films. *Mikrochim. Acta*, 121, 167–181.
157. Guiseppi-Elie A., Wallace G.G., & Matsue T., (1997). In: Skotheim, T., Elsenbaumer, R., Reynolds, J.R. (Eds), *Chemical and biological sensors based on*

electrically conducting polymers. *Handbook of Conducting Polymers* (pp. 963–991, 2nd ed.). New York: Marcel Dekker.

158. Situmorang M., Gooding J. J., Hibbert, D. B., & Barnett, D., (1998). Electrodeposited polytyramine as an immobilization matrix for enzyme biosensors. *Biosens. Bioelectron.*, 13, 953–962.
159. Ahuja T., Mir I. A., Kumar, D., & Rajesh., (2007). Biomolecular immobilization on conducting polymers for biosensing applications. *Biomaterials*, 28, 791-805.
160. Guimard N. K., Gomez N., & Schmidt C. E., (2007). Conducting polymers in biomedical engineering. *Prog. Polym. Sci.*, 32, 876-921.
161. Jang J., Bae J., & Lee, K., (2005). Synthesis and characterization of polyaniline nanorods as curing agent and nanofiller for epoxy matrix composite. *Polymer*, 46, 3677-3684.
162. Plesu N., Ilia G., Pascariu A., & Vlase G., (2006). Preparation, degradation of polyaniline doped with organic phosphorus acids and corrosion essays of polyaniline–acrylic blends. *Synth. Met.*, 156, 230–238.
163. Zhang Z., Wei Z., Zhang L., Wan M., (2005). Polyaniline nanotubes and their dendrites doped with different naphthalene sulfonic acids. *Acta Materialia*, 53:1373-1379.
164. Greene R.L., Street G.B., Suter L.J., (1975). Superconductivity in polysulphur nitride (SN)<sub>x</sub>. *Phys. Rev. Lett.* 34, 577-579.
165. Hong S. Y., & Marnick D. S., (1992). Understanding the conformational stability and electronic structures of modified polymers based on polythiophene. *Macromolecules*, 4652–4657.

166. Kundu K., & Giri, D., (1996). Evolution of the electronic structure of cyclic polythiophene upon bipolaron doping. *Am. Inst. Phys.*, 105, 11075–11080.
167. Bejan D., & Duca A., (1998). Voltammetry of aniline with different electrodes and electrolytes. *Croat. Chem. Acta*, 71, 745-756.
168. Wei Y., Hariharan R., Patel A. S., (1990). Chemical and electrochemical copolymerization of aniline with alkyl ring-substituted anilines. *Macromolecules*, 23:758-764.
169. Aubert P., Bidan G., (1985). Polyhalopyrroles: Electrochemical synthesis and some characteristics. *J. Electroanal. Chem.* 190, 129-139.
170. Saraswathi R., Gerard M., Malhotra B.D., (1999). Characteristics of aqueous polycarbazole batteries. *J. Appl. Polym. Sci.* 74, 145-150.
171. Kawai T., Kuwabara T., Wan S., Yoshino K., (1990). Secondary battery characteristics of poly(3-alkylthiophene). *Jap. J. Appl. Phys.* 29, 602-605.
172. Santhanam K.S.V., Gupta N., (1993). Conducting-polymer electrodes in batteries. *TRIP* 1, 284-289.
173. Friend R.H. (Ed), (1993). *Conductive Polymer II*, Rapra Review Report, 6 (3), 23.
174. Diaz A.F., Logan J.A., (1980). *J. Electroanal. Chem.* 111, 111.
175. a) Chiang J.C, MacDiarmid A.G., (1986). *Synth. Met.* 13, 193. b) MacDiarmid A.G, Chiang J.C, Richter A.F, Epstein A.J. (1987), *Synth. Met.* 18, 285.
176. Cruz G. J., Morales J., Castillo-Ortega M. M., & Olayo R., (1997). Synthesis of polyaniline films by plasma polymerization. *Synth. Met.*, 88, 213–218.



177. Paterno L. G., Manolache S., & Denes F., (2002). Synthesis of polyaniline-type thin layer structures under low-pressure RF-plasma conditions. *Synth. Met.* 130, 85–97.
178. Liao C., & Gu M., (2002). Electroless deposition of polyaniline film via autocatalytic polymerization of aniline. *Thin Solid Films*, 408, 37–42.
179. Gong J., Cui, X. J., Xie, Z. W., Wang, S. G., & Qu, L.Y., (2002). The solid-state synthesis of polyaniline/H<sub>4</sub>SiW<sub>12</sub>O<sub>40</sub> materials. *Synth. Met.*, 129, 187–192.
180. Kim S. -C., Huh P., Kumar J., Kim B., Lee J. -O., Bruno F. F., et al., (2007). Synthesis of polyaniline derivatives via biocatalysis. *Green Chem.* 9, 44-48.
181. Wallace G. G., Spinks G. M., Kane-Maguire L. A., & Teasdale P. R., (2003). *Conductive electroactive polymers: Intelligent materials systems* (2nd ed.). United States of America: Taylor & Francis Group.
182. Iwuoha E. I., Saenz de Villaverde D., Garcia N. P., Smyth M. R., & Pingarront J. M., (1997). Reactivities of organic phase biosensors. 2. The amperometric behavior of horseradish peroxidase immobilized on a platinum electrode modified with an electrosynthetic polyaniline film. *Biosens. Bioelectron.*, 12, 749-761.
183. Tang H., Kitani A., & Shiotani M., (1996). Effects of anions on electrochemical formation and overoxidation of polyaniline *Electrochim. Acta* , 41, 1561-1567.
184. Inzelt G., & Horányi G., (1990). Some problems connected with the study and evaluation of the effect of pH and electrolyte concentration on the behaviour of polyaniline film electrodes. *Electrochim. Acta*, 35, 27-34.
185. Kalaji M., Nyholm L., & Peter L. M., (1991). A microelectrode study of the influence of pH and solution composition on the electrochemical behaviour of

- polyaniline films. *J. Electroanal. Chem.*, 313, 271-289.
186. Chen S. -S., Wen T. -C., & Gopalan A., (2003). Electrosynthesis and characterization of a conducting copolymer having S-S links. *Synth. Met.*, 132, 133-143.
187. Wei Z., Zhang Z., Wan N., (2002). Formation mechanism of self-Assembled polyaniline micro/nanotubes. *Langmuir*, 18: 917-921.
188. Pud A., Ogurstov N., Korzhenko, A., & Shapoval G., (2003). Some aspects of preparation methods and properties of polyaniline blends and composites with organic polymers. *Prog. Polym. Sci.*, 28, 1701-1753.
189. Yue J.; Wang Z. H.; Cromack K. R.; Epstein A.J.; Macdiarmid A. G., (1991). Effect of sulfonic acid group on polyaniline backbone. *J. Am. Chem. Soc.* 113, 2665-2671.
190. Wei X.-L.; Wang Y. Z.; Long S. M.; Bobeczko C.; Epstein A. J., (1996). Synthesis and physical properties of highly sulfonated polyaniline. *J. Am. Chem. Soc.* 118, 2545-2555.
191. Lange U., Roznyatovskaya N. V., & Mirsky V. M., (2008). Conducting polymers in chemical sensors and arrays. *Anal. Chim. Acta.*, 614, 1-26.
192. MacDiarmid A. G., Chiang J. C., Halpern M., Huang W. S., Mu S. I., Somasiri N. L., Wu W., & Yaniger S. I., (1985). Polyaniline interconversion of metallic and insulating forms. *Mol. Cryst. Liq. Cryst.*, 121, 173-180.
193. Watanabe A., Mori K., Mikon M., Nakamura Y., & Matsuda M., (1989). Comparative study of redox reactions of polyaniline films in aqueous and nonaqueous solutions. *Macromolecules*, 22, 3323-3327.

194. Deepa M., Ahmad S., Sood K. N., Alam J., Ahmad S., & Srivastava A. K., (2007). Electrochromic properties of polyaniline thin film nanostructures derived from solutions of ionic liquid/polyethylene glycol. *Electrochim. Acta*, 7453–7463.
195. Bartlett P. N., & Wallace E. N., (2000). The oxidation of  $\beta$ -nicotinamide adenine dinucleotide (NADH) at poly(aniline)-coated electrodes Part II. Kinetics of reaction at PANI–poly(styrenesulfonate) composites. *J. Electroanal. Chem.*, 486, 23-31.
196. Mirmohseni A., Wallace G. G, (2003). Preparation and characterisation of processable electroactive polyaniline- polyvinyl alcohol composite. *Polymer*, 44:3523-3526.
197. Cho M. S., Park S. Y., Hwang J. Y., Choi H. J., (2004). Synthesis and electrochemical properties of polymer composites with nanoparticles, *Material Science and Engineering C*24:15-18.
198. Zhang D., Wang Y., (2006). Synthesis and applications of one-dimensional nano-structured polyaniline; an overview. *Material Science and Engineering B*, 134:9-19.
199. Wessling B., (1998). Dispersion as the link between basic research and commercial applications of conductive polymers (polyaniline). *Synthetic Metals*, 93:143-154.
200. Malinauskas A., Malinauskienė J., Ramnavičius A., (2005). Conducting polymer-based nanostructured materials: Electrochemical Aspects. *Nanotechnology*, 16: R51-R62.
201. Kohut-Svelko N., Reynaud S., François J., (2005). Synthesis and characterization of polyaniline prepared in the presence of nonionic surfactants in an aqueous dispersion. *Synthetic Metals*, 150:107-114.

202. Han D., Chu Y., Liu Y., Lu Z., (2005). Reversed micelle polymerization: a new route for the synthesis of DBSA-polyaniline nanoparticles. *Colloids and surfaces A: Physicochemistry and Engineering aspects*, 259:179-187.
203. Tran D. H., Kaner R.B., (2006). A general synthetic route to nanofibres of polyaniline derivatives. *The Royal Society of Chemistry, Chemical Communications*, 3915-3917.
204. Yang S. M., Chen K. H., Yang Y. F., (2005). Synthesis of polyaniline nanotubes in the channels of anodic alumina membranes. *Synthetic Metals*, 152:65-68.
205. Long Y., Chen Z., Wang N., Zhang Z., Wan M., (2003). Resistivity study of polyaniline doped with protonic acids. *Physica B*, 325:208-213.
206. Han M. G., Cho S. K., Oh S. G., Im S. S., (2002). Preparation and characterization of polyaniline nanoparticles synthesized from DBSA micellar solution. *Synthetic Metals*, 126:53-60.
207. Cruz G. J., Morales J., Castillo-Ortega M. M., Olayo R., (1997). Synthesis of polyaniline films by plasma polymerisation. *Synthetic Metals*, 88:213-218.
208. Palaniappan S., Amarnath C. A., (2006). A novel polyaniline maleic acid-dodecylhydrogensulphate salt: Soluble polyaniline powder. *Reactive and Functional Polymers*, 66:1741-1748.
209. Innis P. C., Norris I. D., Maguire L. A. P. K., Wallace G. G., (1998). Formation of chiral polyaniline colloids codoped with (+) or (-)- 10-camphor sulphonic acid with polystyrene sulphonated. *Macromolecules*, 31:6521-6528.
210. Anand J., Palaniappan S., Sathyanarayana D. N., (1998). Conducting polyaniline blends and composites. *Progress in Polymer Science*, 23: 993-1018.

211. Norris I. D., Kane- Maguire L. A. P., Wallace G. G., (2000). Electrochemical synthesis and chiroptical properties of optically active poly-o- methoxy aniline. *Macromolecules*, 33: 3237-3243.
212. Genies E. M., Tsintavis C., (1995). Redox mechanism and electrochemical behaviour of polyaniline deposits. *Journal of electroanalytical Chemistry*, 195:109-128.
213. Sivakumar R., Saraswathi R., (2003). Redox polyaniline properties of poly-N-methylaniline. *Synthetic Metals*, 138:381-390.
214. Tang Z., Liu S., Wang Z., Dong S., Wang E., (2000). Electrochemical synthesis of polyaniline nanoparticles. *Electrochemistry Communications* 2:32-35.
215. Komsijska L., Tsacheva Ts., Tsakova V., (2005). Electrochemical formation and Copper Modification of Poly-o-methoxyaniline. *Thin Solid Films*, 493:88-95.
216. Lindfors T., Ivaska A., (2002). Potentiometric and UV-Vis characterisation of N-substituted polyanilines. *Journal of electroanalytical chemistry*, 535: 65-74.
217. Rahmanifar M. S., Mousavi M. F., Shamsipur M., Riahi S., (2006). A study of the influence of anionic surfactants on electrochemical degradation of polyaniline. *Polymer degradation and stability*, 91: 3463-3468).
218. Roković M. K., Duć Lj., (2006). Electrochemical synthesis of poly(ortho-ethoxyaniline) from phosphoric and sulphuric acid solutions. *Electrochimica Acta*, 51: 6045-6050.
219. Raposo M., Oliviera O. N., (2002). Adsorption of poly-o-methoxyaniline in Layer-by-Layer films. *Langmuir*, 18:6866-6874.

220. Delvaux M., Duchet Jannick, Stavaux P-Y., Legras R., Demoustier-Champagne S., (2000). Chemical and Electrochemical Synthesis of Polyaniline micro-and nano-tubules. *J. Synthetic Metals*, 113: 275-280.
221. Patil V., Sainkar S. R., & Patil, P. P., (2004). Growth of poly(2,5-dimethoxyaniline) coatings on low carbon steel. *Synth. Met.*, 140, 57-63.
222. Cataldo F., & Maltese P., (2002). Synthesis of alkyl and N-alkyl-substituted polyanilines. A study on their spectral properties and thermal stability. *Eur. Polym. J.*, 38, 1791-1803.
223. MacDiarmid A. G., Manohar S. K., Masters J. G., Sun Y., Weiss H., & Epstein A. J., (1991). *Synth. Met.*, 41, 621-626.
224. Cao Y. (1990). Spectroscopic studies of acceptor and donor doping of polyaniline in the emeraldine base and pernigraniline forms. *Synth. Met.*, 35, 319-332.
225. Kang E. T., Neoh, K. G., Tan T. C., Khor S. H., & Tan K. L., (1990). Structural studies of poly(p-phenyleneamine) and its oxidation. *Macromolecules*, 23, 2918-2926.
226. Kang E. T., Neoh K. G., & Tan K. L., (1998). Polyaniline: A polymer with many interesting intrinsic redox states. *Prog. Polym. Sci.*, 23, 277-324.
227. Cho M. S., Park S. Y., Hwang, J. Y., & Choi, H. J., (2004). Synthesis and electrochemical properties of polymer composites with nanoparticles. *Mater. Sci. Eng., C*, 24, 15-18.
228. Fernandes M. R., Garcia J. R., Schultz M. S., & Nart F. C., (2005). Polaron and bipolaron transitions in doped poly(p-phenylene vinylene films). *Thin Solid Films*, 474, 279-284.

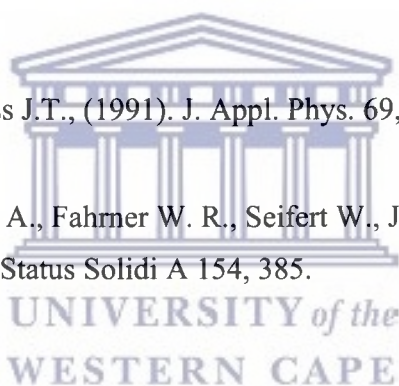
229. Geng Y. H., Sun Z. C., Li, J., Jing X. B., Wang X. H., & Wang, F. S., (1999). Water soluble polyaniline and its blend films prepared by aqueous solution casting. *Polymer*, 40, 5723-5727.
230. Goel S., Gupta A., Sign K. P., Mehrotra R., Kandpal H. C., (2007). Optical studies of polyaniline nanostructures. *Material Science and Engineering A*, 443:71-76.
231. Wei Z., Zhang Z., Wan N., (2002). Formation mechanism of self-Assembled polyaniline micro/nanotubes. *Langmuir*, 18: 917-921.
232. Jayanty S., Prasad G. K., Sreedhar B., Radhakrishnana T. P., (2003). Polyelectrolyte templated polyaniline-film morphology and conductivity. *Polymer*, 44: 7265-7270.
233. Huang J., (2006). Syntheses and Applications of Conducting Polymer Polyaniline Nanofibres. *Pure and Applied Chemistry*, 78: 15-27.
234. Zhang L., Wan M., (2002). Synthesis and characterization of self-assembled polyaniline nanotubes doped with D-10-camphor sulphonic acid. *Nanotechnology*, 13:750-755.
235. Huang J., Wan M., (1998). Temperature and pressure dependence of conductivity of polyaniline by insitu doping polymerization in the presence of organic functional acids as dopants. *Solid State Communications*, 108:255-259.
236. Zhang, D., & Wang, Y., (2006). Synthesis and applications of one-dimensional nanostructured polyaniline: An overview. *Mater. Sci. Eng., B*, 134 , 9-19.
237. Michira, I. N., (2007). Synthesis, electrodynamics and biosensor applications of novel sulphonated polyaniline nanocomposites. Unpublished Ph.D Thesis, University of the Western Cape, South Africa.



238. Perret A, Haenni W, Skinner N, Tang X.M, Gandini D, Comninellis C, Correa B, Foti G, (1999). *Diamond Relat. Mater.* 8, 820.
239. Pleskov Y.V, Russ., (1999). *Chem. Rev.* 68, 381.
240. Vinokur N, Miller B, Avyigal Y, Kalish R., (1996). *J.Electrochem. Soc.* 143, L238.
241. Swain G.M., (1994). *J. Electrochem. Soc.* 141, 3382.
242. Haenni W, Baumann H, Comninellis Ch, Gandini D, Niederman P, Perret A, Skinner N., (1998). *Diamond Relat. Mater.* 7, 569.
243. Granger M.C, Witek M, Xu J, Wang J., Hupert M, Hanks A, Koppang M.D, Butler J.E, Lucazeau G, Mermoux, M., Strojek, J.W, Swain G.M., (2000). *Anal. Chem.* 72, 3793–3804
244. Holt K.B, Bard A.J, Show Y, Swain G.M., (2004). *J. Phys. Chem. B* 108 15117–15127.
245. Fischer A.E, Show Y, Swain G.M., (2004). *Anal. Chem.* 76, 2553–2560.
246. Honda K, Noda T, Yoshimura M, Nakagawa K, Fujishima A., (2004). *J.Phys. Chem. B* 108, 16117–16127.
247. Hupert M, Muck A, Wang J, Stotter J, Cvackova Z, Haymond S, Show Y, Swain G.M., (2003). *Diamond Relat. Mater.* 12, 1940.
248. Martin H.B, Morrison P.W., (2001). *Electrochem. Solid-State Lett.* 4, E17.
249. Isberg J, et al., (2002). *Science* 297, 119.

250. Liu H, Dandy D.S., (1995). *Diamond Relat. Mater.* 4, 1173.
251. Goeting C.H, Jones F, Food J.S, Eklund J.C, Marken F, Compton R.G., Chalker P.R., Johnston C., (1998). *J. Electroanal. Chem.* 442, 207.
252. Koppang M.D, Witek M.A, Blau J, Swain G.M., (1999). *Anal. Chem.* 71, 1188.
253. Show Y, Witek M.A, Sonthalia P, Swain G.M., (2003). *Chem. Mater.* 15, 879.
254. Okano K, Naruki H, Akiba Y, Kurosu T.I, Hirose Y, Nakamura T., (1989). *Jpn. J. Appl. Phys.* 6, 1066.
255. Philip J., Hess P, Feygelson T, Butler J.E, Chattopadhyay S, Chen K.H, Chen. L.C., (1989). *J. Appl. Phys.* 6, 1066.
256. Kalish R., (1999), Doping of diamond. *Carbon* 37, 781-785.
257. Babbs C.F., and Gale M.J., (1988). In *Free Radicals: methodology and concepts* (Rice-Evans C., and B. Halliwell, Eds.), 91-121, Richelieu Press, London.
258. Bard A. J. and Faulkner L. R., (2001). 'Electrochemical methods – Fundamentals And applications', J. Wiley and Sons, Inc., New York.
259. Bockris J. O. M., Devanathan M. A. V., and Mueller K., (1963). *Proc. Phys. Soc. Ser. A*, 274, 55.
260. Beck F. and Schulz H., (1984). *Electrochim. Acta*, 29, 1569.
261. Marcus R. A., (1956). *J. Chem. Phys.*, 24 966.

262. Marcus R. A., (1968). *Electrochim. Acta* 13, 995.
263. Taylor R. J. and Humffray A. A., (1973). *J. Electroanal. Chem.*, 42, 347.
264. Blaedel W. J. and Schieffer G. W., (1977). *J. Electroanal. Chem.*, 80, 259.
265. Kuta J. and Yaeger E., (1975). *J. Electroanal. Chem.* 59, 110.
266. Bindra P, Gerischer H., and Peter L. M., (1974). *J. Electroanal. Chem.*, 57, 435.
267. Kawiak J., Jedral T., and Galus Z., (1983). *J. Electroanal. Chem.*, 145, 163.
268. Fleischmann M., Graves P. R., and Robinson J., (1985). *J. Electroanal. Chem.* 182  
87.
269. Nishimura K., Das K., Glass J.T., (1991). *J. Appl. Phys.* 69, 3142.
270. Werner M., Job R., Zaitzev A., Fahrner W. R., Seifert W., Johnston C.,  
Chalker P.R., (1996). *Phys. Status Solidi A* 154, 385.
271. Yagi I., Notsu H., Kondo T., Tryk D.A., Fujishima A., (1999). *J. Electroanal.  
Chem.* 473, 173.
272. Granger M.C., Witek M., Xu J.S., Wang J., Hupert M., Hanks A., Koppang M.D.,  
Butler J.E., Lucazeau G., Mermoux M., Strojek J.W., Swain G.M., (2000). *Anal.  
Chem.* 72, 3793.
273. Tryk D.A., Tsunozaki K., Rao T.N., Fujishima A., (2001). *Diamond Relat. Mater.*  
10, 1804.

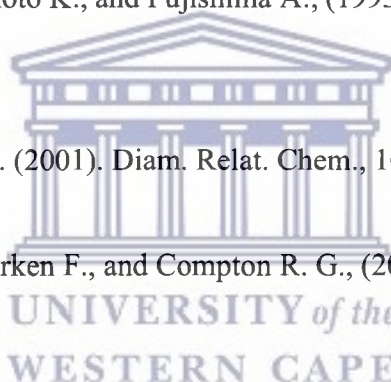


274. Granger M.C., Swain G.M., (1999). *J. Electrochem. Soc.* 146, 4551.
275. Maier F., Riedel M., Mantel B., Ristein J., Ley L., (2000). *Phys. Rev.Lett.* 85, 3472.
276. Mahe' E., Devilliers D., Comininellis Ch., (2005). *Electrochim. Acta* 50, 2263.
277. Rieger P.H., (1987). *Electrochemistry*, N.J., 1-26.
278. Marselli B., (2003). *Journal of Electrochemical Society*, Vol.150, N<sup>o</sup>.3, 79-83.
279. Latto M. N., Riley D. J., and May P. W., (2000). *Diamond Relat. Mater.*, 9, 1181.
280. Looi H. J., Pang L. Y. S., Molloy A. B., Jones F., Foord J. S., and Jackman R. B., (1998), *Diamond Relat. Mater.* 7, 550.
281. Yagi I., Notsu H., Kondo T., Tryk D. A., and Fujishima A., (1999). *J. Electroanal. Chem.*, 473, 173.
282. Tryk D. A., Tsunozaki K., Rao T. N., and Fujishima A., (2001). *Diamond Relat. Mater.*, 10, 1804.
283. Zhang G.-J., Song K.-S., Nakamura Y., Ueno T., Funatsu T., Ohdomari I., Kawarada H., (2006). *Langmuir* 22, 3728–3734.
284. Angus J. C., (1988). *Low Pressure, Metastable Growth of Diamond and Diamondlike Phases. Science (Articles)*, 913-919.
285. Martin T. H.B., Argoitia A., Angus J.C. and Landau U., (1999). *J. Electrochem. Soc.* 146, 2959.
286. Tryk D.A., Kondo T., Fujishima A., (2005). In *Diamond Electrochemistry*; A.

Fujishima, Y. Einaga, T.N. Rao, and D.A. Tryk. Ed.; BKC, Inc. (Tokyo), Elsevier (Amsterdam).

287. Terashima C., Rao T.N., Sarada B.V., Spataru N., (2003), Fujishima A.. J. Electroanal. Chem. 544, 65.
288. Salimi A., Hyde M.E., Banks C.E., Compton R.G., (2004). Analyst 9, 129.
289. Salimi A., Alizadeh V., Hallaj R., (2006). Talanta 68, 1610.
290. Xia Y. B., Sekiguchi T., Zhang W. J., Jiang X., Ju J. H., Wang L. J., and Yao T., (2000). Diam. Relat. Chem., 9, 1636.
291. Uchikado R., Rao T.N., Tryk D.A., Fujishima A., (2001). Chem. Lett. 30, 144.
292. Arefi-Khonsari F., Kurdi J., Tatoulian M., Amouroux J., (2001). Surf. Coat. Technol. 142–144, 437–448.
293. Mueller L. and Dietzsch S., (1981). J. Electroanal. Chem., 121, 255.
294. Lasseter T.L., Clare B.H., Abbott N.L., Hamers R.J., (2004). J. Am. Chem. Soc. 126, 10220–10221.
295. Swain G. M., Anderson A. B., and Angus J. C., (1998). MRS Bull., 23, 56.
296. Tian R.-H., Rao T.N., Einaga Y., Zhi J.-F., (2006). Chem. Mater. 18, 939–945.
297. Xu J., Granger M.C., Chen Q., Lister T.E., Strojek J.W., Swain G.M., (1997). Anal. Chem. 69, 591A.

298. Bouamrane F., Tadjeddine A., Butler J.E., Tenne R., Levy-Clement C., (1996). *J. Electroanal. Chem.* 405, 95.
299. Levy-Clement C., Ndao N.A., Katty A., Bernard M., Deneuille A., Comninellis Ch., Fujishima A., (2003). *Diamond Relat. Mater.*, 12, 606.
300. Pleskov Y. V., Sakharova A. Y., Krotova M. D., Bouilov L. L., and Spitsyn B. P., (1987). *J. Electroanal. Chem.*, 228, 19.
301. Reuben C., Galun E., Cohen H., Tenne R., Kalish R., Muraki Y., Hashimoto K., Fujishima A., Butler J. E., and Levy-Clement C., (1995). *J. Electroanal. Chem.* 396, 233.
302. Tenne R., Patel K., Hashimoto K., and Fujishima A., (1993). *J. Electroanal. Chem.* 347, 409.
303. Fujishima A and Rao, T. N. (2001). *Diam. Relat. Chem.*, 10, 1799.
304. Prado C., Wilkins S. J., Marken F., and Compton R. G., (2002). *Electroanalysis* 14, 262.
305. Manivannan A., Seehra M. S., Tryk D. A., and Fujishima A., (2002). *Anal. Lett.*, 35, 355.
306. Spataru N., Sarada B. V., Popa E., Tryk D. A, and Fujishima A., (2001). *Anal. Chem.* 73, 514.
307. Uchikado R., Rao T. N., Tryk D. A., and Fujishima A., (2001). *Chem. Lett.*, 144.
308. Denisenko A., Aleksov A., and Kohn E., (2001). *Diam. Relat. Chem.*, 10, 667.



309. Hayashi K., Yamanaka S., Watanabe H., T H. Sekiguchi H., Okushi H., and Kajimura K., (1997), *J. Appl. Phys.*, 81, 744.
310. Ristein, (2000). *Diam. Relat. Chem.*, 9, 1129.
311. van de Lagemaat J., Vanmaekelbergh D., and Kelly J. J., (1999). *J. Electroanal. Chem.*, 475, 139.
312. Alehashem S., Chambers F., Strojek J. W., Swain G. M., and Ramesham R., (1995). *Anal. Chem.*, 67, 2812.
313. Wu Z. Y., Yano T., Tryk D. A., Hashimoto K., and Fujishima A., (1998). *Chem. Lett.*, 503.
314. Del Campo F. J., Goeting C. H., Morris D., Foord J. S., Neudeck A., Compton R. G. and Marken F., (2000). *Electrochem. Solid State Lett.*, 3, 224.
315. Pleskov Y. V., Mazin V. M., Evstefeeva Y. E., Varnin V. P., Teremetskaya I. G., and Laptev V. A., (2000). *Electrochem. Solid State Lett.*, 3, 141.
316. Pleskov Y. V., Varnin V. P., Teremetskaya I. G., and Churikov A. V., (1997). *J. Electrochem. Soc.*, 144, 175.
317. Rao T. N., Tryk D. A., Hashimoto K., and Fujishima A., (1999). *J. Electrochem. Soc.* 146, 680.
318. Pehrsson P. E., Long J. P., Marchywka M., and Butler J. E., (1995). *App. Phys. Lett.*, 67, 3414.



319. Okano K., Koizumi S., Silva S. R. P., and Amaratunga G. A. J., (1996).  
Nature 381, 140.
320. Swain G. M., (1994). J. Electrochem. Soc., 141, 3382.
321. Vinokur N., Miller B., Avyigal Y., and Kalish R., (1996). J. Electrochem. Soc.  
143, L238.
322. Sakharova A. Y., Pleskov Y. V., Diquarto F., Piazza S., Sunseri C.,  
Teremetskaya I. G., and Varnin V. P., (1995). J. Electrochem. Soc. 142, 2704.
323. Zhang Z., Wensell M., and Bernholc J., (1995). Phys. Rev.B, 51, 5291.
324. Rohrer E., Nebel C. E., Stutzmann M., Floter A., Zachai R., Jiang X., and Klages  
C. P., (1998). Diam. Relat. Chem., 7, 879.
325. Nebel C. E., Waltenspiel A., Stutzmann M., Paul M., and Schafer L., (2000).  
Diam. Relat. Chem. 9, 404.
326. Pereira L., Pereira E., and Gomes H., (2000). Diam. Relat. Chem., 9, 1621.
327. Alvarez J., Kleider J. P., Bergonzo P., Mer C., Tromson D., Deneuille A.,  
and Muret P., (2002). Diam. Relat. Mater., 11, 635.
328. Ramesham R. and Rose M. F., (1997). Diam. Relat. Chem., 6, 17.
329. Granger M. C., Xu J. S., Strojek J. W., and Swain G. M., (1999). Anal. Chim. Acta,  
397, 145.

330. Samlenski R., Haug C., Brenn R., Wild C., Locher R., Koidl P., (1996). *Diamond Relat.Mater.* 5, 947.
331. Murray R.W., (1984). *Electroanal. Chem.* 13, 191.
332. Kaneko M., Wöhrle D., (1988). *Adv. Polym. Sci.* 84, 141.
333. Kaufman F.B., Engler M.B., (1979). *J. Am. Chem. Soc.* 101, 547.
334. Kaufman, F. B.; Schroeder, A. M.; Engler, E. M.; Kramer, S. R.,(1980). Chambers, J. Q. *J. Am. Chem. Soc.* 102, 483.
335. Lyons. M.E.G., (1994). *Charge Percolation in Electroactive Polymers.* In *Electroactive Polymer Electrochemistry*; Plenum Press: New York.
336. Oyama N., Oshsaka T., in: Murray R.W. (Ed), (1992). *Molecular Design of Electrode Surfaces*, Wiley, N.Y. 333.
337. Martin C.R., Van Dyke L.S., in: Murray R.W., (1992). *Molecular Design of Electrode Surfaces*, Wiley, N.Y. 403.
338. Terashima C., Rao T. N., Sarada B. V., Tryk D. A., and Fujishima A., (2002). *Anal. Chem.*, 74, 895.
339. Rao T. N., Loo B. H., Sarada B. V., Terashima C., and Fujishima A., (2002). *Anal. Chem.*, 74, 1578.
340. Michaud P.-A., Mahe´ E., Haenni W., Perret A., Comninellis Ch., (2000). *Electrochem. Solid-State Lett.* 3, 77.
341. Ferro S., DeBattisti A., Duo I., Comninellis Ch., Haenni W., Perret A., (2000). *J. Electrochem. Soc.* 147, 2614.

342. Wurm J., (2002). *New Diamond Front. Carbon Technol.* 12 (2), 107–114.
343. Rodrigo M. A., Michaud P. A., Duo I., Panizza M., Cerisola G., and Comninellis C., (2001). *J. Electrochem. Soc.* 148, D60.
344. Iniesta J., Michaud P.A., Panizza M., Cerisola G., Aldaz A., Comninellis Ch., (2001). *Electrochim. Acta* 46, 3573.
345. Iniesta J.P., Michaud A., Panizza M., Comninellis Ch., (2001). *Electrochem. Commun.* 3, 346.
346. Troupe C.E., Drummond I.C., Graham C., Grice J., John P., Wilson J.I.B., Jubber N.G., Morrison N.A., (1998). *Diamond Relat. Mater.* 7, 575.
347. Tatsuma T., Mori H., Fujishima A., (2000). *Anal. Chem.* 72, 2919.
348. Rao T.N., Yagi I., Miwa T., Tryk D.A., Fujishima A., (1999), *Anal. Chem.* 71, 2506.
349. Ohnishi K., Einaga Y., Notsu H., Terashima C., Rao T.N., Park S.G., Fujishima A., (2002). *Electrochem. Solid-State Lett.* 5, D1.
350. Ushizawa K., Sato Y., Mitsumori T., Machinami T., Ueda T., and Ando T., (2002). *Chem. Phys. Lett.* 351, 105-108.
351. Worner E., Wild C., MullerSebert W., Locher R., and Koidl P., (1996). *Diam. Relat. Chem.* 5, 688.
352. Kohn E., Adamschik M., Schmid P., Ertl S., and Floter A., (2001). *Diam. Relat. Chem.*, 10, 1684.

353. Troy C. T., (1992). *Photon. Spect.* 26, 28.
354. Hayashi K., Yamanaka S., Watanabe H., Sekiguchi T., Okushi H., and Kajimura K., (1997). *J. Appl. Phys.*, 81, 744.
355. Koenigsfeld N., Philosoph B., and Kalish R., (2000). *Diam. Relat. Chem.* 9, 1218.
356. Mankos M, Tromp R. M, and Cartier M. C. R. a. E., (1996). *Phys. Rev. Lett*, 76 3200.
357. Wang W. L, K. J. Liao, R. Q. Zhang, and C. Y. Kong, (2001). *Mater. Sci. Eng. B-Solid State Mater. Adv. Technol.*, 85, 169.
358. Wild C., (1998). 'Low pressure Synthetic Diamond: Manufacturing and Applications', ed. B. Dischler.
359. Chowalla M., (2001). *Diam. Relat. Chem.*, 10, 1011.
360. Sein H, Ahmed W, and Rego C., (2002). *Diam. Relat. Mater.*, 11, 731.
361. Nutt J.G., Woodward W.R., Hammerstad J.P., (1984). The "on-off" phenomenon In Parkinson's disease. Relation to levodopa absorption and transport. *N. Engl. J. Med.* 310, 483-488.
362. Beckmann H., Athen D., Olteanu M., (1979). DL-phenylalanine versus imipramine: a double-blind controlled study. *Arch Psychiat Nervenkr.* 227, 49-58.
363. Birkmayer W., Riederer P, Linauer W. Knoll, J., (1984). L-deprenyl plus L-phenylalanine in the treatment of depression. *J Neutral Transm.* 59, 81-87.

364. Zho G., (1991). Inherited metabolic aberration of phenylalanine in the family members of patients with essential hypertension and stroke. 71, 388-390.
365. Sabelli H.C., Fawcett J., Gusovsky F., (1986). Clinical studies on the Phenylalanine hypothesis of affective disorder: urine and blood phenylacetic acid and phenylalanine dietary supplements. *J.Clin.Psychiatry*, 47, 66-70.
366. Gardos G, Cole, J.O., Matthews J.D., (1992). The acute effects of a loading dose of phenylalanine in unipolar depressed patients with and without tardive dyskinesia. *Neuropsychopharmacology*, 6, 241-247.
367. Siddiqui A.H., Stolk L.M., Bhagooe R., (1994). L-phenylalanine and UVA irradiation in the treatment of vitiligo. *Dermatology*, 188, 215-218.
368. Mosnik D.M., Spring B., Rogers K., Baruah S., (1997). Tardive dyskinesia Exacerbated after ingestion of phenylalanine by schizophrenic patients. *Neuropsychopharmacology*, 16, 136-146.
369. Gelenberg, A.J.; Gibson, C.J.; Wojcik, J.D., (1982). Neurotransmitter precursors for the treatment of depression. *Psychopharmacol. Bull* 18, 7-18.
370. Meyer J.S., Welch K.M.A, Deshmuckh V.D., (1997). Neurotransmitter precursor amino acids in the treatment of multi-infarct dementia and Alzheimer's disease. *J.Am.Geriatr. Soc.* 7, 289-298.
371. Banderet, L.E.; Lieberman, H.R., (1989). Treatment with tyrosine, a Neurotransmitter precursor, reduces environmental stress in humans. *Brain Res Bull* 22, 759-762.

372. Salter C.A., (1989). Dietary tyrosine as an aid to stress resistance among troops. *Mil Med.* 154, 144-146.
373. Neri D.F., Wiegmann D., Stanny R.R., (1995). The effects of tyrosine on Cognitive performance during extended wakefulness. *Aviat Space Environ Med.* 66, 313-319.
374. Koch R., (1996). Tyrosine supplementation for phenylketonuria treatment. *Am J Clin Nutr.* 64, 974-5.
375. Gjetting Torben, Petersen M., Guldborg P., and Guttler F., (2001). "Missense Mutations in the N-Terminal Domain of Human Phenylalanine Hydroxylase Interfere with Binding of Regulatory Phenylalanine". *The American Journal of Human Genetics.* 68, 1353-1360.
376. Nelson, David, and Michael Cox, (2000). *Lehninger Principles of Biochemistry*, 3<sup>rd</sup> Edition. New York: Worth.
377. Monk P. M. S., (2001). *Fundamentals of electroanalytical chemistry*. Wiley & Sons, NY, USA, pp 17-24.
378. Bard A. J. and Faulkner L. R., (2001). *Electrochemical methods, fundamentals and application*, 2<sup>nd</sup> Edition, Wiley & Sons, US, pp 1, 23-35, 87-102, 161, 240 -250, 580-601.
379. Brett C. M. A and Brett A. M. O., (2005). *Electrochemistry, principles, methods and applications*. Oxford Science Publications, oxford University Press, pp 137-142.
380. Yu.V. Pleskov, Russ., (1999). *Chem. Rev.* 68, 381.
381. Granger M. C, Xu J. S, Strojek J. W, Swain G. M., (1999). *Anal. Chim. Acta* 397, 145.

382. Rao T. N, Fujishima A., (2000). *Diam. Rel. Mater.* 9, 384.
383. Angus J. C, Martin H. B, Landau U, Evstefeeva Y. E, Miller B, Vinokur N., (1999). *New Diam. Front. Carbon Technol.* 9, 175.
384. Yu.V. Pleskov, (2003). In *Advances in Electrochemical Science and Engineering* (Ed: R. Alkire), Wiley, New York.
385. Andrieux C.P, Hapiot P., Saveant J.M., (1990a). Ultramicroelectrodes for fast electrochemical kinetics *Electroanalysis*. *Electroanal.* 2, 183.
386. Souza D.D., Machado S.A.S., Pires R.C., (2006). Multiple square wave voltammetry for analytical determination of paraquat in natural water, food, and beverages using microelectrodes. *Talanta* 69, 1200.
387. Lafleur R.D., Myland J.C., Oldham K.B., (1990). Analytical microelectrode voltammetry with minimal instrumentation. *Electroanal.* 2, 223.
388. Bard, A. J., & Faulkner, L. R., (2000). *Electrochemical methods: Fundamentals And applications* (2nd ed.). New York: John Wiley & Sons.
389. Kounaves S. P., (1997). Voltammetric Techniques, In: *Handbook of Instrumental Techniques for Analytical Chemistry*, Settle F. A, Upper Saddle River, NJ: Prentice Hall, PTR, chp 37: 720-721.
390. Greef, R., Peat, R., Peter, L. M., & Pletcher, D., (1990). *Instrumental Methods in electrochemistry*. England: Ellis Horwood Limited.



391. Yang, Y., Yang, M., Wang, H., Jiang, J., Shen, G., & Yu, R., (2004). An amperometric horseradish peroxidase inhibition biosensor based on a cysteamine selfassembled monolayer for the determination of sulfides. *Sens. Actuators, B*, 102, 162–168.
392. Amine, A., Mohamed, H., Bourais, I., & Palleschi, G., (2006). Enzyme inhibition based biosensors for food safety and environmental monitoring. *Biosens. Bioelectron.*, 21, 1405-1423.
393. Hong, S. Y., Jung, Y. M., Bin Kim, S., & Park, S. M., (2005). Electrochemistry of conductive polymers. 34. Two-dimensional correlation analysis of real-time spectroelectrochemical data for aniline polymerization. *J. Phys. Chem. B*, 109, 3844.
394. Kim, S. -C., Huh, P., Kumar, J., Kim, B., Lee, J. -O., Bruno, F. F., (2007). Synthesis of polyaniline derivatives via biocatalysis. *Green Chem.*, 9, 44-48.
395. Mannino S., Cosio M., (1994), Organic-phase enzyme biosensor for moisture determination in Food products, *Analyst* 119, 2001–2003.
396. Mayer, AM., (2006). "Polyphenol oxidases in plants and fungi: Going places? A review". *Phytochemistry* 67: 2318-2331. PMID 16973188.
397. MacDiarmid A. G., (2001). 'Synthetic Metals': A novel role for organic polymers. *Current Applied Physics*, 1:269-279.
398. Mazur M., Michota-Kamińska A., Bukowska J., (2006). Surface-catalysed growth of poly(2-methoxyaniline) on gold. *Electrochimica Acta*, doi: 10.1016/j.electacta.2006.10.043
399. Hino T., Namiki T., Kuramoto N., (2006). Synthesis and characterization of novel conducting composites of polyaniline prepared in the presence of sodium dodecyl sulfate and several water soluble polymers. *Synthetic Metals*, 156: 1327-1332.

418. Hideo Notsu, Tetsu Tatsuma, Akira Fujishim, (2002). Tyrosinase-modified boron-doped diamond electrodes for the determination of phenol derivatives. *Journal of Electroanalytical Chemistry*, 523, 86–92.
419. Mangombo Z.A., Baker P., Iwuoha E., Key D., (2010). Tyrosinase biosensor based on a Boron-doped diamond electrode modified with a polyaniline-poly(vinyl sulfonate) composite film. *Microchim Acta*, 170, 267-273.



391. Yang, Y., Yang, M., Wang, H., Jiang, J., Shen, G., & Yu, R., (2004). An amperometric horseradish peroxidase inhibition biosensor based on a cysteamine self-assembled monolayer for the determination of sulfides. *Sens. Actuators, B*, 102, 162–168.
392. Amine, A., Mohamed, H., Bourais, I., & Paleschi, G., (2006). Enzyme inhibition based biosensors for food safety and environmental monitoring. *Biosens. Bioelectron.*, 21, 1405-1423.
393. Hong, S. Y., Jung, Y. M., Bin Kim, S., & Park, S. M., (2005). Electrochemistry of conductive polymers. 34. Two-dimensional correlation analysis of real-time spectroelectrochemical data for aniline polymerization. *J. Phys. Chem. B*, 109, 3844.
394. Kim, S. -C., Huh, P., Kumar, J., Kim, B., Lee, J. -O., Bruno, F. F., (2007). Synthesis of polyaniline derivatives via biocatalysis. *Green Chem.*, 9, 44-48.
395. Mannino S., Cosio M., (1994), Organic-phase enzyme biosensor for moisture determination in Food products, *Analyst* 119, 2001–2003.
396. Mayer, AM., (2006). "Polyphenol oxidases in plants and fungi: Going places? A review". *Phytochemistry* 67: 2318-2331. PMID 16973188.
397. MacDiarmid A. G., (2001). 'Synthetic Metals': A novel role for organic polymers. *Current Applied Physics*, 1:269-279.
398. Mazur M., Michota-Kamińska A., Bukowska J., (2006). Surface-catalysed growth of poly(2-methoxyaniline) on gold. *Electrochimica Acta*, doi: 10.1016/j.electacta.2006.10.043
399. Hino T., Namiki T., Kuramoto N., (2006). Synthesis and characterization of novel conducting composites of polyaniline prepared in the presence of sodium dodecyl sulfate and several water soluble polymers. *Synthetic Metals*, 156: 1327-1332.

409. Campuzano S., Serra B., Pedrero M., Villena F.J.M., Pingarrón J.M., (2003). *Anal. Chim. Acta* 494, 187–197.
410. Liu S., Yu J., Ju H., (2003). *J. Electroanal. Chem.* 540, 61–67.
411. Rogers K.R., Becker J.Y., Cembrano, J., (2000). *Electrochim. Acta* 45, 4373–4379.
412. Serra B., Jimenez S., Mena M.L., Reviejo A.J., Pingarrón J.M., (2002). *Biosens. Bioelectron.* 17, 217–226.
413. Hong, J., Moosavi-Movahedi, A. A., Ghourchian, H., Rad, A. M., & Rezaei-Zarchi, S., (2007). Direct electron transfer of horseradish peroxidase on Nafion-Cystein modified gold electrode. *Electrochim. Acta*, 52, 6261-6267.
414. Murray R. W., (1984). In A. J. Bard (Ed.), *Electroanalytical Chemistry* (vol. 13, pp.191). Dekker, New York: Dekker.
415. Toshio Nakamura, Jujie Ren, Kai-mei Zhu, Shinshi Kawara, and Baokang Jin, (2006). Application of the Nanogold-4,4'-bis(methanethiol) biphenyl Modified Gold Electrode to the Determination of Tyrosinase-Catechol Reaction Kinetics in Acetonitrile, *Anal. Sc.* Vol.22, 1261-1264.
416. Hernandez L.; Hernandez P.; Velasco V., (2003). Carbon felt electrode design: application to phenol electrochemical determination by direct oxidation, *Anal. Bioanal. Chem.* 377: 262-266.
417. Slawomir Michalkiewicz, Agata Skorupa, (2009). Anodic oxidation of 3,4-dihydroxyphenylacetic acid on carbon electrodes in acetic acid solutions, *Bioelectrochemistry*, doi: 10.1016/j.bioelechem.2009.11.002.

418. Hideo Notsu, Tetsu Tatsuma, Akira Fujishim, (2002). Tyrosinase-modified boron-doped diamond electrodes for the determination of phenol derivatives. *Journal of Electroanalytical Chemistry*, 523, 86–92.
419. Mangombo Z.A., Baker P., Iwuoha E., Key D., (2010). Tyrosinase biosensor based on a Boron-doped diamond electrode modified with a polyaniline-poly(vinyl sulfonate) composite film. *Microchim Acta*, 170, 267-273.

